Approaches to Overcome the Blood-Brain Barrier in the Chemotherapy of Primary and Secondary Brain Tumors:

Modulation of P-glycoprotein 170 and Targeting of the Transferrin Receptor

Dissertation

zur Erlangung des Doktorgrades der Naturwissenschaften (Dr. rer.nat.)
der Naturwissenschaftlichen Fakultät IV - Chemie und Pharmazie -
der Universität Regensburg

vorgelegt von

Martina Hubensack

aus Ingolstadt

2005

Für Ralph

Die vorliegende Arbeit entstand in der Zeit von August 2001 bis Januar 2005 unter der Leitung von Herrn Prof. Dr. A. Buschauer am Institut für Pharmazie der Naturwissenschaftlichen Fakultät IV - Chemie und Pharmazie - der Universität Regensburg.

Das Promotionsgesuch wurde eingereicht im Januar 2005.

Tag der mündlichen Prüfung: 15. Februar 2005

Prüfungsausschuß:	Prof. Dr. J. Heilmann	(Vorsitzender)
	Prof. Dr. A. Buschauer	(Erstgutachter)
	Prof. Dr. A. Göpferich	(Zweitgutachter)
	Prof. Dr. A. Kurtz	(Prüfer)

An dieser Stelle möchte ich mich bedanken bei:

Herrn Prof. Dr. A. Buschauer für die interessante Aufgabenstellung, die wissenschaftlichen Anregungen und Förderung, sowie für die konstruktive Kritik bei der Durchsicht der Arbeit.

Herrn PD Dr. G. Bernhardt für die umfassende Betreuung, die wissenschaftliche Anleitung sowie für zahlreiche konstruktive Diskussionen während der Laborzeit und der Durchsicht der Arbeit.

Herrn Dr. T. Spruß für die Unterstützung bei der Durchführung der Tierversuche und der histologischen Untersuchungen.

Herrn Prof. Dr. A. Kurtz und Herrn Dr. H. Castrop für die Unterstützung beim Erlernen und der Durchführung der RT-PCR Untersuchungen.

Herrn M. Henry von der Firma GlaxoSmithKline sowie Herrn R. Robey vom NIH für die Bereitstellung der Inhibitoren.

Herrn F. Wiesenmayer und Herrn O. Baumann für die Unterstützung bei der Durchführung der Tierversuche.

Frau P. Pistor und Frau K. Frank für die Erstellung und Färbung der histologischen Schnittserien sowie für die Unterstützung bei der Durchführung der immunhistologischen Färbungen.

Frau S. Bollwein und Frau C. Müller für die Hilfe bei der Homogenisierung der Gewebeproben.

Herrn J. Zimmermann für die Unterstützung und den Platz bei der Durchführung der chemischen Synthesen.

Frau S. Bollwein und Herrn M. Keller für die fachliche Unterstützung und die gute Zusammenarbeit im Labor.

Frau S. Heinrich und Herrn P. Richthammer für die Hilfsbereitschaft und Unterstützung bei vielen organisatorischen und technischen Dingen.

allen Mitgliedern des Lehrstuhls für ihre Kollegialität und Hilfsbereitschaft.

der Schafkopfgruppe (Sigrid, Christian und Erich) für die vielen lustigen und aufheiternden Stunden abseits des Laboralltags.

meinen Kollegen Christine, Edith, Manuela, Sunnhild, Alex, Christian, Erich, Georg, Hendrik, Jochen, Ralf und Stephan für die Unterstützung bei fachlichen Problemen und die vielseitigen Erlebnisse im Laufe der gemeinsamen Zeit.

meiner Schwägerin Claudia für ihre geduldige und unermüdliche Lesebereitschaft.

meiner Famile, vor allem meinen Eltern sowie Herta und Willy für all ihre Unterstützung.

meinem Mann Ralph für Toleranz, Geduld und seine offenen Ohren in den letzten drei Jahren.

Contents

Chapter 1

Introduction

1.1 Barriers inhibiting drug delivery to the brain

Systemic drug delivery to the brain is a difficult challenge for modern drug development. For an effective treatment of diseases in the CNS drugs have to overcome several barriers including the blood-brain barrier and the blood-cerebrospinal fluid (CSF) barrier. If the target of intracranial drug delivery is a CNS tumor an additional barrier, the blood-tumor barrier has to be considered.

1.1.1 The Blood-Brain Barrier

The general concept of a restriction on the passage of dissolved substances out of the blood into the brain was first postulated by Paul Ehrlich (Ehrlich 1902). Edwin Goldmann, a student of Paul Ehrlich, injected the dye trypan blue into the CSF and the dye stained only the brain but not the other organs (Goldmann 1909). This experiment together with the studies of Romanowsky, who used Prussians' blue as a reagent in the late 1890s (Brightman 1992), established the concept of the blood-brain barrier (BBB). The cytoarchitecture of the BBB was discovered in the late 1960s by means of electron microscopic studies (Miller 2002).

The BBB is build up by the endothelial cells of the brain capillaries (Fig. 1.1). Astrocytes, microglial cells, pericytes and nerve endings surrounding the capillaries are considered to be essential for the differentiation of the endothelial cells and the maintenance of

the barrier (Abbott 2002, Brightman 1992, Rubin and Staddon 1999). Astrocytes are the structural frame of the neurons and their adjoining foot processes fully encapsulate the capillaries (Lo et al. 2001). Furthermore, they are necessary for the expression of various growth factors and transport systems such as the glucose transporter GLUT1 (Janzer and Raff 1987). Microglia and pericytes derived from mononuclear blood macrophages enhance the BBB function and are conducive to modulatory signaling (Zenker et al. 2003). Axonal endings that are closely abutted to the endothelial cells, are considered to be important for BBB permeability (Rennels et al. 1983).

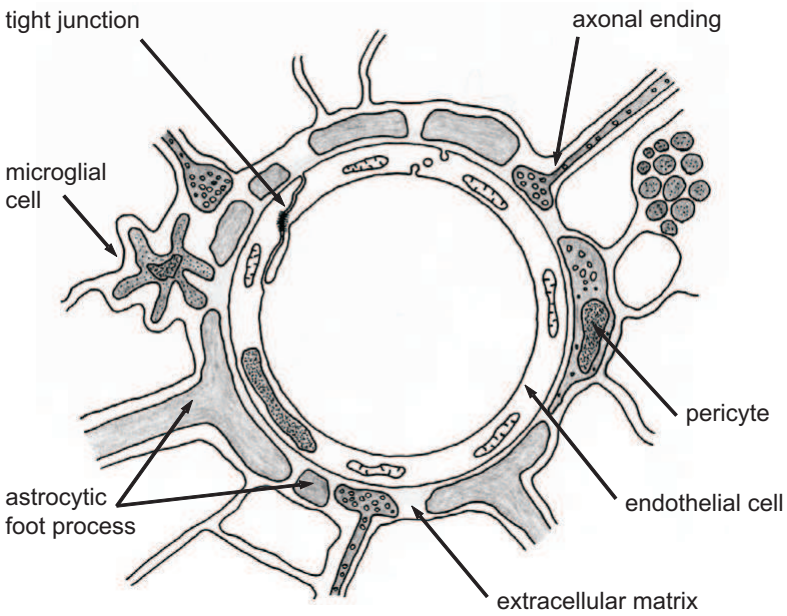

Figure 1.1: Schematic diagram of the cells forming the BBB. Endothelial cells of brain capillaries are sealed by tight junctions. These cells are surrounded by pericytes and foot processes of astrocytes responsible for the structural integrity of the barrier. The microglial cells are part of the immune system due to their descent from macrophages. Axonal endings provide vasoactive neurotransmitters which are important for BBB permeability (from Begley (2004)).

Brain capillaries have a total length of more than 600 kilometers through the human brain, a total surface area of 12 m^2 (Misra et al. 2003, Miller 2002) and are much smaller in diameter as well as thinner walled compared to vessels in other organs. The typical characteristics of blood vessels such as intercellular clefts, pinocytosis and fenestrae are not found in brain capillaries. The endothelial cells form intercellular tight junctions (zona occludes) that completely seal the capillaries and close the paracellular pathway

(Brightman and Reese 1969, Saunders et al. 1999, Fenstermacher 2001). Several transmembrane proteins, particulary occludin and claudin, are responsible for the formation of the junctions by complex interactions with each other (Kniesel and Wolburg 2000). The high seclusiveness of the brain to the other organs and the blood circulation results in an extremely high trans-endothelial electrical resistance of 1500 to 2000 $\Omega \cdot cm^2$ (Butt et al. 1990). Moreover, the brain capillaries are identified by limited paracellular transport due to the low endocytic activity and the absence of fenestration (Kemper et al. 2004a).

All these properties of the endothelial cells contribute to a strongly restricted permeability of the BBB, which is required to protect the brain against foreign and toxic substances as well as neurotransmitters and hormones (van Asperen et al. 1997). Additionally, the relative impermeability supports the maintenance of a constant internal environment, which is very important for proper neuronal function in the brain. Also, the composition of the resulting extracellular fluid of the brain parenchyma can be precisely controlled (Begley 2004). Due to the limited access of substances to the brain, only small lipid soluble compounds can cross the BBB by passive diffusion. To enable the uptake of essential polar substances into the brain, a lot of different transport proteins are expressed at the BBB (Begley 2003). These active transporters include carriers for glucose and amino acids as well as receptor mediated systems for certain peptides such as insulin or transferrin (Begley 1996). Fig. 1.2 shows different possible pathways through the BBB.

Apart from the transporters that are responsible for substance uptake into the brain, two specific mechanisms exist at the BBB. which are concerned with the protection of the brain. In order to degrade unwanted crossing substances the endothelial cells contain a large number of degrading enzymes and a high density of mitochondria, which are metabolically highly active organelles (Misra et al. 2003, Brownlees and Williams 1993). The high ability of the BBB to detoxify and transform compounds has been underestimated in the past. Furthermore, active efflux transport proteins are expressed at high concentrations at the luminal or basolateral membrane of the endothelial cells such as ABCB1 (p-glycoprotein 170), ABCC1 (MRP1) and ABCG2 (BCRP) and are able to transport a broad variety of compounds against a concentration gradient from the endothelial cytoplasm back to the lumen of the brain capillaries (Ramakrishnan 2003). These efflux transporters are described in detail in chapter 1.3.

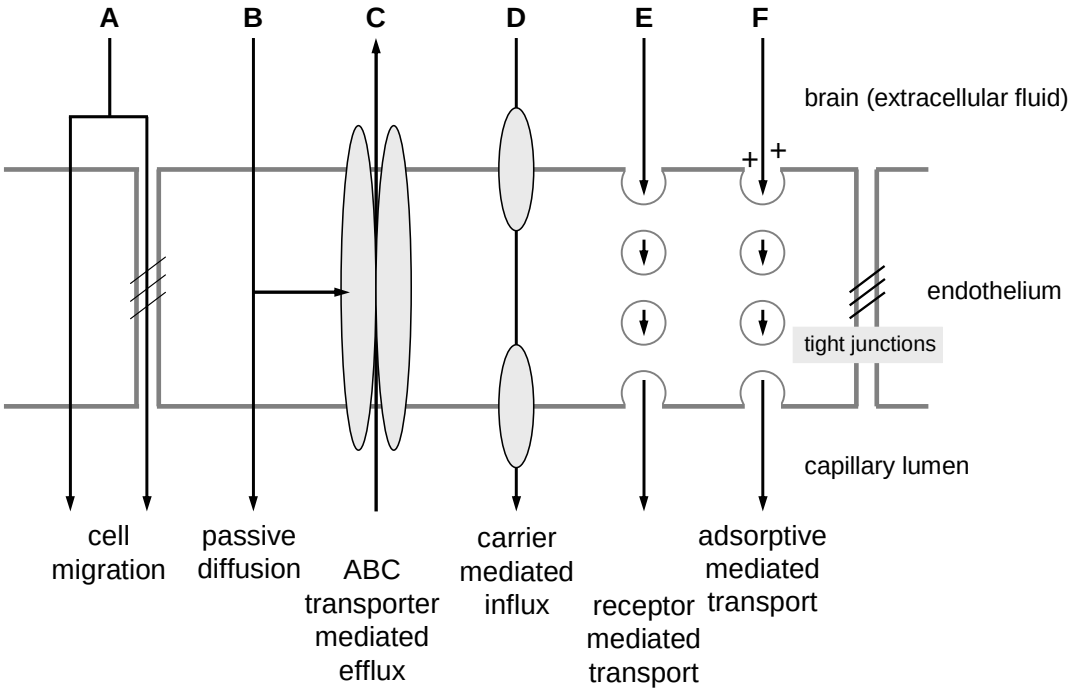

Figure 1.2: Possible routes for transport across the BBB. (A) Cells, particularly leukocytes, cross the BBB adjacent to tight junctions or directly. (B) The most common pathway for compounds is passive diffusion. (C) However, passively transported substances may be carried out by active efflux pumps. (D) Carrier mediated influx is used by essential polar solutes such as glucose. (E) Macromolecules, e.g. insulin, are transported by specific receptors. (F) Alternatively, adsorptive mediated transcytosis may occur induced by negatively charged macromolecules (from Begley (2004) with modifications).

1.1.2 The Blood-CSF Barrier

The most important function of the choroid plexus is the secretion of CSF. To produce this fluid, a broad variety of nutrients and other blood borne solutes are necessary. Since, however, molecules can be exchanged between the CSF and the interstitial fluid of the brain parenchyma (Misra et al. 2003), the uptake of these solutes into the CSF has to be controlled in order to restrict the penetration of cytotoxic agents or other unwanted substances into the brain. This is done by the blood-CSF barrier (BCB) which is formed by the epithelia of the choroid plexus and the circumventricular organs (CVO) (Wolburg et al. 2001). Furthermore, the arachnoid membrane is also involved in the function of the

BCB (Siegal 2001). The arachnoid membrane consists of a double layer of ependymal cells between dura and pia mater. Tight junctions between the ependymal cells seal the arachnoid membrane against the paracellular pathway. Also, the epithelial cells of the choroid plexus, arranged in a close sheet, form tight junctions to prevent macromolecular diffusion into further brain regions. However, these epithelial-like cells show a lower resistance of approximately 200 $\Omega \cdot cm^2$ compared to the endothelial cells of the BBB (Misra et al. 2003). Moreover, paracellular diffusion is impeded at the CVO due to the occurrence of tight junctions between the ependymal cells surrounding the CVO. To enable the passage of peptides, ions and further nutrients from blood into the CSF, the capillaries of the choroid plexus and the CVO are fenestrated and non-continuous. Due to the sealed paracellular pathways at the surrounding epithelia, exchange of molecules can only occur in a small restricted area of the extracellular fluid immediately around the CVO. Within this limited volume, the activity of dendritic processes and neuron receptors can be influenced by blood borne compounds leading to certain neural impulses in distant brain areas (Begley 2004).

However, the surface area of the BCB is approximately 1,000 fold smaller compared to the BBB surface area (Pardridge 1997). Hence, drug entry to the brain via the BCB plays a secondary role in brain drug uptake (Rautio and Chikhale 2004).

1.1.3 The Blood-Tumor-Barrier

Although in brain tumors the BBB is at least partly disrupted, other barriers together with the physiological conditions in the brain tumor tissue such as abnormal blood capillaries, hamper effective drug delivery to the tumor. In contrast to brain capillaries, the blood capillaries within different regions of the tumor tissue show significantly different morphology (Schlageter et al. 1999, Siegal 2001). These changes include alterations in the tight junction structure and the irregular appearance of endothelial cells with either many fenestrations, increased pinocytosis or a totally irregular basal membrane (Bart et al. 2000). The inconsistent spatial density of the capillaries together with the decreased vascular surface compared to the tumor volume contribute to an insufficient brain tumor drug delivery. Furthermore, tumor blood capillaries are sometimes leaky, leading to an

accumulation of interstitial fluid and hence, an increase of the interstitial tumor pressure (Jain 1994). The high intratumoral pressure limits drug penetration into the tumor tissue and could effect the drug permeability of capillaries in tumor adjacent regions of normal brain, resulting in low extratumoral interstitial drug concentrations (Cornford et al. 1982). The term blood-tumor barrier includes all aforementioned aspects of drug delivery to brain tumors.

1.2 Drug delivery into the brain: different approaches to overcome the BBB

Drug delivery to the brain is a major challenge in brain disease treatment nowadays. There are various strategies to circumvent the aforementioned barriers in order to increase drug concentrations in the brain. Generally, the majority of these strategies can be classified in four categories: direct manipulation of the drug itself, disruption of the BBB, direct brain delivery, and alternative drug delivery routes.

1.2.1 Improvement of the physicochemical properties

The common requirements to a compound for penetration through the BBB are a low molecular mass between 150 and 500 Da and an optimal log $P_{o/w}$ between 1.5 and 2.5 (Madrid et al. 1991). Furthermore, the compound has to be uncharged at physiological pH 7.4. Due to the clear relationship between lipophilicity and CNS penetration (Levin 1980), small chemical modifications to compounds that normally do not cross the BBB should lead to lipophilic analogs with the desired characteristics for penetrating the BBB. Besides the increased log $P_{o/w}$ values, the circulatory half life of such compounds may be prolonged and the plasma AUC may be increased, resulting in higher drug concentrations that are available for brain uptake.

However, increasing the lipid solubility often achieves reversed effects on drug uptake into the brain. Improvement of the lipophilicity leads to decreased solubility and unavailability. Moreover, the plasma protein binding of such modified compounds is increased, resulting in lower drug concentrations in the brain and in enhanced systemic toxicity. In

addition, the activity of the drug is influenced by its poor solubility in the interstitial fluid. This was demonstrated with BCNU analogs (reviewed by Pardridge (1988)). The antineoplastic activity of the different derivatives was inversely proportional to their lipid solubility.

Although a compound is sufficiently lipophilic to penetrate the BBB, sometimes no enhanced brain accumulation is observed. Then, the compound is a substrate of an efflux transporter located at the BBB (see 1.2.6 and 1.3). Today it is possible to predict the permeability of compounds and their lipophilic analogs by use of computation techniques. However, these programs provide no information about the affinity of the compounds to certain efflux transporters.

1.2.2 Prodrugs

An alternative approach to improve the delivery to the brain is the preparation of prodrugs, e.g. by esterification of carboxylic acid containing drugs. These prodrugs contain the drug in pharmacologically inactive or only weakly active form, but show improved physicochemical properties such as increased lipophilicity for an enhanced BBB penetration of the drug. The transformation of the prodrug in its active form requires a transient chemical or biochemical modification that should take effect solely in the desired organs (Stella et al. 1985). In case of drug delivery to the brain, the active compound is more polar compared to the prodrug and thus, trapped inside the brain after conversion. Then, the brain concentrations of the compound remain high although the prodrug levels in the blood significantly decrease. The brain delivery of heroin is a good and well known example for the prodrug approach. The structure of heroin is similar to morphine as heroin contains two further acetyl groups leading to an enhanced lipid solubility compared to morphine. The brain accumulation of morphine is about 30 times lower compared to that of heroin (Begley 2004). Inside the brain, however, heroin is transformed to 6-acetyl morphine and subsequently metabolized to morphine which is trapped in the brain because of its hydrophilicity. Morphine is the active form that interacts with the opioid receptors. Hence, heroin is a prodrug form of morphine.

However, the use of prodrugs for brain delivery has its limitations. Besides an en-

hanced brain uptake the prodrug accumulates in other tissues resulting in an increased tissue burden. This loss of selective drug delivery is critical, particularly in case of steroids and cytotoxic agents. Furthermore, the prodrug could be metabolized into other active compounds than the desired one, which may enhance the toxicity of the compound. Therefore, the required metabolic transformations to produce the active compound have to be seriously considered.

1.2.3 Chemical drug delivery systems

The concept of a chemical drug delivery system was developed from the prodrug approach. The drugs used for this system consist of several additionally attached moieties that are introduced into the molecule to improve lipid solubility, protect certain functions of the molecule, and prevent premature metabolic degradation. Furthermore, another moiety is attached to the molecule to target the drug to a specific tissue. This targeting aspect is the major difference to the prodrug concept. Drug modifying and targeting functions can be fulfilled by the same moiety. Once at the targeted tissue, the active drug is released from the system by several enzymatic processes. Bodor and Brewster (1991) developed a chemical delivery system that can be used for brain drug delivery (see Fig. 1.3). 1-Methyl-1,4-dihydronicotinic acid was covalently linked to a drug by esterification. Due to the enhanced lipophilicity by the attachment of the nicotinic acid derivative, the drug is able to penetrate the BBB and accumulate in the brain. Inside the brain parenchyma, the dihydronicotinic acid moiety of the drug is enzymatically oxidized to the quaternary salt by the NAD^+/NADH coenzyme system. The charged drug is locked in the CNS and subsequently, the active form is released slowly from the attached moiety by hydrolysis. However, the modified drug distributes not only in the brain, but also in various other organs. Since the conversion to the salt form takes place ubiquitously in the body, the oxidized salt that is present outside the brain will be rapidly eliminated from the body by liver and kidney. Hence, the use of this chemical delivery system leads to a sustained and brain-specific drug accumulation. Due to the accelerated systemic elimination of the charged drug in the periphery, the systemic toxicity is reduced. Furthermore, since the majority of the drug in the brain is present in the inactive form, the central toxicity of

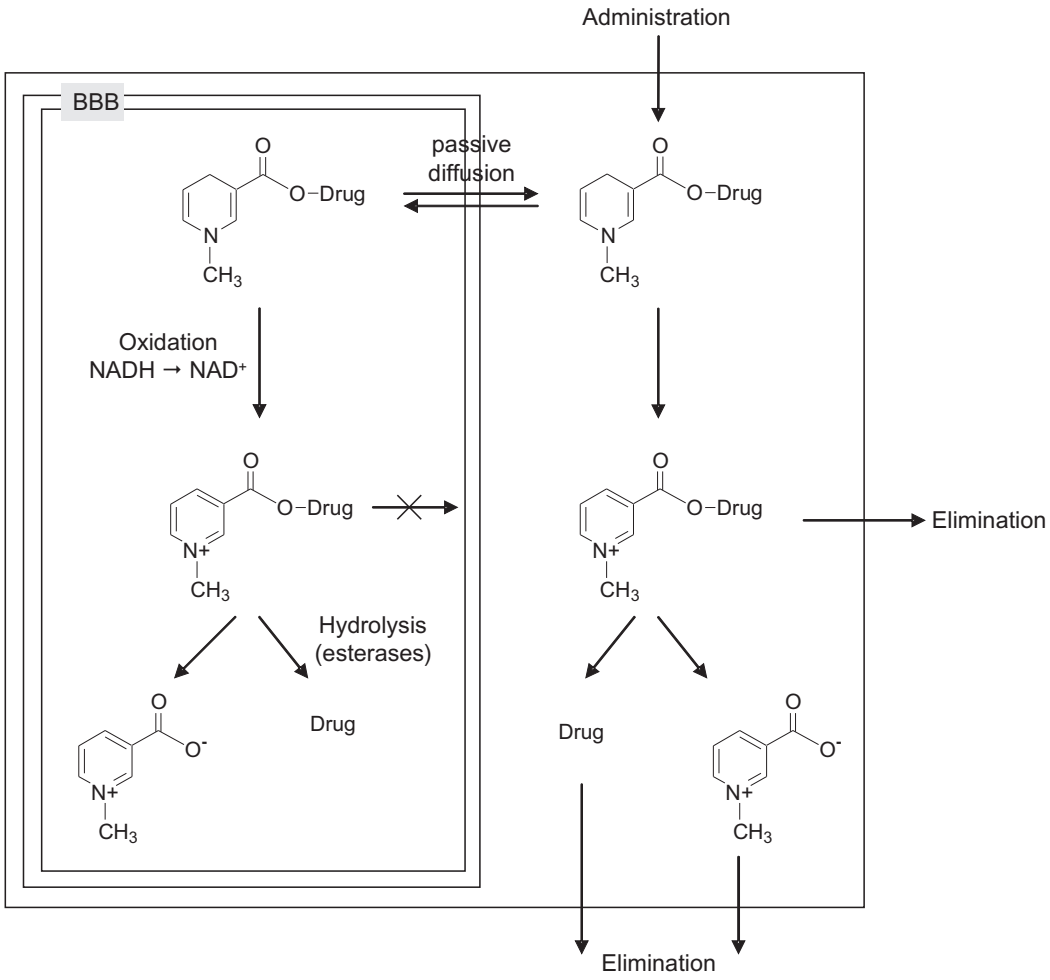

Figure 1.3: Lock-in mechanism of a chemical drug delivery system using a targeting moiety that exploits a 1,4-dihydronicotinic acid to charged nicotinic acid conversion. Covalently linkage to the targeting moiety leads to drug accumulation in the brain and accelerated elimination in the periphery (adopted from Bodor and Brewster (1991)).

the drug is lowered as well. During the last decade, variations of chemical drug delivery systems were developed such as anionic or redox chemical delivery systems. This approach to brain drug delivery is established for various drug classes such as chemotherapeutic agents (Bodor and Buchwald 1999) or estrogens (Bodor and Buchwald 2002).

1.2.4 Carrier- and receptor mediated transport

A broad variety of transporters, carriers, and certain receptors is localized at the BBB. They all are responsible for the uptake of polar metabolites and nutrients that normally

have no access to the brain (Begley and Brightman 2003). These transport pathways through the BBB can be utilized to enhance the brain concentration of certain compounds. Therefore, the stereochemical transport requirements for transport by these carrier systems has to be known in order to use this pathway for compounds that can act as pseudosubstrates (Tamai and Tsuji 2000).

The carrier systems at the BBB include hexose transporters (Pardridge et al. 1990a), the large neutral amino acid transporter (LAT) (Boado et al. 1999), acidic and basic amino acid transporters (Smith 2000), tricarboxylic acid transporters (Walker et al. 1994), nucleoside transporters (Schaddelee et al. 2003), and peptide transporters (Tsuji 2000). There are transport systems with a very high substrate selectivity such as the hexose transporter GLUT1 or the nucleoside transporter, that accept only a very restricted amount of compounds. In contrast, the LAT is less specific for its substrates and accepts the widest variety of pseudosubstrates (Begley 2004). The substrates of the LAT require only a carboxylic acid group and an amino group covalently linked to the same carbon atom, or a conformation that is similar to this grouping. Furthermore, a LAT substrate needs a large hydrophobic side to ensure the correct alignment of the compound to the active site of the transporter (Smith and Stoll 1999). The anticancer drug melphalan, a derivative of L-phenylalanine, shows only low affinity for the LAT. Taken the structure transport relationships of LAT into account for the synthesis of a melphalan derivative with higher affinity to LAT, the compound D,L-2-amino-7-bis[(chloroethyl)amino]-1,2,3,4-tetrahydro-2-naphthoic acid (D,L-NAM) was developed which had a 100-fold greater affinity for LAT compared to melphalan (Takada et al. 1992). The affinity of D,L-NAM for LAT is even higher than that of endogenous substrates, leading to preferred transport into the brain.

In addition to the described transporters and carriers, certain receptor systems are present at the BBB such as transferrin and insulin receptors. Also by means of transcytosis mediated by these receptors, several proteins, peptides, and drugs can gain access to the brain (see also chapter 8). BBB transcytosis can be mediated by either a receptor (RMT) or by absorption (AMT) (Bickel et al. 1994). In case of RMT the compound has to bind directly to the receptor at the luminal site of the capillary endothelial cells. The binding induces internalization of the compound-receptor complex and leads to the formation of a vesicle containing the complex. The vesicle can enter several pathways that carry it

either to the abluminal site of the cell, where exocytosis of the compound takes place, or to a lysosome to fuse forming a secondary lysosome. The latter pathway describes a dead end and may lead to the degradation of the compound. If direct binding of a drug to the receptor is not possible, the drug can be conjugated to a vector by chemical linkers such as Traut's reagent, polyethylene glycol (PEG) linkers or the avidin-biotin technique. The effectiveness of this delivery approach was demonstrated for several peptide based pharmaceuticals, such as vasoactive peptides (Pardridge 1999). Monoclonal antibodies (MAb) that are directed to a certain receptor at the BBB are used as BBB transport vectors. The most common MAb used in experimental studies is the OX26 MAb directed to the rat transferrin receptor (Broadwell et al. 1996). Using the OX26 as a BBB transport vector, specific accumulation of neuropeptides in the brain of rats was shown (Bickel et al. 1993). However, the capacity of RMT systems is very low as only one molecule can bind to the receptor or the vector. Furthermore, the competition with endogenous substrates for the receptors is a major drawback of this strategy particularly in case of direct binding to the receptor.

The concept of absorption mediated transcytosis (AMT) is based on electrostatic interactions between peptides or proteins and the luminal surface of the endothelial cells. These charge interactions induce vesicle formation and internalization. This approach is applicable for compounds with high positive charge as for example cationized albumin (Pardridge et al. 1990b). Furthermore, the structure of the C-terminus and the basicity of the molecule are important for brain uptake via AMT (Tamai et al. 1997).

1.2.5 Disruption of the BBB

Interference with the cytoarchitecture of the BBB is another approach that was developed especially for the treatment of rapidly growing high grade glioma. Here, the function of the tight junctions is disturbed and the BBB is transiently disrupted to open a paracellular transport pathway for the enhanced access of systemically administered drugs. There are several ways to open the BBB. The first attempts were done by infusion of dimethyl sulfoxide or ethanol. Also pathological conditions such as hypertension, hypoxia or ischemia were induced at which disruption of the BBB was observed (Misra et al. 2003). However,

all these techniques have unacceptable side effects.

In the 1970s Rapport et al. demonstrated the osmotic opening of the BBB which is still applied in the treatment of human brain tumors (Rapoport et al. 1972, Rapoport 2000). An inert hypertonic solution is injected via the carotid artery. Generally, a 25 % solution of mannitol is used for the BBB opening that is infused at a rate of 4 to 8 ml/sec over a period of 30 min (Begley 2004). The hypertonic solution initiates shrinkage of the endothelial cells, resulting in the disruption of the tight junctions and the opening of a paracellular pathway for a few hours. Subsequently after the injection of the BBB opener, the chemotherapeutic drug is administered by intraarterial injection. This method was very successful in patients who failed systemic chemotherapy (Rautio and Chikhale 2004). However, the opening of the BBB is nonselective and potentially neurotoxic compounds can easily reach the brain leading to sometimes unreasonable toxicity. Furthermore, the osmotic disruption enhanced the permeability of the tumor capillaries only by 25 %, in contrast to a 10 fold increase in the permeability of normal brain capillaries (Neuwelt et al. 1994). The toxic vs. therapeutic ratio has to be carefully considered for the individual patient.

The opening of the BBB using biochemical techniques is a more reliable alternative to hypertonic solutions. This was demonstrated with an intracarotid infusion of leukotriene C4 (Chio et al. 1992). Here, a selective opening of the tumor capillaries was observed. The adjacent normal brain capillaries were not affected. An explanation of this phenomenon may be the abundant expression of γ-glutamyl transpeptidase in normal brain capillaries, which inactivates leukotriene C4 to leukotriene D4 (Black et al. 1994). This enzyme is downregulated in damaged capillaries or brain tumor capillaries leading to elevated vascular permeability mediated by leukotriene C4 in these regions. Further BBB openers are bradykinin (Cloughesy and Black 1995) and the synthetic bradykinin analog RMP-7 (receptor mediated permeability; cereport; Emerich et al. (2001)). These substances act on the B2 receptors that are expressed in the luminal membrane of the endothelial cells. The stimulated receptors initiate an increase in intracellular free calcium, which leads to an activation of the actin/myosin system within the cells. This activation influences the scaffolding proteins (ZO1-3) that are attached to the tight junction proteins occludin and claudin, resulting in a remove from the cell membrane and thus, modify the functionality of

the tight junctions (Begley 2004). First promising results were obtained in the treatment of glioma bearing rats with carboplatin and RMP-7 (Matsukado et al. 1996). In contrast to leukotriene C4, this opening is unselective due to the overall distribution of B2 receptors in the body which may again result in unwanted toxic side effects. Hence, phase II trials on combination treatment of anticancer drugs with RMP-7 were aborted due to toxicity concerns (Misra et al. 2003, Prados et al. 2003).

Also, allylglyceroles, particularly monoacetyl and diacetyl glycerols, are able to modulate the permeability of the BBB (Erdlenbruch et al. 2003a, Lee et al. 2002). They cause a rapid opening of BBB that remains for up to 120 min. The most effective compound is 1-O-hexyldiglycerol. A possible mechanism for this substance class is the formation of vesicles at the cell membrane due to the detergent properties. Thus, pores are formed through the plasma membrane leading to enhanced access of polar compounds to the brain. Using this approach, Erdlenbruch et al. (2003b) were able to increase the delivery of methotrexate to the rat brain without any signs of toxicity. However, this kind of BBB opening is again unselective as both normal and tumor brain capillaries are affected.

1.2.6 Modulation of efflux transporters

Brain tumor therapy with cytostatic drugs that should be able to penetrate the BBB often failed due to the extremely low drug concentrations in the brain. This is explainable by the high affinity of these compounds to efflux transport systems that are localized at the luminal membrane of the brain capillary endothelial cells, at newly formed capillaries of brain tumors, and in the tumor cells themselves (Bendayan et al. 2002, Toth et al. 1996, Matsumoto et al. 1991). These efflux transport proteins belong to the ABC transporter class including ABCB1, ABCC1 and ABCG2. They are described in detail in chapter 1.3.

The major strategies to overcome the ABC transporter mediated efflux are the application of specific inhibitors in addition to the effluxed compound, and the synthesis of new drugs that lack the affinity to the ABC transport proteins. It is essential for both approaches to know the detailed structure activity relationships of the ABC transport mechanism. As these proteins do not show interactions with their substrates in a classic enzyme-substrate or lock-and-key manner, the determination of these relationships is

hampered. Research effort was mostly directed to the inhibition of the ABCB1 transport protein. Several ABCB1 inhibitors were developed in the past (Tan et al. 2000) that have been shown to successfully enhance CNS concentrations of ABC transporter substrates such as the anticancer agent paclitaxel (see Fig. 1.4). These inhibitors include the second generation inhibitor valspodar (SDZ PSC 833, Fellner et al. (2002)) as well as the third generation inhibitors elacridar (GF 120918, Kemper et al. (2003)) and zosuquidar (LY 335979, Kemper et al. (2004b)). One major problem of ABCB1 inhibitors, especially of first and second generation compounds, is the lack of organ specificity. Valspodar, for example, inhibits ABCB1 not only at the BBB but also in liver and kidney leading to altered drug metabolism and excretion, and hence, to an increased systemic toxicity of the co-administered drug. Furthermore, it influences the cytochrome P450 3A4 drug metabolism, which contributes to the enhanced drug toxicity. Third generation inhibitors have only a slight influence on this metabolism. Chemotherapy in combination with third generation modulators should therefore be better tolerated by patients.

In case of the other two ABC transporters mentioned above, ABCC1 and ABCG2, only a few specific inhibitory compounds are known so far. The leukotriene LTD4 receptor antagonist MK571 modulates the ABCC1 mediated drug efflux (Gekeler et al. 1995). The ABCG2 transporter is inhibited specifically by fumitremorgine C (Rabindran et al. 2000). Some ABC transporter compounds show affinity to more than one transport protein. Biricodar blocks both ABCB1 and ABCC1 drug transport (Litman et al. 2001), whereas elacridar affects the transport activity of the ABCB1 and the ABCG2 transporter (Kruijtzer et al. 2002). In contrast, valspodar and zosuquidar are specific inhibitors of the ABCB1 efflux pump (Shepard et al. 2003). The difference between the efficacy of multispecific and single specific ABC transporter inhibitors in chemotherapeutic treatment studies is part of ongoing research (Bardelmeijer et al. 2004, Kemper et al. 2004c).

Another approach to overcome the drug efflux mediated by the ABCB1 transporter is the use of excipients such as pluronic block copolymers. Two mechanisms are suggested to be involved in the interaction with the ABCB1 protein: depletion of cellular ATP and alteration of physicochemical properties of the lipid membrane (Kabanov et al. 2003, Fricker and Miller 2004). Pluronic P85 block copolymer was shown to be at least in part responsible for the increase in opioid peptide analgesia in the mouse brain (Witt et al.

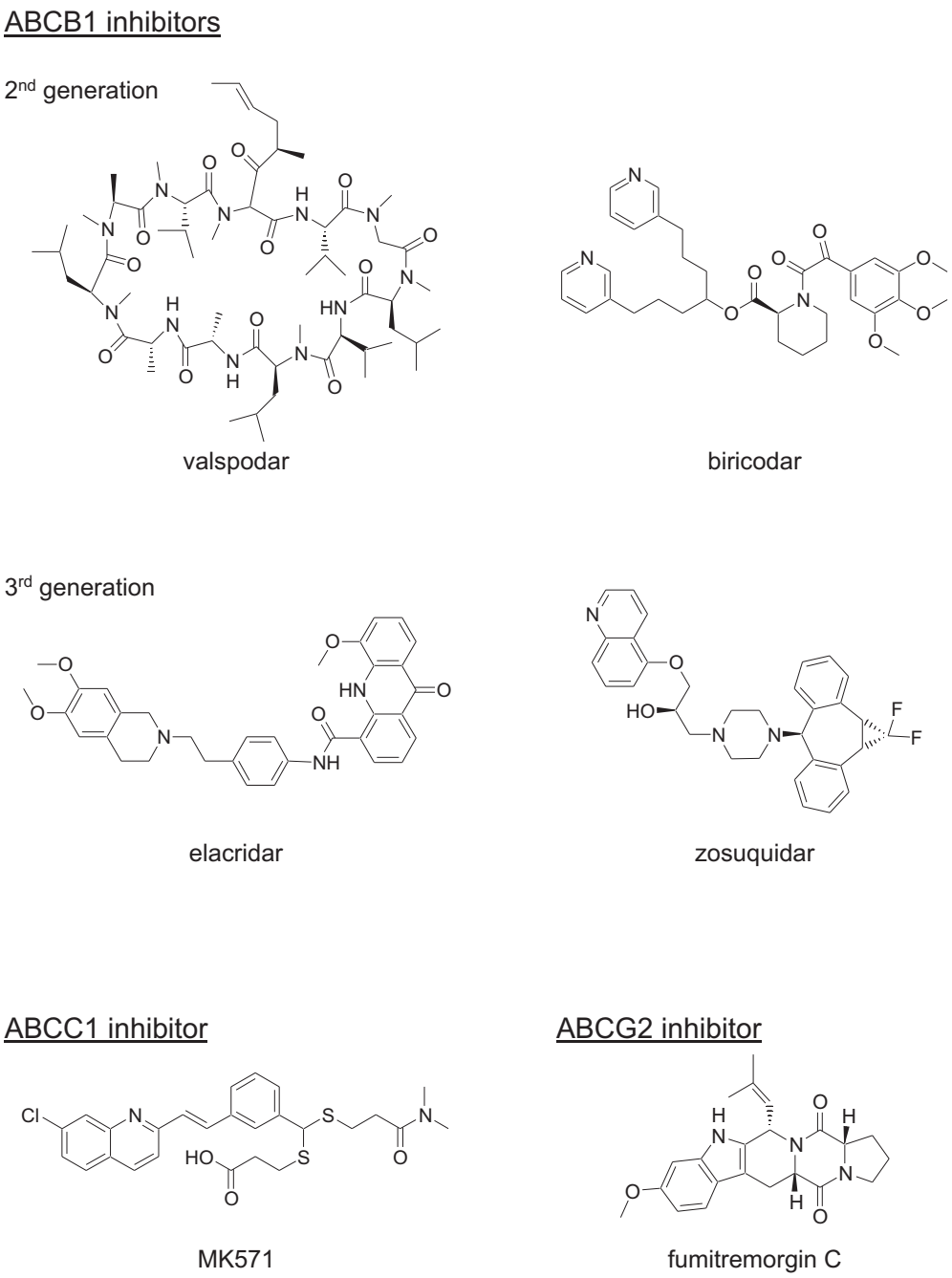

Figure 1.4: Structures of different ABC transporter inhibitors.

2002). However, the inhibition of the ABC transporter mediated efflux that is counted in the self-defense mechanisms of an organism, may lead to an enhanced access to the brain for other toxic substrates resulting in neurotoxic effects. Hence, blockade of these transport mechanisms should only be used for short term treatments.

1.2.7 Liposomes and nanoparticles as carrier systems

The use of liposomes as a drug carrier system to increase brain drug concentrations is a further development of the lipid analog approach. The drug is incorporated in a liposome that is sufficiently lipophilic to cross the BBB. Liposomes have a size of up to 500 nm in diameter and can incorporate large amounts of drug (up to 10,000 molecules). The drug is released from the liposome at the desired tissue by degradation of the liposome. However, to transport drugs into the brain using liposomes, the surface of the liposome has to be modified with brain targeting vectors such as MAbs. Huwyler et al. (2002) demonstrate the specific brain delivery of digoxin incorporated in modified immunoliposomes with the OX26 MAb as brain targeting vector. As digoxin is a substrate of the efflux transporter p-glycoprotein 170 (p-gp), incorporation in an immunoliposome is a possibility of bypassing this efflux mechanism and enhancing brain concentrations of drugs that are normally effluxed from the brain by p-gp. Further modification of the surface with PEG side chains lead to a prolonged half life of the liposomes in the blood stream.

Nanoparticles were developed for the improvement of the stability of liposomes (Benoit et al. 2000). They mostly consist of poly(butyl)cyanoacrylate (PBCA) and are normally 250 nm in diameter, which is a suitable size for intravenous injection. Nanoparticles can be loaded by two different methods: the drug can be incorporated during the initial particle polymerization or it can be absorbed on the nanoparticle surface (Begley 2004). After drug loading, the nanoparticles are coated with Tween 80 (Ramge et al. 2000). The coated particles preferentially absorb the plasma protein ApoE from blood plasma after intravenous injection. With the attached ApoE, the nanoparticles appear to imitate LDL particles and are recognize by LDL-receptors at the BBB, leading to internalization of the nanoparticles (Kreuter et al. 2002; 2003). Using this approach, drugs such as doxorubicin or dalargin are successfully delivered to the brain (Gulyaev et al. 1999, Alyautdin et al. 1995). Moreover, chemotherapy of glioma bearing rats with nanoparticles containing doxorubicin led to 40 % cure (Steiniger et al. 2004). Two requirements for the design of appropriate nanoparticles are deducible from the published experiments. The carrier has to provide long lasting circulation of the particle in the blood stream. Also the surface has to be modified with certain characteristics that enable specific interactions with the targeted cells.

1.2.8 Direct intracerebral delivery

The most obvious way of increasing drug concentrations inside the brain is the direct injection of the drug into the brain or in case of a solid tumor into the brain tumor parenchyma. Several methods including infusion of active agents or implantation of drug loaded polymer wafers are available. The advantages of these techniques are the circumvention of the BBB and the low systemic toxicity. Furthermore, direct intracerebral delivery is the sole method by which 100 % of the administered dose of a drug is delivered to the targeted tissue.

Direct injection into the brain could be done intraventricularly, intrathecally or directly into the brain parenchyma. These highly invasive approaches of brain drug delivery are suitable for the treatment of primary brain tumors at best as these tumors rarely develop systemic metastases. Intraventricular and intrathecal drug injection is performed into the lumbar subarachnoid space or the cerebral ventricles. This kind of intracerebral injection is used for patients with tumors developed at the CSF spaces or adjacent brain regions. Of course, the injection of certain drug volumes damage the brain at least in an extension of the administered volume. Moreover, the distribution of the drug in the brain is hardly predictable due to interstitial pressure gradients, and the convection and diffusion of the drug itself. Although the initial drug concentration is very high at the injection site after the injection, it decreases very fast due to the steady turnover of newly secreted brain extracellular fluid (Cserr and Patlak 1992). Even after intraventricular injection, the drug is carried away by the continuous production of CSF by the choroid plexus (Begley et al. 2000). Hence, the administered drug volume has to be given via long term infusion.

Several infusion systems have been developed, the first in the late 1960s. This system is called Ommaya reservoir (Ratcheson and Ommaya 1968). Here, an inert plastic reservoir is implanted subcutaneously in the scalp and can be refilled by subcutaneous injection of drug solutions. The drug is delivered from the reservoir to the targeted brain tumor region through an outlet catheter by manual compression. Further infusion systems were designed working with different pump mechanisms. The Infusaid pump (Chandler et al. 1988) uses compressed vapor pressure. A solenoid pump is part of the MiniMed PIMS system (Lord et al. 1988) and in case of the Medtronic SynchroMed system (Heruth 1988),

a peristaltic mechanism delivers the drug to the brain tissue. All mentioned infusion systems have successfully shown to provide high intratumoral drug concentrations of certain anticancer agents such as doxorubicin or cisplatin (Walter et al. 1995) with only mild side effects. However, infection and damage of brain parenchyma along the catheter, enhanced neurotoxicity and high discomfort for the patient limit the applicability of brain drug delivery by infusion techniques.

Continuous drug delivery can also be achieved with implanted polymer matrices. Particularly after brain tumor surgery, the remaining space is packed with a drug loaded implant that slowly releases chemotherapeutic agents for the treatment of remaining tumor cells. The implants are based on lipid or polymeric materials such as polyanhydrides that deliver the containing molecules at defined rates for specific periods of time. Also, biodegradable polymeric implants such as the BCNU loaded Gliadel™ are introduced in the chemotherapy of glioma. The use of Gliadel™ resulted in prolonged survival in patients with recurrent glioblastoma multiforma (Brem and Gabikian 2001). Despite this encouraging improvement of brain drug delivery, brain implants are only useful in a very limited number of patients due to diffusion problems. The chemotherapeutic agent that is released by the polymer implant is only effective in the brain parenchyma directly surrounding the implant. Krewson et al. (1995) proved this by examination of the concentration of a nerve growth factor adsorbed on a plastic disk in the rat brain. Even in a distance of 1 mm from the disk the brain concentrations of the nerve growth factor are undetectably low. Furthermore, interstitial therapy with implanted polymers may result in an increased risk of local neurotoxicity. Also, once implanted in the brain, the release of the drug from the matrix can not be controlled and breakdowns of polymer structures followed by a complete release of drug may occur.

1.2.9 Brain drug uptake using the olfactory pathway

An alternative and interesting approach to deliver drugs to the brain is the use of the olfactory pathway (Illum 2002). The intranasal route is based on the fact that olfactory neurons that penetrate the cribriform plate are surrounded by a part of the arachnoid membrane. A fraction of the CSF inside the arachnoid membrane flows into the local

lymphatic system, but an other part of the CSF seems to be recirculated back into the subarachnoid CSF. Compounds that are attached to the olfactory mucosa may be transported via this CSF fraction into the subarachnoid space (Begley and Brightman 2003, Begley 2004). Besides this extraneuronal route, an intraneuronal pathway is postulated by Illum (2003). According to this, the olfactory nerves themselves may carry drugs by the retrograde axonal cytoplasmic flow into the brain. The intranasal approach is a non-invasive and very fast transport way to the brain, as compounds administered to the nose are detected in the brain within a few minutes (Sakane et al. 1991). Various drugs have been transported to the brain using the olfactory pathway including sulfonamides (Sakane et al. 1991) and polypeptides such as insulin and hyaluronidase (Fehm et al. 2000). Lipophilicity of a compound increases the intranasal transport indicating the participation of a transmembrane movement in the drug transport process (Sakane et al. 1991). Further investigations are required to elucidate the exact delivery process. However, it is questionable, if the achieved brain concentrations are sufficient to achieve therapeutic effects.

1.2.10 Alternative routes

Cell penetrating peptides. A relatively new research field regarding drug delivery to the brain is the development of cell penetrating peptides. These peptides seem to wind directly through the cell membrane without damaging the cell, similar to signal peptides. The mechanism of this cell penetration is for the most part unknown. Several hypotheses are described in the literature. According to Torchilin et al. (2001), the peptides initiate the formation of reverse micelles in an energy independent process. In contrast, Richard et al. (2003) suggest, that endocytic events are induced at the plasma membrane similar to the interactions observed at AMT.

Cell penetrating peptides include TAT (transactivating-transduction) peptide that penetrates the nuclear membrane by the process of replication of the HIV virus, and penetratin. They characteristically consist of an amphiphatic α-helix as well as repeating sequences of positively charged and lipophilic amino acids (Begley 1996). Schwarze et al. (1999) demonstrate the transport of biologically active proteins such as the β-galactosidase

protein across the BBB mediated by TAT in the mouse. When doxorubicin is linked to penetratin, the doxorubicin brain concentrations are 3 to 8 times higher compared to doxorubicin alone as shown in a rat in situ brain perfusion model (Rousselle et al. 2000).

Implanted biological tissue as drug distributor. This invasive technique uses the naturally ability of certain tissues to produce the desired therapeutic agent. This tissue is implanted in the brain to provide the required compounds. The success of this approach was shown in the treatment of Parkinson's disease (Madrid et al. 1991). However, a major drawback is the low vascularization of the implanted foreign tissue resulting in a reduced supply with nutrients and consequently in the decay of the transplanted tissue. The survival of the implanted tissue may be improved by co-cultivation of certain cells. Thus, two different types of cells are implanted in the brain, one for the expression of the therapeutic agent and the second for the secretion of tissue stabilizing factors. Since it is difficult to find cells that release appropriate compounds for the therapy of brain diseases, an alternative method was developed. The cells are genetically modified to express specifically active compounds. The success of the genetically modified tissue was demonstrated in the treatment of gliomas (Lal et al. 1994).

1.2.11 Conclusion

The presented approaches to overcome the BBB and enhance intracranial drug concentrations are summarized with respect to their advantages and drawbacks in table 1.2.11.

The variety of the methods listed above reveals the current opinion about the BBB. The BBB is no longer thought to be a static barrier between blood and CNS. In light of the enormous knowledge about the BBB that was collected in recent years, the BBB is considered a highly complex structure with bidirectional transport properties. The barrier function and the activity can be modified by several factors and signals from CNS and the blood.

Nowadays, the research for CNS active drugs as well as the development of brain drug delivery systems is changing away from the mere synthesis of compounds and the direct delivery of drugs irrespective of the applicability in the human body. Using the knowledge from modelling techniques and modern cell biology methods, highly potent CNS active

Table 1.1: Advantages and drawbacks of various invasive and non-invasive approaches for circumvention of the BBB.

Approach	**Advantages**	**Drawbacks**
invasive		
direct intracerebral delivery	bypass of BBB, immediate high drug concentrations; controlled drug delivery	brain damage; neuronal toxicity; restricted to local therapy
non-invasive		
improvement of physicochemical properties	increased lipophilicity leads to enhanced brain uptake	poor aqueous solubility; peripheral distribution; reduced therapeutic activity
prodrug	trapping of active drug inside the brain after transformation of the prodrug	poor selectivity, poor retention; risk of toxic metabolites
chemical drug delivery systems	site specific drug delivery; slow and constant release of active drug at targeted site	oxidative and hydrolytic instability
carrier- and receptor-mediated transport	utilization of endogenous transport pathways; great variety of brain transport vectors	similar structure to natural substrate is needed; attachment of transport vectors alters drug activity
BBB disruption	promising strategy for high grade glioma therapy; selective BBB opening with LTC4 derivatives	unfavorable toxic/therapeutic ratio; breakdown of self-defense mechanism of the brain
modulation of efflux transport proteins	no modification of therapeutic agent; reduced side effects by third generation modulators	opening not specific for therapeutic agent; breakdown of self-defense mechanism
liposomes and nanoparticles	capable for receptor-mediated transport through BBB	modified surface required (vectors, coating) for specific brain delivery

agents may be developed. Furthermore, new or improved drug delivery systems based on immunoliposomes and nanoparticles approaches as well as on RMT pathways, might provide specific transport systems for brain drug delivery and thus, the treatment of brain diseases in the future.

1.3 ABC transporters

ABC transporters were first discovered in tumor cells in the 1970s when Dane demonstrated the active outward transport of daunorubicin in drug resistant Ehrlich ascites tumor cells (Dano 1973). The family of the ABC transporters is widely distributed from bacteria to man (Holland et al. 2003). An ATP binding cassette (ABC) is characteristic for these proteins. They transport a broad variety of compounds including amino acids, peptides, and xenobiotics against a concentration gradient enabled by ATP hydrolysis across biological membranes. ABC transporters are typically composed of two hydrophobic halves, each comprising six transmembrane domains, and two ATP binding domains. The ATP binding domains are also termed as nucleotide binding domains (NBD) and contain four motifs: Walker A, Walker B, Q-loop and H-loop (Higgins 1995, Linton et al. 2003). A diagnostic signature sequence called LSGGQ motif is located between the Walker A and the Walker B region. It is unique for ABC transporters and highly specific for each family. The transport proteins are clustered according to their LSGGQ motif by the human genome nomenclature committee (HUGO) creating the ABC nomenclature (Klein et al. 1999). Table 1.2 provides an overview of three subfamilies of ABC transporters (ABCB, ABCC and ABCG) and their most important members with respect to their localization in the human body, their substrate specificity, and the diseases that are linked to these proteins.

P-glycoprotein 170 (p-gp, ABCB1), MRP1 (ABCC1) and a recently discovered protein, called ABCG2 (MXR, BCRP), are the most important proteins of the three subfamilies regarding the involvement in MDR. They are discussed concerning their predicted structure, their localization, their mode of action and their physiological role.

Structural data of these transport proteins were obtained from single-particle analysis and electron crystallography leading to low-to-medium resolution structures with a resolution of 10 to 25 Å (Rosenberg et al. 1997; 2001a). However, these structures are only estimations. X-ray crystallographic data for a complete ABC transporter exist only for the lipid transporter MsbA both from *Escherichia coli* (Chang and Roth 2001) and from *Vibrio cholera* (Chang 2003), and for the *Escherichia coli* vitamin B_{12} transporter BtuCD (Locher et al. 2002). As these proteins are homologous to the multidrug resistance ABC

Table 1.2: Overview of the most important members of the ABC transporter subfamilies ABCB, ABCC and ABCG.

member	HUGO term	further names	main tissue localization	substrates	linked disease
MDR1	ABCB1	PGY1, p-gp	BBB, adrenal cortex, kidney, liver, placenta, intestine	hydrophobic, amphiphilic drugs, cationic organic compounds	MDR resistance in cancer
MDR3	ABCB4	PGY3, MDR2/ MDR3	liver	phosphatidyl choline	progressive familial intrahepatic cholestasis
MRP1	ABCC1	MRP, GS-X	ubiquitous	organic anions, glutathione conjugates	MDR resistance in cancer
MRP2	ABCC2	COAT	liver, intestine, kidney	similar to MRP1, non-bile salt organic anions	Dubin-Johnson syndrome
MRP3	ABCC3	cMOAT2, MOAT-D, MLP2	intestine, liver, pancreas, kidney	glucuronide bile salts	
MRP4	ABCC4	MOAT-B	prostate, lung pancreas, testis, ovary, intestine	organic anions, nucleoside analogs	
MRP5	ABCC5	SMRP, MOAT-C	ubiquitous	similar to MRP4	
MRP6	ABCC6	ARA, MLP1, MOAT-E	liver, kidney,	anionic peptides	pseudo-xanthoma elasticum
MRP7	ABCC10		liver, heart, kidney	glutathione conjugates	
MXR	ABCG2	BCRP, ABCP	placenta, liver, intestine, BBB, breast	mitoxantrone hydrophobic, amphiphilic drugs	MDR resistance in cancer

transporters these structures are used for the elucidation of transport processes and substrate recognition. Moreover, most research effort was done on p-gp. Therefore, the mode of action and the transport of substrates by ABC transporters are discussed for p-gp.

1.3.1 ABCB1 - P-glycoprotein 170

P-gp was first described by Juliano et al. in 1976, who found that chinese hamster ovary cells selected for resistance to colchicine showed cross resistance to a broad range of drugs (Juliano and Ling 1976). The authors detected a transport protein in the cell membranes of the resistant cells that was not found in wild type cells and named it P-glycoprotein 170. Besides this localization at tumor cell membranes, where p-gp is responsible for the development of multi drug resistance in chemotherapy, p-gp was found in several tissues of the human body. It is expressed at the biliary canalicular membrane of hepatocytes as well as at the brush border membrane of the intestinal epithelium (Thiebaut et al. 1987). In kidney, abundant p-gp is found at the luminal membrane of the proximal tubules. In liver, kidney and intestine, p-gp has excretory and detoxifying functions. Moreover, p-gp is expressed in the brain. It was detected both in the choroid plexus (Rao et al. 1999) and at the BBB (Thiebaut et al. 1989). The precise localization of p-gp at the BBB is a topic of controversy. On the one hand, there is evidence for the expression of p-gp at the luminal membranes of endothelial cells of the brain capillaries. Beaulieu et al. (1997) detected strong enrichment of p-gp by Western blotting in brain capillary luminal membranes, compared with brain capillaries (17-fold) and whole membranes (400-500-fold). On the other hand, other work groups used the MRK-16 MAb against human p-gp for the detection of the transport protein. According to their findings p-gp expression at the BBB is similar to the localization of glial fibrillary acidic protein (GFAP) which is found in astrocytes. Hence, they postulated that p-gp is localized at the astrocyte foot processes (Pardridge et al. 1997). In the meantime several studies have demonstrated that p-gp is co-localized at the astrocytes as well as at the luminal membrane of the endothelial cells (Decleves et al. 2000). However, much more p-gp is expressed at the endothelial cell membrane compared to astrocytes foot processes. Furthermore, the co-cultivation of astrocytes and brain capillary endothelial cells (BCEC) in in vitro models of the BBB led to an increased p-gp expression compared to BCEC monolayer models indicating an important role of the astrocytes regarding the expression of p-gp (Gaillard et al. 2000). Due to the localization of p-gp at the endothelial membrane of the capillaries the role of p-gp is the protection of the brain from foreign and toxic compounds.

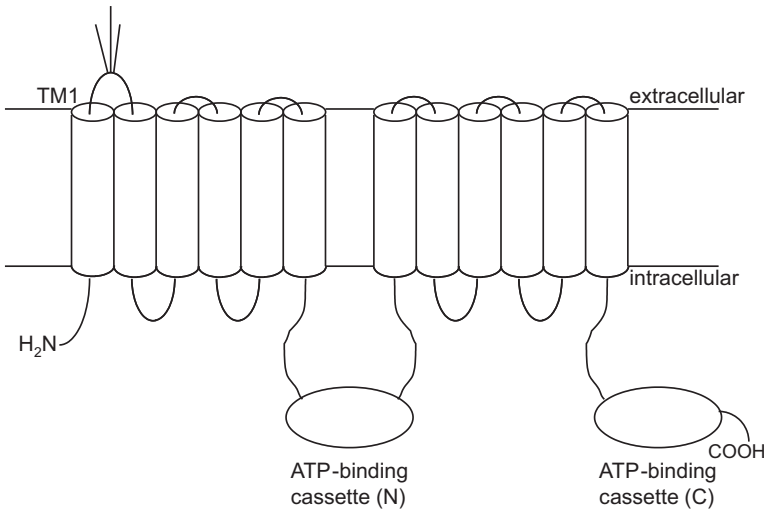

Figure 1.5: Predicted membrane topology of human p-gp. The ABC transport protein p-gp is thought to be organized in two hydrophobic halves, each half consisting of six TMDs and one cytoplasmic ATP-binding domain (NBD). The protein is glycosylated at three sites on the first extracellular loop.

A model for the predicted structure of p-gp is presented in Fig. 1.5. P-gp is a 170 kDa transmembrane protein that is encoded by the MDR1 gene. This gene consists of 27 exons distributed over 100 kb and is located on the long arm of chromosome 7 (Fardel et al. 1996). The human p-gp is composed of 1280 amino acids. They are organized in two halves each containing 610 amino acids in 6 hydrophobic transmembrane domains (TMD) and one hydrophilic NBD. The protein is N-glycosylated on the first extracellular loop in three different locations. This glycosylation appears to be necessary for the effectiveness of the protein (Ramakrishnan 2003). The TMDs play an important role for the substrate recognition as single mutations in all transmembrane regions affect the transport function of the protein either directly through alteration of the binding site or by interference in the conformational changes (Litman et al. 2001). Therefore, the binding sites are broad interaction regions. Using photoaffinity labelling studies and epitope mapping with iodomycin (Demmer et al. 1997) two major regions were identified within the TMDs: TMD 5 and 6 in the N-terminal half, and TMD 11 and 12 in the C-terminal half. However, there are much more interaction points between substrates and amino acids. These are particularly localized at TMD 4 and 10 and have been discovered by means of cysteine scanning mutagenesis of all TMDs combined with thiol modification (Loo and Clarke 2000; 2001, Van Veem and Callaghan 2003). Within these TMDs, specific amino acids

are responsible for substrate recognition. For example, charged substrates are able to interact with the π face of aromatic residues in tyrosine, phenylalanine and tryptophan. This binding is as strong as electrostatic interactions between ion pairs (Dougherty 1996, Kwan et al. 2000). Until now, at least four binding sites are identified by several work groups (Martin et al. 2000, Ekins et al. 2002, Wang et al. 2003). These binding sites are in part transport sites, but regulatory sites also exist. Both site types appear to switch between high and low affinity conformations (Martin et al. 2000).

In contrast to the TMDs, the NBDs are not integrated in the process of substrate recognition. NBDs are involved in the transport mechanism of ABC transporters. Liu and Sharom (1996) demonstrated by 2-(4-maleimidoanilino)naphthalene-6-sulfonic acid (MIANS) labelling of cysteine residues located within the Walker A motif of the NBD that the NBDs change their positions relative to the cell membrane in the presence of p-gp substrates. MIANS is fluorescent in an aqueous environment, but in lipophilic solutions the fluorescence is quenched. Therefore, the quenching of the MIANS fluorescence during the efflux process indicates conformational changes of the transporter including the NBDs. These changes can be seen directly by cryo-electron microscopy of p-gp trapped in different stages of the transport cycle (Rosenberg et al. 2001b). The energy for these changes which are essential for the releasing of a compound, is provided by hydrolysis of ATP at the NBDs. The binding and hydrolysis of ATP are crucial steps in the transport process, which can be divided in four steps (see Fig. 1.6). First, the substrate has to be recognized and bound by p-gp. ATP binds to one NBD in this first step. In the second step, ATP hydrolysis at the NBD leads to the aforementioned conformational changes. The affinity of the binding site is switched to the low affinity status and the drug binding site is oriented to the extracellular site to release the substrate. Uptake of a second ATP molecule in the third step results in a further conformational change at the NBD, whereas the drug binding site remains in the low affinity status. In the last step after hydrolysis of the second ATP molecule the protein returns to the original conformation with high affinity status of the binding site to recognize a new substrate. ATP hydrolysis takes place during the second and the fourth step. To supply the energy for the conformational changes of the TMDs, the NBDs have to be in contact with the TMDs. This exchange takes places via the intracellular loops (Van Veem and Callaghan 2003).

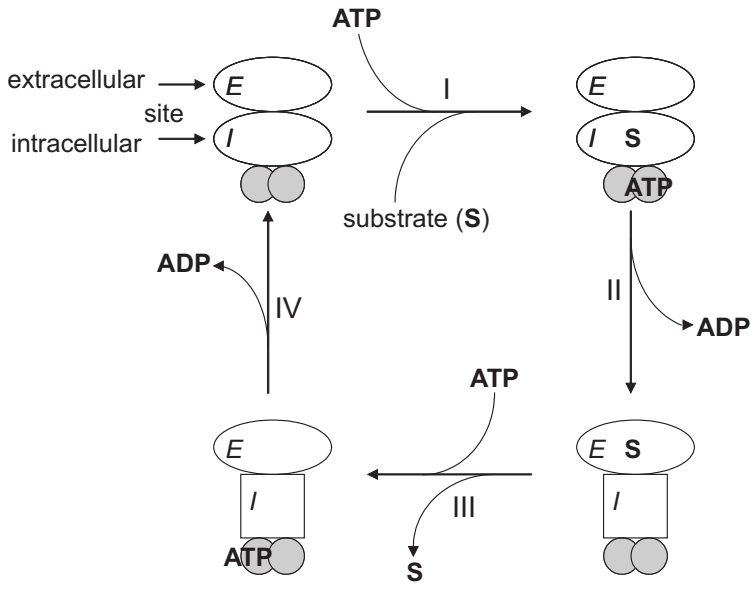

Figure 1.6: Proposed mechanism of p-gp function. The ellipses represent the substrate-binding face of the protein, the extra- and the intracellular location. The square describes the intracellular site with reduced affinity. The NBDs are represented by two overlapping circles indicating that both sites are required for ATP hydrolysis (according to Druley et al. (2001), Sauna and Ambudkar (2001)).

It is important to note that both NBDs are required for the efflux process. For a complete transport cycle, both NBDs have to be activated by the binding of ATP, but it is indifferent which NBD binds to ATP first. Sauna and Ambudkar (2000) proved this by investigation of the affinity of [I^{125}]iodoarylazidoprazosin for p-gp in the presence of the nonhydrolyzable nucleotide 5'-adenylylimidodiphosphate and vanadate, as well as for p-gp that is trapped in transition-state conformation by ADP and vanadate. The affinity is clearly reduced ($>$ 30-fold) to low affinity state if p-gp is trapped, whereas it is not influenced by the nonhydrolyzable compounds. Furthermore, they found an inverse correlation between ADP release and the recovery of substrate binding. Therefore, Sauna et al. summarized that one ATP molecule is necessary for the efflux of a bound substrate resulting in the aforementioned change to the low affinity status. In addition, a second ATP molecule is required to reset the status of the binding sites to the high affinity conformation in order to prepare the next catalytic cycle.

Three different models are described in the literature concerning the mechanism of transport at the multiple drug binding sites of ABC transporters. The "altering ac-

cess/single site model" (Bruggemann et al. 1992, Martin et al. 2000) suggests that the sites are localized within a single binding region which is alternately oriented to the extracellular or to the intracellular site. Dey et al. (1997) postulated in the "fixed two side model" the existence of two static binding regions. The high affinity "on"-site is located in the C-terminal half of the protein, whereas the low affinity "off"-site is found in the N-terminal half. The bound substrate moves from the "on" to the "off" site during the first ATP hydrolysis. This model agrees well with the process of ATP hydrolysis described by Sauna and Ambudkar (2000) mentioned above. Furthermore, the "altering two-site (two-cylinder engine) model" is a combination of the aforementioned models; two distinct binding regions are alternately exposed to the inner and outer membrane. Here, ATP hydrolysis leads to simultaneous or sequential movement of the two regions (van Veen et al. 2000). The differences between the three models may be related to the different localization of the substrate binding sites.

The establishment of a complete transport model is difficult since many factors that influence the transport function both directly and indirectly have to be taken into account. These factors include conformational changes, the existence of multiple binding sites, the role of NBDs, as well as the variable effects of p-gp inhibitors (Litman et al. 2001). Nowadays, there is more knowledge about the number of binding sites, their interactions among each other, and various pharmacophores of substrates. However, only little research is focused on the reactions of the protein caused by substrate binding which is important for the design of new modulators and for the development of agents with low p-gp affinity.

1.3.2 ABCC1 - MRP1

MRP1 is a member of the largest subfamily of the ABC transporters. It was discovered in HL60/ADR cells which did not overexpress p-gp, but showed a MDR phenotype (McGrath and Center 1987). The resistance was attributed to a 190 kDa protein and was classified in the family of the ABC transporters due to its immunoreactivity with peptide antisera directed at the conserved NBD of p-gp (Marquardt et al. 1990). The cDNA of the new transport protein was isolated in 1992 by Cole et al. in the MDR resistant

doxorubicin-selected human lung cancer cell line H69AR and was then designated as multidrug resistance-associated protein (Cole et al. 1992). In addition to the expression at the cell membrane of tumor cells, MRP1 is localized at the basolateral membrane of epithelial cells in all tissues in the human body (Ambudkar et al. 2003). It is also expressed at the BBB together with MRP3 and MRP5 (Bart et al. 2000). However, MRP1 has only 15 % homology to p-gp, but a higher relation to the cystic fibrosis transmembrane regulator gene (CFTR). Also, within the MRP subfamily the sequence identity of MRP1 compared to MRP2-6 ranges between 35 and 58 %, although the overall membrane topology appears to be similar in this subfamily (Litman et al. 2001).

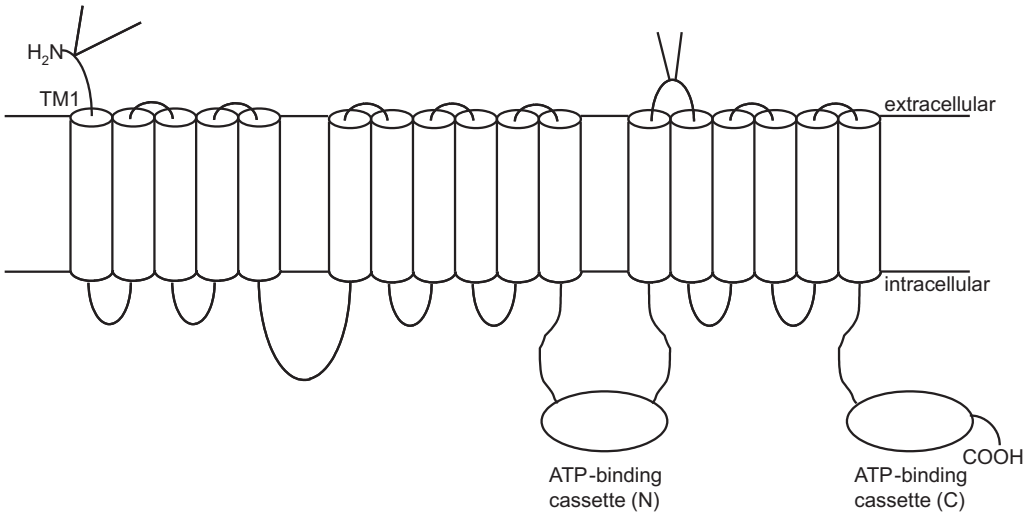

Figure 1.7: Predicted structure model of the ABC transport protein MRP1. The protein consists of 17 transmembrane domains that are organized in three groups. The orientation of the two NBDs and the TMD 6 to 17 is similar to p-gp. Compared to the p-gp structure five TMDs (1-5) are added resulting in an extracellular N-terminus.

The predicted structure of MRP1 consists of 1531 amino acids and 17 TMDs. These are divided into three membrane spanning domains (MSD) in the following organization: MSD1 (5 TMDs), MSD2 (6 TMDs), NBD1, MSD3 (6 TMDs), NBD2 (see Fig. 1.7). The structure of MSD2 and MSD3 together with the NBDs is similar to p-gp. The additional 5 TMDs are attached to the N-terminus of this p-gp similar structure by a linker region that seems to be necessary for the MRP1 mediated transport of organic anions (Bakos et al. 1998). Hence, in contrast to p-gp, the N-terminus of MRP1 is oriented to the extracellular site. MRP1 transports hydrophobic anions and drugs that are conjugated

to glutathione, glucuronic acid or sulfate as well as exogenous compounds. MRP1 is one of the best characterized proteins of this subfamily regarding its physiological role. In tumor cells it is involved in the development of MDR. Due to its expression in liver, kidney and at the BBB it is part of the self defense system of the human body against toxic xenobiotics, particularly against anthracyclins, epipodophyllotoxins, vinca alkaloids and camptothecins. These compounds are also substrates of p-gp, indicating a large overlap of the resistance profiles of these transport proteins. Exceptions from this overlap are taxanes which are specific substrates of p-gp. Glutathione and glucuronate conjugates are products of the phase II metabolism. The role of MRP1 as an efflux pump which is responsible for the cellular extrusion of these conjugates in phase II underlines the MRP1 function as a cellular detoxifying factor (Kruh and Belinsky 2003). P-gp transports exogenous compounds to the bile and intestine for elimination out of the body due to its luminal localization. In contrast, MRP1 is expressed at the basolateral membrane resulting in the transport into tissues beneath the basement membrane. Recently, a further key function of MRP1 was discovered by Wijnholds et al. (1997). As mice lacking MRP1 show a decreased inflammatory response and leukotriene C4 is a MRP1 substrate, MRP1 may play a major role in the leukotriene depending inflammatory response.

The clinical relevance of MRP1 mediated efflux in cancer chemotherapy has not been determined yet due to the broad variety of resistance factors that are found in tumor cells and tissues with barrier functions in the human body (Kruh and Belinsky 2003). The lack of specific MRP1 inhibitors contributes to this issue. Development of such inhibitors and their application to clinical studies may help to elucidate the importance of MRP1 in MDR.

1.3.3 ABCG2 - BCRP

ABCG2 belongs to the "white subfamily" that is named after the white ABC transporter gene in Drosophila melanogaster. This protein was discovered by three different work groups in the late 1990s. Doyle et al. (1998) detected cross resistance to other anthracyclins than doxorubicin in multidrug-resistant human breast cancer MCF-7/AdrVp cells. They postulated the existence of another efflux pump as the cells did not overexpress

p-gp or MRP1 and contributed the observed resistance to a certain gene that was subsequently designated as breast cancer resistance protein (BCRP) gene. At the same time this gene was cloned from human DNA sequences by searching for novel human ABC transporter (Allikmets et al. 1998). Since the identified sequence is highly expressed in placenta, the gene was named ABCP (ABC transporter highly expressed in placenta). Also, a third work group was able to clone this gene from mitoxantrone-resistant S1-M1-80 human colon carcinoma cells which lack the overexpression of p-gp and MRP1 (Miyake et al. 1999). Due to the used anticancer drug for resistance, Miyake et al. called the gene mitoxantrone resistance (MXR). In the following, the transport protein is designated as ABGC2 according to the HUGO nomenclature.

ABCG2 is frequently observed in plasma membranes of tumor cells especially breast, colon, gastric, lung and ovarian cancer cells (Maliepaard et al. 1999, Ross et al. 1999, Litman et al. 2000). Inside the human body, the protein is found with the highest expression levels in placenta and at lower levels in breast, liver, intestines, prostate and at the BBB (Litman et al. 2001). The physiological role of ABCG2 is similar to that of p-gp and MRP1. Due to its detection in multidrug resistant tumor cells, a part of the low response rate to chemotherapy is attributable to this protein. ABCG2 plays an important role in the natural defense mechanism against xenobiotic compounds because it is expressed in tissues that are involved in excretion processes or have certain barrier functions like liver, placenta and BBB (Cooray et al. 2002). The localization of ABCG2 in stem cells again shows a protective function of this protein (Zhou et al. 2002).

ABCG2 is a 72 kDa half ABC transporter that consists of 655 amino acids. In contrast to full length ABC transporters of other subfamilies, the domain orientation is reversed. ABCG2 has one NBD located at the N-terminal site followed by six TMDs at the C-terminal site (see Fig. 1.8). The largest extracellular loop is located between TMD 5 and TMD 6 and is therefore a potential target for antibody recognition (Han and Zhang 2004). The protein is heavily glycosylated. However, in contrast to p-gp, the glycosylation has no influence on the transport function of ABCG2 since recombinant ABCG2 generated in insect and bacterial cell is functional although it is unglycosylated (Janvilisri et al. 2003). In some cell lines expressing ABCG2 after selection with various anticancer drugs, different substrate specificities were observed particularly concerning the transport of the

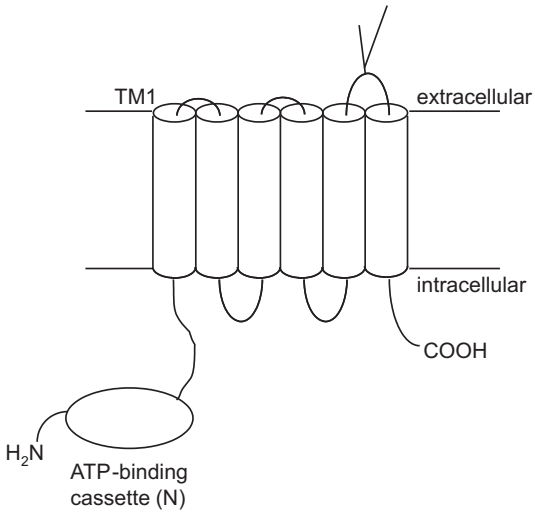

Figure 1.8: Predicted membrane orientation of TMDs of human ABCG2. This half transporter consists of six TMDs and one NBD. In contrast to the other ABC transporters, the NBD is at the N-terminal end of ABCG2 leading to a reverse orientation of the protein. ABCG2 is thought to act as a homodimer.

fluorescent dye rhodamine 123. This finding led to the detection of the mutation hot spot Arg^{482} which is located at the start of TMD 3 and significantly affects the transport profile of ABCG2 (Honjo et al. 2001). If this amino acid is replaced with glycine, threonine, methionine or serine, the cells show higher resistance to anthracyclins, relatively lower resistance to topotecan, and an enhanced efflux of rhodamine 123 (Han and Zhang 2004). Honjo et al. (2001) suggested that the exchange of the amino acid at position 482 results in an altered position of the TMD 3.

As ABCG2 is a half transporter, it must have a dimerization partner to fully achieve effectiveness. There are several studies indicating that ABCG2 works as a homodimer (Kage et al. 2002, Janvilisri et al. 2003). Janvilisri et al. expressed human ABCG2 in the gram-positive bacterium *Lactococcus lactis* and were able to generate a functional transport protein that could be inhibited by the potent ABCG2 specific modulator fumitremorgine C. Therefore, the human protein has to function by itself inside the bacterium. Litman et al. (2002) used immunoblot analysis performed after treatment with cross-linking reagents to demonstrate a molecular mass shift from 72 kDa to several bands of 180 kDa and higher molecular mass. They postulated from these results that higher forms of oligomerization may exist. Also, the possibility of the formation of heterodimers

can not be excluded. This may also be possible with other members of the subfamily such as ABCG1, a protein that is mostly expressed in lung, placenta and liver (Han and Zhang 2004).

The clinical relevance of ABCG2 in cancer chemotherapy was proven in studies by temporal inhibition of the ABCG2 function in patients in order to increase the availability of orally administered anticancer drugs (Malingre et al. 2001). However, these studies were conducted with the nonspecific modulator elacridar. Hence, development of new and specific ABCG2 inhibitors may lead to an improvement of cancer chemotherapy regarding higher bioavailabilities of anticancer drugs as well as the overcoming of MDR caused by ABCG2. The elucidation of the drug binding sites and the dimerization domain will be necessary for a more precise understanding of the function of the ABCG2 transporter.

Chapter 2

Objectives

Up to now, the therapy of primary and secondary brain tumors still remains a major problem in cancer chemotherapy. Although surgery and radiotherapy are becoming even more effective and precise, cancer treatment with chemotherapeutic agents offers interesting therapeutic approaches with a broad range of applications concerning brain drug delivery (see introduction). However, an important obstacle in brain cancer chemotherapy is the BBB, limiting the brain access of several highly potent anticancer drugs such as paclitaxel or vinblastine by efflux transport proteins such as the P-glycoprotein 170 (p-gp). Very recently successful treatment studies on glioblastoma multiforma were done by Fellner (2001) with a combination of the cytostatic agent paclitaxel and the p-gp inhibitor valspodar. In continuation of these investigations, the main goal of this thesis was the further development of this treatment strategy, particularly with respect to secondary brain tumors from different lung cancer types due to the higher incidence of lung carcinomas compared to primary brain tumors, and newly developed p-gp inhibitors.

Lung cancer cell lines had to be characterized in view of the establishment of tumor models in animals. The examinations comprise the determination of cell proliferation characteristics and chemosensitivity of the lung cancer cell lines against several cytostatic agents (see chapter 3).

To determine the potency of p-gp inhibitors and the p-gp activity of cells, a fluorescence assay based on calcein-AM can be used. The establishment of this assay system is part of preliminary investigations of this thesis (see chapter 4).

The lung cancer cells had to be investigated with respect to their suitability for sim-

ulating brain metastases in nude mice. Subsequently, the aforementioned combinatory approach should be applied to the resulting tumor models using the well established p-gp inhibitor valspodar and appropriate anticancer drugs due to the chemosensitivity determined in the first part of the project (see chapter 5).

Recently, new p-gp inhibitors were developed, designated as elacridar and tariquidar, which are described as more selective for p-gp at the BBB and should lead to better tolerated treatment in combination with anticancer drugs. The two compounds had to be characterized in vitro with respect to their p-gp inhibition activity and their selectivity for other efflux transporters and had to be compared to valspodar (see chapter 6). In case of higher potency of the two new modulators regarding the inhibition of p-gp activity in vitro, the ability of elacridar and tariquidar to block p-gp at the BBB resulting in higher cytostatic drug concentrations in the brain should be examined in comparison to valspodar in order to get information about a possible improvement of the therapy by a combination treatment with the new modulators (see chapter 7).

In addition to the investigation of the inhibition of efflux transporters at the BBB, another part of the thesis was concerned with the transferrin receptor mediated transcytosis at the BBB as a method to increase intracerebral drug concentrations. For this purpose, a model of primary brain tumors in nude rats had to be established that should enable treatment studies with immunoliposomes targeted to the transferrin receptor both at the BBB and in tumor cells (see chapter 8).

Chapter 3

Characterization of human lung cancer cell lines

3.1 Introduction

Malignant tumors of the lung were the most common form of cancer and the most common cause of cancer death in the world in the year 2000 in the male population according to the WHO (Globocan 2000). These tumors are subdivided into two classes, the small cell lung cancers (SCLC) and the non-small cell lung cancers (N-SCLC) comprising adenocarcinoma, squamous cell carcinoma and large cell carcinoma (Travis et al. 1999, Mitsuuchi and Testa 2002). N-SCLC, which amounts to 80 % of the cases includes various histological subtypes depending on the origin in the lung, whereas SCLC is relatively undifferentiated. The latter tumors, except for the bronchial carcinoids, a rare form of SCLC, are characterized by a rapid growth, the ability to metastasize early and the expression of neuroendocrine markers, e.g. adrenocorticotropin (ACTH), bombesin and calcitonin (Hay et al. 1994). The prognosis to recover from lung cancer, irrespective of histological classification, is very poor as the 5 year survival amounts to 15 % (Van Houtte and Albain 1999). Nowadays the therapy of lung cancer is based on three modalities of treatment: surgery, radiation and chemotherapy.

For chemotherapy various cytostatic drugs, e.g. cisplatin and vinorelbin for the treatment of advanced N-SCLC (Wozniak et al. 1998), are combined and radiation is often

added to polychemotherapy (Eberhardt et al. 1998). However, combination therapies often prolong the patient's life for several months only. The tendency of the tumor to metastasize to the brain is another problem of the therapy as 50 % of all brain metastases derive from lung cancer (Staab and Drlicek 1988). The treatment of these brain metastases is additionally hampered because many cytostatic drugs are substrates of the P-glycoprotein (p-gp), an efflux pump located in the blood-brain barrier, and thus cannot reach the brain and the brain metastases. To solve this problem Fellner et al. (2002) investigated the treatment of nude mice bearing human brain tumors by co-application of the cytostatic paclitaxel, a p-gp substrate, with the p-gp inhibitor valspodar. By this combination the paclitaxel level in the mouse brain was significantly increased and the tumor volume was reduced by 90 % (for details see chapter 5). Stimulated by these results human lung cancer cell lines were selected to investigate the application of the aforementioned combination therapy to the treatment of secondary brain tumors. First of all the cell lines were characterized with regard to their in vitro and in vivo morphology, their growth characteristics and their chemosensitivity to select cell lines which are representative for the broad variety of lung tumors.

3.2 Materials and methods

3.2.1 Drugs and chemicals

Cisplatin, doxorubicin, etoposide, paclitaxel and vinblastine were purchased from Sigma (München, Germany). Docetaxel (Taxotere®) was obtained from Aventis (Bad Soden, Germany), topotecan (Hycamtin®) from GlaxoSmithKline (München, Germany), vincristine (Vincristine 1mg/ml®) from Rhone-Poulenc (Strasbourg, France) and vinorelbin (Navelbine®) from Pierre Fabre Pharma (Freiburg, Germany). Stock solutions of all drugs were prepared in 70 % ethanol with exception of cisplatin (DMSO), docetaxel (pure ethanol) and vinorelbin (sterile deionized water). The stock solutions of topotecan and vinorelbin were stored at 4 °C, all other stock solutions were stored at -80 °C. Fetal calf serum (FCS) was obtained from Biochrom. All other chemicals and reagents were procured either from Merck or from Serva. Water was de-ionized by Milli Q wa-

ter system (Millipore). Phosphate buffered saline (PBS) contained 8.0 g/l NaCl, 1.0 g/l $Na_2HPO_4x2H_2O$, 0.2 g/l KCl, 0.2 g/l KH_2PO_4 and 0.15 g/l $NaH_2PO_4xH_2O$. Bouin's solution consisted of 300 ml of aqueous saturated picric acid, 100 ml of formaldehyde and 20 ml of glacial acetic acid.

3.2.2 Culture conditions

Lung cancer cell lines were obtained from the ATCC (Rockville, USA). The tumor cells were cultured as "monolayer cultures" in 75 cm^2 flasks (Nunc, Wiesbaden, Germany). The cell cultures were maintained at 37 °C/5 % CO_2 in different culture media. For the NCI-H460 cell line RPMI 1640 culture medium (Sigma) was used containing 10 mM HEPES, 1 mM sodium pyruvate, 2.5 g/l glucose, 1.5 g/l sodium hydrogen carbonate and 10 % FCS. The small cell lung cancer cell lines DMS 53, DMS 114 and DMS 153 were cultivated first in Waymouth's MB 752/1 culture medium (Sigma, München, Germany) supplemented with 2.24 g/l sodium hydrogen carbonate and 10 % FCS, and then adapted to EMEM culture medium (Sigma, München, Germany) supplemented with 110 mg/l sodium pyruvate, 2.2 g/l sodium hydrogen carbonate and 5 % FCS. All culture media were adjusted to pH 7.4. Subculturing was carried out with 0.2 % trypsin/EDTA (Viralex, Paa Laboratories, Pasching, Austria) in PBS once a week. Mycoplasm contamination was monitored by a mycoplasma PCR detection kit (Venor Dem, Minerva Labs, Worcester, USA) periodically. A tumor bank according to the seed stock concept (Hay 1988) was created to have suitable cell material available at any time. For that purpose, the cells were expanded in lower passages and frozen in culture medium with an addition of 10 % DMSO in an ampule for storage in liquid nitrogen. To thaw a sample the ampule was put into water (40 °C) and afterwards, the cells were cultivated in the appropriate culture medium.

3.2.3 Cytological and histological staining

For cytological staining cells were cultivated on microscopic slides that were prepared in accordance to the chromosome preparation. The cells were fixed for 30 min with Carnoy's solution (ethanol:chloroform:glacial acetic acid 6:3:1) and stained by the method

of Papanicolaou (Takahashi 1987). Harris' haematoxylin, orange G6 and eosin azure 31 were utilized as dye reagents to stain plasma turquoise, nuclei blue and nucleoli deep blue. For histological sections of the tumor tissue NMRI(nu/nu) nude mice with subcutaneous solid tumors were killed, and the tumor and part of the dermal tissue were removed and fixed for at least three days in Bouin's solution. The tissues were embedded in paraffin by a standard procedure in a Histokinette (Shandon, Frankfurt/Main, Germany), cut by a Microtome Leitz 1516 (Leitz, Wetzlar, Germany) in sections with a thickness of 6 μm and put on object slides prepared with poly-L-lysin. Prior to each staining procedure the sections were deparaffinized with xylol and various ethanol solutions with descending concentrations. For the haematoxylin-eosin (HE) staining the method described elsewhere (Romeis 1989) was used with Mayer's haematoxylin and eosin. With these dye reagents the nuclei appear blue, whereas the rest of the section is stained pink or red. The Masson-Goldner (MG) staining was also carried out according to Romeis in consideration of the modification of Jerusalem. Here, Weigert's haematoxylin, acid fuchsin-ponceau, orange G and light green were used to stain nuclei violet, erythrocytes red and connective tissue green. All stained sections were evaluated with a BH2 microscope (Olympus, Hamburg, Germany) mounted with a CCD-camera for digital imaging.

3.2.4 In vitro growth determination

For the in vitro growth characterization the lung cancer cells were cultured in 96 well (100 μl/well) flat-bottomed microtitration plates (Greiner, Frickenhausen, Germany) at an appropriate density of 10 to 20 cells per microscopic field (320x, Diavert microscope, Leitz, Wetzlar, Germany) depending on the cell line. After an incubation at 37 ℃/5 % CO_2 for 24 h another 100 μl/well culture medium were added. Cell growth was stopped at various periods of incubation time and the cell density was determined by a crystal violet staining as described in chapter 3.2.6. The absorbance of the cells was measured by a BioTek EL 309 Autoreader (Bad Friedrichshall, Germany) and the average and standard deviation values were calculated. Absorbance values outside of the confidence interval (95 %) were not considered for the calculation. The incubation time was plotted against the absorbance. The doubling time was computed using a computer analysis program (Reile et al. 1990) and plotted against the incubation time.

3.2.5 Metaphase chromosomes preparation

Metaphase chromosomes of the tumor cell lines were prepared by the following procedure. Microscopic slides were prepared according to the method of Rooney and Czepulkowski (1986). For that purpose the slides were degreased for 24 h in ethanol hydrochloric acid (6 ml of concentrated hydrochloric acid in 200 ml 70 % ethanol), rinsed with de-ionized water and dried. Before culturing the cells the slides were autoclaved. Cells were cultured on the prepared slides in Quadriperm 4-well lux-multiplates up to a confluence of 50 %. Metaphase cells were arrested with colcemide (0.04 mg/ml). After an incubation time of 3 h at 37 ℃/5 % CO_2, the culture medium was removed by suction and replaced with 37 ℃ warm hypotonic potassium chloride solution (75 mM) for 30 min to lyse the cells. Afterwards, an equal volume of icecold fixative (methanol/glacial acetic acid 3:1) was added and removed at once. This step was repeated twice and after the last fixation the slides were stored at 4 ℃ for 10 min. The fixative was removed and the slides were dried. Chromosomes were stained with a Giemsa dye solution (10 ml filtered Giemsa solution + 90 ml 0.025 M KH_2PO_4 , pH 6.8) for 8 min. After washing and drying the slides were mounted with DePex. The chromosome numbers were determined by an Olympus BH-2 microscope (Olympus, Hamburg, Germany) with 60x and 100x SPlanApo oil immersion objective. For each cell line 50 metaphases were counted. In addition, digital imaging was performed by means of an Axiovent 200 M microscope (Zeiss, Jena, Germany) and LSM 510 imaging software.

3.2.6 Chemosensitivity assay

The chemosensitivity of the tumor cells was quantified by the crystal violet assay described elsewhere (Bernhardt et al. 1992, Reile et al. 1990). In brief: tumor cells were seeded (100 μl/well) in 96 well flat-bottomed microtitration plates (Nunc, Wiesbaden, Germany) at an appropriate density of 10 to 20 cells per microscopic field (320x, Diavert microscope, Leitz, Wetzlar, Germany) depending on the cell line. After incubation at 37 ℃/5 % CO_2 for 48 h to 72 h according to the cell growth characteristics, the medium was carefully removed by suction and replaced with fresh medium (200 μl/well) containing either drug or pure solvent. The drug solutions were diluted 1:1,000 with culture medium. In 16

wells on every plate culture medium with vehicle was given, so that these wells served as control. For every drug concentration 16 wells were used. After various periods of incubation at 37 ℃/5 % CO_2 the culture medium was shaken off and the cells were fixed with 100 μl 1 % glutardialdehyde in PBS per well for 30 min. The fixative was replaced by 180 μl PBS per well, and the plates were stored at 4 ℃. At the end of the experiment the cells were simultaneously stained with 100 μl of 0.02 % crystal violet solution (N-hexamethylpararosanilin · HCl in water) per well for 20 min. To remove excess dye the plates were rinsed with demineralized water for 20 min and dried. The stain bound by the cells was redissolved in 70 % ethanol (180 μl/well) while shaking the microplates for about 3 h on a Köttermann 4010 shaker. Absorbance was measured at 578 nm using a BioTek EL 309 Autoreader (Bad Friedrichshall, Germany) and the average and standard deviation values were calculated. Absorbance values outside of the confidence interval (95 %) were not considered for the calculations. The drug effects were expressed as corrected T/C values according to

$$T/C_{corr.}[\%] = \frac{T - C_0}{C - C_0} \cdot 100\%$$

where T is the mean absorbance of the treated cells, C the mean absorbance of the control and C_0 the mean absorbance of the cells at the time when the drug was added (t=0). When the absorbance of the treated cells T is less than that of the culture at t=0 (C_0) the extent of cell killing must be calculated as

$$\text{cytocidal effect}[\%] = \frac{T - C_0}{C_0} \cdot 100\%$$

3.2.7 In vivo experiments

For the characterization of the in vivo growth of the lung cancer cells NMRI(nu/nu) nude mice obtained from the nude mice laboratory of the department were used. The mice were allowed to take water and food, a combined breed and maintenance nutrition (Altromin), ad libitum. The water was supplemented with 1.33 g/l of potassium sorbate, 2 g/l of chloramphenicol and 1 g/l of hydrochloric acid leading in a pH value of 2.5. The animals were housed under specific pathogen free conditions at a 12 h light/dark cycle at a

temperature of 25 ℃ and a relative humidity of 70 %. At an age of 6 weeks the mice were used for studies. For the subcutaneous injection cell suspensions of the corresponding cells were prepared in vitro. Cells were detached from the culture flask with trypsin/EDTA and FCS free medium and washed twice with FCS free medium. To adjust the appropriate cell quantity (2 mill. cells/100 μl in case of the NCI-H460 cell line and 4 mill. cells/100 μl for DMS 53 and DMS 114 cell lines, respectively) cells were resuspended in FCS free medium. Under aseptic conditions 100 μl of the cell suspensions were injected under the thoracic dermis. To maintain the subcutaneous tumors in the mice the solid tumor was excised when the tumor growth reached an area of about 150 mm^2. Pieces of 2 mm^3 were prepared in sterile PBS and transplanted into new mice. The NCI-H460 tumor was grafted every three weeks whereas the other tumors were transplanted at an average period of seven weeks.

3.3 Results

The selected four lung cancer cell lines NCI-H460 (N-SCLC), DMS 53, DMS 114 and DMS 153 (all SCLC) were examined with respect to their suitability for establishing a lung cancer tumor model. The tumor cell lines were obtained from the American Type Culture Collection (ATCC) and characterized with respect to their in vitro and in vivo morphology and growth as well as their chemosensitivity against various cytostatic drugs.

3.3.1 Origin and morphology of selected lung cancer cell lines

The large cell carcinoma cell line NCI-H460 (ATCC HTB 177) was isolated by A.F. Gadzar et al. from the pleural fluid of a male patient with large cell carcinoma in 1982 prior to therapy. NCI-H460 cells were obtained in the 140^{th} passage and grew as a monolayer culture with epithelial morphology and easily distinguishable cells. When cultured in flasks over 5 days multilayered cell clusters were observed.

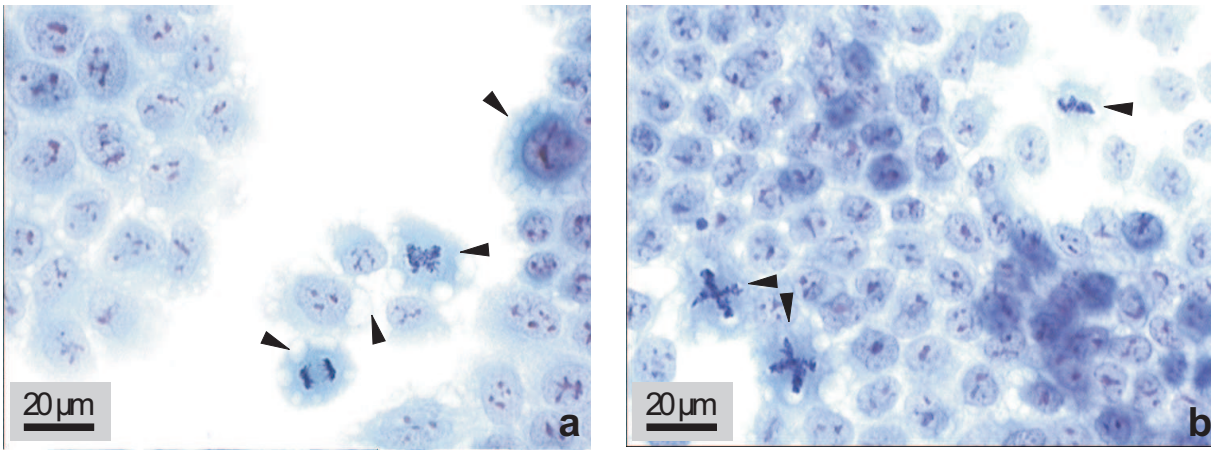

Figure 3.1: In vitro morphology of human NCI-H460 lung cancer cells (Papanicolaou staining). The highly vacuolated round cells (a) form adherent cell aggregates and show a high mitotic activity (a,b). Cells are of the same size, occasionally large cells are observed (a). Two cells in metaphase exhibit abnormal mitotic figures (b).

The round to oval large cells displayed in Fig. 3.1 form tight adherent cell sheets and are of different sizes. The cell cytoplasm is highly vacuolated and the round nuclei, that fill a major portion of the cells, contain multiple prominent nucleoli scattered within the nuclei. A high mitotic activity of the cells is observed. The aggressiveness of NCI-H460 tumors is clearly deducible from the abnormal mitotic figures (tetrapolar spindles) in cell

metaphases shown in Fig. 3.1b (indicated by arrows).

The small cell lung cancer cell line DMS 53 (ATCC CRL 2062) was isolated from a mediastinal biopsy at the time of diagnosis by O.S. Pettengill et al. from a 54-year old male Caucasian in 1974 prior to treatment (Pettengill et al. 1980b). DMS 53 cells were purchased in the 34^{th} passage. The DMS 53 cell line is an example of a SCLC cell line with a well differentiated neuroendocrine phenotype (Mabry et al. 1989).

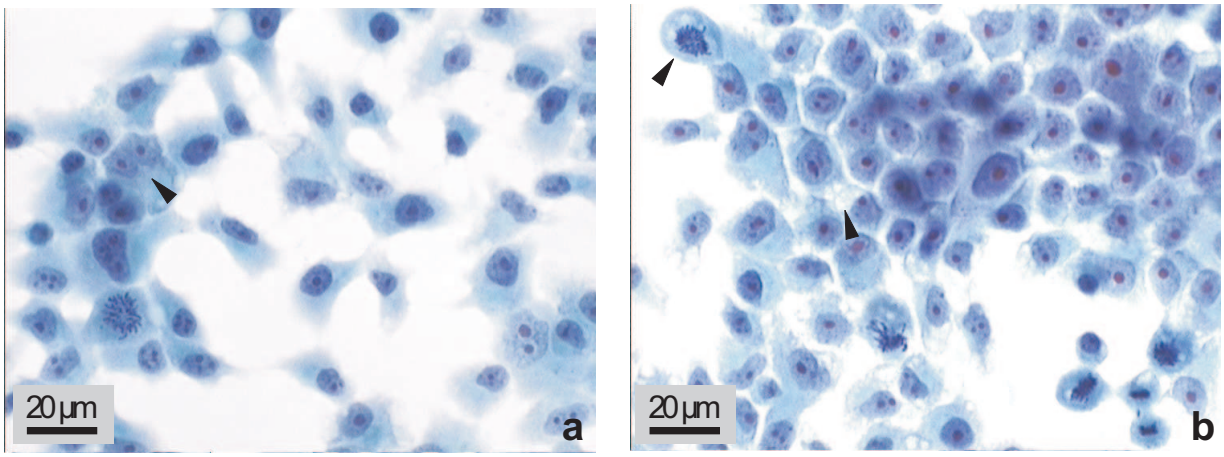

Figure 3.2: In vitro morphology of human DMS 53 lung cancer cells (Papanicolaou staining). The oval cells have small appendages and are slightly vacuolated. The tumor cells grow as tight adherent cell cluster (b) with less mitotic activity (a,b). Cells with more than one nucleus are observed (a).

The DMS 53 cell line is a typical SCLC cell line because of its oval cells with scant cytoplasm that are small to moderate in size in contrast to NCI-H460 tumor cells. The cells have short appendages and are slightly vacuolated (Fig. 3.2). The majority of the cells have one oval nucleus and mostly one prominent, round nucleolus. Cells with two nuclei and multiple nucleoli are observed, too. The mitotic activity was not as high as in the case of the NCI-H460 cell line.

The human small cell lung cancer cell line DMS 114 (ATCC CRL 2066) was established from a mediastinal biopsy by O.S. Pettengill and associates from a 68-year old male Caucasian at the time of diagnosis prior to therapy in 1975 (Pettengill et al. 1980b). DMS 114 cells were obtained in the 36^{th} passage and were described as tumorigenic in athymic mice (Pettengill et al. 1980a). DMS 114 cells as well as the DMS 53 cell line are classified to SCLC type IV as both cell lines grew attached to the culture flask (Carney et al. 1985)

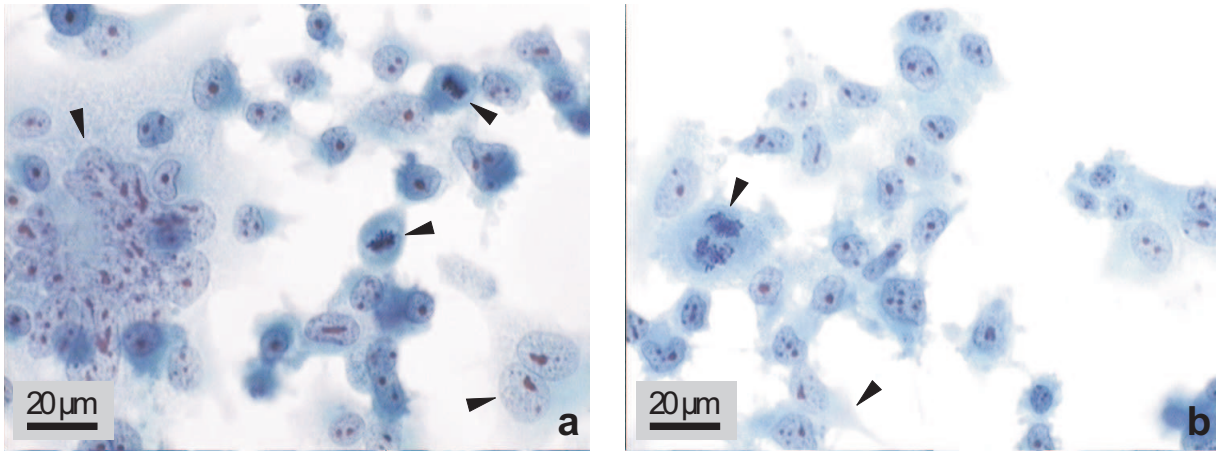

Figure 3.3: In vitro morphology of human DMS 114 lung cancer cells (Papanicolaou staining). The oval to polymorphic cells with appendages form loose cell aggregates (b). Multinucleated cells are frequently observed, that are sometimes of giant size (a). The cells show relatively high mitotic activity (a,b).

The irregularly formed cells shown in Fig. 3.3 have appendages and form loose cell clusters without vacuolization. The oval nuclei have two or more prominent nucleoli. The nucleocytoplasmic ratio is nearly 3:1. Multinucleated giant cells are frequently observed. The high malignancy of SCLC tumors is clearly deducible from the relatively high mitotic activity of the cells.

The human small cell lung cancer cell line DMS 153 (ATCC CRL 2064) was isolated from liver tissue taken at an autopsy of a patient with small cell carcinoma in the lung, who received therapy with cyclophosphamide and methotrexate (Pettengill et al. 1980b). DMS 153 cells were obtained in the 26^{th} passage. Unfortunately, the cell line is a mixture of adherent cells and cells growing in suspension. Therefore, the cultivation of DMS 153 cells was stopped as the planned assays are unsuitable for suspension cells.

3.3.2 In vitro growth and doubling time

In permanent in vitro cultivation it is important to monitor growth parameters like duration of G_0- and M-phase and minimal doubling time. Modifications of these parameters could affect chemosensitivity, as the antiproliferative effect of cytostatic agents is heavily depending on the growth kinetics of the examined cell line. Therefore, the selected cell lines were incubated for at least 250 hours. At various time points the cell proliferation

was stopped by fixation with glutardialdehyde. The cells were stained with crystal violet solution and the absorbance was measured. The absorbance is an indication of the cell density: the higher the absorbance, the higher is the cell density. The absorbance was plotted against the incubation time to assess the growth of the different lung cancer cell lines.

All three curves are characterized by a steep increase at the beginning followed by a plateau phase with constant absorbance values (Fig. 3.4). The NCI-H460 cell line is the fastest growing cell line of the selected human lung cancer cell lines. The growth curves of the SCLC cell lines DMS 53 and DMS 114 are similar in their characteristics in consideration of the different cell densities at the beginning of the measurements. Both SCLC cell lines grew slower in comparison to the NCI-H460 cell line. Confluently grown NCI-H460 and DMS 53 cells reached a higher absorption level compared to confluently grown DMS 114 cells.

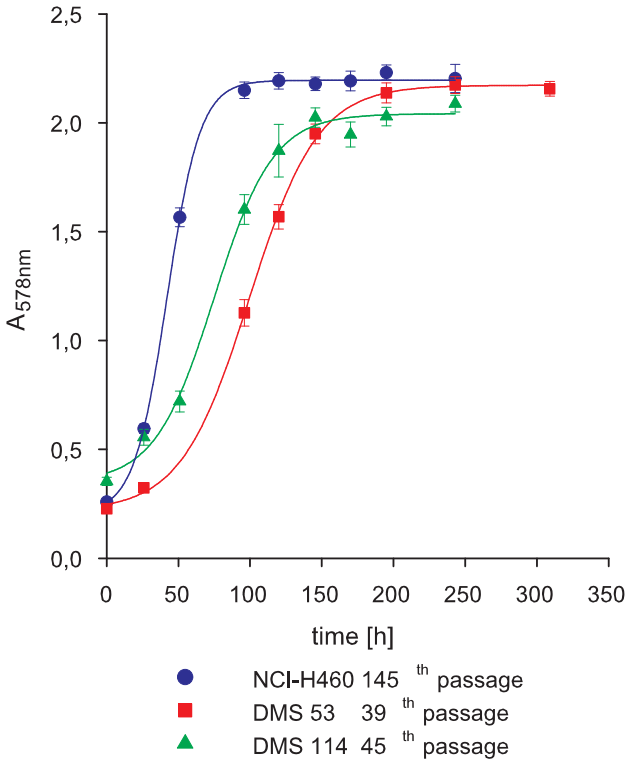

Figure 3.4: Representative growth curves of NCI-H460, DMS 53 and DMS 114 human lung cancer cell lines in lower passages. Absorbance as a parameter for cell growth is plotted against the incubation time.

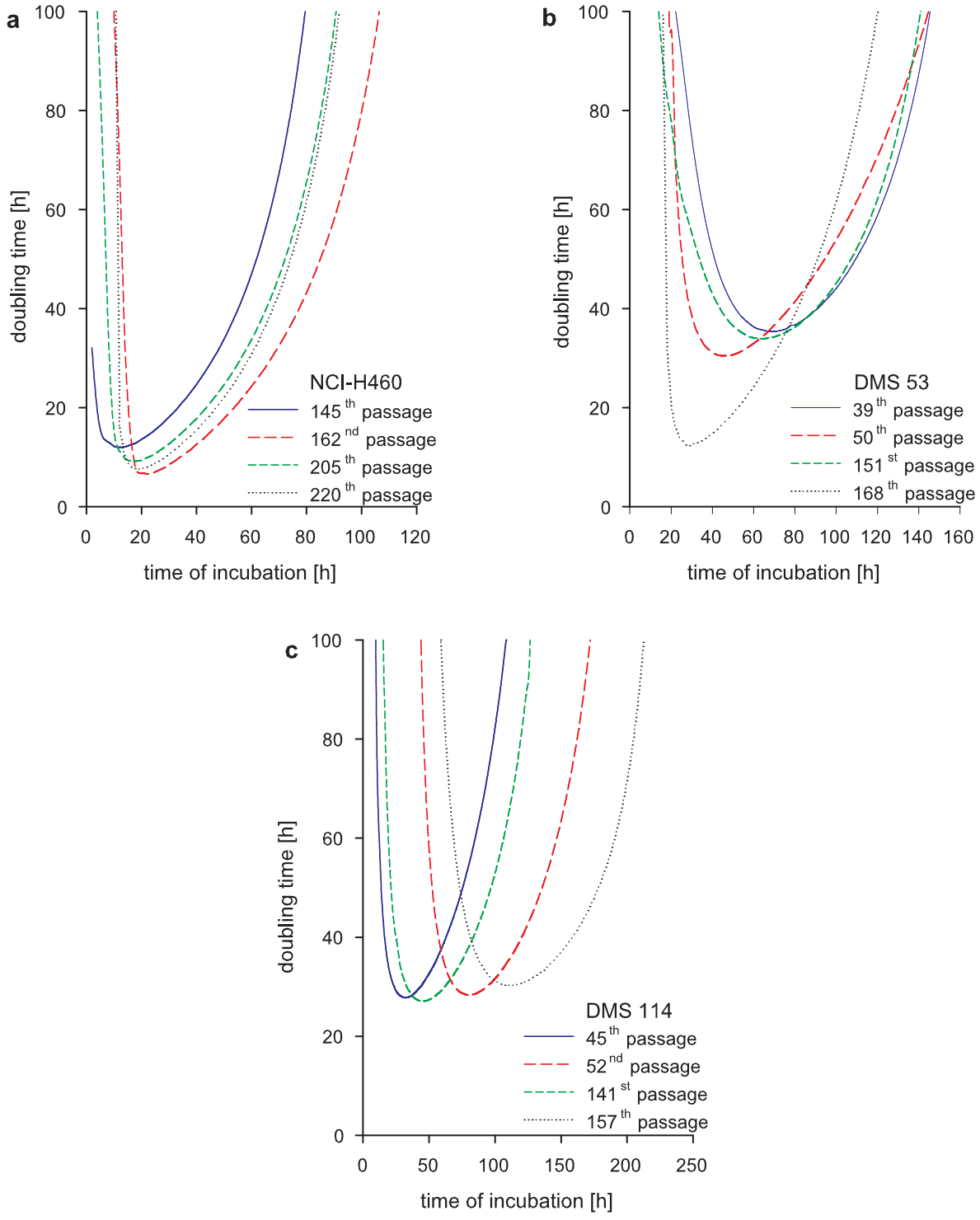

Figure 3.5: Long time cultivation of NCI-H460 (a), DMS 53 (b) and DMS 114 (c) lung cancer cells. Doubling times in various passages are plotted against the incubation time.

To determine the minimal doubling times of the cell lines the doubling time was plotted against the incubation time (Fig. 3.5). NCI-H460 cells exhibited the shortest minimal doubling times (about 9 h), so the cell line was the most rapidly growing cell line among the selected ones. DMS 53 and DMS 114 cells had similar minimal doubling times of 34 h and 28 h, respectively, indicating a slower cell growth in comparison to NCI-H460 cells.

The doubling time curves are used to indicate logarithmic cell growth, which is characterized by constant doubling times. At logarithmic growth, a characteristic for normal growing cells, the doubling time curve results in a parallel line to the x-axis. This curve progression was not observed in any of the three selected cell lines.

The minimal doubling times did not alter during long term cultivation in the case of the NCI-H460 and DMS 114 cell lines. In contrast, the minimal doubling time of DMS 53 cells determined in the 168^{th} passage was three times less compared to the minimal doubling time examined in the 151^{st} passage. This marked decrease of the doubling times indicates a rapid cell growth with increasing cultivation period. Therefore, the DMS 53 cell line is unsuited for a stable long term cultivation, which is necessary for the establishment of a tumor model.

3.3.3 Chromosome distribution

Genetic alterations play a decisive role in genesis and progression of cancer (Kaye 2001). For lung cancer multiple molecular genetic changes are known concerning oncogenes and tumor suppressor genes, which are typical for SCLC. Prevalent expression of oncogenes is mainly existent in N-SCLC (Mitsuuchi and Testa 2002). The most common genetic modification (SCLC >90 %, N-SCLC >50 %) is the loss of heterozygosity at chromosome 3p (Whang-Peng et al. 1982, Sekido et al. 2001) and this change is one of the first alterations in the development of lung cancer. In comparison to SCLC the modifications of N-SCLC karyotypes are more complex. Depending on the N-SCLC tumor species various alterations and imbalances take place at the chromosomes and certain chromosomal aberrations show evidence for the tumor malignancy, e.g. gain of 7q and 8q. Therefore, it is of great importance to examine the chromosome distribution and the karyotype of cell lines to estimate genetic stability and the aggressiveness of lung cancer cell lines.

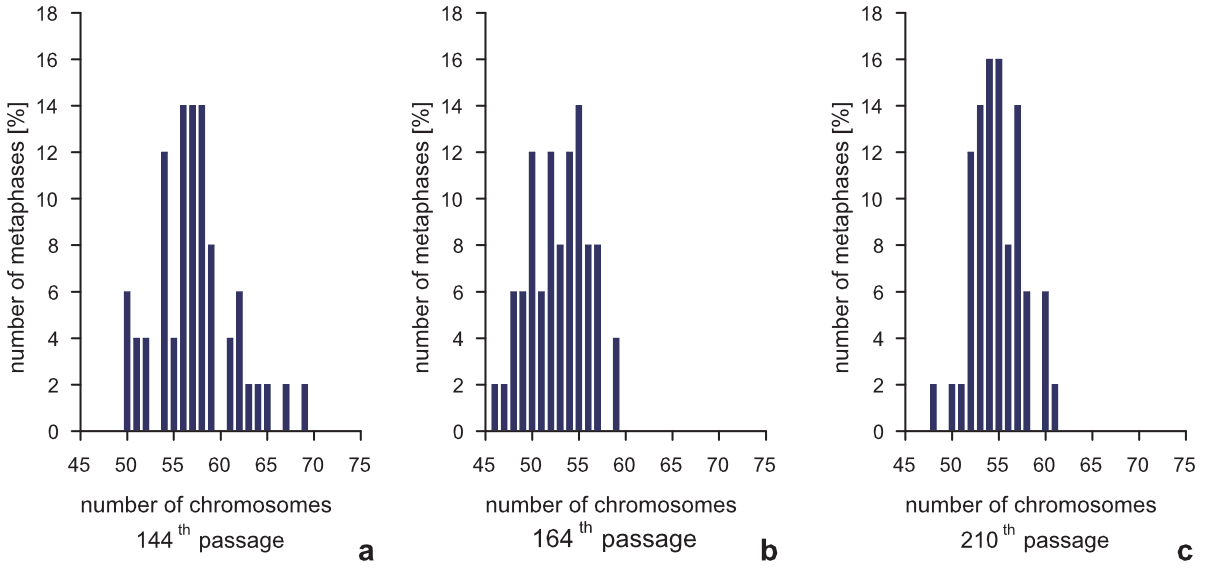

Figure 3.6: Effect of long term cultivation on the chromosome distribution of human lung cancer cell line NCI-H460. The chromosome distribution of the 144^{th} (a), the 164^{th} (b) and the 210^{th} (c) passage is shown.

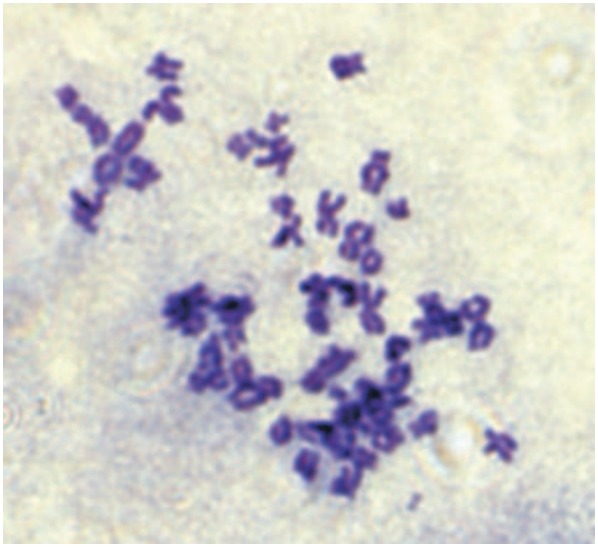

Figure 3.7: Representative metaphase chromosomes of NCI-H460 cell line. Chromosomes were stained with Giemsa solution.

The results of the chromosome distribution for NCI-H460 cells during several passages are shown in Fig. 3.6. The modal chromosome number of 57 specified in the ATCC manual remained nearly unchanged. At higher passages it was only reduced by two chromosomes to 55 chromosomes. The chromosome number was distributed in a close range during

the cultivation period (overall range: 44-69 chromosomes per cell), so the majority of the NCI-H460 cells possessed a hypotriploid set of chromosome.

The chromosome distribution of DMS 53 cells during different passages are described in Fig. 3.8. Here the modal chromosome number of 58 remained constant. In long time

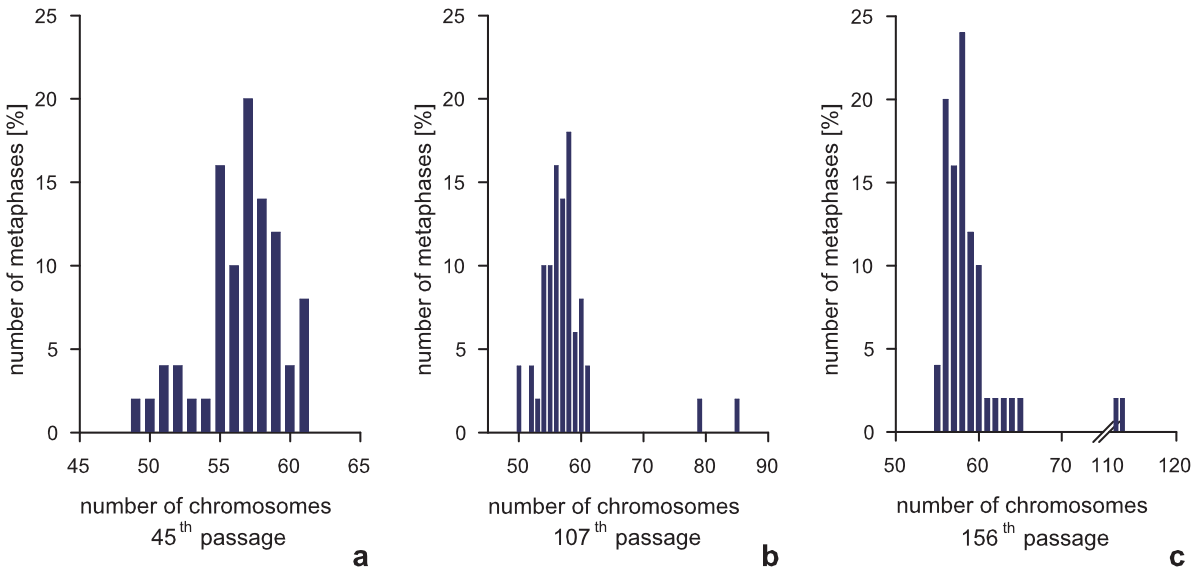

Figure 3.8: Effect of long term cultivation on the chromosome distribution of human small cell lung cancer cell line DMS 53. The chromosome distribution of the 45^{th} (a), the 107^{th} (b) and the 156^{th} (c) passage is shown.

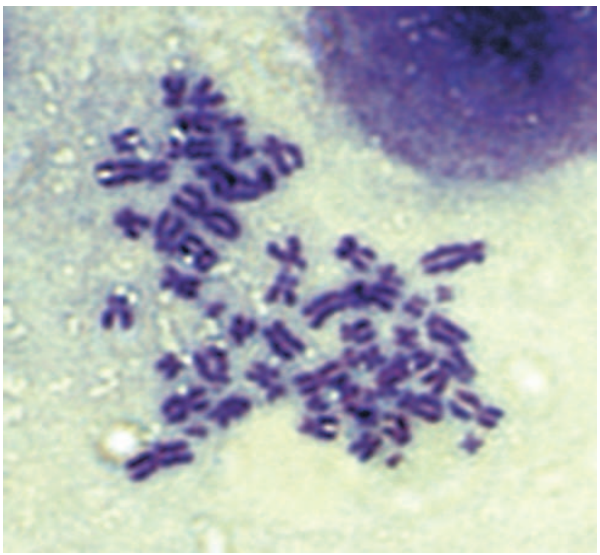

Figure 3.9: Representative metaphase chromosomes of DMS 53 cell line. Chromosomes were stained with Giemsa solution.

cell cultures several nuclei with 80 and more chromosomes per cell were observed. Apart from these nuclei the chromosome number ranged from 49 to 65 chromosomes per cell.

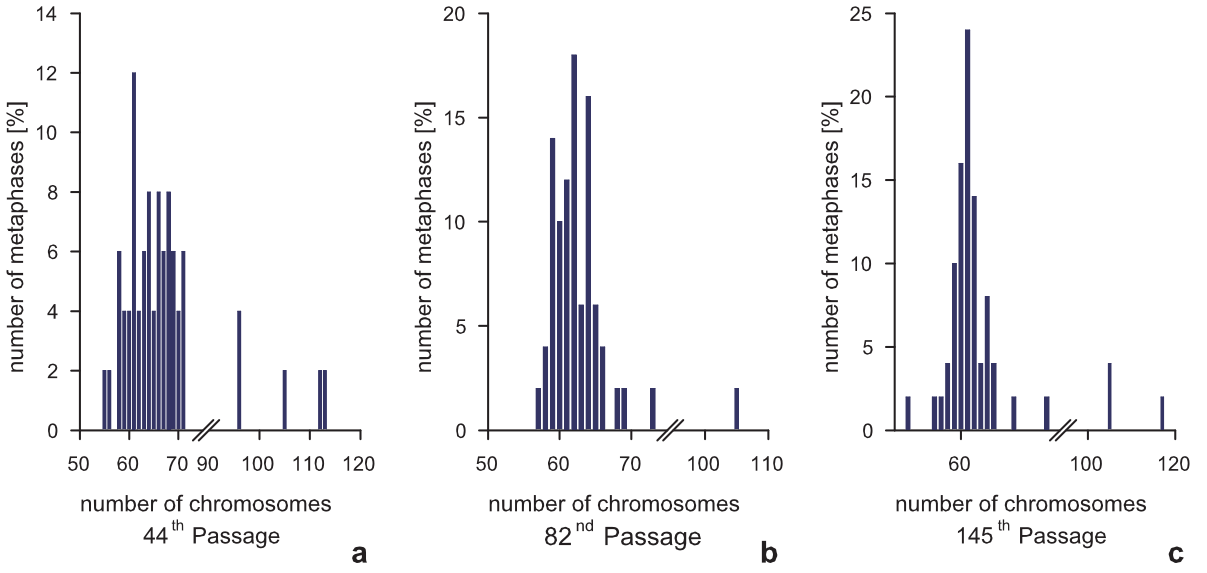

Figure 3.10: Effect of long term cultivation on the chromosome distribution of human small cell lung cancer cell line DMS 114. The chromosome distribution of the 44^{th} (a), the 82^{nd} (b) and the 145^{th} (c) passage is shown.

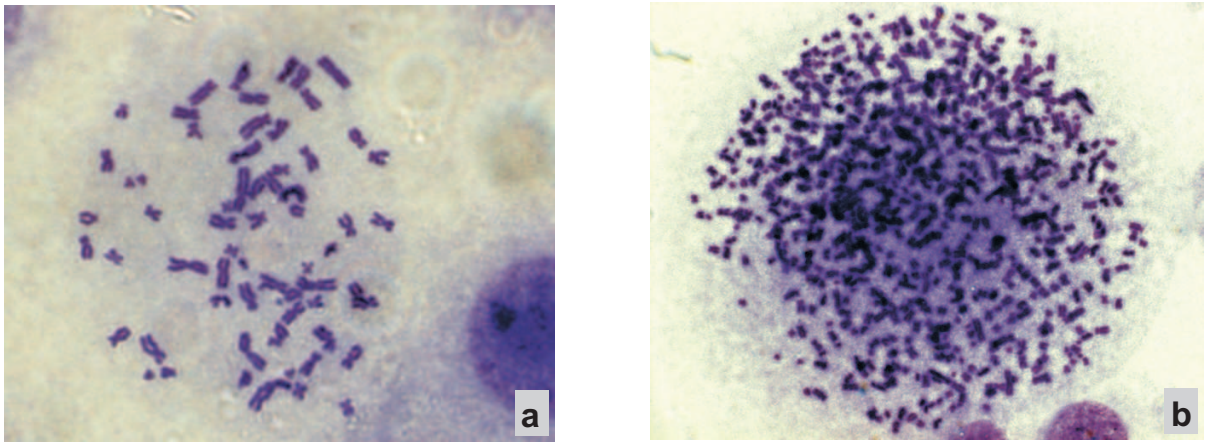

Figure 3.11: Representative metaphase chromosomes of DMS 114 cell line. Chromosomes were stained with Giemsa solution. Metaphase chromosomes of a multinucleated giant cell (b).

The chromosome distributions of cell line DMS 114 are presented in Fig. 3.10. Two metaphase chromosomes are shown in Fig. 3.11, whereas in Fig. 3.11 b the chromosome

set of a multinucleated giant cell mentioned in chapter 3.3.1 is depicted. Such chromosome sets were excluded from the chromosome number determination, but they represent about 10 % of all cells in the examined passages. Modal chromosome numbers of 62 in the 44^{th} passage, 66 in the 82^{nd} passage and 61 in the 145^{th} passage were determined showing nearly no alteration in the modal chromosome number. The range of the chromosome number was similar over the cultivation period (52 to 74 chromosomes per cell).

Thus all three human lung cancer cell lines had a relatively constant number of chromosomes during the cultivation period and are suitable for the establishment of a lung cancer model.

3.3.4 Chemosensitivity against selected cytostatic drugs

Many cytostatic drugs which are utilized for the treatment of lung cancer and its metastases cannot cross the blood-brain barrier because they are substrates of p-gp. One aim of this work was the development of a treatment for brain metastases of lung cancer by analogy with the combination therapy investigated by Fellner et al. (2002) (see 3.1). Therefore, only those chemotherapeutics were selected, which are p-gp substrates (Fisher et al. 1996, Van Veem and Callaghan 2003) and established in clinical lung cancer therapy (Thomas et al. 2002). In addition, the modes of action of the substances should be different. The following classes of substances were chosen (Fig. 3.12): mitotic inhibitors (paclitaxel, docetaxel, vincristine, vinblastine and vinorelbin), topoisomerase inhibitors (etoposide and topotecan), and anthracyclins (doxorubicin). Additionally, cisplatin was used as a chemotherapeutic agent which is not a p-gp substrate.

A screening of the antiproliferative activities of the selected cytostatic drugs was performed by a chemosensitivity assay using the three human lung cancer cell lines NCI-H460, DMS 53 and DMS 114. In Figs. 3.13 to 3.24 the proliferation kinetics of the corresponding controls are shown, and the corrected T/C values, calculated from the proliferation kinetics are plotted against the incubation time. The correction for the initial cell number allows discrimination between cytotoxic, cytostatic and cytocidal drug action at any time of incubation. Clear dose-response relationships were obtained for all selected cytostatic substances and specific effects were derived from these relationships.

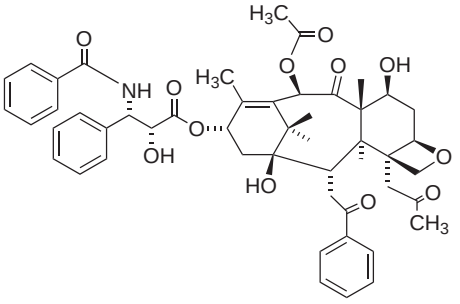

paclitaxel

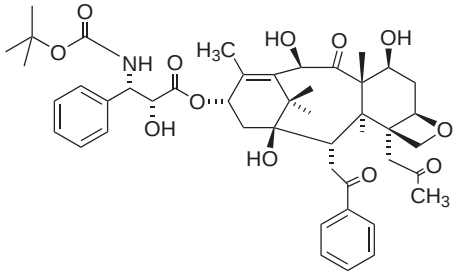

docetaxel

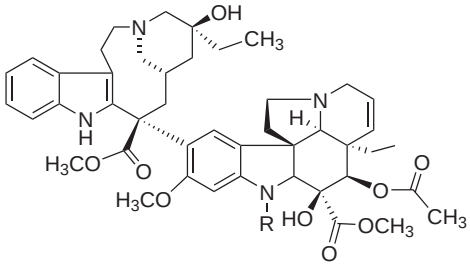

R = CH_3 vinblastine
R = CHO vincristine

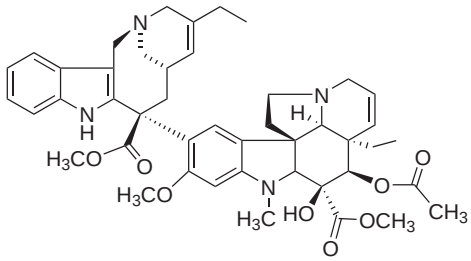

vinorelbin

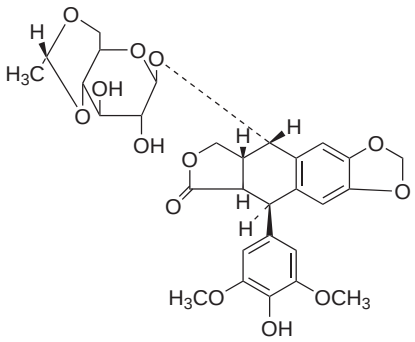

etoposide

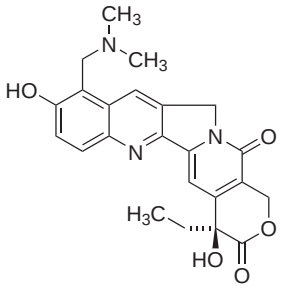

topotecan

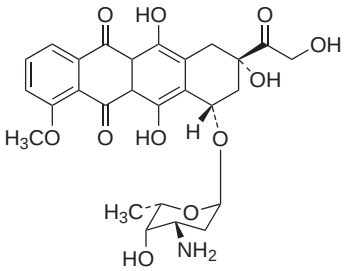

doxorubicin

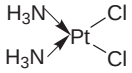

cisplatin

Figure 3.12: Structures of the selected chemotherapeutic agents

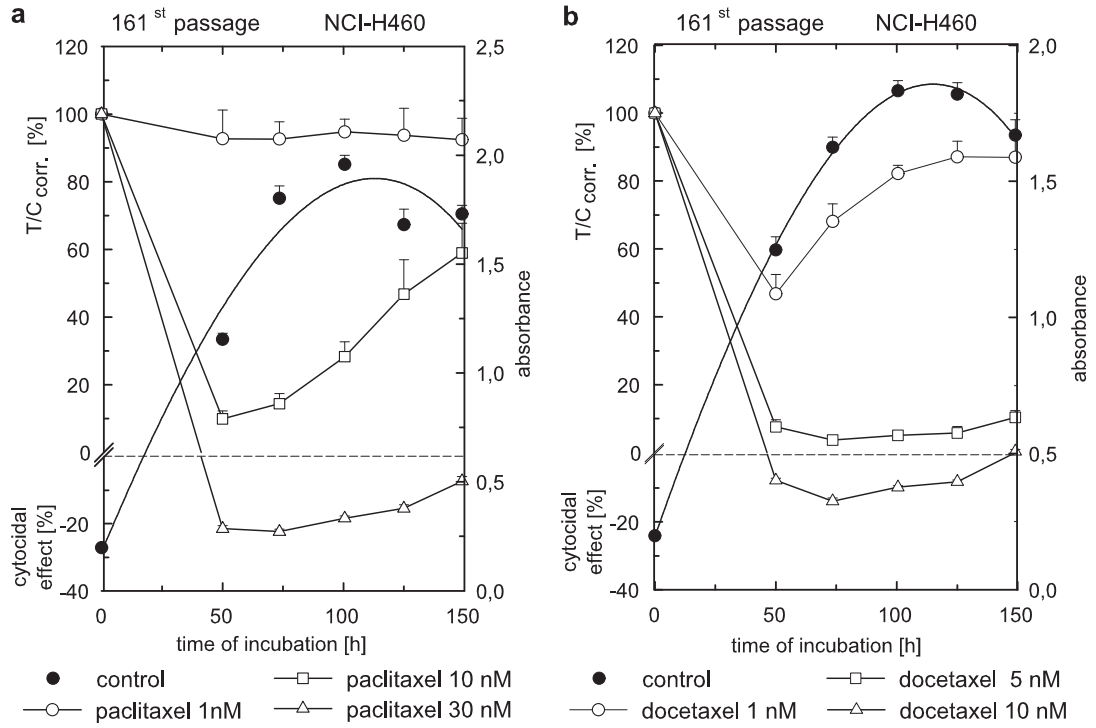

Figure 3.13: Chemosensitivity of NCI-H460 cells against the mitotic inhibitors paclitaxel (a) and docetaxel (b)

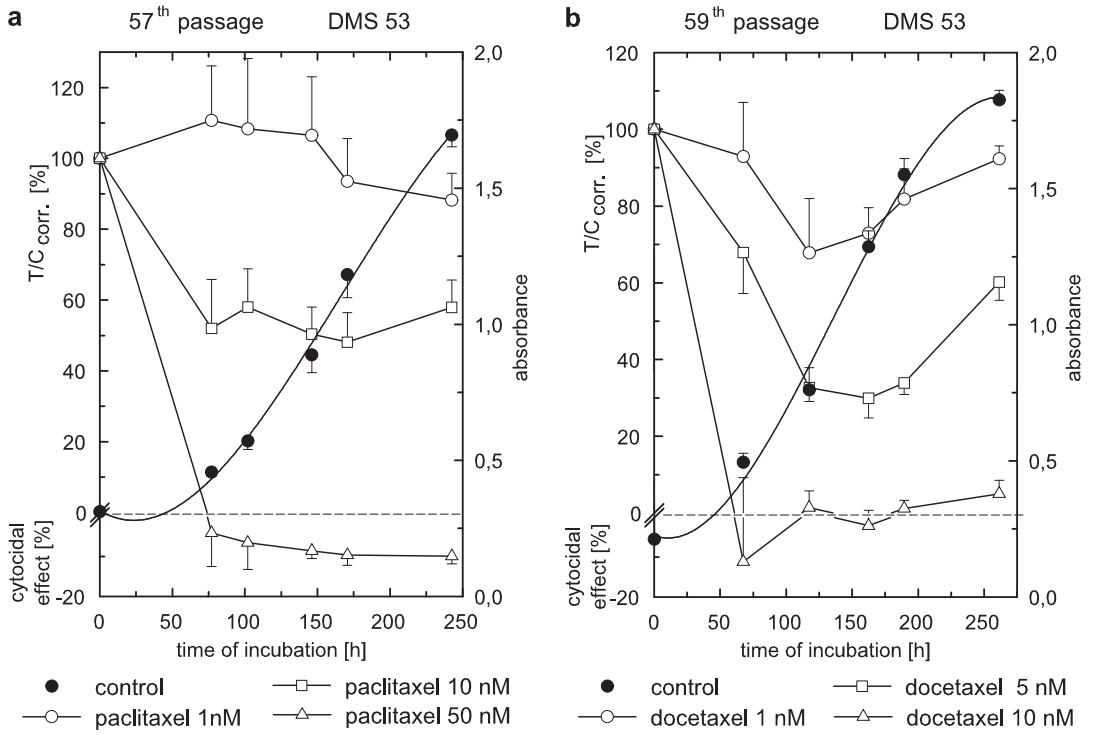

Figure 3.14: Chemosensitivity of DMS 53 cells against the mitotic inhibitors paclitaxel (a) and docetaxel (b)

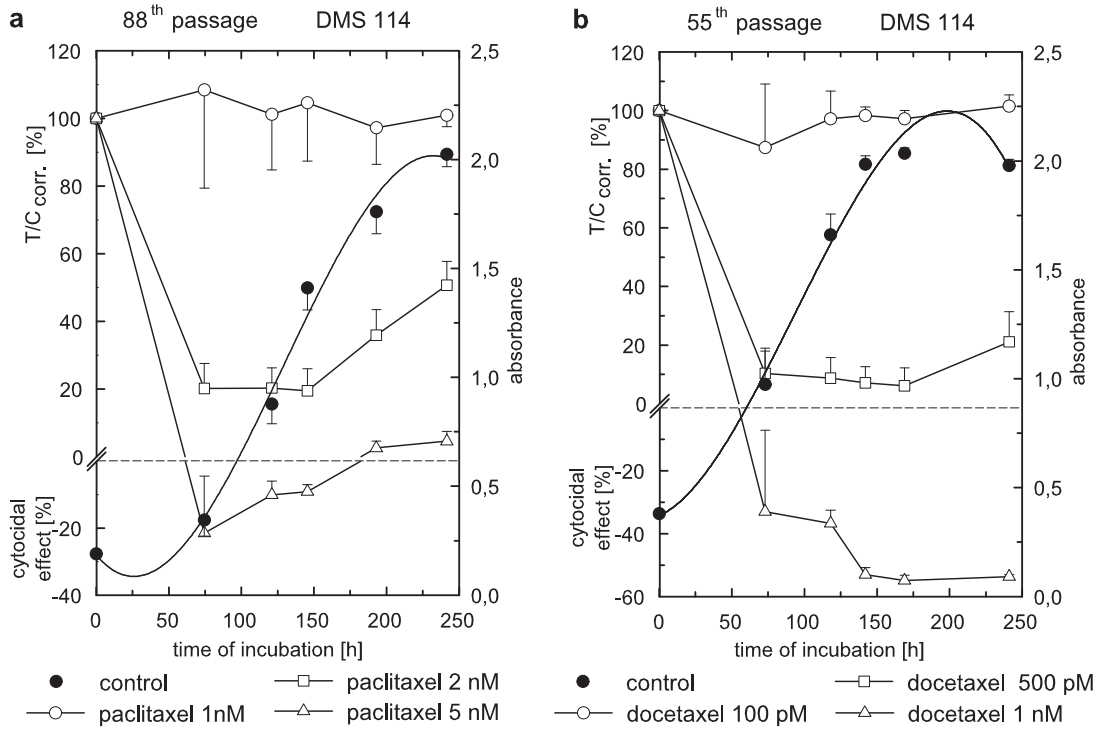

Figure 3.15: Chemosensitivity of DMS 114 cells against the mitotic inhibitors paclitaxel (a) and docetaxel (b)

Mitotic inhibitors paclitaxel and docetaxel. In Fig. 3.13, Fig. 3.14 and Fig. 3.15 the results of the chemosensitivity of the respective cell lines to the taxanes paclitaxel and docetaxel are presented. Paclitaxel and docetaxel, two mitotic inhibitors, prevent the deaggregation of the spindle in G2 phase by binding to microtubules. Effects on the growth of the lung cancer cell lines were already achieved at low concentrations for both substances. In the case of paclitaxel (a) the cell proliferation of NCI-H460 and DMS 53 cells was transiently inhibited at 10 nM paclitaxel. DMS 114 cell growth was already inhibited at a paclitaxel concentration of 2 nM. A cytocidal effect on DMS 114 cells was observed at 5 nM paclitaxel. Compared to the impact of paclitaxel a more powerful cytostatic effect on the cell proliferation was noticed for docetaxel, the semi-synthetical paclitaxel analogue. For example DMS 114 cells disintegrated at 1 nM docetaxel (b). The sensitivity of the selected lung cancer cell lines against the taxanes paclitaxel and docetaxel may be summarized according to the following order:

DMS 114 cells > NCI-H460 cells > DMS 53 cells

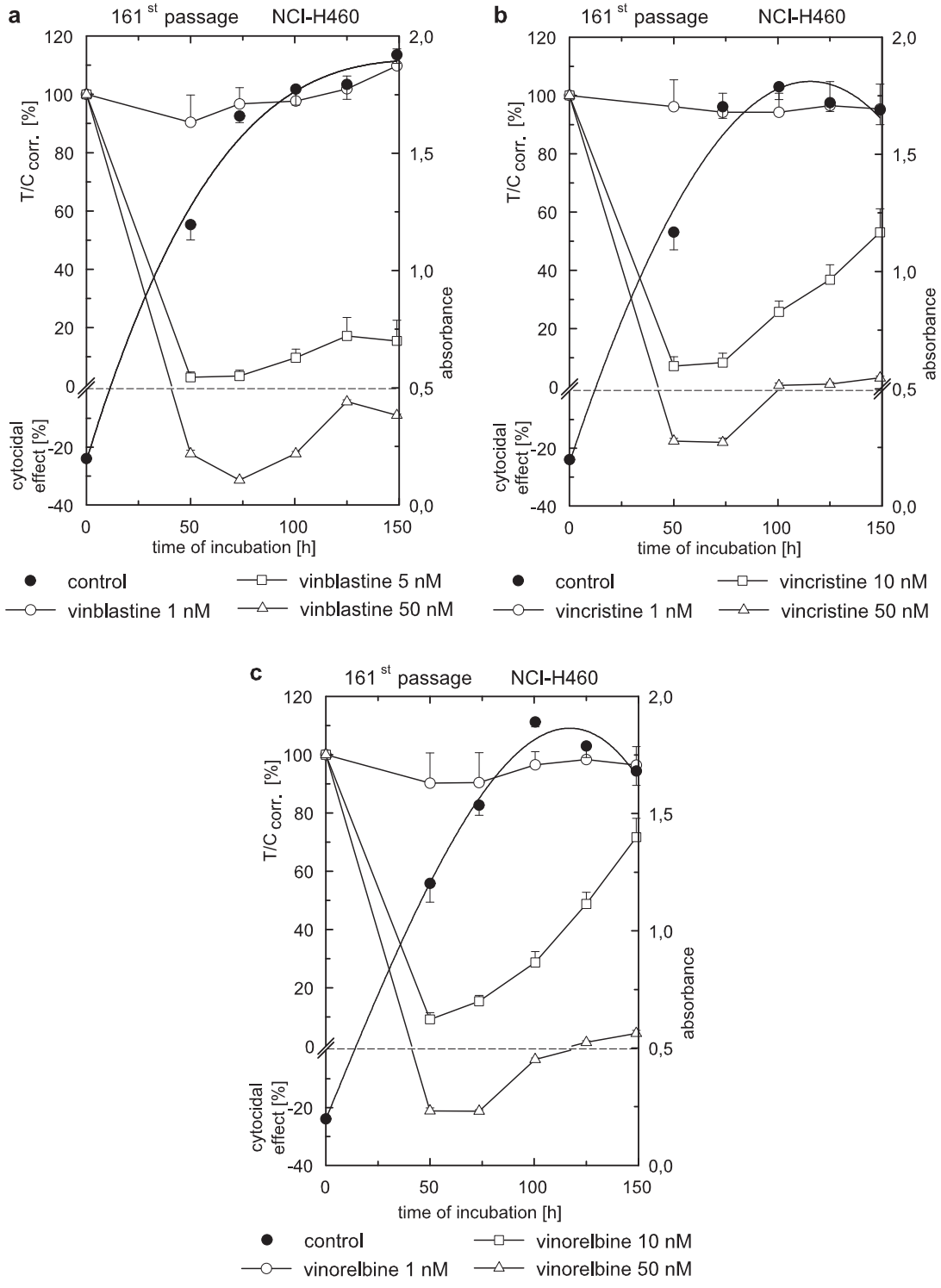

Figure 3.16: Chemosensitivity of NCI-H460 cells against the mitotic inhibitors vinblastine (a), vincristine (b) and vinorelbin (c)

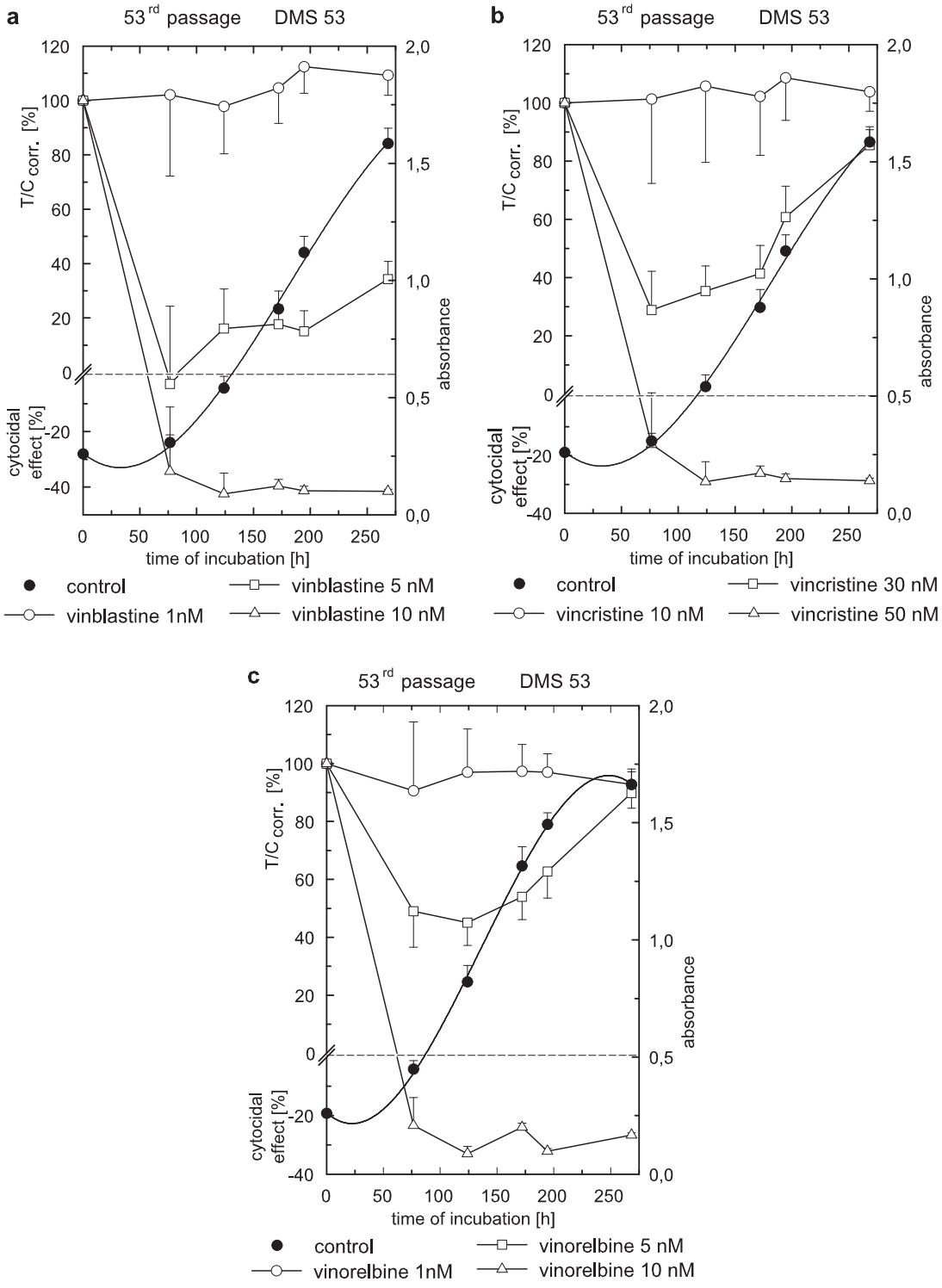

Figure 3.17: Chemosensitivity of DMS 53 cells against the mitotic inhibitors vinblastine (a), vincristine (b) and vinorelbin (c)

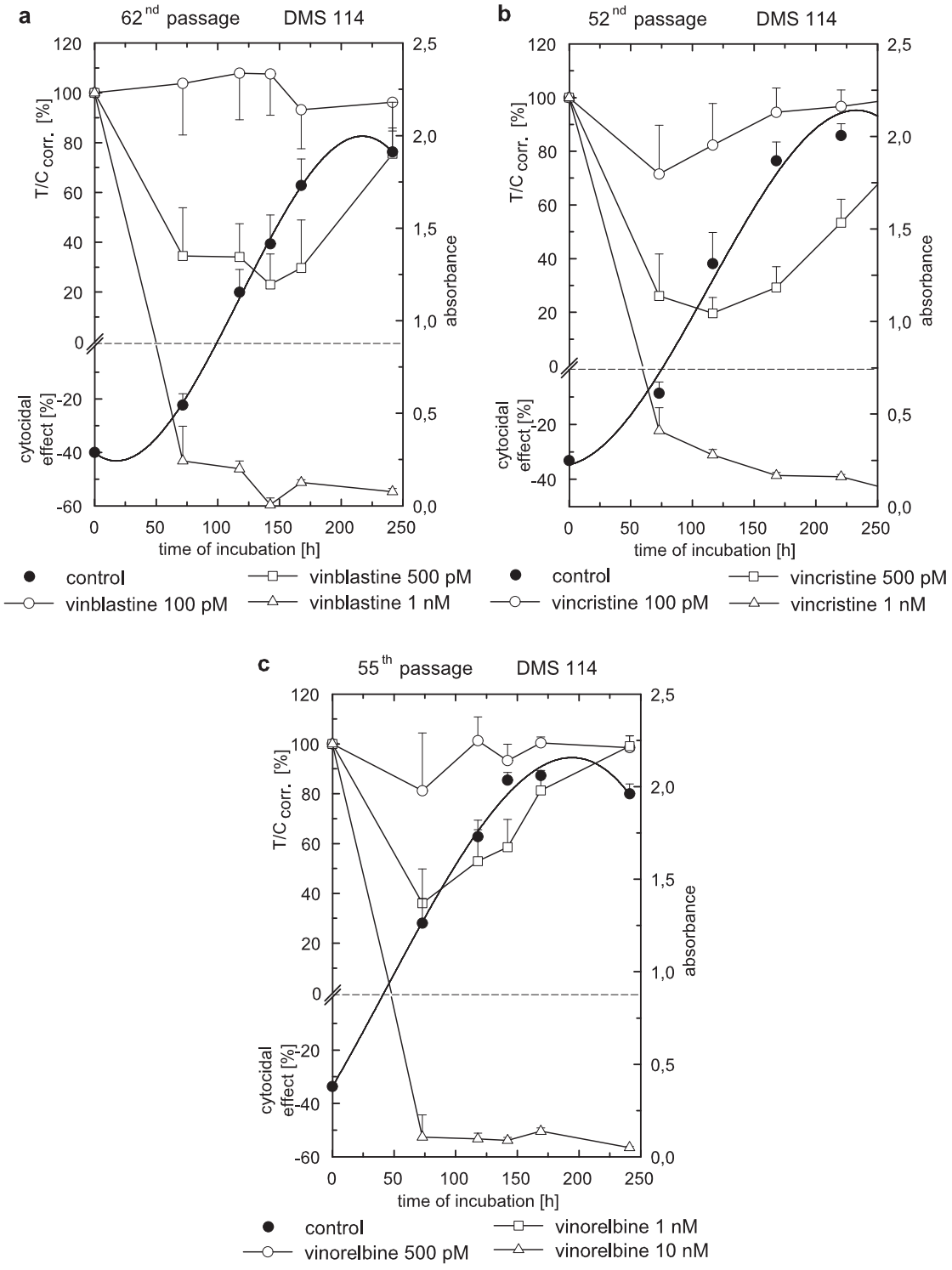

Figure 3.18: Chemosensitivity of DMS 114 cells against the mitotic inhibitors vinblastine (a), vincristine (b) and vinorelbin (c)

Vinca alkaloids vinblastine and vincristine, vinorelbin. Fig. 3.16, Fig. 3.17 and Fig. 3.18 illustrate the effects of the vinca alkaloids vinblastine (a), vincristine (b) and vinorelbin (c) on the growth of the lung cancer cell lines. Vinblastine and vincristine are genuine products of the Madagascar periwinkle leaves and vinorelbin is the semi-synthetical derivative of vinblastine. In contrast to taxanes, vinca alkaloids inhibit the assembly of microtubules. Vinblastine affected the growth of the lung cancer cells similar to docetaxel in case of DMS 53 and DMS 114 cells (cytocidal effect at 10 nM and 1 nM, respectively), whereas a concentration of 50 nM vinblastine is required for a cytocidal effect on NCI-H460 cells (10 nM with docetaxel). Compared to vinblastine higher concentrations of vincristine were needed to inhibit the growth of DMS 53 cells (cytotoxic effect at 30 nM and cytocidal effect at 50 nM). The effect of vincristine on NCI-H460 and DMS 114 cells was comparable to that of vinblastine. Vinorelbin was expected to be more efficient than the genuine vinca alkaloids. However, there was no increase in chemosensitivity compared to vincristine and vinblastine in case of NCI-H460 and DMS 53 cells. The DMS 114 cell line was even less sensitive to vinorelbin than to the other vinca alkaloids. Here, with 1 nM vinorelbin only a cytotoxic effect was achieved compared to a cytocidal effect at 1 nM vinblastine and vincristine, respectively. Hence, vinorelbin was not superior to the genuine vinca alkaloids in inhibiting the investigated lung cancer cell lines. The sensitivity of the human lung cancer cells may be summarized according to the following ranking:

Vinblastine: DMS 114 cells > DMS 53 cells > NCI-H460 cells

Vincristine: DMS 114 cells > NCI-H460 cells > DMS 53 cells

Vinorelbin: DMS 114 cells > DMS 53 cells > NCI-H460 cells

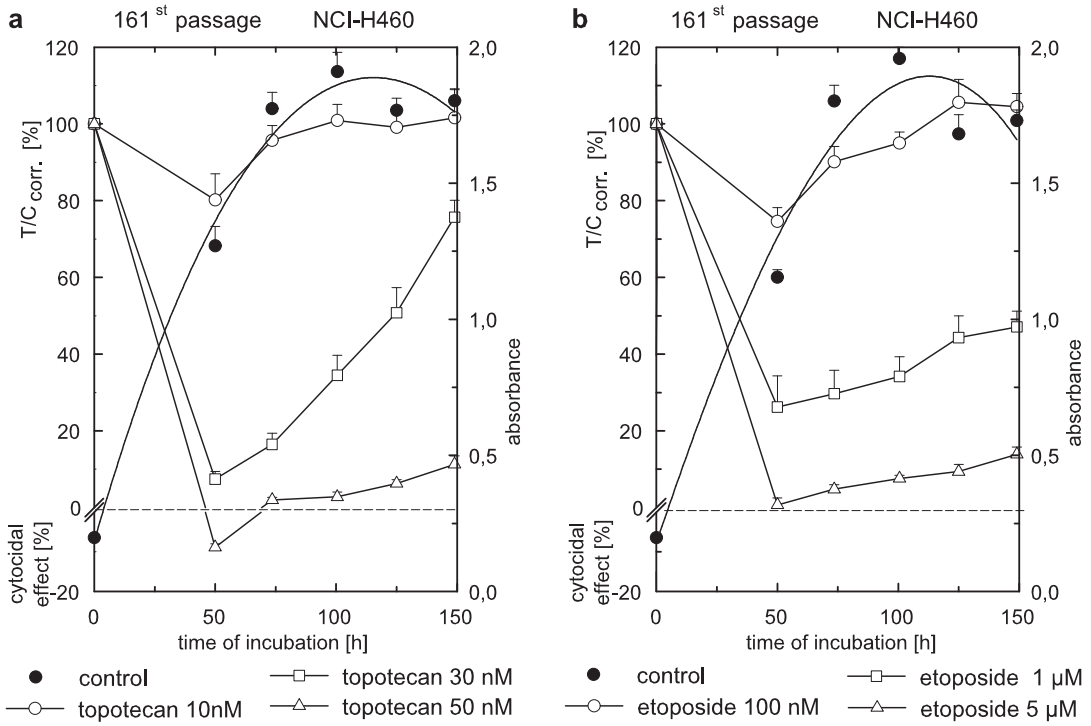

Figure 3.19: Chemosensitivity of NCI-H460 cells against the topoisomerase inhibitors topotecan (a) and etoposide (b)

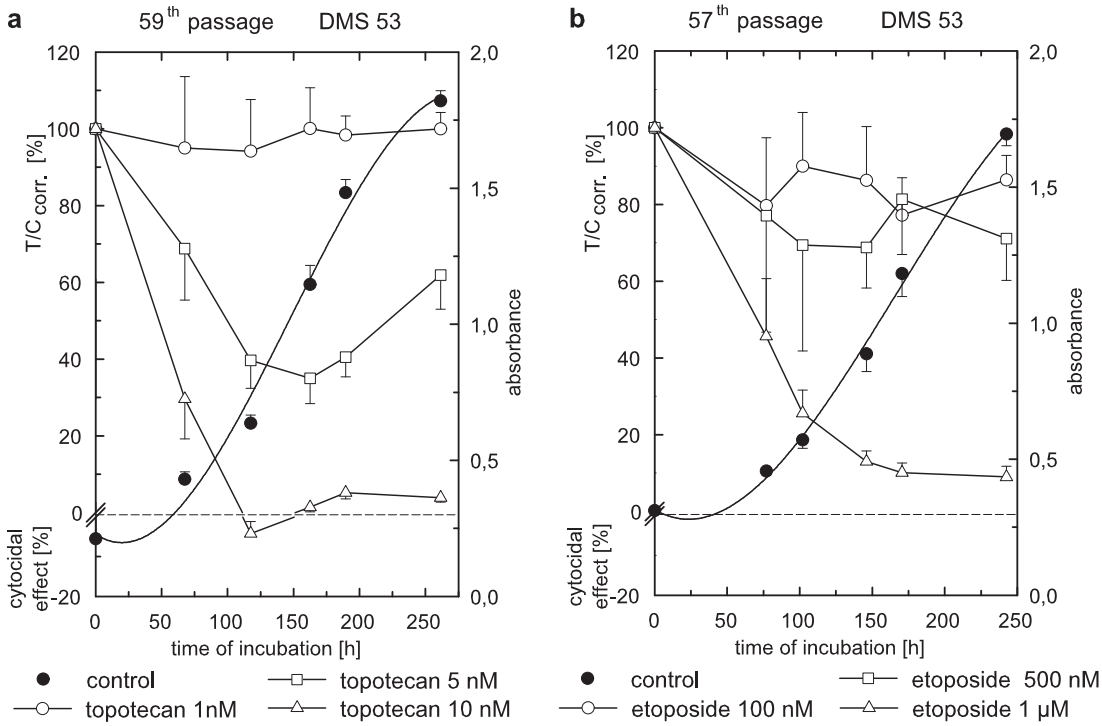

Figure 3.20: Chemosensitivity of DMS 53 cells against the topoisomerase inhibitors topotecan (a) and etoposide (b)

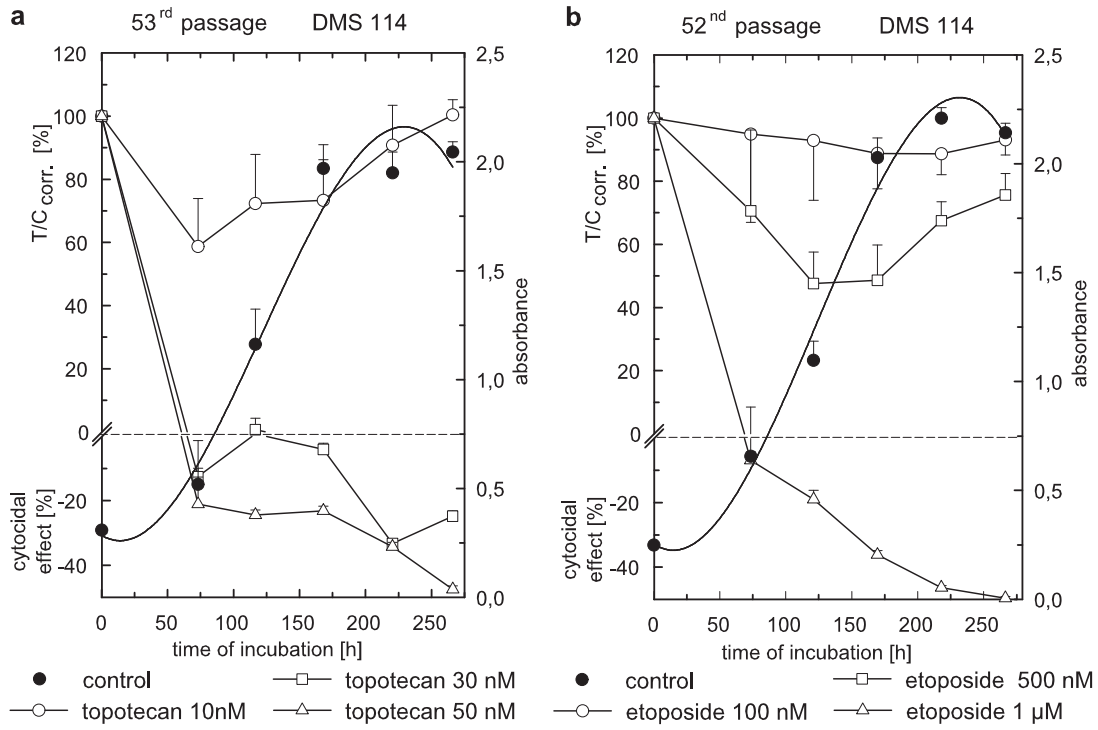

Figure 3.21: Chemosensitivity of DMS 114 cells against the topoisomerase inhibitors topotecan (a) and etoposide (b)

Topoisomerase inhibitors etoposide and topotecan. The chemosensitivities of the selected cell lines against topotecan and etoposide are represented in Fig. 3.19, Fig. 3.20 and Fig. 3.21. Both substances act as topoisomerase inhibitors, inducing DNA strand breaks and cell apoptosis. Topotecan inhibits the type I and etoposide the type II topoisomerase. All three cell lines were much more sensitive against topotecan than against etoposide. A concentration of 50 nM topotecan was required to induce a cytocidal effect on NCI-H460 and DMS 114 cells. In case of etoposide concentrations of 5 μM and 1 μM were necessary to produce comparable effects on NCI-H460 and DMS 114 cells respectively. Topotecan had already a cytocidal effect on DMS 53 cells at 10 nM. At this low concentration the growth of the other cell lines was not effected at all. In case of etoposide the DMS 53 cell line was similar in its sensitivity to the NCI-H460 cell line and thus about 200 times less sensitive compared to the results received with topotecan. The following list summarizes the rank order of sensitivity of the human lung cancer cell lines against the topoisomerase inhibitors topotecan and etoposide:

Topotecan: DMS 53 cells > DMS 114 cells > NCI-H460 cells

Etoposide: DMS 114 cells > DMS 53 cells > NCI-H460 cells

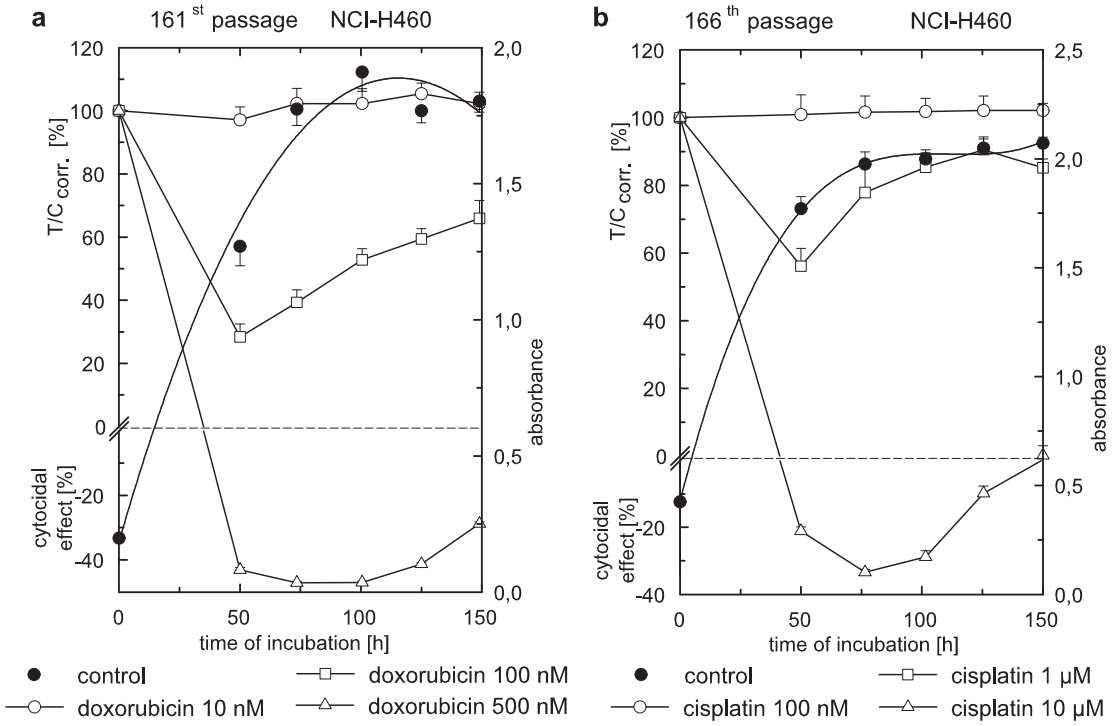

Figure 3.22: Chemosensitivity of NCI-H460 cells against the anthracyclin doxorubicin (a) and cisplatin (b)

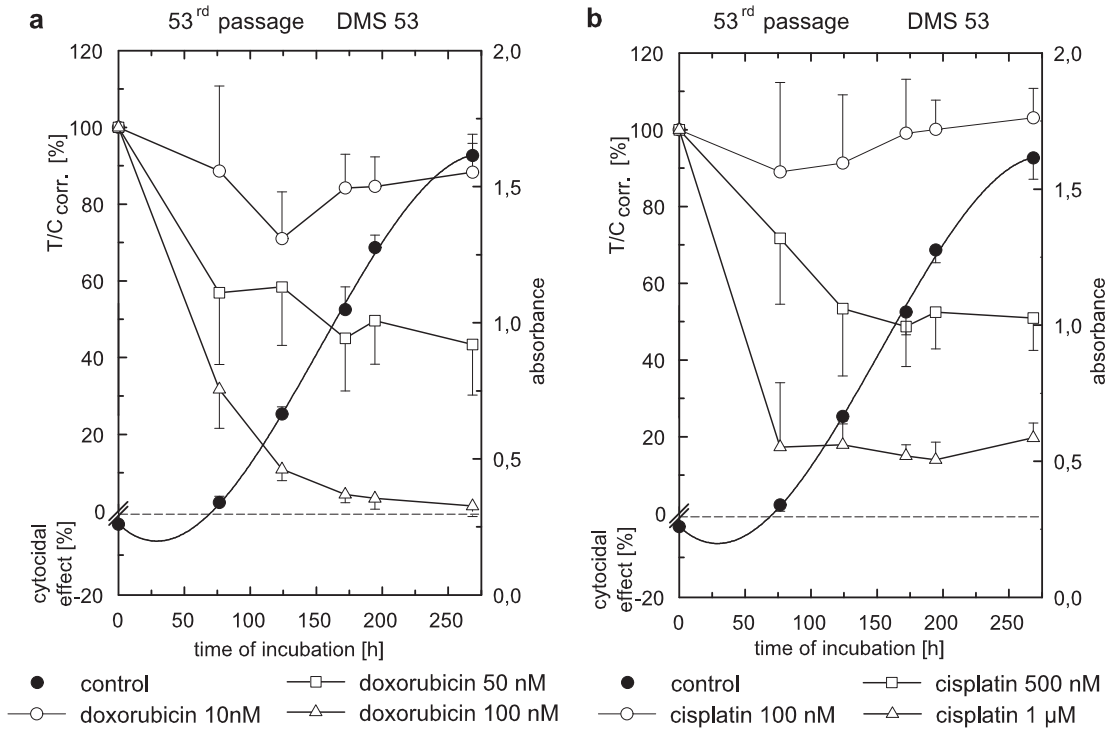

Figure 3.23: Chemosensitivity of DMS 53 cells against the anthracyclin doxorubicin (a) and cisplatin (b)

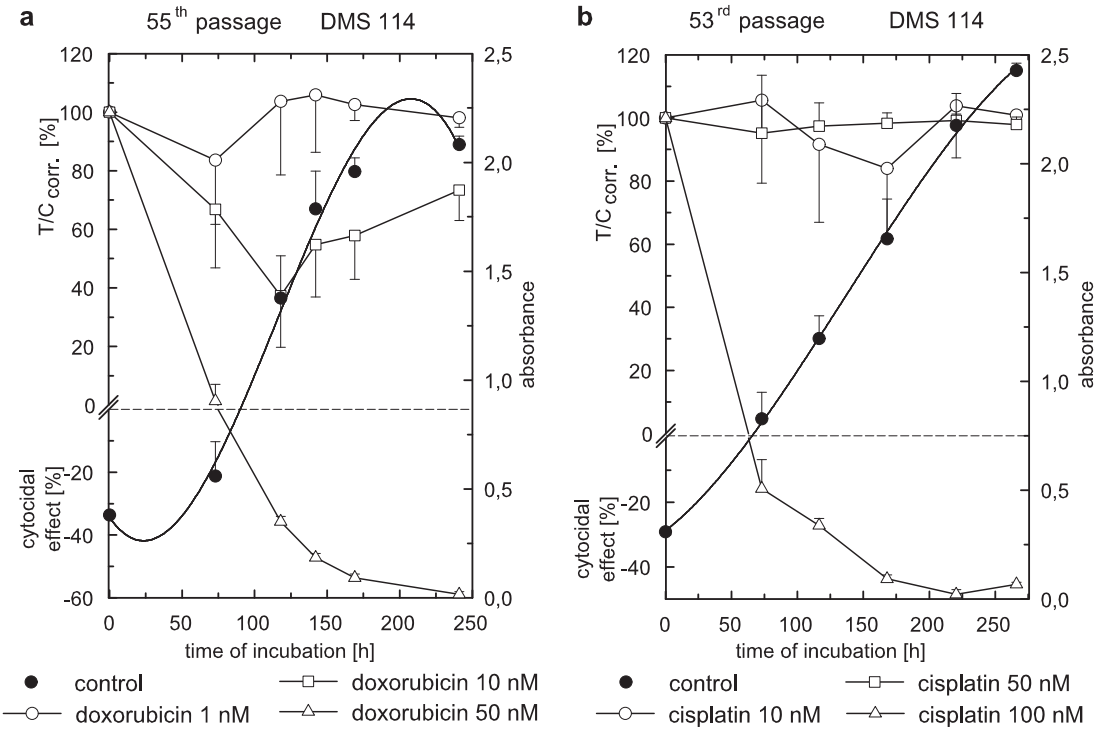

Figure 3.24: Chemosensitivity of DMS 114 cells against the anthracyclin doxorubicin (a) and cisplatin (b)

Doxorubicin and cisplatin. The chemosensitivity of the three lung cancer cell lines against doxorubicin and cisplatin is shown in Fig. 3.22, Fig. 3.23 and Fig. 3.24. At least two mechanisms of action account to the cytotoxic effect of the anthracyclin doxorubicin: on the one hand it intercalates with DNA by wedging between the DNA bases thereby blocking DNA replication and transcription, and on the other hand it inhibits topoisomerase type II. Cisplatin arrests the DNA synthesis mainly by formation of intrastrand crosslinks. Compared to the mitotic inhibitors, doxorubicin is a moderately active cytostatic agent as concentrations of 10 nM in case of DMS 114 or higher (50 nM and 100 nM for DMS 53 and NCI-H460 respectively) were needed to achieve a cytotoxic or cytostatic effect. The cell lines were less sensitive to cisplatin than to doxorubicin. This becomes evident from the comparison of doxorubicin and cisplatin effects on the cell growth of NCI-H460 and DMS 53 cell lines: 10 times higher concentrations were required to induce similar effects on the cell proliferation of the NCI-H460 and DMS 53 cell lines. The sensitivity of the investigated cell lines against doxorubicin and cisplatin may be summarized as follows:

DMS 114 cells > DMS 53 cells > NCI-H460 cells

In summary, the DMS 114 cells were most sensitive to all cytostatic drugs except topotecan, which was most effective against DMS 53 cells. In general, the chemosensitivities of NCI-H460 and DMS 53 cells were comparable. Generally, all lung cancer cell lines responded excellently to mitotic inhibitors. Compared to the other investigated drugs the topoisomerase inhibitor etoposide required the highest concentrations to achieve a cytostatic effect, whereas topotecan affected the cell growth at moderate concentrations. Among the mitotic inhibitors the taxanes, especially docetaxel, were the most potent antitumor agents in this assay.

3.3.5 In vivo growth characteristics

The lung cancer cell lines NCI-H460, DMS 53 and DMS 114 were established in vivo as subcutaneous and intracerebral tumor models, respectively. The intracerebral model is described in detail in chapter 5. In the literature the SCLC cells are described as tumorigenic in athymic mice (Pettengill et al. 1980a). To study new tumor treatment approaches in animals it is indispensable to have a stable tumor growth which is reproducible over several passages. Therefore, the size of the established tumor has to be measured and the growth had to be compared in different passages by plotting the tumor area against the time after tumor implantation.

In Fig. 3.25 the in vivo growth of the selected cell lines in the nude mouse is illustrated during various passages. The implantation of NCI-H460 and DMS 114 cells produced stably growing subcutaneous tumors of sufficient size in different passages (about 140 mm^2 for NCI-H460 tumors, Fig. 3.25 a, and 200 mm^2 in case of DMS 114 tumors, Fig. 3.25 c). In contrast, DMS 53 tumors (Fig. 3.25 b) were growing slower and were smaller. Furthermore, the DMS 53 cells were poorly tumorigenic in mice: only two of five mice developed a subcutaneous tumor after DMS 53 cell injection. The NCI-H460 and DMS 114 tumors were well tolerated by mice. A rapidly growing subcutaneous tumor model was established using the NCI-H460 cell line; this tumor was passaged every 30 days. The DMS 114 cell line should be used for a slowly growing subcutaneous tumor model, that requires a duration greater than 40 days.

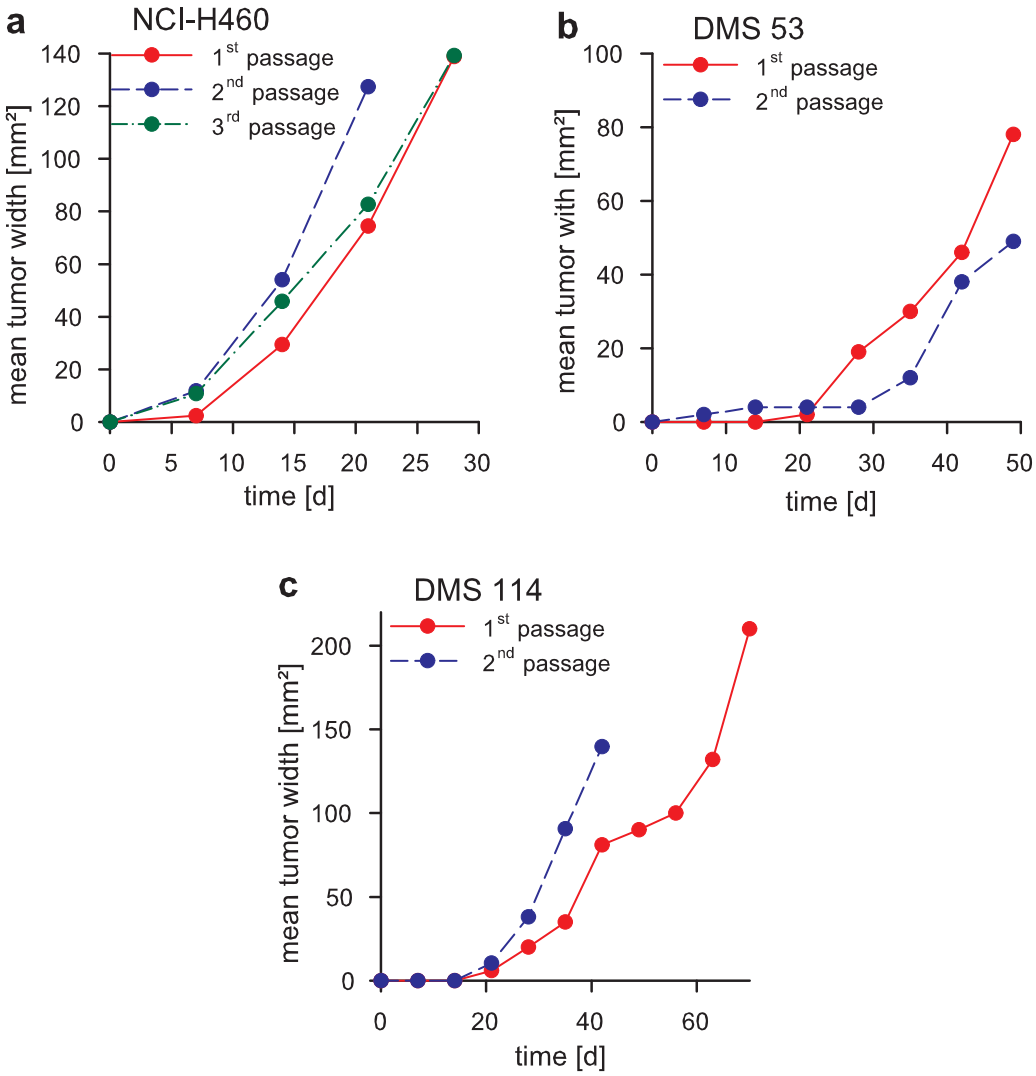

Figure 3.25: In vivo growth curves of subcutaneously growing human lung cancer cell lines NCI-H460 (a), DMS 53 (b) and DMS 114 (c) in mice during various passages

When tumors were passaged tissue samples were taken from the tumor for histological characterization by HE- and MG-staining. MG-stained sections of subcutaneously grown NCI-H460 cells in the 3^{rd} passage are displayed in Fig. 3.26. The subcutaneously growing NCI-H460 cells form a heterogenous tumor with large undifferentiated cells. The cells have round to oval nuclei with large irregularly formed nucleoli and the nucleocytoplasmic ratio is approximately 1 : 2. The high malignancy of the tumor is deducible from the intense mitotic activity and abnormal mitotic figures (tripolar spindle, Fig. 3.26 b). Infiltration of blood vessels is clearly visible in Fig. 3.26 a. The tumor is pervaded with necrotic areas.

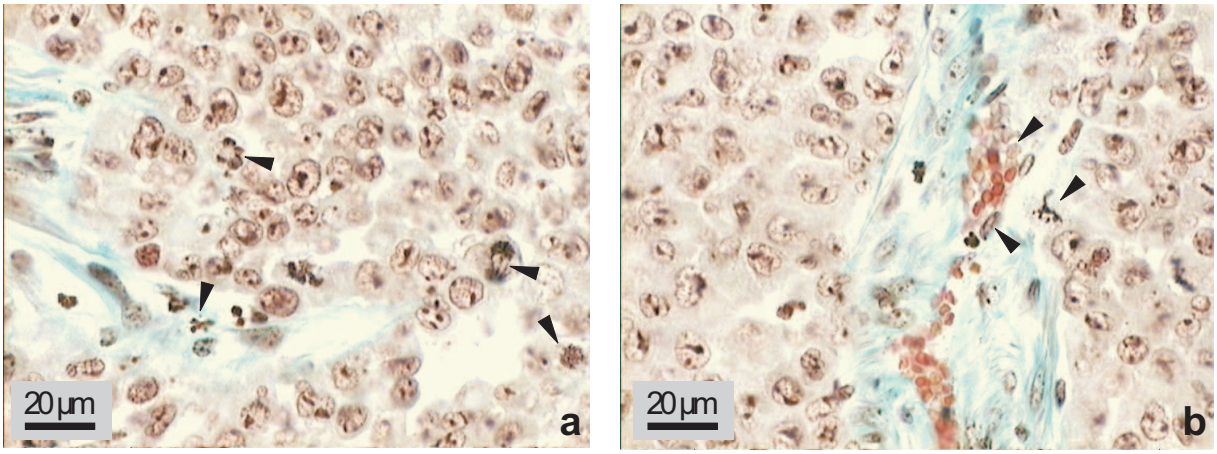

Figure 3.26: MG-staining of subcutaneously growing NCI-H460 tumor. The large undifferentiated cells have irregularly formed nucleoli. Abundant mitosis (a,b) and abnormal mitotic figures (b) are observed. The tumor tissue is necrotic (a) and blood vessels are infiltrated by the tumor cells (b).

In Fig. 3.27 the MG-stained sections of subcutaneously grown DMS 53 tumor in the 1^{st} passage are presented. The homogenous DMS 53 tumor consists of round to oval cells with dense nuclei, prominent round nucleoli and scanty cytoplasm. The tumor is more differentiated in comparison to the NCI-H460 tumor, i.e. a glandular cell formation is observed (Fig. 3.27 b). The tumor tissue is well provided with blood vessels and shows only a few cells in metaphase indicating a lower mitotic activity.

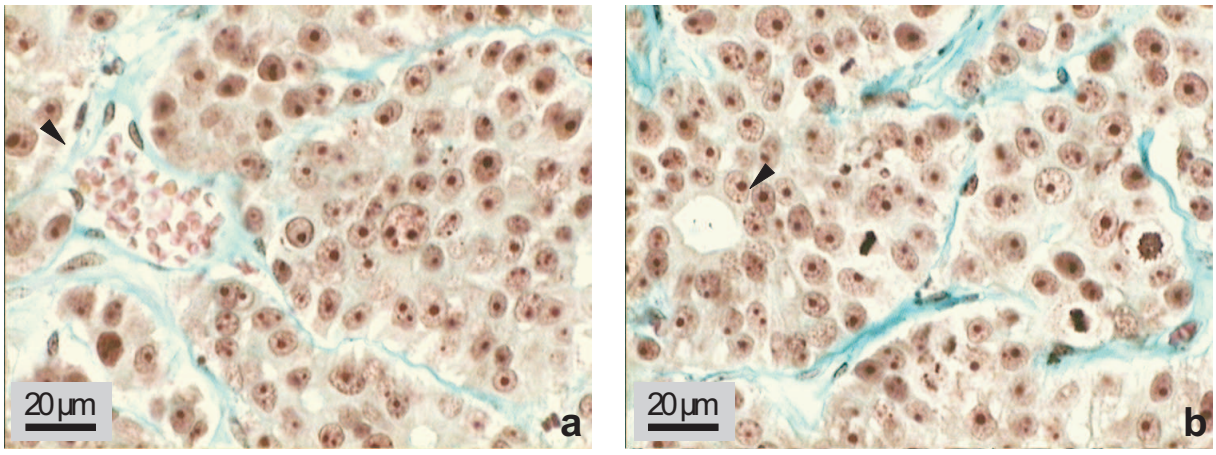

Figure 3.27: MG-staining of subcutaneously growing DMS 53 tumor. Large blood vessels are observed in the tissue (a). The round to oval cells with dense nuclei and scanty cytoplasm are less undifferentiated compared to NCI-H460 tumors as glandular structures are observed (b).

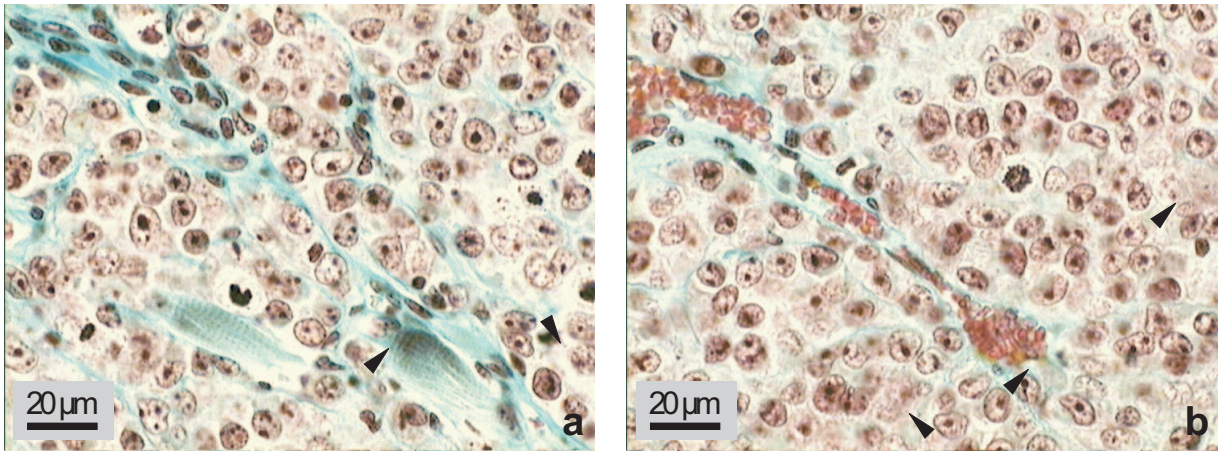

Figure 3.28: MG-staining of subcutaneously growing DMS 114 tumor. The inhomogeneous tumor consists of oval cells with indistinct cytoplasm and polymorphic nuclei. Infiltration of smooth muscles (a) and blood vessels (b) is observed. Multinucleated giant cells are seen as well (b).

MG-stained sections of subcutaneous grown DMS 114 tumor in the 1^{st} passage are depicted in Fig. 3.28. The DMS 114 cells produce xenografts consisting of inhomogeneously formed cells with round to oval nuclei and indistinct cytoplasm. The majority of the cells has one prominent, commonly central nucleolus. The cell density of the tumor is very high. The mitotic activity is lower in mice than in vitro (see page 46). In addition, the malignancy of the DMS 114 tumor is obvious from the infiltration of smooth muscles and blood vessels. Multinucleated giant cells are observed, too.

In summary, all three human lung cancer cell lines were tumorigenic in athymic mice. The DMS 53 cell line is poorly tumorigenic, and hence, unsuited for the establishment of a tumor model in animals as mentioned on page 65. Subcutaneously growing NCI-H460 tumors are highly malignant, rapidly growing tumors, which could be used to produce a stable xenograft model in athymic mice. A subcutaneous tumor model was established with DMS 114, too, but this model is more suitable for experiments of longer duration. The in vivo results confirmed the in vitro morphology and the growth characterization: NCI-H460 was the fastest growing cell line in vitro and in vivo. Moreover, this tumor was found to have the highest malignancy among the investigated lung cancers, indicated by the intense mitotic activity both in vitro and in vivo.

3.4 Summary and conclusion

Three human lung cancer cell lines obtained from the ATCC were characterized with the objective to establish a subcutaneous and an intracerebral tumor model in nude mice for in vivo treatment experiments. Therefore, the cell lines were examined with respect to their in vitro and in vivo morphology and growth, respectively, their number of chromosomes, and their chemosensitivity against several selected cytostatic agents. The NCI-H460, a N-SCLC cell line, and the SCLC cell line DMS 114 proved to be particularly suited.

NCI-H460 was identified as a highly malignant cell line both in vitro and in vivo. The cells were tumorigenic in athymic mice and generated solid subcutaneous tumors. The growth of the NCI-H460 cells in vitro and the subcutaneous tumors in vivo was stable and reproducible. The cell proliferation was significantly effected by various cytostatic drugs, particularly by taxanes such as docetaxel. The cell line NCI-H460 is suitable for the establishment of a tumor model in nude mice with an aggressively and rapidly growth as a human lung cancer.

The DMS 114 cell line showed the well-known characteristics of tumor cells such as intense mitotic activity both in vitro and in vivo. The chromosome distribution of the DMS 114 cells remained constant during the cultivation period. Giant multinucleated cells were visible in Papanicolaou stained cells as well as in MG-stained tumor sections. The portion of the giant cells remained unchanged during the cultivation period. DMS 114 cells grew slower compared to NCI-H460 cells. Furthermore, they were most sensitive to the selected cytostatic drugs. The cell growth was affected already at nanomolar concentrations of the drugs. Therefore, a subcutaneous model in mice was established with the DMS 114 lung cancer cell line as well, which was very suitable for long time studies.

In contrast to NCI-H460 and DMS 114, the minimal doubling time of the third lung cancer cell line, DMS 53, decreased with higher passages, and the cells were poorly tumorigenic in nude mice. Thus, the DMS 53 cell line was excluded from further investigations.

In summary, subcutaneous tumor models were established in nude mice using the human lung cancer cell lines NCI-H460 and DMS 114.

Chapter 4

Establishment and application of a calcein-AM efflux assay

4.1 Introduction

P-glycoprotein 170 (p-gp) is an unusual member of the highly conserved superfamily of ATP-binding cassette (ABC) transport proteins as it recognizes a broad variety of structurally and mechanistically unrelated agents in comparison to other transport proteins (Seelig 1998). The literature describes three different drug transport models: the classical pump, the vacuum cleaner and the flippase model (Sharom 2003). In case of the pump model p-gp interacts with its substrate at the cytosolic side of the plasma membrane and pumps the substrate across the membrane to the extracellular site via a transport channel. The vacuum cleaner model suggests that hydrophobic substrates are delivered by p-gp to the extracellular side after interaction with p-gp within the lipid bilayer of the plasma membrane. In the flippase model it is assumed that the hydrophobic p-gp substrates interact with p-gp within the inner leaflet of the cytoplasmic membrane leading to a translocation into the outer leaflet (Higgins and Gottesman 1992). However, the exact transport mechanism seems to be very complex and is still unclear. Hence, the determination of p-gp transport activity as well as the identification and classification of p-gp substrates is difficult.

Various in vitro screening assays have been developed to examine p-gp activity by

quantification of ATPase activity or by means of radioactively labelled ligands or fluorescent dyes using isolated cells, cell monolayer cultures or isolated tissues (Bauer et al. 2003, Schwab et al. 2003). Cell monolayer cultures are routinely used in industry to investigate the effect of p-gp mediated efflux on the penetration of different drugs across the monolayer. The assays are mainly performed with the p-gp overexpressing cell lines Caco-2 and MDKC (Horio et al. 1989, Kim et al. 1998). For compounds, which are studied in this monolayer system, low to moderate passive permeability is required to detect the influence of p-gp on their transport across the cell monolayer (Lentz et al. 2000).

In the ATPase assay the high-capacity ATP hydrolytic activity of p-gp is measured by monitoring the release of inorganic phosphate with a colorimetric reaction (Urbatsch et al. 1994). Since the ATPase activity is drug dependent, it directly reflects the drug transport capability of p-gp and can be used to identify high-affinity substrates of p-gp (Scarborough 1995). However, several well known p-gp substrates such as vincristine or ivermectine show no stimulation of the ATPase activity (Schwab et al. 2003) and thus, are not identified as p-gp substrates by the ATPase assay.

Another approach to determine the transport activity of p-gp are micro-pH measurements presented by Landwojtowicz et al. (2002). This method is based on the observation that p-gp ATPase activation causes a cytosolic alkalinization in p-gp overexpressing cells (Roepe et al. 1993). The increased cytosolic pH results in an acidification of the cell culture medium which can be detected by pH microsensors (McConnell et al. 1992). However, the mechanism of proton translocation is still unknown.

Assays with radioactively labelled compounds such as [^{3}H]colchicine or [^{3}H]vinblastine are another possibility to identify p-gp substrates and to examine p-gp activity. Begley et al. (1996) used this method to prove the expression of p-gp in the immortalized cell line RBE4, derived from rat cerebral capillary endothelial cells. However, the separation of cell associated radioactivity from unbound radiolabeled ligands in the surrounding medium is a major obstacle of this method. In addition, screening assays should be performed without the use of radioactivity due to safety and environment protection aspects.

Fluorescence assays, which are mostly performed with rhodamine 123 or calcein-acetoxymethylester (calcein-AM) present an alternative to the aforementioned radiochemical assays. They allow a rapid screening of both cell lines and compounds concerning p-gp

expression and affinity, respectively, in a relatively short time. Before these two compounds were used for detecting p-gp substrates, transport studies were mostly carried out on the basis of doxorubicine (Wall et al. 1993). As rhodamine 123 is a substrate of p-gp, the rhodamine 123 uptake in p-gp expressing cells is decreased compared to the rhodamine 123 uptake in cells without a MDR1 phenotype. There is an inverse correlation between expression of p-gp and cellular uptake of rhodamine 123. The use of rhodamine 123 in such a fluorescence screening assay to identify p-gp substrates or inhibitors is hampered by the mitochondrial trapping of the dye (Scaduto and Grotyohann 1999). Furthermore, rhodamine 123 is a fluorescent substance, which leads to similar problems as in radiochemical experiments with respect to the separation of rhodamine 123 loaded cells from free rhodamine. The separation step may affect the integrity of the cells and may cause leakage of the dye (Bauer et al. 2003). On the contrary, calcein-AM is most suitable for the use in a fluorescence assay to identify either p-gp expression in cells or p-gp substrates and p-gp inhibitors (Schwab et al. 2003). Non-fluorescent calcein-AM is transformed into calcein, which is strongly fluorescent and trapped inside the cells (see chapter 4.3). Hence, in contrast to the fluorescent rhodamine 123, high concentrations of calcein-AM located in buffer do not interfere with the measurements of cell associated fluorescence. Moreover, additional preparation steps are not required and the adulterations of the measured fluorescence due to dye leakage are minimized. In contrast to micro-pH measurements the mechanism of calcein-AM efflux is well-known (see chapter 4.3). The calcein-AM efflux assay can be performed within a few hours compared to one day in case of radiochemical assays. Nowadays, calcein-AM is widely used in cell biology studies of intracellular ion activities.

In this chapter a calcein-AM efflux assay is described and different applications of the assay such as the determination of p-gp expression in tumor cells or identification of p-gp substrates are exemplified. Additionally, the feasibility of the calcein-AM efflux assay in common cuvette measurement and at the flow cytometer is compared.

4.2 Materials and methods

4.2.1 Drugs and reagents

Calcein-AM was obtained from Molecular Probes (Eugene, OR, United States). Calcein-AM was dissolved in DMSO (Merck, Darmstadt, Germany) to achieve a final concentration of 1 mM and aliquoted into stock solutions that were stored at -20 ℃. Calcein was prepared by cleaving the ester bonds of calcein-AM with 0.2 % porcine esterase (Sigma, München, Germany) in phosphate buffer, pH 7.4, at 37 ℃ for 1 hour. Vinblastine and R-verapamil were received from Sigma. SDZ PSC 833 (Valspodar®) was a gift from Novartis (Nürnberg, Germany). Rapamycin (Sirolimus®) was kindly provided by Wyeth Pharma (Nürnberg, Germany). The suppliers of the other chemicals are mentioned in chapter 3. Loading buffer consisted of 120 mM NaCl, 5 mM KCl, 2 mM $MgCl_2 \cdot 6H_2O$, 1.5 mM $CaCl_2 \cdot 2H_2O$, 25 mM HEPES and 10 mM glucose and was adjusted to pH 7.4. Loading suspension contained loading buffer supplemented with 20 mg/ml of bovine serum albumin (Serva, Heidelberg, Germany) and 5 μl/ml of Pluronic F127 (20 % in DMSO). PBS composition is specified in chapter 3.

4.2.2 Cell culture

All cell lines were purchased from the American Type Culture Collection (ATCC, Rockville, MD, USA) and cultured as monolayers in 75 cm^2 flasks (Nunc, Wiesbaden, Germany). The cell cultures were maintained at 37 ℃/5 % CO_2 in different culture media. Kb-V1 cells (wildtype) were cultivated in DMEM culture medium (Sigma) supplemented with 3.7 g/l of sodium hydrogen carbonate, 110 mg of sodium pyruvate and 10 % of FCS and adjusted to pH 7.4. The cultivation of NCI-H460 is described in chapter 3. Subculturing was carried out with 0.2 % trypsin/EDTA (Viralex, Paa Laboratories) in PBS once a week. The p-gp overexpressing subclones of Kb-V1 and NCI-H460 cells, termed Kb-V1/VBL and NCI-H460/VBL, respectively, were obtained by adding increasing amounts of a vinblastine solution after subculturing to achieve a vinblastine concentration of 300 ng/ml culture medium within a period of about 90 days (66.7 μl of 10^{-4}M vinblastine in 70 % ethanol). After 3 passages the modified cell lines expressed sufficient quantities of p-gp. New cells were thawed after Kb-V1/VBL cell line was cultivated for about 15 weeks.

4.2.3 Calcein-AM efflux assay

Flow cytometry The assay was carried out with slight modifications according to Hollo et al. (1994), Homolya et al. (1993) and Homolya et al. (1996). Cells were trypsinized 3 or 4 days after the passaging and washed with PBS at 25 ℃. To 0.75 ml cell suspension containing $1 \cdot 10^6$ cells in loading buffer 0.25 ml loading suspension was added. The samples were mixed with different concentrations of test compounds and vortexed. After 15 min calcein-AM solution (1 mM in DMSO) was added to achieve a concentration of 1 μM. If cells were examined regarding their p-gp functionality, calcein-AM was given directly to the samples. After an incubation for 10 min at 37 ℃/5 % CO_2 the supernatant was discarded after centrifugation for 7 min at 4 ℃ and 1100 rpm. The cell pellet was rinsed once with ice cold PBS and resuspended in 0.5 ml of loading buffer per $1 \cdot 10^6$ cells. Calcein fluorescence was measured by a FACS Calibur™ (Becton Dickinson, Heidelberg, Germany) flow cytometer in the FL1-H channel. In each measurement 30,000 gated events were evaluated. The photomultiplier settings were as follows: E-1 for FSC, 270 for SSC and 300 for FL1-H. Data were analyzed by the WinMDI 2.8 software.

Conventional fluorimetry Cells were seeded in black 96-well plates with transparent bottom (Nunc) at a density of 10 and 25 cells per well in case of the Kb-V1 and Kb-V1/VBL cell line, respectively. After an incubation of 4 days at 37 ℃/5 % CO_2, the subconfluent cells were washed with PBS and preincubated for 15 min at room temperature with 50 μl loading buffer which contained test compounds in various concentrations. Then, 50 μl of 2 μM calcein-AM in loading buffer were added so that the final calcein-AM concentration amount to 1 μM. The cells were incubated for 10 min at 37 ℃/5 % CO_2 and rinsed three times with ice cold PBS. PBS was carefully removed by suction and replaced with 200 μl of Triton-X-100 solution per well to lyse the cells. Subsequently, plates were gently shaken on a Köttermann 4010 shaker for 30 min. Calcein fluorescence was measured by Fluoroskan Askent Labsystem™ microplate reader (Franklin, MA, Unites States) with an excitation wavelength of 485 nm and an emission wavelength of 538 nm.

4.2.4 Time-resolved measurements on the flow cytometer

Cells were prepared as described in the calcein-AM-efflux assay for the flow cytometer. Each sample contained $3 \cdot 10^6$ cells in 3 ml of loading buffer. After preincubation with the test compounds, the samples were measured with a FACS Calibur™ flow cytometer at the same parameter as used for the calcein-AM efflux assay. Calcein-AM addition was carried out after 30 s with a Hamilton syringe. Care was taken that the sample tubes were at a stable temperature of 37 ℃ during the experiment. The fluorescence intensity increase at FL1-H channel was recorded over a period of 7.5 min. Data were analyzed by the WinMDI 2.8 software and the fluorescence events in channel FL1-H were plotted against the time.

4.3 Principle of the calcein-AM efflux assay

Calcein-AM is a non-fluorescent, lipophilic ester, that rapidly penetrates the plasma membrane of cells (Fig. 4.1 a). Inside the cells the ester bonds are cleaved by nonspecific esterases and highly fluorescent calcein is generated (Fig. 4.2 a). Calcein (Fig. 4.1 b) is hydrophilic and thus, trapped inside the cells, so that intracellular fluorescence can be measured. Calcein-AM is a substrate of p-gp. In cells of the MDR1 phenotype calcein-AM is extruded by p-gp before esterases can cleave the ester bonds and calcein is not accumulated (Fig. 4.2 b).

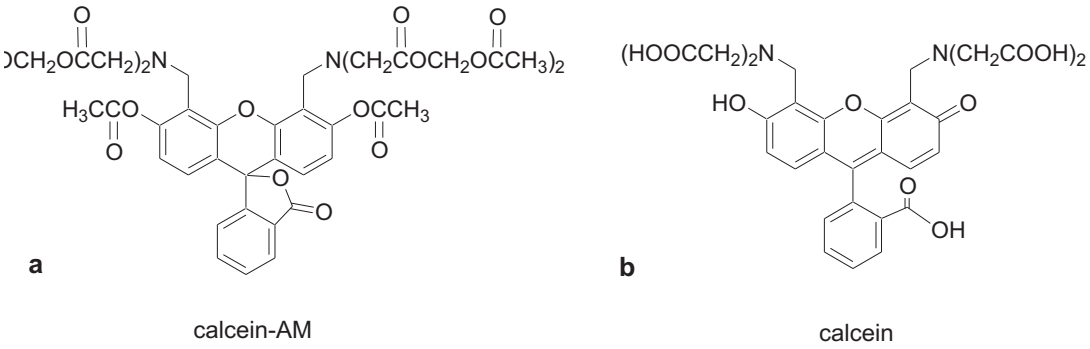

Figure 4.1: Structures of calcein-AM (a) and calcein (b)

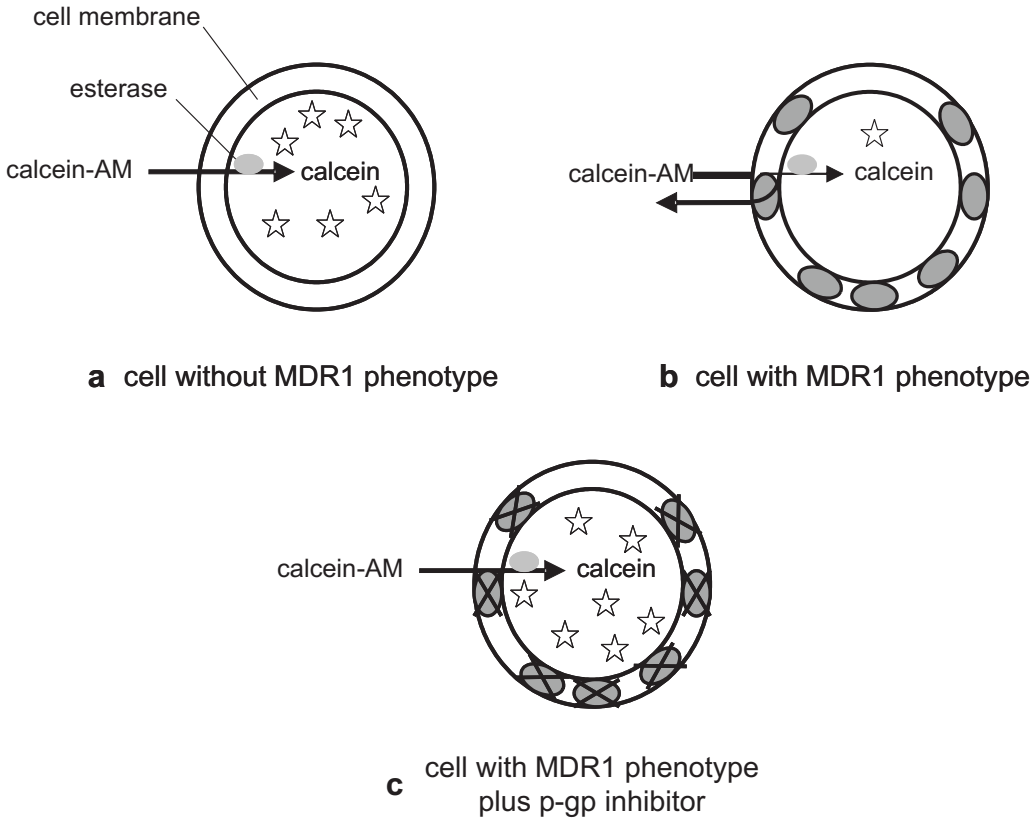

Figure 4.2: Principle of the calcein-AM efflux assay: in cells without MDR1 phenotype the fluorescence dye calcein is formed by intracellular hydrolysis of non-fluorescent calcein-AM, a p-gp substrate, by esterases (a). In MDR positive cells overexpression of p-gp increases extrusion of calcein-AM from the cell membrane before hydrolysis takes place, leading to a reduced accumulation of calcein (b). The calcein-AM efflux is blocked by addition of a p-gp inhibitor (c).(from Bauer et al. (2003) with modifications)

Thus, the intracellular fluorescence is significantly higher in cells with low or no p-gp expression than in multidrug resistant cells. Inhibition of p-gp mediated calcein-AM transport by certain modulators decreases the calcein-AM efflux. Depending on the modulator concentration this results in an intracellular calcein fluorescence comparable with cells without a MDR1 phenotype. Therefore, intracellular fluorescence is indicative for either an inhibition of p-gp by an added p-gp inhibitor or of cells expressing non-functional p-gp.

The intracellular calcein fluorescence can be detected by means of conventional fluorimetry, flow cytometry and laser-scanning microscopy (Hollo et al. 1994). The fluorescence excitation and emission maxima of calcein are 496 and 517 nm, respectively (Fig. 4.3).

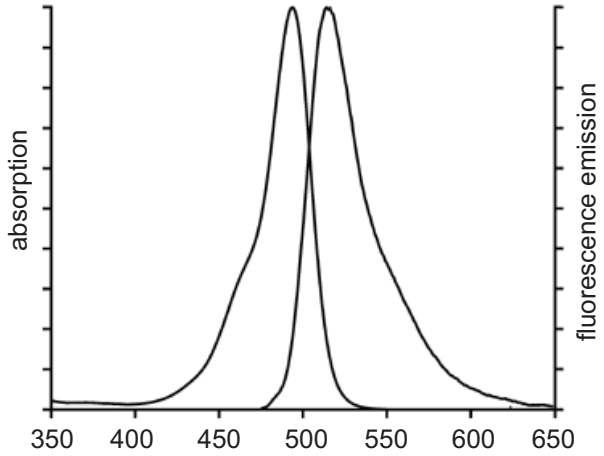

Figure 4.3: Excitation (λ_{em}=517 nm) and emission (λ_{ex}=496 nm) spectrum of calcein in phosphate buffer pH 9.

Preceding investigations such as examination of the autohydrolysis of calcein-AM and the photostability of calcein proved the high stability of the compounds (data not shown) and confirmed the suitability of this fluorescent dye system for the investigation of p-gp efflux in cells.

4.4 Optimization of the calcein-AM efflux assay for flow cytometry

Various experimental procedures for the calcein-AM efflux assay are described in literature (Homolya et al. 1993, Hollo et al. 1994, Feller et al. 1995, Liminga et al. 1994, Legrand et al. 1998). They differ in several parameters such as incubation time, incubation temperature, calcein-AM concentration and cell number in the sample. The calcein-AM loading concentration of the cells is depending on the used calcein-AM concentration and the number of cells per sample. Homolya et al. (1996) examined the appropriate conditions for the calcein-AM efflux assay in great detail and found that at calcein-AM concentrations between 0.1 to 1 μM and cell numbers between $5 \cdot 10^4$ ml^{-1} and $1 \cdot 10^6$ ml^{-1}, clearly distinguishable fluorescence differences between p-gp expressing cells and cells without a MDR1 phenotype can be detected.

In our department a fluorescence assay was established for the determination of intra-

cellular calcium using fluo-4 at the flow cytometer (Schneider et al. 2002). Calcein-AM is analogous to fluo-4. Fluo-4, an acetoxymethylester, can easily penetrate the cell membrane. Inside the cell the ester bonds of fluo-4 are cleaved by intracellular esterases and the resulting fluo-4 can complex intracellular calcium. Due to the similar uptake and transformation mechanism of both fluo-4 and calcein-AM the loading procedure of the fluo-4 assay can be adapted to the calcein assay using Pluronics F-127 to improve the solubility of calcein-AM and its penetration into the cells (Granados et al. 1997).

To optimize the aforementioned assay conditions for the calcein-AM efflux assay several experiments were carried out using Kb-V1 cells (wildtype) which are negative for the MDR1 phenotype. In a first series of experiments the incubation time and the incubation temperature were altered (Fig. 4.4 and Fig. 4.5). Subsequently, the optimal calcein-AM loading concentration was determined by incubation of cells with different calcein-AM concentrations ranging from 0.5 to 2.0 μM under the optimized conditions described above (Fig. 4.6).

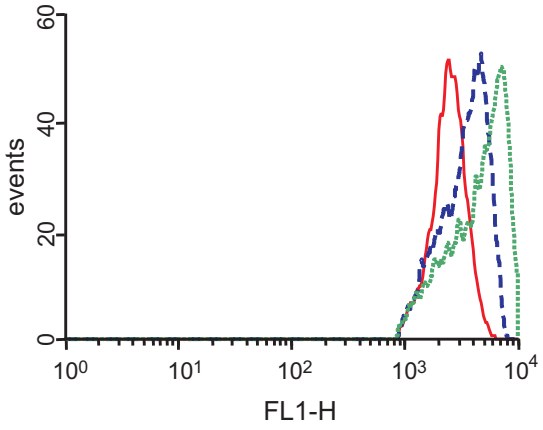

Figure 4.4: Optimization of calcein-AM efflux assay conditions by variation of incubation times using Kb-V1 wildtype cells (10 min - solid line, 30 min - dashed line, 60 min - dotted line). All experiments were carried out at 25 °C using a cell number of $1 \cdot 10^6$ ml^{-1} and a calcein-AM concentration of 1.25 μM.

In Fig. 4.4 the results of the calcein-AM assay carried out at 10, 30 and 60 min, respectively, are displayed in histograms. The cell associated fluorescence increased with longer incubation times. However, the fluorescence intensity measured after an incubation time of 10 min is even high enough for p-gp activity measurements compared to that after

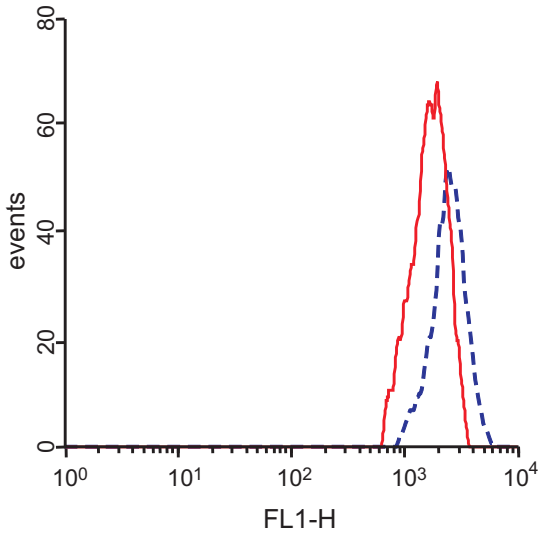

Figure 4.5: Optimization of calcein-AM efflux assay conditions by variation of incubation temperatures using Kb-V1 wildtype cells (37 ℃ - solid line, 25 ℃ - dashed line). All experiments were carried out using a cell number of $1 \cdot 10^6$ ml^{-1}, a calcein-AM concentration of 1.25 μM and an incubation time of 10 min.

a 60 min incubation. Therefore, the calcein-AM efflux assay can be performed with an incubation time of 10 min. In a next step, the incubation temperature was varied (Fig. 4.5). The cell associated fluorescence after an incubation at 37 ℃ was similar compared to the fluorescence intensity after an incubation at 25 ℃. As with an incubation at 37 ℃

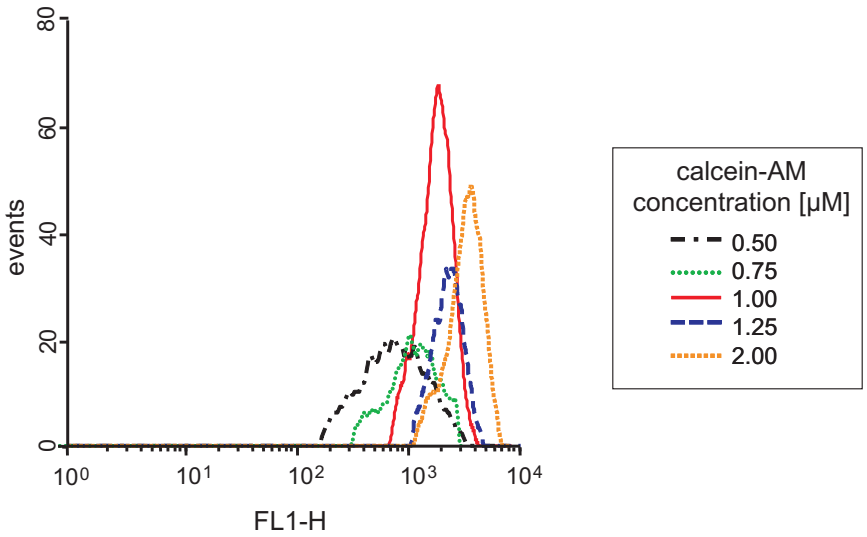

Figure 4.6: Optimization of calcein-AM efflux assay conditions by variation of calcein-AM loading concentrations using Kb-V1 wildtype cells. All experiments were carried out at the optimized incubation conditions using a cell number of $1 \cdot 10^6$ ml^{-1}.

physiological conditions can be simulated, this temperature was chosen for the calcein-AM incubation.

After the optimization of the incubation conditions the appropriate calcein-AM concentration was determined (Fig. 4.6). The fluorescence intensities increased with increasing calcein-AM concentrations. The maximum fluorescence intensities did not differ very much. However, the distribution of the fluorescence intensities after an incubation with 0.5 and 0.75 μM, respectively were relatively broad compared to incubation with higher calcein-AM concentrations. Thus, in order to get a narrow distribution of fluorescence intensities and to use only a minimum of calcein-AM, the optimal calcein-AM concentration was determined to 1.0 μM.

Analyzing the calcein-AM efflux in Kb-V1/VBL cells, that are a p-gp overexpressing subclone of the Kb-V1 cell line, a much lower cell assiciated fluorescence intensity was detected compared to the fluorescence intensity of calcein loaded Kb-V1 cells due to the p-gp mediated efflux of calcein-AM before its transformation into calcein. Both signals were well separated from each other (Fig. 4.7). Hence, Kb-V1/VBL cells provide a system that can be used for the examination of substances with respect to their influence on p-gp mediated efflux. Kb-V1 wildtype cells serve as a positive control for the p-gp mediated calcein-AM efflux. Using the determined parameters for the calcein-AM assay MDR1

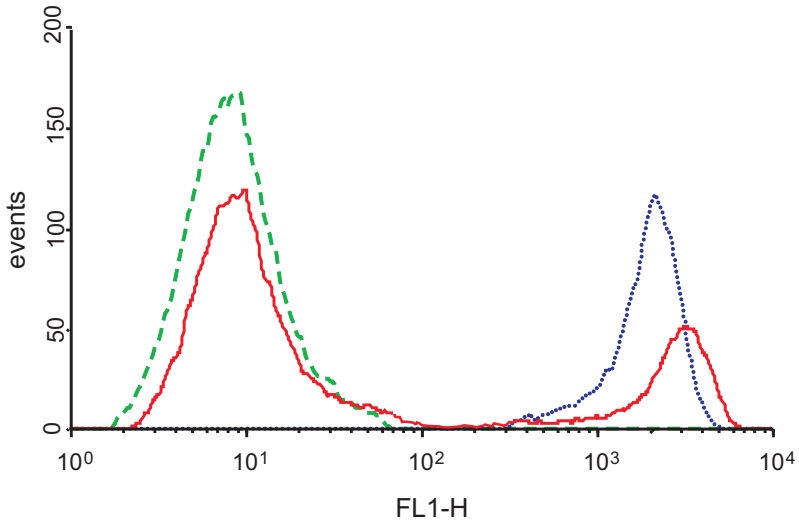

Figure 4.7: Calcein-AM efflux assay with Kb-V1 (dotted line) and Kb-V1/VBL (dashed line) cells carried out at the optimized assay parameters (mixed population - solid line; 10 min, 37 °C, 1 μM calcein-AM, $1 \cdot 10^6$ ml^{-1} cells)

positive and MDR1 negative Kb-V1 cells could be even detected with this assay if they are examined in a mixed cell population (Fig. 4.7).

In summary, the appropriate conditions for the calcein-AM efflux assay to identify p-gp expression in cells and to investigate p-gp substrates and inhibitors are an incubation temperature of 37 ℃, an incubation time of 10 min and a calcein-AM concentration of 1 μM using $1 \cdot 10^6$ cells ml^{-1} in each sample.

4.5 Applications of the calcein-AM efflux assay

4.5.1 Identification of p-glycoprotein expressing cells

In order to identify expression of functional p-gp in cell lines, it is not sufficient to examine the transcription of p-gp encoding mRNA by PCR or the p-gp expression with immunohistochemistry. Using these methods no further information can be obtained concerning the functionality of p-gp in the cells (Krishan et al. 1997). In contrast, the calcein-AM efflux assay provides an analytical system for the determination of functional p-gp. For this purpose, cells were incubated with calcein-AM according to the method described in chapter 4.3. The lower the intensity of the intracellular calcein fluorescence, the greater is the activity and therefore, the expression of functional p-gp.

In Fig. 4.8 the results of the calcein-AM efflux assay of wildtype and MDR resistant NCI-H460 cells are illustrated. Although the NCI-H460 cell line characterized in chapter 1 possessed the mRNA encoding p-gp (Fig. 4.8 b), it showed an intense intracellular fluorescence in the calcein-AM efflux assay (Fig. 4.8 a). This leads to the assumption that p-gp is not or at least not functionally expressed in this cell line. Different cell subclones of NCI-H460/VBL were prepared by cultivation of the NCI-H460 wildtype cells with increasing vinblastin concentrations. After 3 weeks of cultivation the subclones expressed functional p-gp resulting in significantly lower intracellular fluorescence of the NCI-H460/VBL cells compared to the wildtype. The intensity of the intracellular fluorescence decreased with increasing p-gp expression.

In conclusion, the calcein-AM efflux assay is a suitable method to determine the p-gp activity of a cell line in a very short time. Results are available in a few hours rather than in more than one day in the case of using PCR or immunohistochemistry methods.

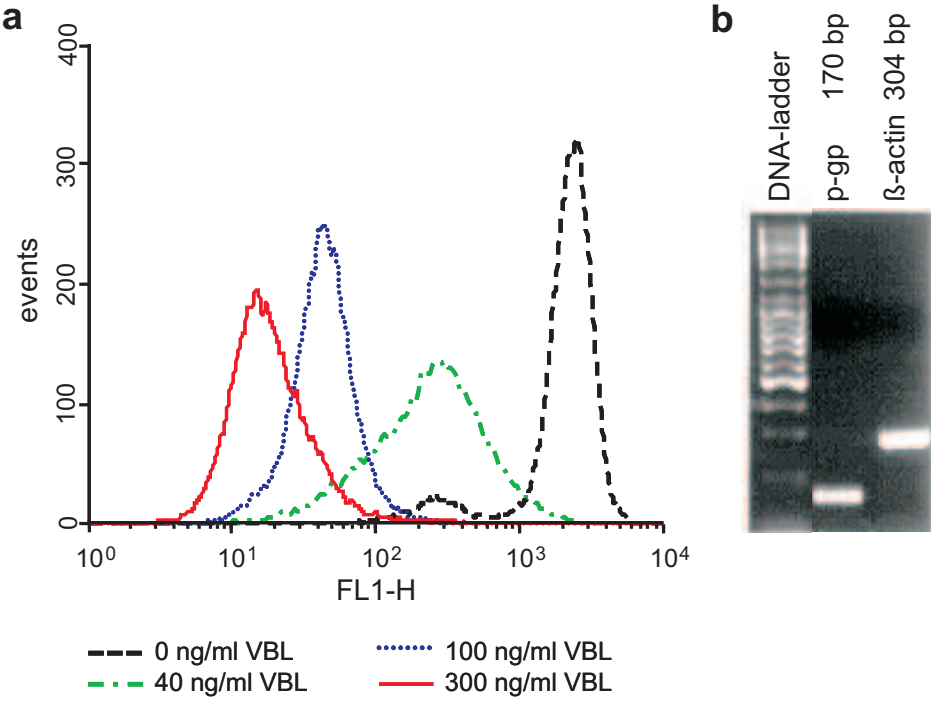

Figure 4.8: (a) Induction of MDR1 phenotype in NCI-H460 cells by cultivation with increasing vinblastine concentrations over 90 days quantificated by the calcein-AM efflux assay. (b) Qualitative determination of mRNA encoding p-gp in wildtype NCI-H460 cells (ethidiumbromide stained agarose gel after RT-PCR (34 cycles); β-actin served as a control)

Additionally, a close relationship between the intracellular fluorescence intensity and the quantity of expressed p-gp is obvious.

4.5.2 Characterization of p-glycoprotein substrates and modulators

Ineffectivity of tumor chemotherapy is often caused by the multidrug resistance of malignant cells and by the localization of multidrug transporters such as p-gp at several barriers inside the body. Various substances are developed which are not transported by p-gp but modulate the p-gp mediated efflux of p-gp substrates. The efficacy of these modulators was studied in p-gp overexpressing Kb-V1/VBL cells using the calcein-AM efflux assay. Cells were preincubated with the test compound for 15 min, and the assay was carried out subsequently according to the procedure described in chapter 4.3. If the test compound interacts with p-gp as a modulator, the intracellular fluorescence intensity increases be-

cause p-gp transport of calcein-AM is blocked and calcein is formed and accumulates in the cells (see Fig. 4.2 c). As a representative of 1^{st} generation modulators, R-verapamil (Fig. 4.9 a) and of 2^{nd} generation modulators, valspodar (Fig. 4.9 b), were examined. Both are well known as p-gp modulators in the literature (Holland et al. 2003).

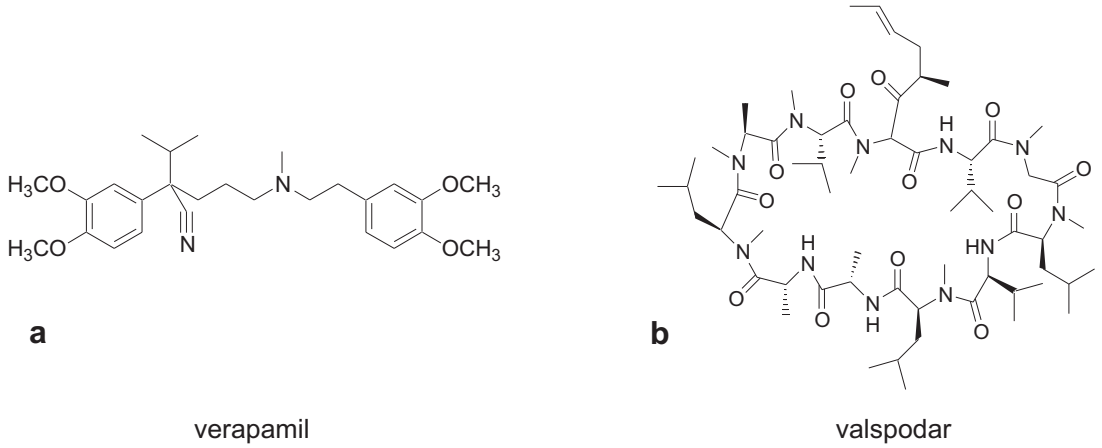

Figure 4.9: Structures of the 1^{st} generation p-gp modulator verapamil (a) and the 2^{nd} generation p-gp modulator valspodar (b)

Increasing concentrations of either verapamil or valspodar led to an elevated intracellular calcein fluorescence (Fig. 4.10 a and Fig. 4.11 a). This is explained by the increasing inhibition of the p-gp activity mediated by the two p-gp modulators. Concentration-response profiles were acquired by incubation with various concentrations of the respective modulator. For that purpose, the geometric means of the obtained histograms were plotted against the modulator concentrations (Fig. 4.10 b and Fig. 4.11 b) and the IC_{50} values were determined. An IC_{50} value of 248 μM was calculated using the Hill equation for the p-gp modulation by verapamil. In case of valspodar an IC_{50} value of 1.63 μM was determined. The intensity shift caused by the inhibition of the p-gp mediated efflux is different for the two modulators. In the case of valspodar the fluorescence intensity abruptly increased at valspodar concentrations higher than 0.3 μM. However, when verapamil was used to inhibit p-gp, the fluorescence intensity increased gradually (for further investigations see chapter 4.5.3). Moreover, the p-gp modulation by verapamil was not maximal as the fluorescence intensity was still increasing at 300 μM of verapamil. Verapamil concentrations higher than 300 μM were not used due to solubility problems. Therefore, the half maximum inhibitory concentration of 248 μM represents only an estimation.

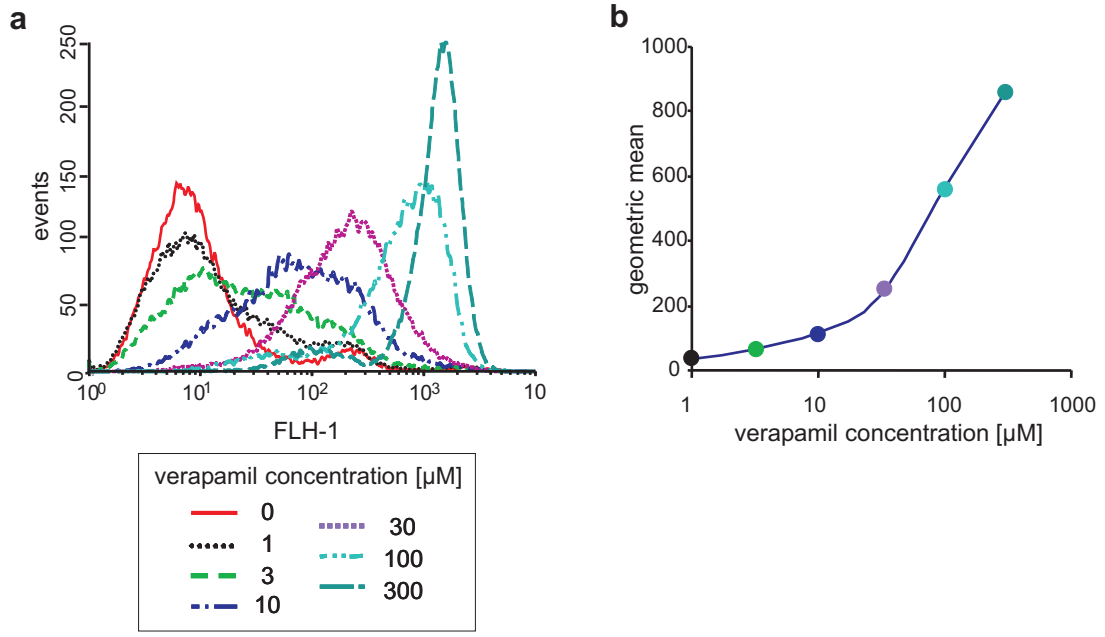

Figure 4.10: Modulation of p-gp activity by increasing concentrations of R-verapamil. Fluorescence intensity increased with increasing R-verapamil concentrations (a). Plotting of geometric means against the R-verapamil concentration leads to concentration response curves (b).

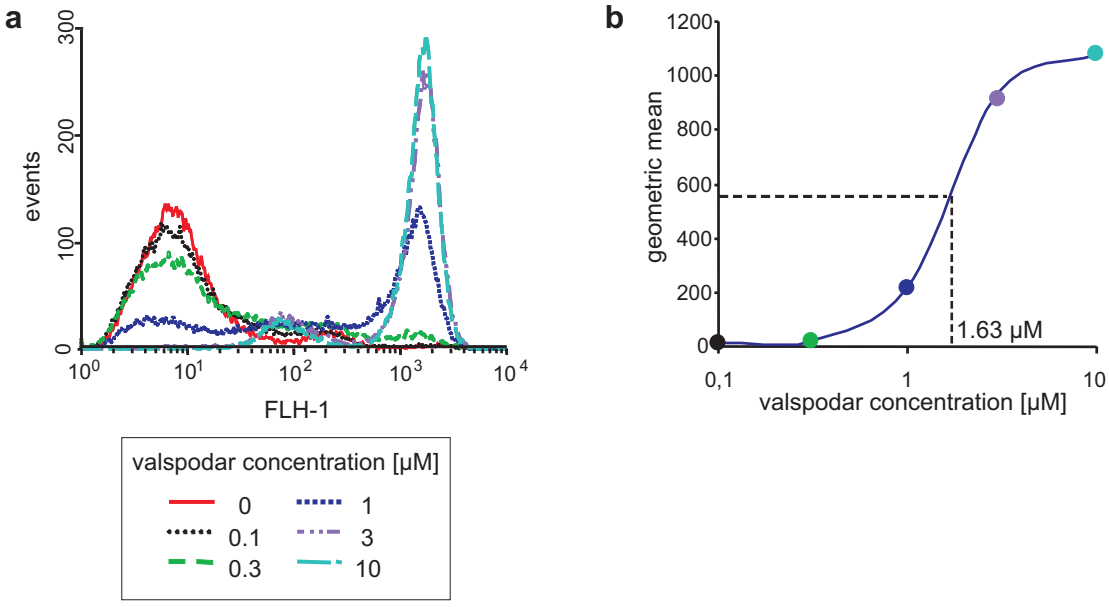

Figure 4.11: Modulation of p-gp activity by increasing concentrations of valspodar. Fluorescence intensity increased with increasing valspodar concentrations (a). Plotting of geometric means against the valspodar concentration leads to concentration response curves. The calculated IC_{50} value is 1.63 μM. (b).

In addition to a complete inhibition of the p-gp activity, it is important to regard the limited solubility of the test compounds in the aqueous assay system to calculate precise IC_{50} values. The results of the p-gp modulation by the immunosuppressant rapamycin in the calcein-AM efflux assay are shown in Fig. 4.12. A correlation between the shift of the fluorescence intensity in channel FL1-H and the added rapamycin could not be established. The fluorescence intensities decreased at high amounts of rapamycin. Considering the solubility of rapamycin in water (Fig. 4.13), it becomes obvious that rapamycin is only partially soluble in aqueous systems at concentrations higher than 30 μM. In literature

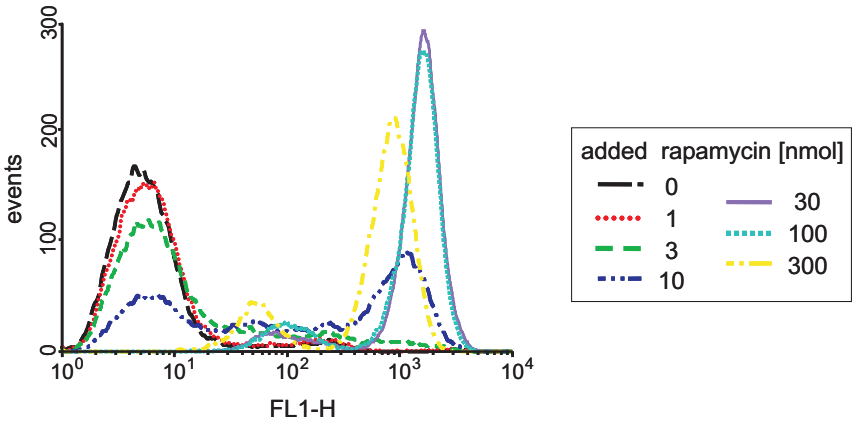

Figure 4.12: Modulation of p-gp activity by increasing amounts of rapamycin. There is no correlation between the shift of the fluorescence intensity and the added rapamycin.

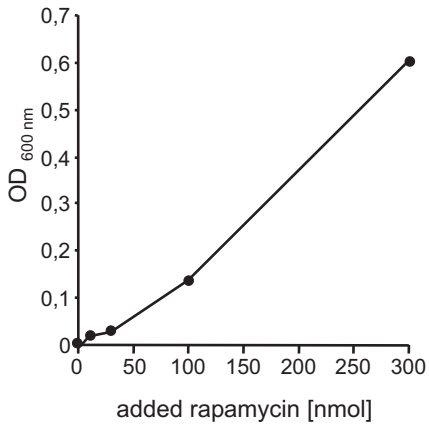

Figure 4.13: Solubility of rapamycin in loading buffer determined by turbidimetric analysis at λ_{600nm}. Rapamycin is not soluble in aqueous solutions in concentrations higher than 30 μM.

the solubility of rapamycin in water is even given as low as 0.3 μM. Hence, conclusions about the exact concentration of the drug responsible for the p-gp modulation in the calcein-AM efflux assay cannot be drawn.

It becomes clear that accurate results in the calcein-AM efflux assay can only be obtained for those substances that are sufficiently soluble in aqueous systems. Furthermore, false negative results are achieved if the affinity of a test compound for p-gp is lower compared to the p-gp affinity of calcein-AM (Homolya et al. 1993). In that case calcein-AM is the preferred substrate of p-gp and is being effluxed by p-gp.

In summary, the distinction between p-gp substrates and inhibitors is difficult. Using the calcein-AM efflux assay, the potency of p-gp modulation can be assessed. However, only interactions of p-gp substrates with a higher affinity to p-gp compared to calcein-AM can be detected.

4.5.3 Investigation of transport mechanisms by time-resolved measurements

The 1^{st} generation modulator verapamil and the 2^{nd} generation modulator valspodar significantly differ regarding the steepness of the corresponding concentration-response curves (Fig. 4.10 b and Fig. 4.11 b). This could be a hint to different inhibition mechanisms of the p-gp mediated efflux and was investigated by means of time-resolved measurements based on the calcein-AM efflux assay during the incubation period. Flow cytometry offers the possibility to observe changes in the fluorescence over an arbitrary period of time. In Fig. 4.14 the results of the time resolved measurements are shown. An increase in fluorescence intensity during the incubation period was observed as expected.

Calcein-AM was added after 30 s, and the experiment was aborted after 7.5 min when the fluorescence intensity of the control cells (Kb-V1 wildtype cells) was nearly constant. The diagrams show the measurements with the most pronounced changes of the slope of the concentration response curves. Immediately after calcein-AM addition, fluorescence rises irrespective of the modulator. The higher the modulator concentration, the faster is the increase in calcein fluorescence. Fluorescence intensities in channel FL1-H reached after 7.5 min correspond to the results depicted in Fig. 4.10 and Fig. 4.11. In conclusion,

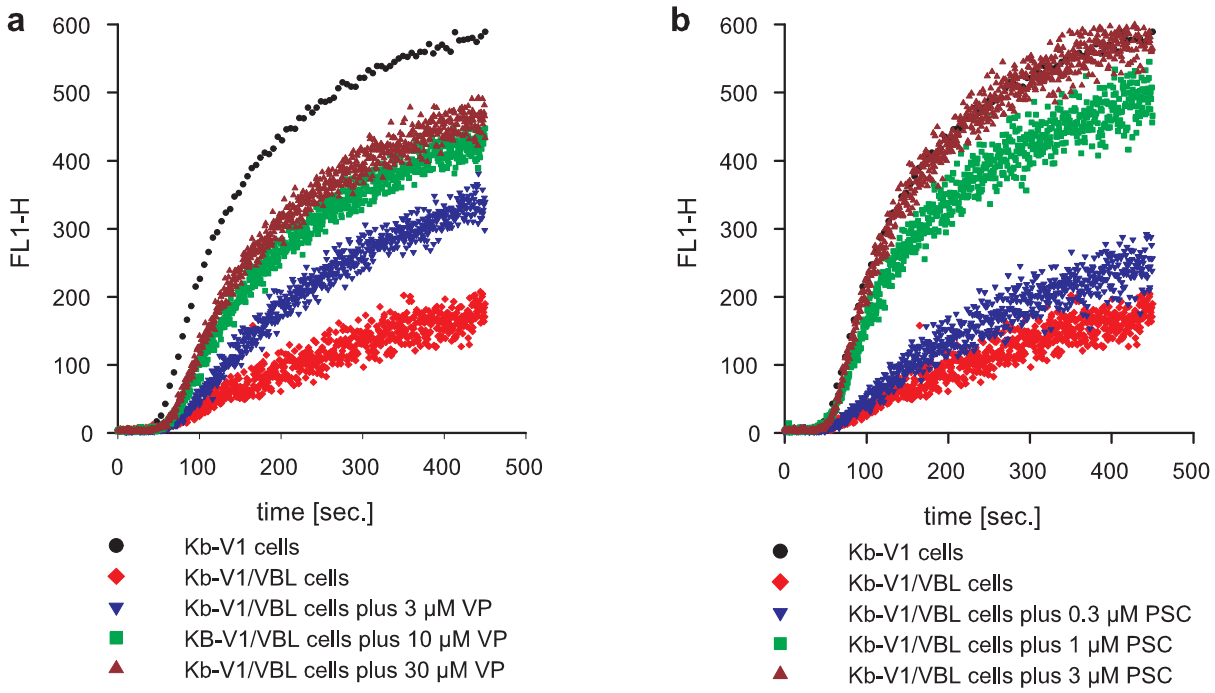

Figure 4.14: Time-resolved measurements of calcein fluorescence during incubation with different concentrations of verapamil (VP, a) and valspodar (PSC, b)

with respect to the explanation of the different slopes of the concentrations response curves no additional information could be obtained by this approach. Calculations of typical kinetic parameters (i.e. Michaelis constant K_m and maximum velocity v_{max}) based on the fluorescence intensity increase were impossible as well. Therefore, insight into the kinetic processes could not be gained. It is difficult to assess the transport procedures with respect to kinetic aspects, as the formation of calcein is controlled by two subsequent steps. First, calcein-AM has to be incorporated into the cells and in the second step the ester bonds have to be cleaved to form calcein. The first step is the more interesting one when characterizing the p-gp transport process. However, the separation of the two processes for a calculation is difficult and additional assays have to be carried out to clarify the transport processes.

4.6 Comparison of flow cytometry and fluorimetry with respect to the calcein-AM efflux assay

The calcein-AM efflux assay was adapted to the fluorimeter to confirm the reliability of the method. Advantages and drawbacks of the newly developed flow cytometric method in comparison to the conventional fluorimetric procedure are explained in the following. The assay was carried out in microtiter plates. As with conventional fluorimetry the fluorescence of a number of cells is measured at once, it is important to ensure the same cell density in each well. This aspect is negligible, if the assay is performed with the flow cytometer, since the fluorescence signals of single cells are detected in this case. To determine the intracellular calcein fluorescence with the fluorimeter cells were washed several times after loading with calcein-AM and then lysed to release the calcein.

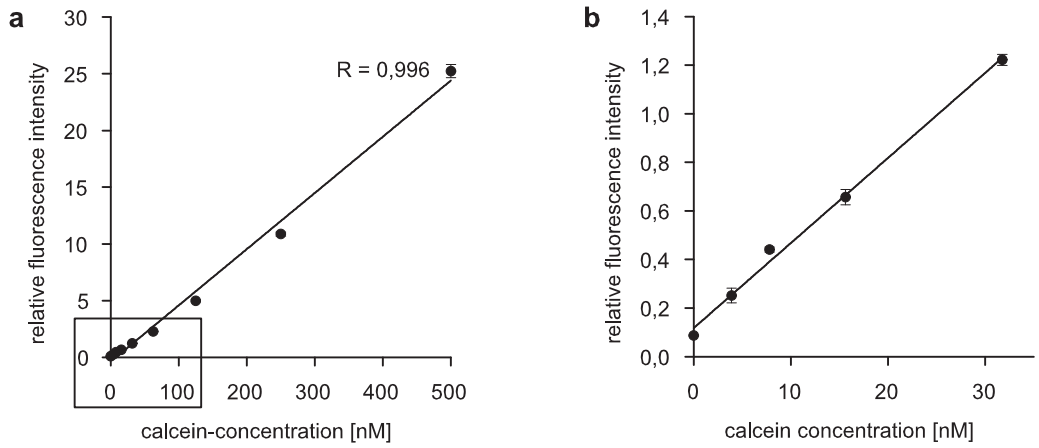

Figure 4.15: Calibration curve of calcein at the conventional fluorimeter. The framed data in (a) is presented in detail in (b) (λ_{ex} = 485 nm, λ_{em} = 538 nm)

As the sensibility of the fluorimeter for calcein fluorescence is a crucial point, a calibration curve was recorded (Fig. 4.15 a). As shown in Fig. 4.15 b even in low fluorescence intensity ranges the linearity of the calcein calibration was maintained.

To assess the reliability of the calcein-AM efflux assay, p-gp modulation experiments with valspodar were performed both with the fluorimeter and the flow cytometer using Kb-V1/VBL cells (Fig. 4.16). The curve shape was similar in both cases. The curves showed similar steepness and the IC_{50} values of 1.63 μM and 1.80 μM determined by flow

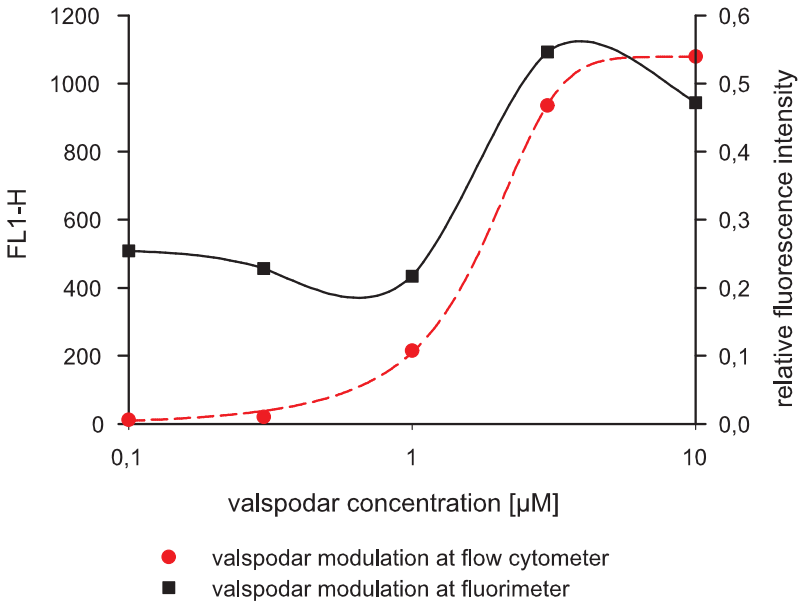

Figure 4.16: Comparison of p-gp activity modulation by valspodar with the flow cytometer and the fluorimeter using Kb-V1/VBL cells (10 min, 37 °C, 1 μM calcein-AM). The measurements at the fluorimeter are performed at lysed cells with $\lambda_{ex} = 485$ nm and $\lambda_{em} = 538$ nm. The fluorescence intensity at the flow cytometer is recorded in channel FL1-H.

cytometry and fluorimetric measurements, respectively, are in good agreement. Thus, the measurements of the p-gp activity in cells using the calcein-AM efflux assay, give reliable results.

The KB-V1 cells and the corresponding chemoresistant subclones grew irregularly leading to different cell concentrations in microtiter plates used in fluorimetry. In contrast, flow cytometry measurements are independent of cell growth due to the aforementioned single cell measurement principle. Moreover, the lysis of the cells, that is necessary to release the intracellular calcein for the measurements with the conventional fluorimeter, leads to an intensive light scattering. This results in a low signal-to-noise ratio that impairs the fluorescence intensity measurements up to valspodar concentrations of 1 μM. Exact fluorescence intensities can not be determined in this concentration range. In contrast, the flow cytometric determination of the calcein fluorescence intensities in dependence of p-gp modulation by valspodar resulted in significant concentration-response curves. Hence, the flow cytometric measurement is superior to the conventional fluorimetric procedures.

Therefore, all further calcein-AM efflux assay measurements were carried out with the flow cytometer.

4.7 Conclusions and summary

The calcein-AM efflux assay represents a convenient method to characterize the MDR1 phenotype with respect to the activity of expressed p-gp in cells. The method is useful for the investigation of p-gp modulators. However, the assay is not able to distinguish between transported substrates of p-gp and compounds with inhibitory properties. The prediction of the p-gp interaction is important for the screening of drug candidates. Furthermore, the characterization of the kinetics of the p-gp transport process has to be investigated for the development of potent p-gp inhibitors. This is especially true for agents with CNS activity. Further efforts have to be made to elucidate p-gp binding sites and the complex allosteric interactions (Martin et al. 2000) as well as to develop new assays for differentiation between inhibitors, transported substrates and non-transported substances. Today it is difficult to perform this classification with only one assay (Schwab et al. 2003) and the characteristics of substances in different assays must be considered to obtain information about the site of interaction for the tested compound (Polli et al. 2001). Computer based models are also used as computational filters to select drugs lacking the interaction with p-gp (Penzotti et al. 2002). However, the calcein-AM efflux assay is most suitable for primary screening of drug candidates and should be confirmed by transport assays and in vivo experiments.

Chapter 5

In vivo models of human lung cancer brain metastases

5.1 Introduction

Multidrug resistance (MDR) is one of the major obstacles to successful tumor therapy. The overexpression of P-glycoprotein 170 (p-gp) is the best characterized phenotype of MDR, although this is not the only mechanism involved (Gottesman and Pastan 1993). P-gp is not only expressed in chemoresistant tumor cells but also within normal cells of the human body, particularly in liver, kidney and the blood-brain-barrier (BBB). The localization of p-gp at the BBB is one of the drawbacks in the chemotherapy of primary and secondary brain tumors because of the protective function of p-gp that results in efflux transport of chemotherapeutic agents (Schinkel et al. 1995). A further problem in the treatment of brain metastases is the primary chemoresistance of tumors preferably metastasizing to the brain (Sawaya and Bindal 1995). However, in case of secondary brain tumors chemotherapy is preferred to locally acting methods such as radiation therapy and surgery because the whole brain is treated. In addition, the cytostatic drugs can act on the primary tumor as well as on metastases in organs other than the brain.

Secondary brain tumors represent approximately 40 % of intracranial neoplasms. In the United States annually approximately 170,000 cancer patients develop brain metastases. In adults, primary tumors that often metastasize to brain are lung cancer (50 %), breast

cancer (15 - 20 %), unknown primary neoplasms (10 - 15 %), melanoma (10 %), renal and colon cancer (both 5 %) (Kaye and Laws 1995). Brain metastases from unknown primary tumors are most likely from lung cancer (72 %). Furthermore, breast, renal and colon cancer produce single metastases, whereas metastases from lung cancer and melanoma are normally multiple (Wen and Loeffler 1999, Khosla 2004). Brain metastases contribute to cancer morbidity and mortality, and are responsible for the neurologic breakdown in cancer. As mentioned before the majority of secondary brain tumors originate from lung cancer which is characterized by a high fatality rate due to the advanced stage of disease at time of diagnosis and its aggressive biologic nature (Tuveson and Jacks 1999). Hence, need for new approaches to the treatment of lung tumor brain metastases is obvious. Possible new treatment strategies, e.g. the combination of anticancer drugs with ABC efflux transporter modulators, have to be examined first regarding their effectiveness in preclinical studies. For that purpose animal models are required that simulate the situation in the human body. At present, various mouse models are established including mice, which develop lung tumors spontaneously or after chemical induction, as well as transgenic mice, which express viral and cellular oncogenes (Tuveson and Jacks 1999). However, none of these models account for the development of brain metastases.

At our department an orthotopic tumor model, using nude mice bearing intracerebral human gliobalstoma, was developed to study the therapy of primary brain tumors (Fellner et al. 2002). For that purpose, human glioblastoma cells were injected intracerebrally into nude mice according to Altenschöpfer (1998). The anticancer agent paclitaxel was co-administered intravenously with valspodar, an inhibitor of the efflux transporter p-gp, to increase the paclitaxel concentration in the brain. The paclitaxel dose had to be reduced from 3 to 2 mg paclitaxel per kg body weight within the experiment due to the body weight reduction that is an indication of the toxicity of the combination with valspodar. In this study a significant increase in the brain paclitaxel concentration and a reduction of the tumor volume by 90 % was achieved with the combination treatment. Since the glioblastoma cells expressed no p-gp, the observed effect could only be explained by the p-gp inhibition at the BBB.

The aforementioned model was very useful to demonstrate that the combination strategy is a promising approach to the treatment of primary brain tumors. In principle, this

animal model can be adapted to study secondary brain tumors from lung cancer, and to investigate the therapeutic benefit of a treatment with a cytostatic in combination with p-gp modulators. Hence, this study was focussed on the treatment of secondary brain tumors originating from the lung. After an extensive characterization of selected human lung cancer cell lines (see chapter 3) the suitability of these cell lines for the presented brain tumor model was examined. In addition, the simulation of lung cancer brain metastases and their response to a combination treatment with valspodar was investigated.

5.2 Material and methods

5.2.1 Drugs and chemicals

SDZ PSC 833 (Valspodar®) was a gift from Novartis (Nürnberg, Germany). Paclitaxel and vinblastine used for the in vitro tests were purchased from Sigma (München, Germany). Stock solutions of all drugs were prepared in 70 % ethanol. For the treatment experiments Cellblastin® (Cellpharm, Hannover, Germany) and Taxol® (Bristol-Myers-Squibb, München, Germany) were used. All other chemicals and reagents were purchased either from Merck (Darmstadt, Germany) or from Serva (Heidelberg, Germany). The valspodar vehicle consisted of 52.2 g of cremophor RH40 (Caelo, Hilden, Germany), 15 g of absolute ethanol (Merck), 0.1 g of DL-α-tocopherol (Sigma), 7.5 g of propylene glycol (Merck) and 15 g of Labrafil M2125CS (Gattefosse, Weil am Rhein, Germany). The PCR primers were purchased from MWG Biotech (Ebersberg, Germany). Solution D contained 250 g guanidine thiocyanate (Merck), 293 ml demineralized water with DEPC, 17.6 ml sodium citrate (0.1 M, pH 7) and 26.4 ml 0.5 % N-lauryl sarcosine sodium salt (sacrosyl, Merck). All ingredients were dissolved at 64 °C. The composition of PBS and Bouin's solution is specified in chapter 3.

5.2.2 RNA-Isolation and RT-PCR

The isolation of total RNA was carried out according to the procedure of Chomczynski and Sacchi (1987). Human lung cancer cells were grown in 75 cm^2 flasks. When the cells were confluent, the culture medium was removed, and 5 ml of solution D was added

to lyse the cells. The solution was mixed with 0.5 ml of sodium acetate (pH 4, 2 M), 5 ml of water-saturated phenol and 1 ml of chloroform, and was vortexed for 20 s. After incubation on ice for 15 min and centrifugation at 10,000 g for 15 min at 4 ℃, the two phases were separated and isopropyl alcohol p.a. (Merck, Darmstadt, Germany) was added to the upper phase to yield a 1:1 mixture. RNA was precipitated by incubation for 1 h at -20 ℃ followed by centrifugation at 15,000 g for 15 min at 4 ℃. The supernatant was removed by suction, and the RNA pellet was resuspended in 1 ml of solution D. After the addition of 1 ml of isopropyl alcohol p.a., the RNA was precipitated for a second time by incubation for 1 h at -20 ℃ followed by centrifugation at 13,000 g for 30 min at 4 ℃. Again, the supernatant was removed and the pellet was washed with 70 % ethanol. After centrifugation at 15,000 g for 15 min at 4 ℃ the pellet was dried at room temperature, dissolved in water containing DEPC (DEPC water), and stored at -80 ℃. The concentration and purity of the isolated RNA were measured using an ultraviolet spectrophotometer, confirming $A_{260/280}$ ratio values between 1.6 and 1.8.

The reverse transcription (RT) reaction was carried out with 1 μg of total RNA and 1 μl of oligo(dT_{12-18}) primer (Invitrogen, Karlsruhe, Germany) in DEPC water. The mixture was heated at 70 ℃ for 5 minutes and afterwards cooled on ice. To 10 μl of the mixture the following reagents were added: 200 U of M-MLV reverse transcriptase (Invitrogen, Karlsruhe, Germany), 0.5 μl of RNAsin (Promega, Mannheim, Germany), 10 mM dNTP (MBI Fermentas, St. Leon-Rot, Germany), 2 μl of dithiothreitol (DTT, Roche, Basel, Germany) and 4 μl of first strand buffer (Invitrogen, Karlsruhe , Germany). cDNA was synthesized at 37 ℃ for 1 h followed by incubation at 95 ℃ for 2 min. cDNA samples were stored at -20 ℃.

The polymerase chain reaction (PCR) was performed according to standard procedures. 2 μl of cDNA solution were mixed with 1 U of Taq (Roche, Mannheim, Germany), 2 μl of 10x PCR buffer, 2 μl of 10 mM dNTPs, 1 μl of sense and anti-sense primer and DEPC water to yield a volume of 20 μl. The used primer sequences are displayed in table 5.1.

The PCR encompassed 34 cycles at a denaturation temperature of 95 ℃ for 30 s, an annealing temperature of 60 ℃ for 60 s, and an extension temperature of 72 ℃ for 30 s. The last cycle contained a 2 min extension step at 72 ℃. Following PCR, 10 μl of PCR reaction mixture was subjected to electrophoresis on 1.5 % agarose gels. The

Table 5.1: Primer sequences used for RT-PCR

Primer		Sequence	bp
β-actin	sense	5'-CGGGATCCCCAACTGGGAC-3'	304
	antisense	5'-GGAATTCTGGCGTGAGGGA-3'	
MDR1	sense	5'-CGGGATCCCCCATCATTGCAATAGCAGG-3'	167
	antisense	5'-GGAATTCGTTCAAACTTCTGCTCCTGA-3'	

PCR products were visualized by staining with ethidium bromide (2 %) and analyzed by a GelDoc imaging system (BioRad, München, Germany).

5.2.3 Immunocyto- and Immunohistochemistry

Subconfluent tumor cells, cultured on chambers slides, were fixed in 4 % phosphate buffered paraformaldehyde, pH 7.4, for 30 minutes and washed three times with PBS. The deparaffinizing of paraffine embedded tumor tissue sections is described in chapter 3.2.3. The staining procedure was similar for cells and tissue sections.

Endogenous peroxidase was blocked by incubation in PBS containing 3 % H_2O_2 and 10 % methanol for 30 min, followed by two incubations in PBS with 0.04 % Triton-X-100 (PBST) for 5 min. Nonspecific binding was prevented by incubation for 30 min in 10 % natural goat serum (NGS, Sigma, München, Germany), 2.5 % skimmed milk powder (Milupa, Friedrichsdorf, Germany), and 0.3 % Triton-X-100 in PBS. Subsequently, cells were washed three times with PBST. Primary antibody AB-1 (PC03) (polyclonal anti-human/mouse p-gp, Dianova) was diluted 1:10 (1:50 in case of immunocytochemistry) with washing buffer consisting of 10 ml of PBST, 100 μl of 1 % NGS, and 0.3 % Triton-X-100. After incubation with AB-1 over night at room temperature, the slides were washed three times with PBST and treated with biotinylated goat anti-rabbit antibody as secondary antibody (1:200, Dianova, Hamburg, Germany) for 2 hours at room temperature in a humid chamber. Afterwards, slides were washed three times in PBST and incubated for 1 hour with horseradish-conjugated avidin-biotin complex (Vectastain Elite Kit ABC, Vectorlabs, Burlingame, United Kingdom) in PBST. Slides were washed for 5 min in PBST before incubation in a diaminobenzidine (DAB) solution for 10 min

(0.05 % DAB, 0.02 % ammonium nickel sulfate in PBST). H_2O_2 (10 %) was added to a final concentration of 0.006 %, and slides were incubated for 1.5 min. Afterwards, they were washed three times with PBS and counterstained with nuclear fast red solution for 50 s. Subsequently, the slides were given in PBS and demineralized water, processed in an ascending alcohol series and mounted with DePex. All stained slides were evaluated with a BH2 microscope (Olympus, Hamburg, Germany) mounted with a CCD-camera for digital imaging.

5.2.4 Calcein-AM efflux assay

The exact assay procedure is described in chapter 4.2.3.

5.2.5 Chemosensitivity assay

The procedure is described in detail in chapter 3.2.6.

5.2.6 Intracerebral tumor cell implantation

The breeding of the used NMRI(nu/nu) nude mice is reported in chapter 3.2.7.

The intracerebral model has been described at Altenschöpfer (1998). In brief: the parietal bone of anaesthetized nude mice was drilled with a 1-mm-diameter bit 3 mm to the right-hand side of the sagittal line and 3 mm rostral of the coronal line. Human lung cancer cells ($5{\cdot}10^4$ and $1 \cdot 10^5$ cells in case of NCI-H460 and DMS 114 cell line, respectively) suspended in 5 μl of serum-free RPMI 1640 culture medium (NCI-H460 cell line) or Eagle's minimum essential medium (DMS 114 cell line) were injected 3 mm deep into the brain tissue, and the wound was closed with a surgical clamp.

5.2.7 Treatment of intracerebrally growing lung cancer

In the intracerebral model, the 7- to 9-week old nude mice were assigned to 5 groups (n = 6-8). For each experiment only animals of the same sex were used. In the co-application studies of valspodar and vinblastine mice were assigned to 5 groups of 6 to 8 animals. The control groups received either 0.9 % NaCl solution (vehicle of cytostatic

drug, group 5), complex vehicle of valspodar (group 4) or valspodar alone (50 mg/kg, p.o., group 3). Two additional groups were treated either with a combination of valspodar and the cytostatic drug (50 mg/kg valspodar, p.o.; 0.8 mg/kg vinblastine, i.p.; group 1) or with the cytostatic drug alone (0.8 mg/kg vinblastine, i.p., group 2). Solutions were administered in a volume of 0.1 ml/20 g body weight. Valspodar and its vehicle were given orally every 5 days 4 h before the intraperitoneal injection of vinblastine and its vehicle. The survival rate was calculated by a Kaplan-Meyer analysis.

In case of co-application of valspodar and paclitaxel the treatment of mice, which were assigned in groups according to the co-application of valspodar and vinblastine, was as follows: valspodar (50 mg/kg) and vehicle were administered orally 4 h before the intravenous injection of two doses of paclitaxel and its vehicle, i.e., 3 mg/kg on day 8 and another 2 mg/kg on day 15 after tumor implantation. Animals were killed at day 20, and brains were fixed in Bouin's solution for histological examination. Serial 5 μm coronal sections were prepared every 150 μm from the paraffine embedded brains starting and ending 1.5 mm rostral and caudal to the region of tumor cell implantation. The sections were stained according to the HE-staining procedure described in detail in chapter 3.2.3.

5.3 Results

5.3.1 Prerequisites of an intracerebral in vivo model for the p-gp modulation in the nude mouse brain

The orthotopic brain tumor model is suitable for studies on the p-gp modulation at the BBB (see also chapter 7). Furthermore, it is used for treatment experiments of primary and secondary brain tumors. Selected tumor cell lines for these tests have to comply with the following requirements. To observe a p-gp modulatory effect only at the BBB, the cells have to be negative for the MDR1 phenotype. As a second prerequisite, the cells should be chemosensitive in the presence of low concentrations of cytostatic drugs. In addition, the cells have to be tumorigenic in the brains of nude mice.

5.3.1.1 Investigations on the MDR phenotype of human lung cancer cell lines

The MDR phenotype of the selected lung cancer cell lines NCI-H460 and DMS 114 was examined in three ways. The existence of p-gp encoding mRNA was detected by PCR. The p-gp expression was demonstrated with immunohistochemical methods, and the functionality of an eventually expressed p-gp was determined by the calcein-AM efflux assay.

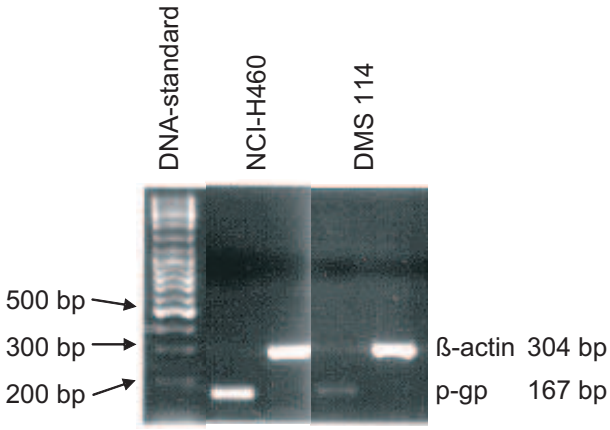

Figure 5.1: Determination of p-gp encoding mRNA in NCI-H460 and DMS 114 cells. mRNA encoding for the MDR1 phenotype was only detected in NCI-H460 cells (ethidium-bromide stained RT-PCR gel after 34 cycles. β-Actin served as a control.)

The results of the RT-PCR for the MDR1 encoding mRNA are shown in Fig. 5.1. mRNA encoding for p-gp was detected in PCR products of the NCI-H460 cells. DMS 114 cells possessed no p-gp encoding gene, because no PCR product of 167 base pairs was observed. β-Actin served as a control for proper RT-PCR procedure.

The expression of p-gp was examined with an avidin-biotin-method on paraffine sections as well as on fixed cells. No typical p-gp staining was observed on any examined slide. Hence, although NCI-H460 cells have MDR1 encoding mRNA, p-gp is not expressed at the protein level. In case of the DMS 114 cell line, the negative MDR phenotype of the cells determined in the RT-PCR experiment was confirmed.

Fig. 5.2 shows the results of the calcein-AM efflux assay that was used to investigate the cell lines regarding p-gp activity. Both NCI-H460 and DMS 114 cells took up calcein-AM very well leading to high fluorescence intensities. Therefore, no active p-gp was expressed in the two cell lines despite the genetic disposition of NCI-H460 cells. However, NCI-H460 cells could presumably become MDR resistant by the addition of p-gp inducers like

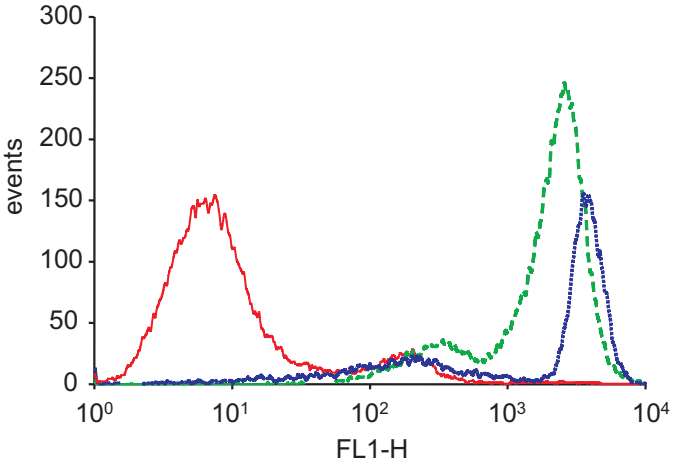

Figure 5.2: Comparison NCI-H460 (dashed line), DMS 114 (dotted line) and p-gp overexpressing Kb-V1/VBL (solid line) cells with respect to their p-gp activity. Both NCI-H460 and DMS 114 cells show higher fluorescence intensities compared to Kb-V1/VBL cells indicating an inactive p-gp or the lack of p-gp.

vinblastine.

In conclusion, the selected cell lines do not exhibit a MDR1 phenotype. Therefore, the study of p-gp modulation exclusively at the BBB is possible using NCI-H460 or DMS 114 cells in an orthotopic brain tumor model.

5.3.1.2 Chemosensitivity of human lung cancer cell lines

With respect to a successful treatment experiment the selected tumor cell lines have to be sensitive against chemotherapeutic agents. For our treatment studies the cytostatic drugs paclitaxel and vinblastine were chosen due to their applicability in treatment experiments in nude mice (Fellner et al. 2002, Spruss et al. 1995). Fig. 5.3 and Fig. 5.4 illustrate the chemosensitivity of DMS 114 and NCI-H460 cells against the two cytostatic drugs. Both substances are very potent cytostatics and thus, cytocidal effects were achieved in low concentrations. For example, 5 nM paclitaxel had a transiently cytocidal effect on DMS 114 cells, i.e. not all cells died and cells began to recover after 100 hours. In contrast, a concentration of 1 nM vinblastine was already sufficient for a permanent cytocidal effect. In general, the NCI-H460 cells were less sensitive to the selected cytostatic drugs than the DMS 114 cells (see also chapter 3.3.4). Concentrations of 30 nM paclitaxel and 50 nM vinblastine, respectively, were necessary to achieve cytocidal effects.

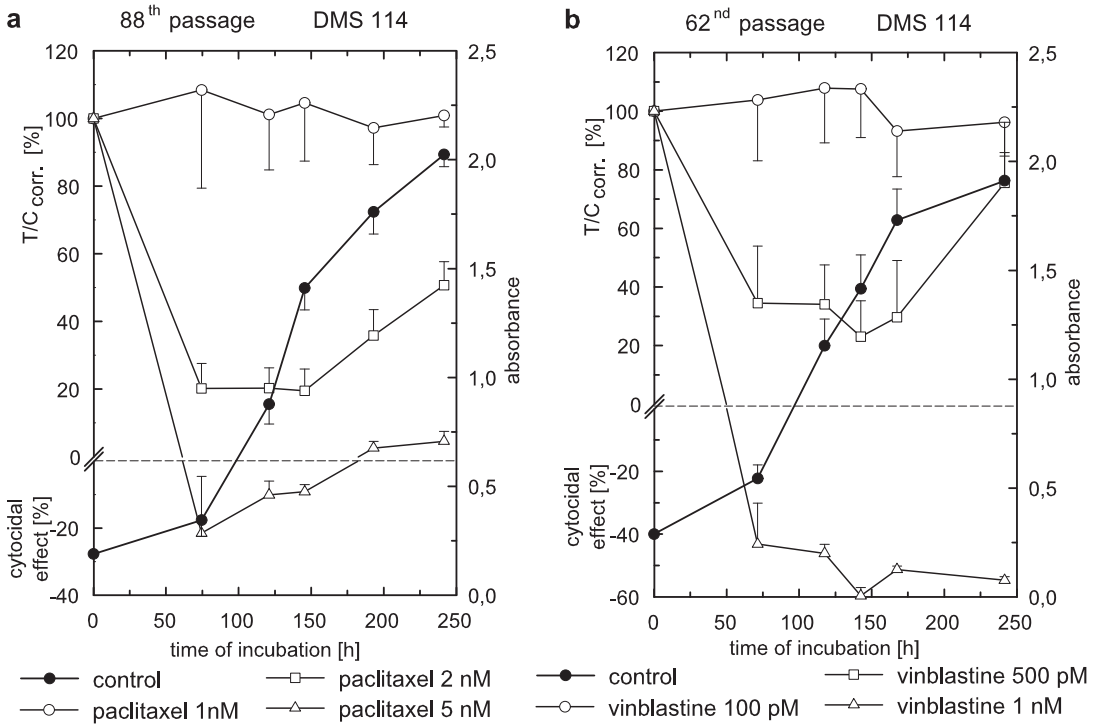

Figure 5.3: Chemosensitivity of DMS 114 cells against paclitaxel (a) and vinblastine (b)

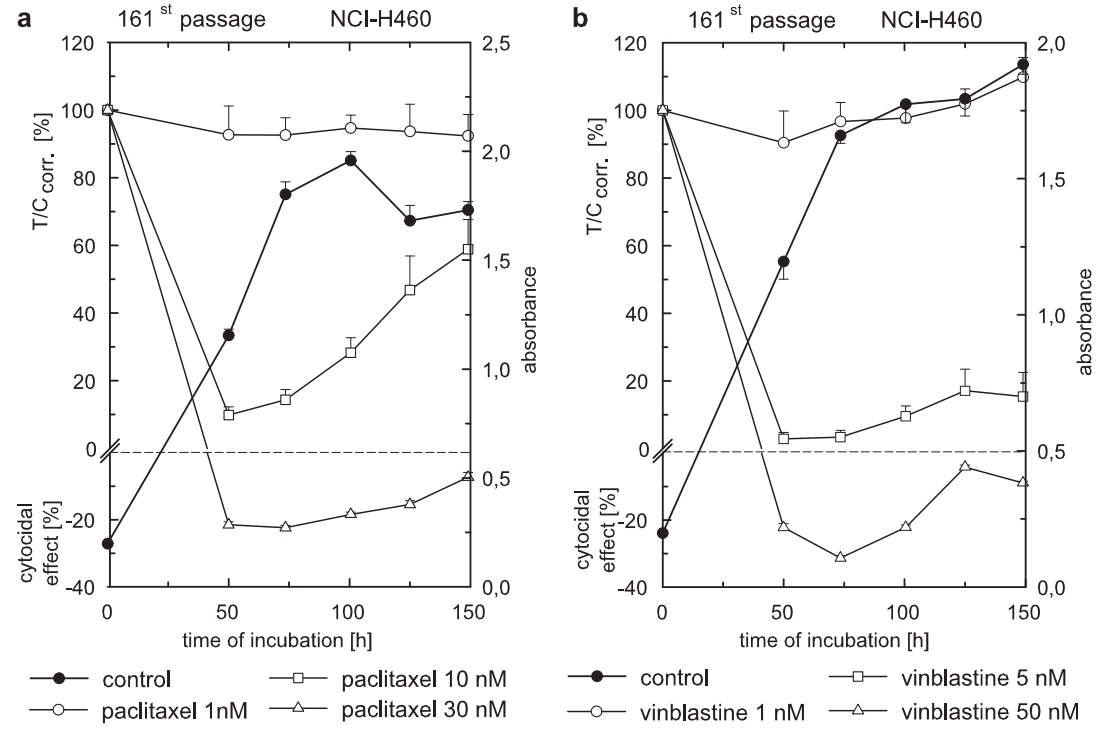

Figure 5.4: Chemosensitivity of NCI-H460 cells against paclitaxel (a) and vinblastine (b)

Hence, NCI-H460 as well as DMS 114 cells were sensitive against low concentrations of the chemotherapeutic drugs paclitaxel and vinblastine.

5.3.1.3 Intracerebral in vivo growth

To investigate the tumorigenicity of the selected tumor cells three different tumor cell quantities were injected into the brain of nude mice to determine the optimal cell concentration. After three to four weeks, the intracerebral tumor growth was controlled. Fig. 5.5 and Fig. 5.6 illustrate an intracerebrally grown DMS 114 tumor. In this case 100,000 cells were injected.

The appearance of the brain tumor is similar to that of the subcutaneously grown tumor (see chapter 3.3.5). Here as well, the cells have mostly one prominent nucleolus. Multinucleated cells are observed, too. The tumor is not well-delimited against the brain tissue. The infiltration into other brain areas is clearly visible.

In case of NCI-H460 tumors the characteristics of the subcutaneously grown tumor are similar to those of the intracerebral tumor (Fig. 5.7 and Fig. 5.8). The cells with scanty cytoplasm have round to oval nuclei with irregularly formed prominent nucleoli. Mitotic

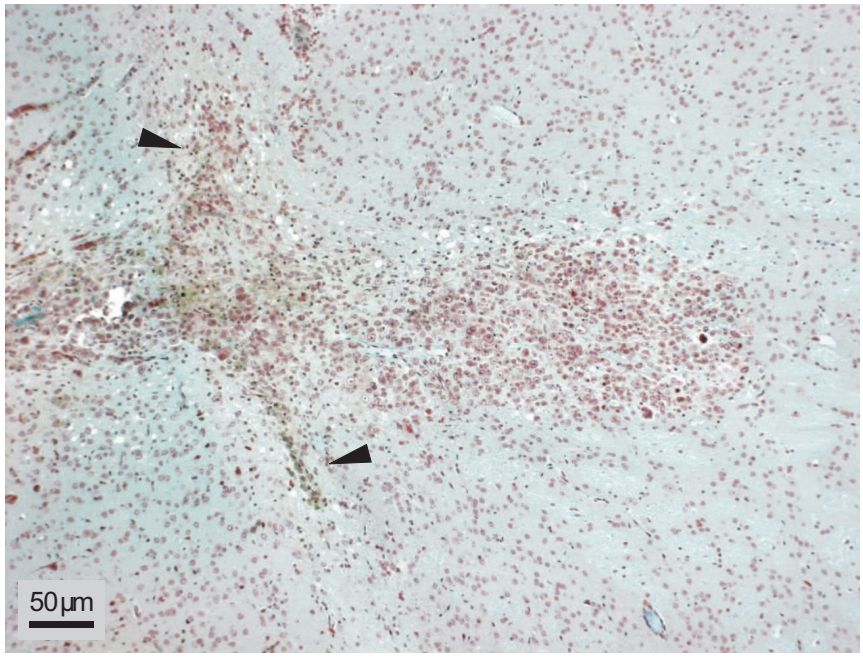

Figure 5.5: MG-staining of an intracerebrally grown DMS 114 tumor. The diffuse tumor infiltrates other brain regions (indicated by arrows).

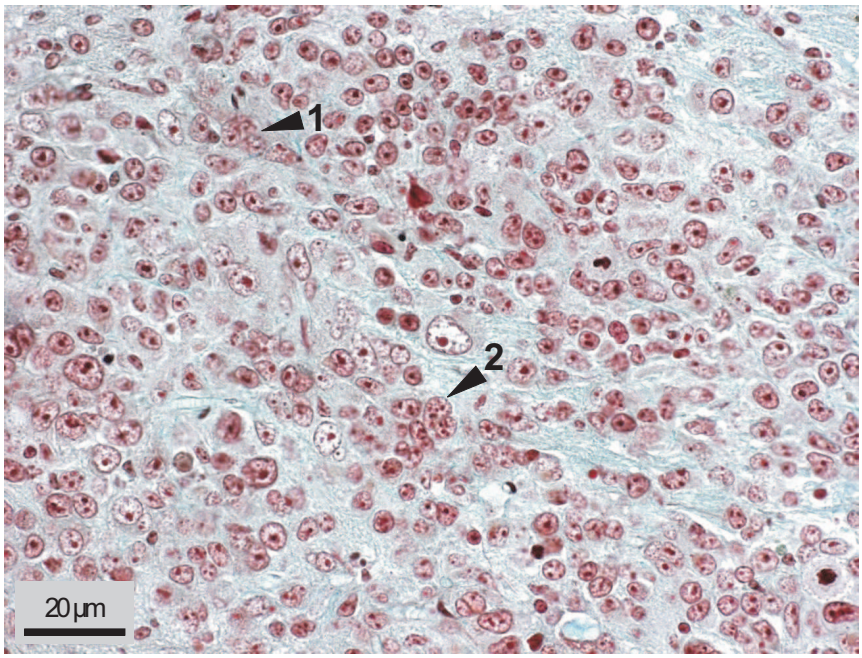

Figure 5.6: MG-staining of an intracerebrally grown DMS 114 tumor. The anisometrically formed cells are occasionally multinucleated (indicated by arrow 1). The irregular formed nuclei are of different size and have several prominent nucleoli (indicated by arrow 2).

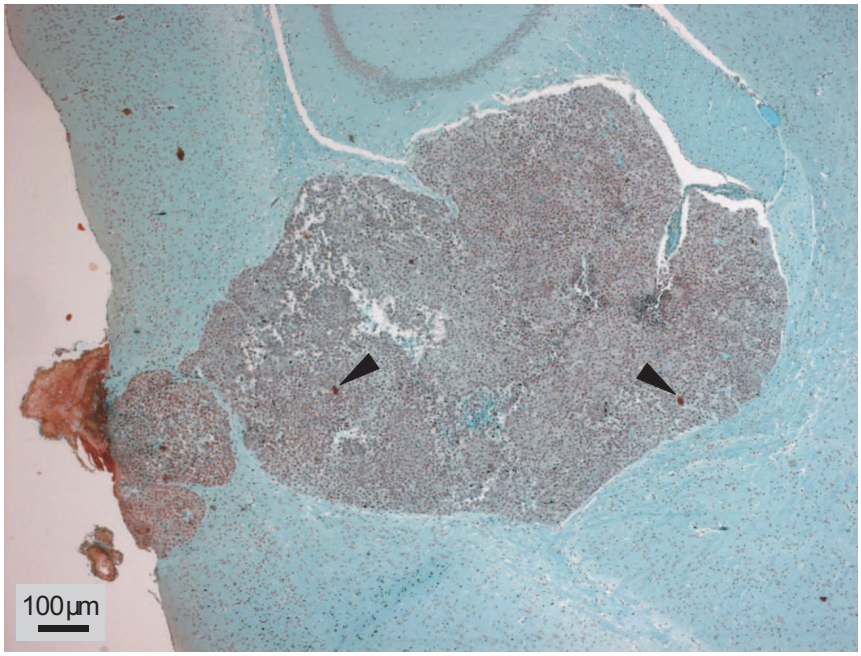

Figure 5.7: MG-staining of an intracerebrally grown NCI-H460 tumor. Many blood vessels (indicated by arrows) are observed in this well-delimited tumor.

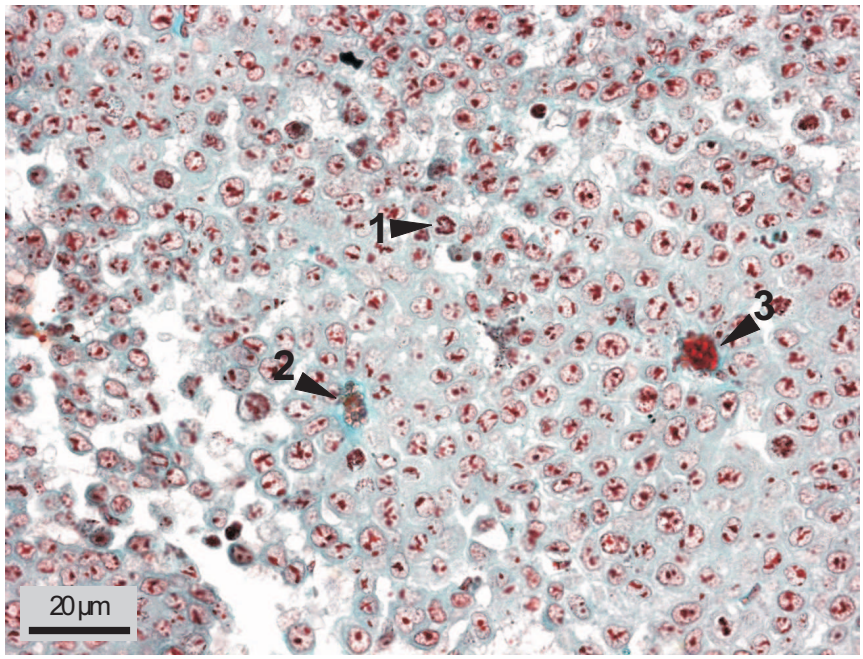

Figure 5.8: MG-staining of an intracerebrally grown NCI-H460 tumor. The cells have round to oval nuclei with several irregularly shaped nucleoli. Mitotic activity (arrow 1) and the vascularization of the tissue (arrows 2 and 3) is marked by arrows.

activity is not as high as seen in the subcutaneously grown tumor. The tumor tissue is well vascularized, but infiltration of the vessels is not observed. After three weeks nearly all mice were dead because the tumor grew very rapidly and aggressively in the brain.

A tumor was detectable in all examined brains. Thus, both cell lines were tumorigenic in the nude mouse brain.

In summary, the selected lung cancer cell lines NCI-H460 and DMS 114 fulfill all three prerequisites. They are suitable to establish an orthotopic tumor model simulating brain metastases of lung cancer. Furthermore, the cell lines are sensitive to the selected chemotherapeutic agents. Since NCI-H460 and DMS 114 cells do not express a MDR1 phenotype, the effect of a specific p-gp modulation at the BBB could be examined in a treatment experiment.

5.3.2 Treatment experiments

The results of Fellner et al. (see page 94) showed that valspodar pretreatment increased the brain levels of administered paclitaxel to concentrations which were sufficient to pro-

duce a therapeutic effect on a paclitaxel sensitive transplanted tumor. Therefore, the adaptation of this successful approach to the treatment of brain metastases was investigated.

5.3.2.1 Combination of valspodar with cytostatic drugs in vitro

First, the efficacy of valspodar co-administered to certain cytostatic drugs was investigated in vitro. MDR resistant Kb-V1 cells (Kb-V1/VBL, see chapter 4.4) were incubated with paclitaxel or vinblastine in combination with various concentrations of valspodar. The cytostatic drugs as well as the modulator valspodar were given at concentrations that did not affect the growth of the Kb-V1/VBL cells when the compounds were administered as single drugs. The results of the chemosensitivity assay are illustrated in Fig. 5.9.

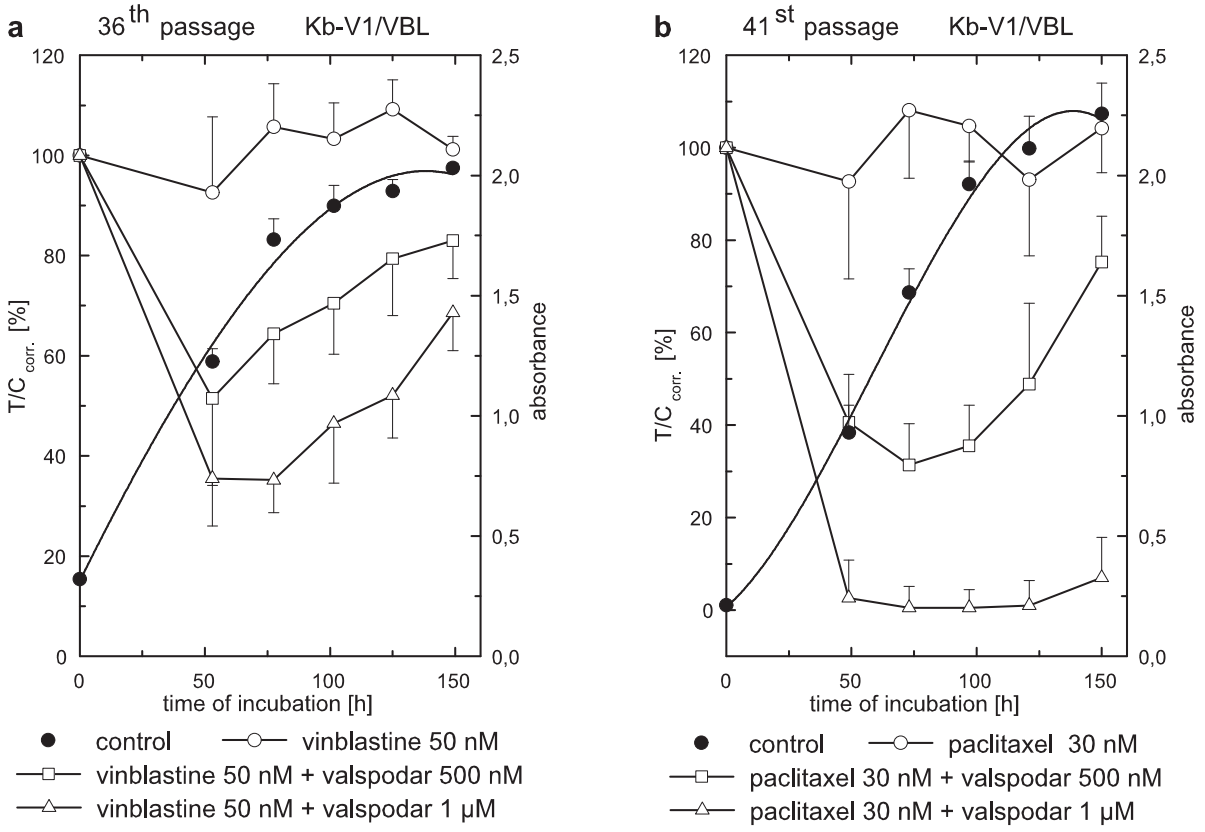

Figure 5.9: Chemosensitivity of p-gp expressing MDR resistant Kb-V1/VBL cells against vinblastine (a) and paclitaxel (b) in combination with different concentrations of valspodar. The chemosensitivity of the cells is increased by valspodar.

The co-incubation of paclitaxel or vinblastine with valspodar led to a transient inhi-

bition of the Kb-V1/VBL cell proliferation due to the blockade of the p-gp activity in a valspodar concentration dependent manner. A valspodar concentration of 1 μM even fully restored the paclitaxel sensitivity of the Kb-V1/VBL cells as indicated by the complete growth inhibition. Using vinblastine as cytostatic drug the cell proliferation was at least transiently inhibited. The co-application of valspodar led to enhanced toxicity of the co-administered cytostatic drug. This proves the ability of valspodar to inhibit p-gp activity.

5.3.2.2 Co-application of valspodar with vinblastine for the treatment of NCI-H460 lung cancer in the brains of nude mice

NCI-H460 human lung cancer cells were intracerebrally implanted into nude mice. This procedure resulted in aggressively growing intracerebral neoplasms (see chapter 3 and 5.3.1.3). Every five days nude mice received 0.8 mg/kg of vinblastine intraperitoneally with (group 1) or without (group 2) 50 mg/kg valspodar. Valspodar was given orally 4 h before the vinblastine injection. In the literature, valspodar is described as a cytotoxic agent with an anticancer effect independent from the modulatory action on MDR (Kreis et al. 2001). Therefore, it was given to another group of mice that served as a control (group 3). The valspodar vehicle was also administered to mice as a control (group 4) because cremophor RH40, a derivative of cremophor EL, is an ingredient of the vehicle.

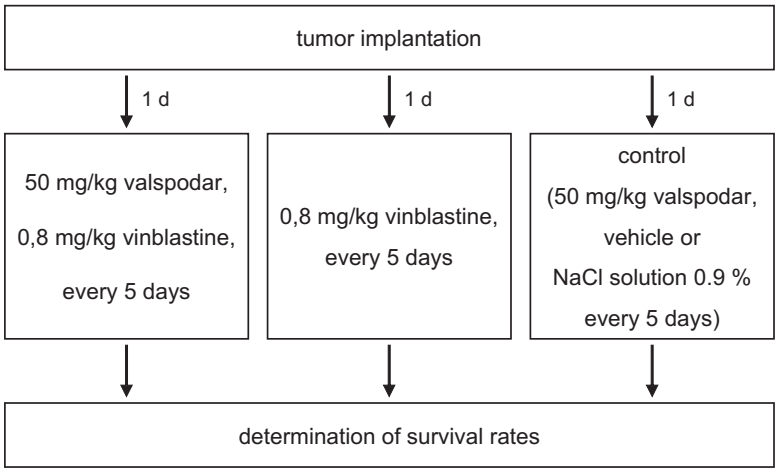

Figure 5.10: Application scheme for the treatment of NCI-H460 brain metastases in nude mice with vinblastine co-administered with valspodar. Each group consists of 6 to 8 nude mice.

For cremophor EL a modulating effect on p-gp is described in literature (Chervinsky et al. 1993, Woodcock et al. 1990). In addition, mice received 0.9 % sodium chloride solution, the vehicle of vinblastine, to represent the "untreated" control (group 5). The survival plot was determined according to Kaplan-Meyer.

Survival did not significantly differ within the five groups (Fig. 5.11). Until day 15 the combination treatment seemed to exhibit an advantage compared to the other groups because no mouse died in group 1 until this day. In contrast, in the other groups at least 2 mice had died by day 15 indicated by a survival rate of 80% at best. On day 20 all living animals were very weak and apathetic, and the experiment was aborted. In group 1 where mice received the combination of vinblastine and valspodar, 2 of 8 mice (25 %) were still living. In the control groups 3 and 4, all animals had died. However, 1 animal remained alive in the vinblastine group 2 (16.7 %) as well as in the untreated group 5

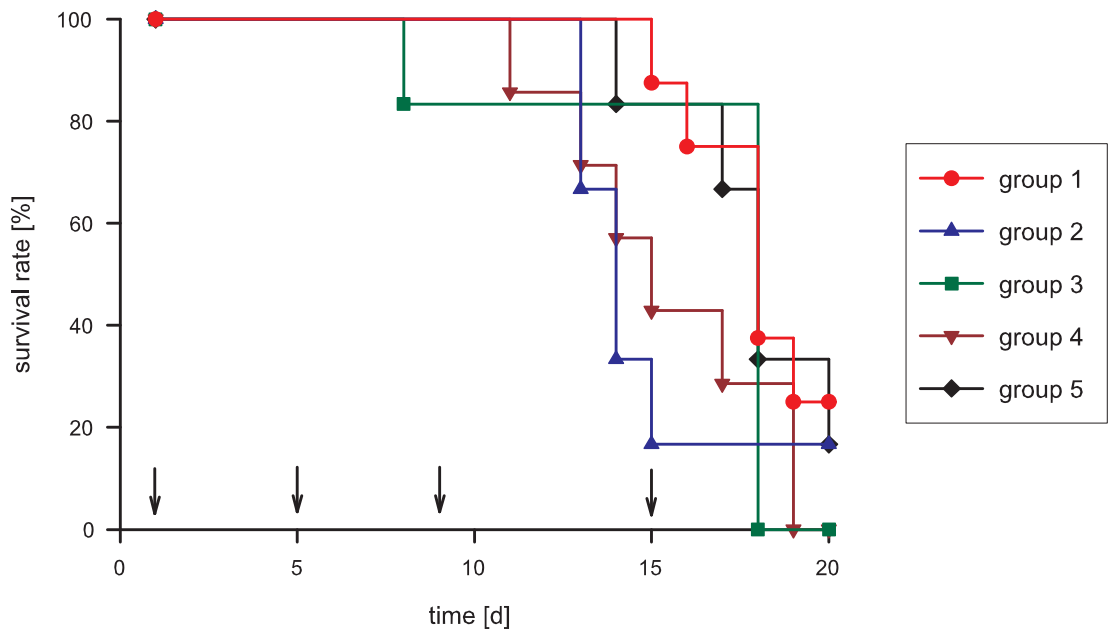

Figure 5.11: Kaplan-Meyer survival plot for the treatment of intracerebrally grown NCI-H460 lung cancer in nude mice with vinblastine and valspodar. The animals (n = 6 - 8) were treated every 5 days starting on day 1. Group 1 received vinblastine (0.8 mg/kg, i.p.) and valspodar (50 mg/kg, p.o., 4 h before vinblastine), group 2 vinblastine alone and the groups 3 to 5 served as control groups and received either valspodar, valspodar vehicle or sodium chloride solution, respectively. No significant differences within the five groups were observed.

(16.7 %). In this model no significant increase in survival time was achieved by systemic treatment with vinblastine and even the co-application of valspodar had no significant effect on the life span of the nude mice.

Up to day 5 the mice put on weight slightly (data not shown). Two to 3 days after the 2^{nd} treatment a clear decrease in body weight was observed in the treated groups 1 and 2 and also in the control groups 3 to 5 on day 10 after the 3^{rd} treatment. There are no differences between the vinblastine/valspodar group and mice, which received vinblastine alone. There are at least three reasons for the obvious body weight reduction. The first one is the increased toxicity of vinblastine caused by the co-administration of valspodar; this is well known from clinical studies (Bates et al. 2001). Another reason for the decrease in body weight in the vinblastine treated groups is the narrow therapeutic index of vinblastine and the corresponding systemic toxicity. The third reason is the aggressive and rapid growth of the NCI-H460 cell line (see chapter 3).

The experiment was repeated and this time the brains were supposed to be ana-

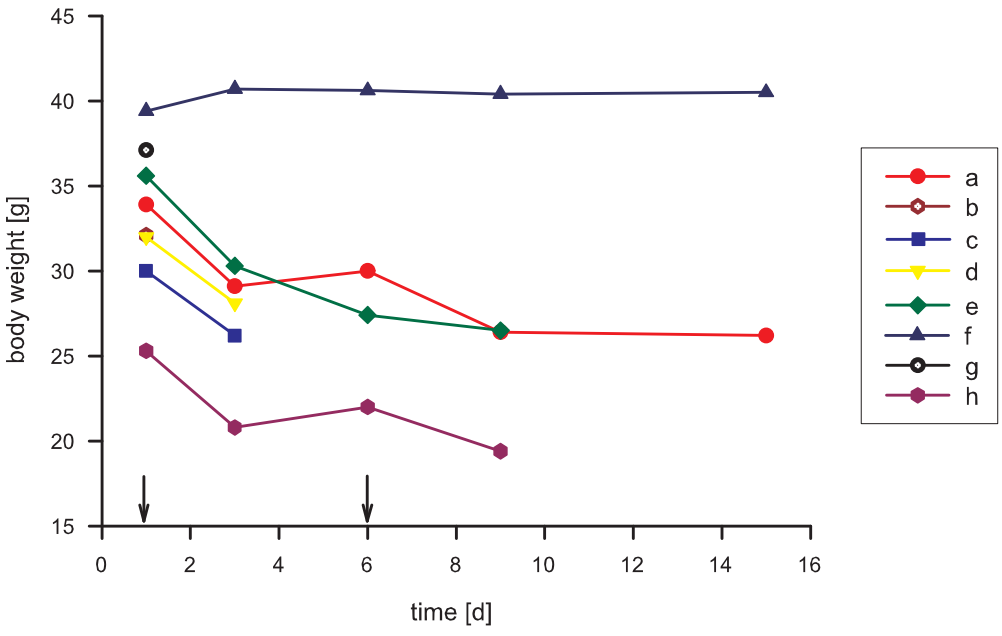

Figure 5.12: Tolerance experiment for the vinblastine/valspodar combination. Mice received 50 mg/kg valspodar p.o. 4 h before i.p. injection of 0.8 mg/kg vinblastine. Decrease in body weight is an indicator of systemic toxicity. The combination of vinblastine and valspodar was only tolerated by 2 mice (a,f).

lyzed by a morphometrical method described at Fellner (2001). Unfortunately, the mice treated with vinblastine and valspodar already died 2 days after the 1^{st} treatment. Therefore, the experiment was not repeated. The intraperitoneal administration of vinblastine 0.8 mg/kg, every 5 days, to 5 tumor-free female nude mice was well tolerated. The application of the vinblastine/valspodar combination was tested in healthy mice as well and in contrast to the result described above most of the mice did not withstand the treatment. Fig. 5.12 shows the body weights of 8 male nude mice, which received 50 mg/kg valspodar orally, and 4 h later 0.8 mg/kg vinblastine intraperitoneally.

Two days after the 1^{st} treatment 2 mice died (b,g), another 2 mice (c,d) died 4 days after the 1^{st} treatment. Again 3 days after the 2^{nd} treatment 2 mice (e,h) died. Only 2 mice (a,f) sustained the combination treatment with vinblastine and valspodar. Subsequently performed HPLC investigations of the used vinblastine solutions proved that incorrect preparation of the vinblastine solutions can be excluded as a possible cause of the fatalities.

5.3.2.3 Co-application of valspodar with paclitaxel for the treatment of DMS 114 lung cancer in the brain of nude mice

In a second study nude mice with intracerebrally grown DMS 114 tumors were treated with a combination of paclitaxel and valspodar. The animals were treated with 3 mg/kg of paclitaxel intravenously on day 8 after tumor cell implantation and with 2 mg/kg of

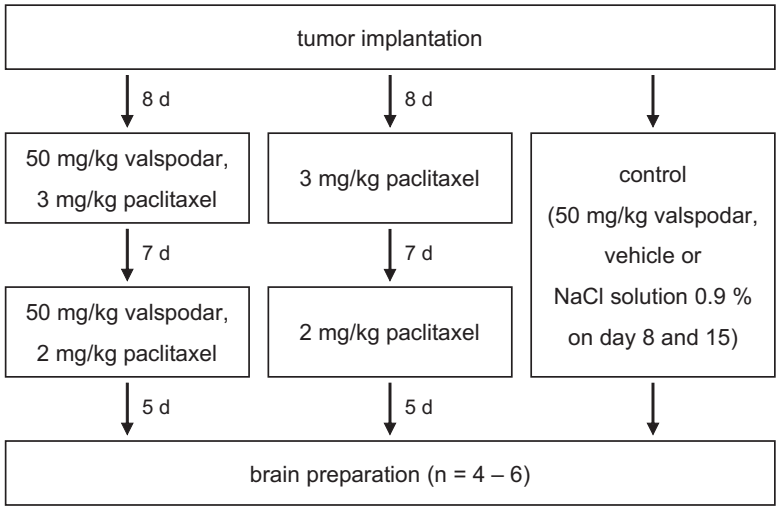

Figure 5.13: Application scheme for the treatment of DMS 114 brain metastases with paclitaxel co-administered with valspodar. Each group consists of 6 to 8 nude mice.

paclitaxel on day 15, with (group 1) and without (group 2) orally administered 50 mg/kg of valspodar 4 h before each paclitaxel dose. The control groups received either 50 mg/kg of valspodar (group 3), the valspodar vehicle (group 4) or 0.9 % sodium chloride solution (group 5), the vehicle of paclitaxel (cp. chapter 5.3.2.2). The mice were killed 20 days after implantation and the tumor volume in each brain was determined morphometrically.

In each group 4 brains were used for the morphometric analysis. After the HE-staining of the brains of group 1, a tumor of enormous size was detected in one brain. Paclitaxel and valspodar had been administered to mice in group 1. In theory, the brains of group 1 should possess small or no tumors due to a therapeutical benefit of the valspodar pretreatment. Thereupon, only the brains of the mice assigned to the control group 4 (valspodar vehicle) were examined as the morphometric examination is very time consuming. Assuming a globular or ellipsoidal tumor growth, the tumor volumes were estimated from the HE-stained sections.

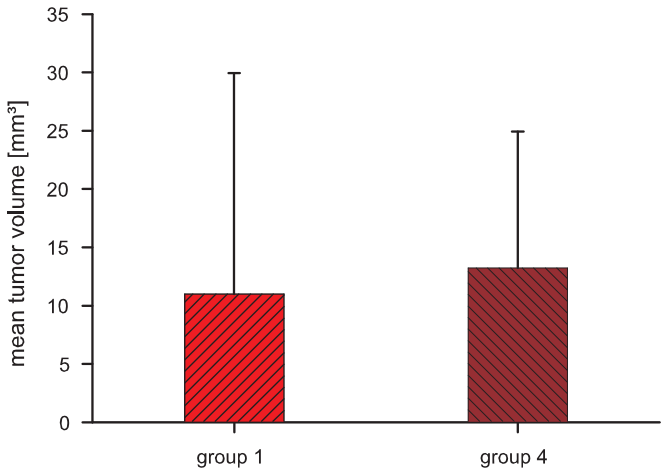

Figure 5.14: Mean estimated tumor volumes of treated group 1 (50 mg/kg valspodar p.o., 4 h before 3 and 2 mg/kg paclitaxel i.v., respectively) and untreated group 4 (valspodar vehicle). There is no significant difference within the two groups. Paclitaxel administration even in combination with valspodar, did not have a tumor reducing effect on intracerebrally grown DMS 114 tumors.

Fig. 5.14 presents the estimated tumor area for the paclitaxel/valspodar treated group 1 and the control group 4. In this study, there were no statistically significant differences between the mean tumor volumes within the two examined groups. Only 3 of the 4

examined brains per group could be used for the volume estimation. In group 4, one brain was incorrectly prepared, so only part of the brain which did not contain any tumor was available for evaluation. In group 1 no tumor was detected in one brain. It cannot be excluded that the injection of the tumor cells had failed in this animal as the tumor volume of another DMS 114 brain tumor was assessed to 39 mm^3. Hence, no therapeutic benefit could be achieved in this tumor model by systemic treatment with paclitaxel even in combination with valspodar.

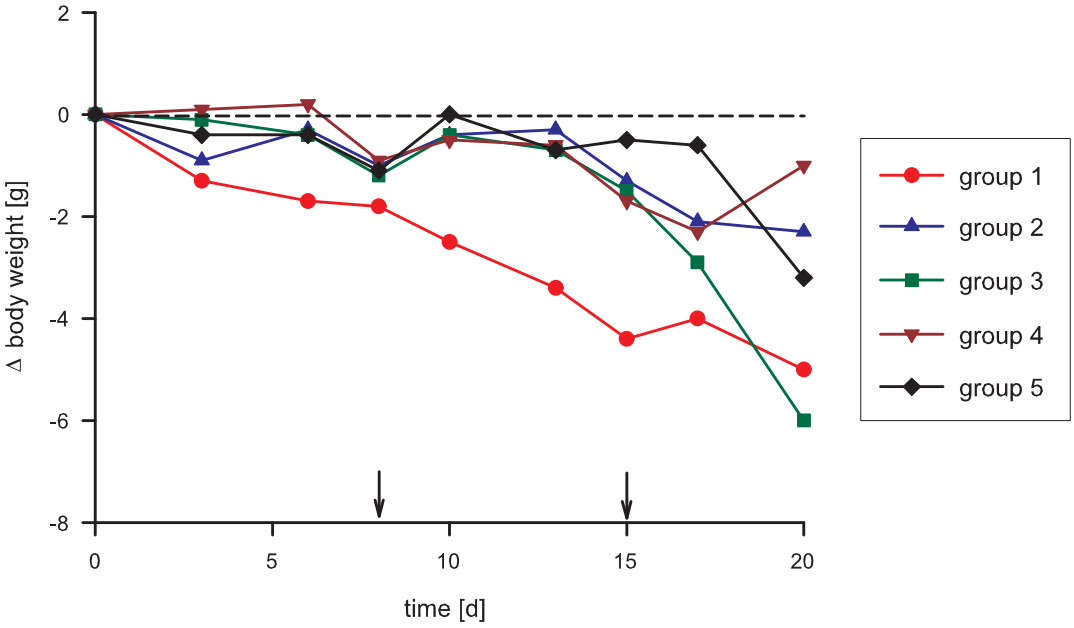

Figure 5.15: Decrease in body weight is an indicator of systemic toxicity. The arrows indicate drug administration. The animals (n = 6 - 8) were treated on day 8 (3 mg/kg paclitaxel i.v.) and on day 15 (2 mg/kg paclitaxel i.v.). Group 1 received paclitaxel and valspodar (50 mg/kg, p.o., 4 h before paclitaxel), group 2 paclitaxel alone and the groups 3 to 5 served as control groups and received either valspodar, valspodar vehicle or sodium chloride solution, respectively.

The changes in body weight are depicted in Fig. 5.15. Particularly in mice treated with the paclitaxel/valspodar combination (group 1) the body weight was reduced after each treatment. The body weight of mice assigned to the control groups 3 to 5 remained relatively constant over a long period of time and decreased at the end of the experiment due to the tumor burden. The body weight reduction of animals which received pacli-

taxel alone, was lower than in case of the paclitaxel/valspodar treated mice. Thus, the co-application of valspodar increases the toxicity of paclitaxel. This finding is in good agreement with results of clinical trials (Advani et al. 2001).

5.3.3 Discussion

In both studies no therapeutic effect of valspodar co-administration on the growth of brain tumors was observed. The dosage of valspodar (50 mg/kg) was sufficient to inhibit p-gp activity in the mouse. Lemaire et al. (1996) investigated the brain-to-blood partition coefficient of valspodar in rats 2 h after the intravenous administration of radioactively labelled valspodar in doses of 0.1 to 30 mg/kg. A valspodar dosage of 10 mg/kg achieved a saturation effect of the p-gp inhibition at the BBB. As the oral bioavailability of valspodar reached 53 % (Covelli 1998), a concentration of 20 mg/kg should already be sufficient for a complete p-gp inhibition at the BBB.

The ineffectiveness of the co-application of vinblastine and valspodar is discussed in the literature. Lyubimov et al. (1996) and Drion et al. (1996) described that the increase in vinblastine concentration achieved by co-administration of valspodar, was lower in the brain than in liver and kidney. Similarly, in our study the vinblastine concentrations in the brain were too low to achieve an antitumor effect. The intolerance of the combination treatment in mice could be explained by the narrow therapeutic index of vinblastine. Alterations of the pharmacokinetic parameters of vinblastine caused by the combination with valspodar have profound consequences on the safety of the treatment. In other studies, the co-application was only tolerated with acceptable toxicities in case of a vinblastine dose reduction (van Asperen et al. 1996, Bates et al. 2004). But with the optimized dosage only a slight benefit was observed in both studies, because the vinblastine concentration was too low after the dose reduction to have an effect on the tumor growth.

In the literature, studies with the combination of paclitaxel and valspodar are described as well. By co-application of the p-gp modulator increased paclitaxel brain levels were achieved (Fellner et al. 2002, Kemper et al. 2003) and toxicity remained acceptable due to paclitaxel dose reduction (Fracasso et al. 2000). Moreover, Fellner (2001) determined a paclitaxel concentration of 146 nmol/g in the nude mouse brain 24 h after the intra-

venous injection of 4 mg/kg of paclitaxel when the animals were pretreated with 50 mg/kg valspodar p.o. (4 h before paclitaxel injection). The in vitro chemosensitivity of DMS 114 against paclitaxel was tested within the scope this thesis (see chapter 5.3.1.2). A paclitaxel concentration of 5 nM (equivalent to 5 nmol/g) had a cytocidal effect on the in vitro growth of DMS 114 cells. Hence, the paclitaxel brain levels detected by Fellner should be intrinsically high enough to achieve a therapeutic effect on the DMS 114 brain tumors in nude mice. However, under the conditions described by Fellner et al. the treatment of DMS 114 brain metastases failed. It is conceivable that the chemosensitivity of the selected DMS 114 tumor against paclitaxel in vivo is reduced compared to the chemosensitivity in vitro.

Furthermore, the injected number of tumor cells plays a decisive role for the success of a treatment experiment. In preliminary tests with different cell numbers (30,000 to 300,000 DMS 114 cells) tumors of sufficient size grew after an injection of 30,000 and 100,000 tumor cells, respectively. As in the treatment experiment the investigated tumors were partly too big in size for a morphometric analysis, the preliminary tests were repeated with 10,000 and 30,000 cells, respectively (4 mice per group). After 22 days the brains were collected and the prepared sections were analyzed. Only in 5 of 8 brains tumors were detectable. Since the mice received no treatment, probably the injection of the tumor cells was incorrect. In one brain, no injection channel was detected and in another case, the tumor had grown between the skull and the dura mater. The detected tumors differed in size independent of the injected tumor cell number. Thus, the procedure of the tumor cell injection is complicated and it is difficult to produce tumors of a sufficient size (10 - 15 mm^3) especially in case of the DMS 114 cell line.

In case of the NCI-H460 cell line, the cell injection is important as well. Additionally, the tumor growth is aggressive and rapid both in vitro and in vivo. Since the cells possess the mRNA encoding for p-gp (see chapter 5.3.1.1), it is possible that the cells became chemoresistant during therapy due to the continuous contact with the p-gp inducer vinblastine. Thus, this cell line is unsuited for the brain metastases model studying effects of p-gp inhibition at the BBB, because of its rapid growth, the high chemoresistance and the existence of p-gp encoding mRNA.

For further treatment studies with the DMS 114 tumor, the model should be improved.

The application scheme could be optimized by reduction of the valspodar concentration. Then the paclitaxel dose can be increased as analogously described for a combination with vinblastine (Bates et al. 2004). Moreover, the tumor cells should be stably transfected to express fluorescent proteins like GFP and EGFP (Yang et al. 2000, Hoffman 2002). The intracerebral tumor growth may then be controlled in the living animal and similar to the subcutaneous tumor model only mice which developed a solid brain tumor can be selected for the experiments.

5.4 Summary

In this chapter the suitability of the lung cancer cell lines NCI-H460 and DMS 114 for the intracerebral in vivo model and the treatment of these tumors were examined. The NCI-H460 and DMS 114 cell lines were tumorigenic in the brain of nude mice and were used to simulate brain metastases of lung cancer. Furthermore, no MDR1-phenotype was exhibited despite the detection of MDR1 encoding mRNA in NCI-H460 cells. Therefore, the cell lines were suited for experiments on the selective p-gp modulation at the BBB. Also, the lung cancer cells were sensitive against low concentrations of the selected cytostatic drugs vinblastine and paclitaxel.

Whereas the combination of the potent p-gp modulator valspodar with the chemotherapeutic agents vinblastine or paclitaxel resulted in a restoration of the chemosensitivity of p-gp expressing Kb-V1/VBL cells in vitro, no therapeutic benefit was observed in the treatment experiments of the simulated NCI-H460 and DMS 114 brain metastases in the intracerebral in vivo model.

The highly aggressive and rapid growth of the intracerebral NCI-H460 tumors could not be affected by the treatment with vinblastine. Furthermore, the increase in vinblastine brain concentration caused by the co-administration of valspodar seemed to be extremely low. Although the vinblastine concentrations in brains of mice which received additionally valspodar were not determined within these experiments, other studies indicated only a slight increase in vinblastine brain levels after valspodar pretreatment (Lyubimov et al. 1996, Drion et al. 1996). Additionally, vinblastine has a narrow therapeutic index. The neurotoxic side effects of vinblastine were too serious to allow for a continuation of the

experiments. Therefore, the NCI-H460 cell line is unsuited for treatment experiments using the intracerebral in vivo model.

The DMS 114 cell line seemed to be less chemosensitive against paclitaxel in vivo compared to the in vivo tests. Moreover, the tumorigenicity of the cells was heavily dependent upon the injected number of cells. Hence, the control of the intracerebral tumor growth is indispensable. This may be achieved by transfection of the tumor cells with the fluorescent proteins GFP or EGFP. Furthermore, the use of newly developed p-gp modulators such as elacridar, tariquidar (see chapter 6 and 7) or zosuquidar (Kemper et al. 2004b) is recommended, as according to literature these compounds do not alter the pharmacokinetic parameters of co-administered substances. Using these new 3^{rd} generation p-gp modulators, the paclitaxel concentration could be increased leading to an improvement of the therapy of DMS 114 brain tumors in the intracerebral tumor model.

Chapter 6

Characterization of the 3^{rd} generation p-gp inhibitors elacridar and tariquidar[1]

6.1 Introduction

Inhibiting P-glycoprotein 170 (p-gp, ABCB1) as a way of reversing multidrug resistance (MDR) has been extensively studied for more than two decades (Thomas and Coley 2003). A broad range of substances that interact with p-gp and block p-gp mediated drug efflux have been reported. These compounds include calcium channel blockers, calmodulin inhibitors, steroidal derivatives, antibiotics, cardiovascular drugs and cyclosporins (Ford 1996, Krishna and Mayer 2000). The calcium channel antagonist verapamil has been one of the best studied compounds in clinic (Dalton et al. 1989, Miller et al. 1991). However, these compounds were developed for other pharmacological purposes than the reversal of MDR, they are very weak and non-specific p-gp modulators, and p-gp substrates. The use of high doses of these 1^{st} generation modulators was necessary because of their low binding affinity resulting in unacceptable toxicity (Ferry et al. 1996).

The development of more selective and potent inhibitors led to the 2^{nd} generation of p-gp modulators such as biricodar (VX-710, Germann et al. (1997b)) and the non-immunosuppressive cyclosporin D analogue valspodar (SDZ PSC 833, Boesch et al. (1991)). Although these substances were more potent and less toxic in comparison to the 1^{st}

[1]Parts of this work were presented at the BBB Expertentreffen 2004 in Bad Herrenalb

generation modulators, they retained some characteristics that limited their clinical usefulness. These compounds caused alterations of the pharmacokinetic parameters of the co-administered cytotoxic drugs, whereby the toxicity of these cytotoxic agents increased. This led to dose reductions and to limited success in cancer chemotherapy (Rowinsky et al. 1998, Fischer et al. 1998).

Agents lacking the alteration of pharmacokinetic parameters when co-administered with cytostatic drugs were developed by using structure-activity relationships and combinatorial chemistry (Robert and Jarry 2003). These so-called 3^{rd} generation modulators include zosuquidar (LY 335979, Dantzig et al. (1996)), laniquidar (R 101933, van Zuylen et al. (2000)), ONT 093 (Newman et al. 2000), elacridar (GF 120918, Hyafil et al. (1993)) and tariquidar (XR 9576, Mistry et al. (2001)). The latter two are shown in Fig. 6.1.

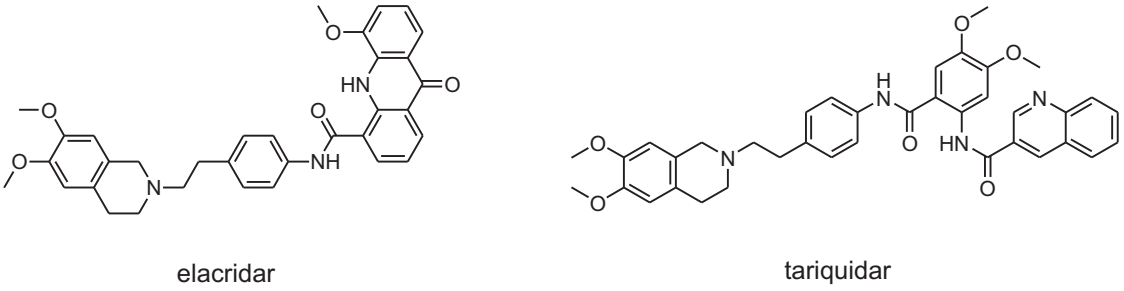

Figure 6.1: Structures of the acridone carboxamide derivative elacridar and the anthranilamide derivative tariquidar. Both substances are 3^{rd} generation p-gp modulators.

Elacridar and tariquidar are two of the most promising chemosensitizing inhibitors of p-gp (Myer et al. 1999). According to the literature both substances are suitable for combination therapy with cytostatic drugs (Ward and Azzarano 2004). The compounds are no p-gp substrates, e.g. tariquidar inhibits p-gp function by binding at a site which is distinct form the site of interaction of transported substances (Martin et al. 1999). In the present study these inhibitors were characterized with respect to their spectroscopical properties, their potential toxicity and their in vitro efficacy.

P-gp is not the only ATP-binding cassette (ABC) transporter that is associated with MDR. Besides p-gp, the members of the MDR associated protein (MRP) family have been extensively studied since 1992 (Cole et al. 1992). In 1998 another ABC transporter called ABCG2 was identified independently by three different groups (Doyle et al. 1998,

Allikmets et al. 1998, Miyake et al. 1999). ABCG2, that is also known as BCRP, MXR or ABCP, consists of 6 transmembrane domains. Thus, it is a half transporter member of the ABC superfamily. It probably requires dimerization in order to become a functional full transporter molecule (Litman et al. 2001). The different transporters have in part the same substrates. Doxorubicin efflux is mediated by all three ABC transporters. However, topotecan is transported by p-gp and ABCG2 (Bates et al. 2000). Therefore, it is important to know if an inhibitory substance acts multispecificly on more than one ABC transporter or if the modulator is selective for only one transport protein. Zosuquidar, for example, specifically inhibits p-gp and does not affect MRP1 or ABCG2 (Shepard et al. 2003). The specificity of the two modulators elacridar and tariquidar was investigated in this study, too.

6.2 Materials and methods

6.2.1 Drugs and chemicals

Starting materials and solvents for the synthesis of tariquidar were purchased from Lancaster Synthesis (Frankfurt, Germany), Sigma (München, Germany) and Merck (Darmstadt, Germany). Elacridar (GF 120918·HCl) was kindly provided by GlaxoSmithKline (Research Triangle Park, North Carolina, Unites States). Valspodar (SDZ PSC 833) was a gift from Novartis (Nürnberg, Germany). Fumitremorgin C was provided by the work group of Susan Bates (NIH, Bethesda, Maryland, United States). Papaverine and the solvents acetonitrile, ethanol and methanol were purchased from Merck. Mitoxantrone was obtained from Sigma. The suppliers of the other cytostatic drugs are mentioned in chapter 3. The PCR primers were ordered from MWG Biotech (Ebersberg, Germany). Calcein-AM was purchased from Molecular Probes (Eugene, Oregon, United States). For details concerning calcein-AM storage see chapter 4. PBS composition is specified in chapter 3. The ingredients of the loading buffer are mentioned in chapter 4.

6.2.2 Cell culture

All cell lines were purchased from the American Type Culture Collection (ATCC), Rockville, MD, USA and cultured as monolayers in 75 cm^2 flasks (Nunc, Wiesbaden, Germany). The cells were maintained at 37 ℃/5 % CO_2 in different culture media. MCF-7 cells were cultivated in RPMI 1640 culture medium (Sigma) supplemented with 1.5 g/l of sodium hydrogen carbonate and 10 % FCS, adjusted to pH 7.4. The cultivation of the Kb-V1/VBL cells is described in chapter 3. Subculturing was carried out with 0.2 % trypsin/EDTA (Viralex, Paa Laboratories, Pasching, Austria) in PBS once a week. The chemoresistant variant of the MCF-7 cell line, MCF-7/Topo, was obtained by adding increasing volumes of a topotecan solution within a period of about 40 days to achieve a topotecan concentration of 500 ng/ml culture medium (11.9 μl of 10^{-3} M topotecan in 70 % ethanol). After 3 passages the treated cells expressed sufficient quantities of ABCG2.

6.2.3 Synthesis of tariquidar

General conditions. Melting points (Mp) were determined on a BÜCHI 510 electrically heated copper block apparatus using an open capillary and are uncorrected. Silica gel 60 (0.063 - 0.200 nm, Merck) was used for column chromatography, and thin layer chromatography (TLC) was performed with silica gel plates (Merck F_{254}). Elemental analysis was carried out by the department of microanalysis of the faculty. Mass spectrometry analysis (MS) was performed on a Varian MAT 112 (PI-EIMS 70 eV). The peak intensity is indicated relatively to the strongest signal in %. Nuclear Magnetic Resonance (^{1}H-NMR) spectra were recorded using a Bruker ARX-300 spectrometer with deuterated chloroform or DMSO. The chemical shift δ is given in parts per million (ppm) with reference to the chemical shift of the residual protic solvent compared to tetramethylsilane (TMS, $\delta = 0$ ppm).

Synthesis. The preparation of tariquidar was performed according to Dodic et al. (1995), Roe et al. (1999) and Sharp et al. (1998) with slight modifications. A solution of 4-nitrophenethyl bromide **1** (10.5 g, 43.4 mmol), 6,7-dimethoxy-1,2,3,4-tetrahydro-

isoquinoline hydrochloride **2** (10.9 g, 47.5 mmol) and potassium carbonate (13.9 g, 100 mmol) in 100 ml DMF was heated at 100 °C for 6 h. The mixture was filtered and evaporated, the residue was taken up in water and extracted with dichloromethane (3 x 30 ml). The organic layer was dried over sodium sulphate and the solvents were removed under reduced pressure. The resulting solid was recrystallized from ethanol to give 10.52 g of 6,7-dimethoxy-2-[2-(4-nitrophenyl)ethyl]-1,2,3,4-tetrahydroisoquinoline **3** as orange crystals (mp 115 °C, yield: 65.3 %). This product was hydrogenated in ethanol (200 ml) at room temperature at a pressure of 5 bar in the presence of Pd/C (10 %, 1 g). After completion of hydrogenation the catalyst was filtered off and the solution was concentrated to give 8.16 g of 4-[2-(6,7-dimethoxy-3,4-dihydro-1*H*-isoquinolin-2-yl)ethyl]phenylamine **4** as a creamy solid (mp 125 °C, yield: 85.2 %).

^{1}H-NMR ([D$_6$]DMSO) of compound 4. δ[ppm] = 2.52-2.74 (m, 8H, CH_2), 3.51 (s, 2H, NCH_2C), 3.69 (s, 3H, OCH_3), 3.70 (s, 3H, OCH_3), 4.83 (br, 2H, NH_2), 6.45-6.51 (m, 2H, AA'BB'), 6.63 (s, 1H, Ar-H), 6.65 (s, 1H, Ar-H), 6.85-6.91 (m, 2H, AA'BB')

For the next step 2-amino-4,5-dimethoxybenzoic acid **5** (2.37 g, 12 mmol) and HOBt (1.84 g, 12 mmol) were dissolved in DMF (120 ml) for 10 min at room temperature. Compound **4** (3.75 g, 12 mmol) and DCC (2.48 g, 12 mmol) were successively added, and the reaction mixture was stirred at room temperature overnight. Subsequently, the solution was filtered and concentrated under reduced pressure. The residue was treated with sodium hydroxide solution (2 N) and extracted with dichloromethane (3 x 30 ml). The organic layers were separated, washed with water (3 x 30 ml) and brine (3 x 30 ml), dried over sodium sulphate and evaporated. The product was purified by column chromatography on silica gel using a mixture of dichloromethane and methanol (90:10, v/v) for elution, followed by recrystallization from isopropyl alcohol. Another column chromatography (elution with dichloromethane and methanol, 97:3, v/v) and recrystallization from ethyl acetate with petroleum ether gave 3.67 g of 2-amino-*N*-4-[2-(6,7-dimethoxy-3,4-dihydro-1*H*-isoquinolin-2-yl)-ethyl]phenyl-4,5-dimethoxy benzamide **6** (mp 180 °C, yield: 62:3 %) as a yellow solid.

Quinoline-3-carboxylic acid **7** (1.1 g, 6.38 mmol), compound **6** (3.14 g, 6.38 mmol) and HOBt (0.98 g, 6.38 mmol) were dissolved in dichloromethane at room temperature. DCC

(1.32 g, 6.38 mmol) was added, and the reaction mixture was stirred at room temperature over night. After filtration the solution was washed with a saturated solution of sodium hydrogen carbonate (3 x 30 ml), water (3 x 30 ml) and brine (3 x 30 ml). The solution was dried over sodium sulphate and the solvent was evaporated. The product was purified by column chromatography on silica gel by elution with a mixture of dichloromethane and methanol (97:3, v/v) followed by recrystallization from chloroform to give 1.5 g of tariquidar (quinoline-3-carboxylic acid (2-4-[2-(6,7-dimethoxy-3,4-dihydro-1*H*-isoquinolin-2-yl)ethyl]phenylcarbamoyl-4,5-dimethoxyphenyl)amide **8**.

Yield: 1.5 g (2.72 mmol, 36 %, creamy solid)

Mp: decomposition at 260 °C

^{1}H-NMR ([D$_6$]DMSO): δ[ppm] = 2.62 (m, 8H, CH_2), 3.55 (s, 2H, NCH_2C), 3.69 (s, 3H, OCH_3), 3.70 (s, 3H, OCH_3), 3.88 (s, 3H, OCH_3), 3.89 (s, 3H, OCH_3), 6.63 (s, 1H, Ar-H), 6.65 (s, 1H, Ar-H), 7.23-7.29 (m, 2H, Ar-H), 7.52 (s, 1H, Ar-H), 7.57-7.62 (m, 2H, Ar-H), 7.69-7.76 (m, 1H, Ar-H), 7.88-7.96 (m, 1H, Ar-H), 8.05-8.18 (m, 2H, Ar-H), 8.26 (s, 1H, Ar-H), 8.88 (d, ^{4}J = 2.2, 1H, COCCHC), 9.34 (d, ^{4}J = 2.2, 1H, COCCHN), 10.33 (s, 1H, NH), 12.30 (s, 1H, NH)

MS (PI-EIMS 70 eV): m/z (%) = 646 ([$M^{\cdot+}$], 6), 335 ([M-NH-C_6H_4-CH_2-CH_2-C_9H_8N(OCH_3)]$^+$, 25), 206 ([CH_2-$C_9H_8N(OCH_3)$]$^+$, 100), 164 ([CO-$C_6H_2(OCH_3)$]$^+$, 58)

Analysis:

calculated	C:	70.57	H:	5.92	N:	8.66
found	C:	69.78	H:	6.01	N:	8.87

$C_{38}H_{38}N_4O_6$ (646.74)

6.2.4 Spectroscopic methods

Absorption spectra were recorded on a Cary 100 conc UV visible spectrophotometer (Varian, Darmstadt, Germany). The fluorescence spectra were measured on a Perkin Elmer LS50B luminescence spectrophotometer (Wiesbaden, Germany). Solutions of the p-gp modulators were prepared with concentrations from 0.1 to 10 μM in ethanol, methanol

or phosphate buffer, pH 7.4, by dilution of a 1 mM stock solution (DMSO).

To determine the water solubility of the p-gp modulators, a Kontron UV-VIS spectrophotometer was used. Stock solutions (1 mM) made in DMSO were diluted in loading buffer to achieve concentrations in the range from 0.1 nM to 30 μM. The solutions were measured at a wavelength of 600 nm in polystyrene cuvettes. An optical density higher than 0.05 indicates insolubility of the tested compound.

6.2.5 Chemosensitivity assay

The chemosensitivity assay was performed according to the procedure developed by Bernhardt et al. (1992). Details are given in chapter 3.2.6.

6.2.6 Calcein-AM efflux assay

The calcein-AM efflux assay is described in detail in chapter 4.

6.2.7 RT-PCR

The RT-PCR was performed as described in chapter 5.2.2. The following primer sequences were used to detect the ABCG2 gene.

Table 6.1: Primer sequences used for RT-PCR

Primer		Sequence	bp
β-actin	sense	5'-CGGGATCCCCAACTGGGAC-3'	304
	antisense	5'-GGAATTCTGGCGTGAGGGA-3'	
ABCG2	sense	5'-TTCCAAGCAGGATAAGCCACT-3'	589
	antisense	5'-AGCCACCATCATAAGGGTAAA-3'	

6.2.8 ABCG2 assay

The assay was performed according to de Bruin et al. (1999), Lee et al. (1994), Maliepaard et al. (1999) and Robey et al. (2001a) with modifications. In brief: ABCG2 expressing

MCF-7/Topo cells were used for this assay. Cells that were passaged 3 or 4 days before the assay was carried out, were trypsinized and washed with PBS at 25 ℃. A number of $1 \cdot 10^6$ cells per ml was adjusted with culture medium. Mitoxantrone was added to the cell suspensions to achieve a concentration of 20 μM (6.67 μl of 3 mM stock solution in 70 % ethanol). After short vortexing, test compounds were added in different concentrations. The cell solutions were vortexed again and incubated for 30 min at 37 ℃/5 % CO_2. According to the literature an incubation period of 30 min is sufficient for complete uptake of mitoxantrone in cells. Subsequently, the cells were washed with ice cold PBS at 4 ℃ and resuspended in culture medium. Then, the samples were incubated for 1 h at 37 ℃/5 % CO_2. After an incubation period of 1 h an equilibrium had developed between mitoxantrone inside the cells and in the surrounding medium, i.e. no further mitoxantrone efflux can be determined. The medium was removed by centrifugation, and the cell pellet was rinsed once with ice cold PBS, resuspended in 0.5 ml of PBS per $1 \cdot 10^6$ cells and placed on ice in the dark. A FACS Calibur™ (Becton Dickinson, Heidelberg, Germany) was used to analyze the samples. A minimum of 10,000 events was collected per sample and the events were gated according to forward scatter and sideward scatter to exclude clumps and debris. The photomultiplier settings were as follows: E-1 for FSC, 200 for SSC, 450 for FL1-H and 700 for FL4-H. FL4-H histograms were analyzed by the WinMDI 2.8 software.

To determine the mitoxantrone efflux two control samples were prepared. The first control sample was used for the determination of the 100 % mitoxantrone uptake. Therefore, fumitremorgin C (2 μl of 3 mM stock solution in DMSO) was added to a sample containing $1 \cdot 10^6$ cells per ml and mitoxantrone (20 μM). After short vortexing, the control sample was incubated for 30 min at 37 ℃/5 % CO_2 and washed with ice cold PBS at 4 ℃. The cells of this control sample were then resuspended in ice cold PBS and placed on ice in the dark until measurement to avoid mitoxantrone efflux. In the second control sample ($1 \cdot 10^6$ cells per ml) cells were loaded with mitoxantrone (20 μM) during an incubation period of 30 min at 37 ℃/5 % CO_2. After a washing step, the cells of the second control sample were resuspended in culture medium and incubated for 1 h at 37 ℃/ 5 % CO_2 to determine the residual mitoxantrone fluorescence after mitoxantrone was effluxed. Subsequently, the cells were washed, resuspended in ice cold PBS and measured

at a flow cytometer according to the aforementioned settings. The difference between the fluorescence intensities of the second control sample and the 100 % mitoxantrone uptake value determined with the first control sample represents the 100 % mitoxantrone efflux. All other samples were related to the 100 % efflux value resulting in mitoxantrone efflux expressed in [%] depending on the added test compound concentration.

6.3 Results and discussion

The two newly developed p-gp modulators elacridar and tariquidar were characterized regarding their in vitro efficacy to inhibit p-gp mediated drug efflux as well as their potential cytotoxicity. Furthermore, the inhibitory effect of compound **4** on p-gp was examined to identify structure activity relationships. Compound **4** is a common structural part of the two modulators. The selectivity to other multidrug transporters responsible for MDR was investigated, too. As tariquidar could not be procured, the modulator was synthesized in our department. The spectroscopical characteristics that were important for analytical detection were also determined.

6.3.1 Synthesis of tariquidar

The 3^{rd} generation p-gp modulator tariquidar (XR 9576) was developed by Roe et al. (1999) by evaluation of a series of commercially available compounds which contained features common to known p-gp modulators such as verapamil, S 9788 (Dhainaut et al. 1992), CP 100356 (Kajiji et al. 1994), biricodar, elacridar and zosuquidar. These structural characteristics include a tertiary amine, a dimethoxyphenyl group and an amide group (Wang et al. 2003), and seemed to be important for p-gp inhibition (see chapter 6.3.4). In our department tariquidar was synthesized as depicted in Fig. 6.2.

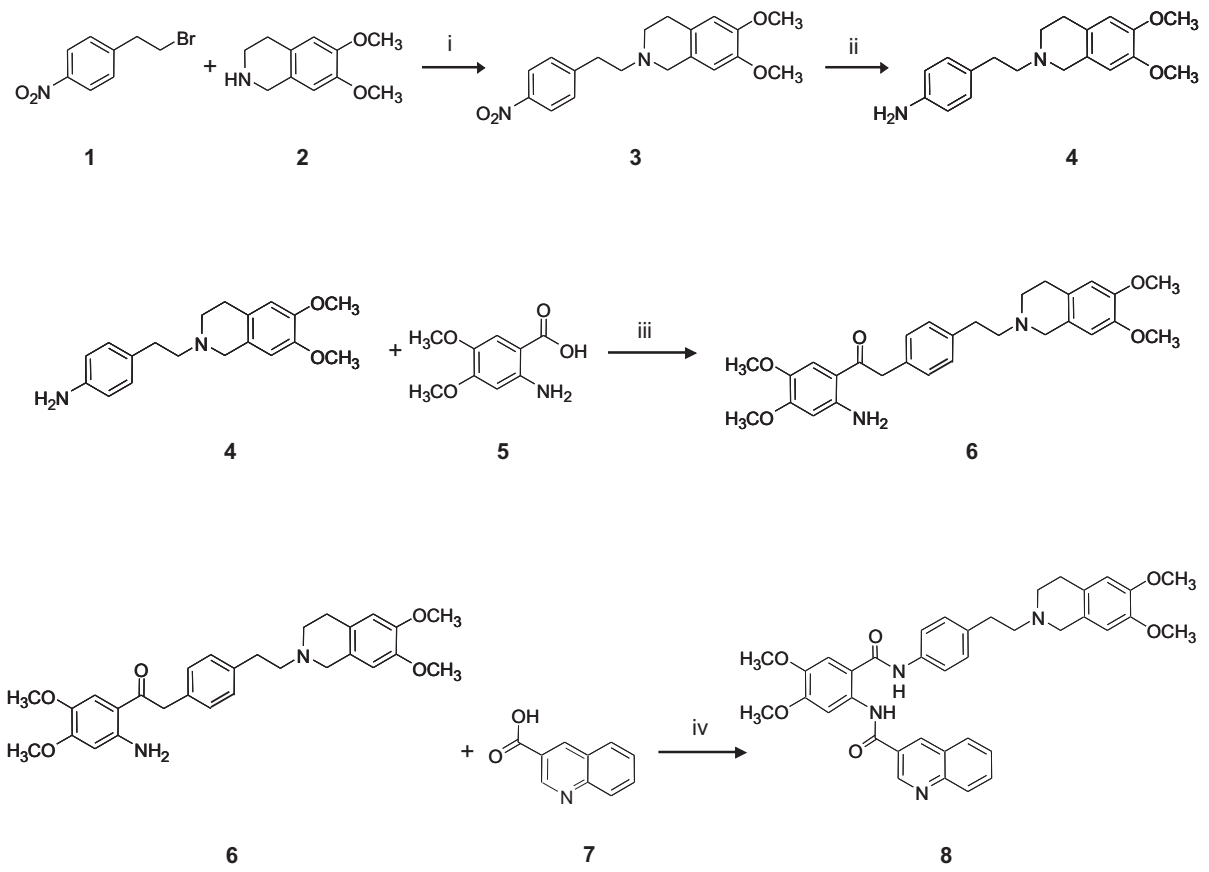

Figure 6.2: Strategy of tariquidar **8** synthesis reported by Dodic et al. (1995) and Roe et al. (1999). The following reagents were used: i) K_2CO_3, DMF, 100°C; ii) Pd/C, 5 bar; iii) HOBt, DCC, DMF; iv) HOBt, DCC, CH_2Cl_2

The commercially available bromide derivative **1** was allowed to react with isoquinoline **2** according to a nucleophilic substitution in the presence of potassium carbonate in DMF. The subsequent hydrogenation of the nitro compound **3** was carried out according to standard procedures using palladium on charcoal (10 % Pd/C) at 5 bar hydrogen pressure. In the next step the resulting amine **4** was coupled to the anthranilic acid **5** using HOBt and DCC as coupling reagents to yield the intermediate 2-aminobenzamide **6**. The same reagents were used in the last step. Here, reaction of **6** by activation of the carboxylic acid **7** with HOBt led to the anthranilamide derivative tariquidar **8**.

6.3.2 Spectroscopic characterization

After the in vitro characterization of the two selected modulators, pharmacokinetic investigations were planned. To be able to detect the modulators by HPLC using a fluorescence or UV/VIS detector, the spectroscopical characteristics of the substances have to be known. Moreover, this information is necessary for the in vitro investigation of the p-gp modulation in the calcein-AM efflux assay and the MDR transporter selectivity using the ABCG2 assay, that the modulators do not show fluorescence signals interfering with the respective fluorescence agents calcein and mitoxantrone. For this reason, fluorescence and UV spectra were recorded and the respective maxima were determined.

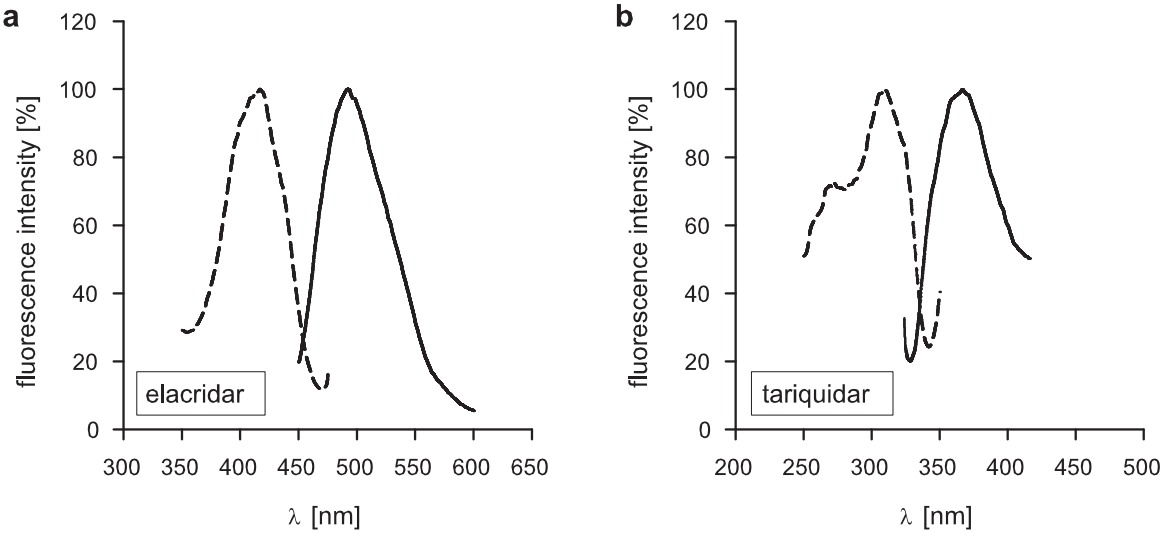

Figure 6.3: (a) Excitation (λ_{em} = 492 nm) and emission (λ_{ex} = 418 nm) spectrum of elacridar in phosphate buffer pH 7.4. (b) Excitation (λ_{em} = 367 nm) and emission (λ_{ex} = 308 nm) spectrum of tariquidar in phosphate buffer pH 7.4.

Fig. 6.3 shows representative fluorescence spectra of elacridar and tariquidar. The fluorescence spectra were measured in three different solvents: loading buffer, ethanol and methanol. The excitation and emission maxima were determined as presented in table 6.2.

The excitation and emission maxima corresponded well for the solvents ethanol and methanol. The fluorescence spectra obtained in loading buffer (pH 7.4) differed in the positions of the maxima, compared to spectra in ethanol and methanol. Tariquidar emitted

Table 6.2: Excitation and emission maxima of elacridar and tariquidar in different solvents.

solvent		buffer, pH 7.4	ethanol	methanol
elacridar	λ_{ex} [nm]	417	407	405
	λ_{em} [nm]	492	469	475
tariquidar	λ_{ex} [nm]	308	318	316
	λ_{em} [nm]	366	360	359

at shorter wave lengths than elacridar. This was expected because the elacridar structure includes an acridine system which is responsible for the fluorescence at higher wave lengths.

Representative UV spectra of elacridar and tariquidar are depicted in Fig. 6.4. The UV spectra were measured in three different solvents: loading buffer, ethanol and methanol. The excitation and emission maxima were determined as presented in table 6.3.

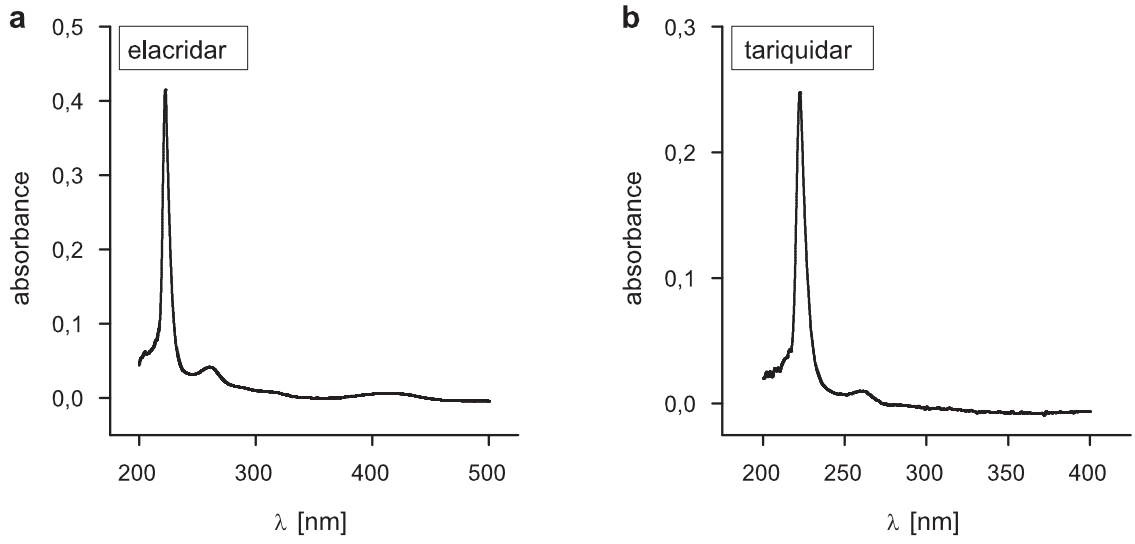

Figure 6.4: (a) UV spectrum of elacridar (100 nM in phosphate buffer, pH 7.4) (b) UV spectrum of tariquidar (100 nM in phosphate buffer, pH 7.4)

The excitation and emission maxima corresponded well for all examined solvents. The UV maxima of tariquidar were determined at shorter wave lengths compared to the maxima of elacridar. Furthermore, an additional maximum was observed in the elacridar UV spectra at a wave length of about 410 nm due the acridine system of the elacridar

Table 6.3: UV maxima of elacridar and tariquidar in different solvents.

solvent	buffer pH 7.4	ethanol	methanol
elacridar	226 nm	225 nm	228 nm
	260 nm	258 nm	258 nm
	413 nm	410 nm	408 nm
tariquidar	222 nm	220 nm	223 nm
	247 nm	245 nm	244 nm

structure and the resulting light yellow color of substance and prepared solutions.

The solubility of a compound is another important criterion for analytical examinations. The modulators were dissolved in different solvents at various concentrations from 1 nM to 30 μM and measured at 600 nm in an UV/VIS-spectrophotometer (data not shown). Aqueous loading buffer, methanol and acetonitrile were used as solvents. Elacridar and tariquidar are readily soluble in the three examined solvents within the tested concentration range. However, aqueous solutions with modulator concentrations higher than 30 μM are not recommended for the use in in vitro experiments. At this concentration the measured optical density of the aqueous solutions slightly increased indicating insolubility at modulator concentrations higher than 30 μM. This was not observed in ethanol and methanol solutions.

In conclusion, the two examined modulators are detectable with both fluorescence and UV spectroscopy. The fluorescence of elacridar and tariquidar has no influence on the assays that are used for the investigation of the selectivity and the in vitro efficacy (see 6.3.4 and 6.3.5). In the ABCG2 assay an excitation wavelength of 635 nm is used and calcein is excited at 488 nm in the case of the calcein-AM efflux assay. At both wavelengths the two modulators are not excited. Elacridar and tariquidar are easily soluble in different solvents such as methanol and acetonitrile. In aqueous solutions the modulator concentrations should be kept below $1{\cdot}10^{-4}$ M to avoid solubility problems.

6.3.3 Cytotoxicity of the p-gp modulators elacridar and tariquidar

To test the cytotoxicity of an anticancer drug depending on the presence of a p-gp inhibitor the latter can only be used in concentrations that do not affect the cell proliferation. Hence, the in vitro cytotoxicity was investigated to obtain an indication for these modulator concentrations. Kb-V1/VBL and MCF-7/Topo cells were used in chemosensitivity assays for the p-gp modulator characterization. According to the chemosensitivity assay procedure the cells were incubated for up to 168 hours with elacridar and tariquidar using concentrations from 5 to 500 nM (Kb-V1/VBL) and 0.1 to 10 μM (MCF-7/Topo), respectively. Fig. 6.5 and Fig. 6.6 present the results for the in vitro cytotoxicityof the two modulators.

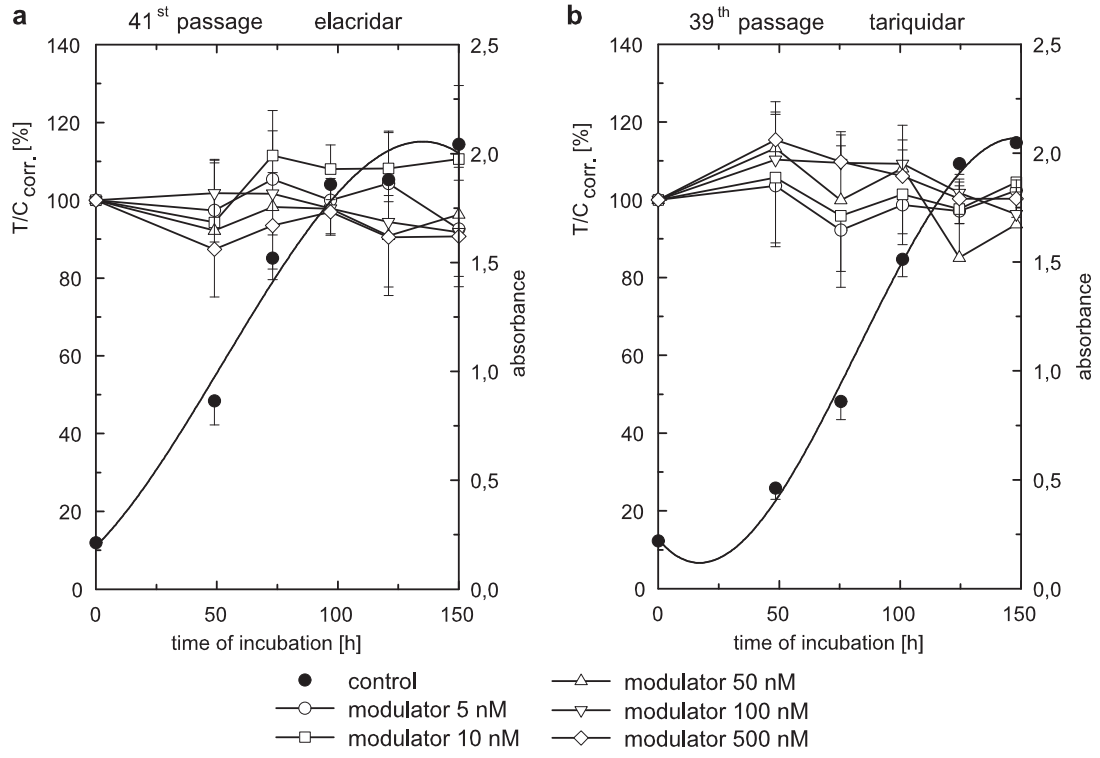

Figure 6.5: Impact of different concentrations of elacridar (a) and tariquidar (b) on the growth of Kb-V1/VBL cells. The incubation with the modulators has no effect on the cell proliferation.

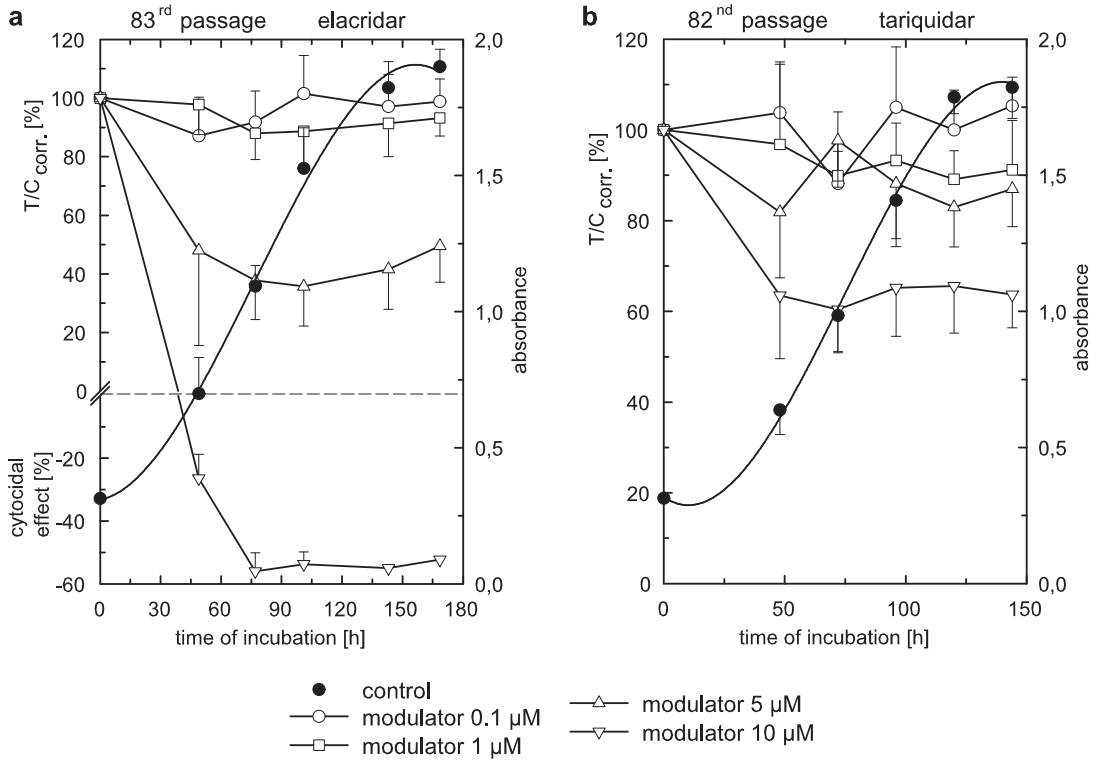

Figure 6.6: Impact of different concentrations of elacridar (a) and tariquidar (b) on the growth of MCF-7/Topo cells. Addition of high elacridar concentrations (10 μM) results in a cytocidal effect. The cytotoxicity of tariquidar is obvious at a concentration of 10 μM, at which the cell growth is inhibited by 40 %.

The growth of the Kb-V1/VBL cells was not influenced by long term incubation with elacridar and tariquidar at the examined modulator concentrations. Even 500 nM of modulator, a concentration 10-fold higher than that required for a complete reversal of drug resistance, had no effect on the Kb-V1/VBL cells. By contrast, the MCF-7/Topo cell line showed sensitivity to the new modulators at high concentrations, particularly to elacridar. At a concentration of 10 μM elacridar had a cytocidal effect.5 μM of elacridar were sufficient to induce a cytostatic effect and to reduce the cell proliferation by 50 %. Tariquidar did not affect the growth of MCF- 7/Topo cells to such an extent. Tariquidar concentrations higher than 5 μM were necessary to influence the cell proliferation, e.g. at a concentration of 10 μM, a growth inhibition by 40 % was observed. The IC_{50} values determined in the ABCG2 assay were 5 (elacridar) and 2 (tariquidar) times lower than the concentrations that caused growth inhibition.

Thus, the achieved potentiation of the cytostatic effects of anticancer drugs by co-

application of MDR modulators in the respective long term incubation studies may be attributed to inhibition of p-gp or ABCG2 function since the cytotoxicity of the modulators is irrelevant at the concentrations used in the corresponding assays.

6.3.4 In vitro efficacy of p-gp inhibitors

The Kb-V1/VBL cell line which was used to investigate the p-gp inhibitors, exhibited an acquired MDR phenotype as a result of p-gp overexpression (see chapter 4). The in vitro efficacy of elacridar, tariquidar and valspodar was examined in two different test series. The ability of the modulators to potentiate the cytotoxicity of several drugs was evaluated in the chemosensitivity assay. The impact of the modulators on the p-gp efflux activity was investigated in the calcein-AM efflux assay.

6.3.4.1 Determination of the inhibition of the p-gp mediated efflux by the chemosensitivity assay

Over the whole incubation period of up to 150 hours Kb-V1/VBL cells were exposed to cytostatic drugs that are known p-gp substrates. The drugs were used at low concentrations that did not affect the growth of Kb-V1/VBL cells. Additionally, the cells were incubated with combinations of drugs and 3 different concentrations of the modulators elacridar, tariquidar and valspodar, respectively. The modulators had no cytotoxic effects in the used concentrations. The ability of elacridar and tariquidar to reverse resistance of the Kb-V1/VBL cells to various cytostatic agents is shown in Figs. 6.7 to 6.10.

The resistance to all examined drugs was completely reversed by the addition of the new modulators elacridar and tariquidar at a concentration of 50 nM, indicated by the cytocidal effect. The two modulators produced significant reversal of resistance at concentrations of 10 nM in the case of doxorubicin (Fig. 6.7) and topotecan (Fig. 6.9).

The potentiation of the cytotoxic effect of topotecan was delayed when compared to the other cytostatic drugs, which showed cytocidal effects 50 hours after addition of 50 nM of the modulators. The potency of elacridar was comparable with that of tariquidar with respect to the reversal of resistance against the cytostatic drugs.

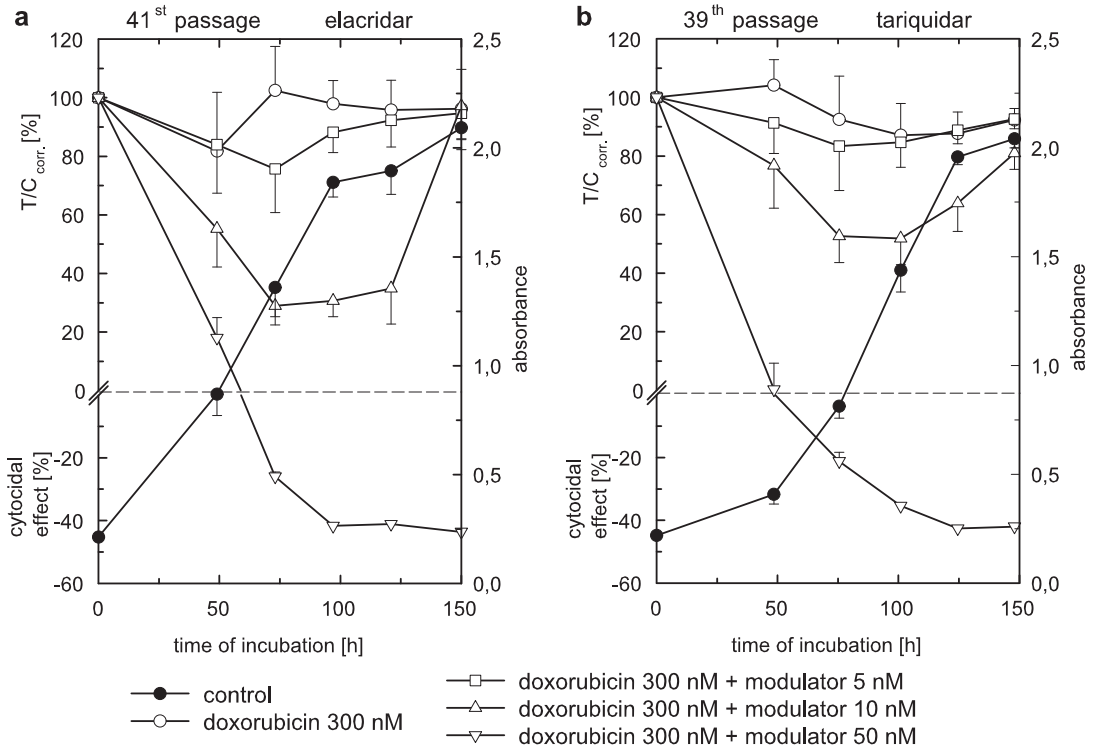

Figure 6.7: Impact of different concentrations of elacridar (a) and tariquidar (b) on the chemosensitivity of Kb-V1/VBL cells against doxorubicin (300 nM). The chemoresistance of the cells is fully reversed after addition of 50 nM of modulator.

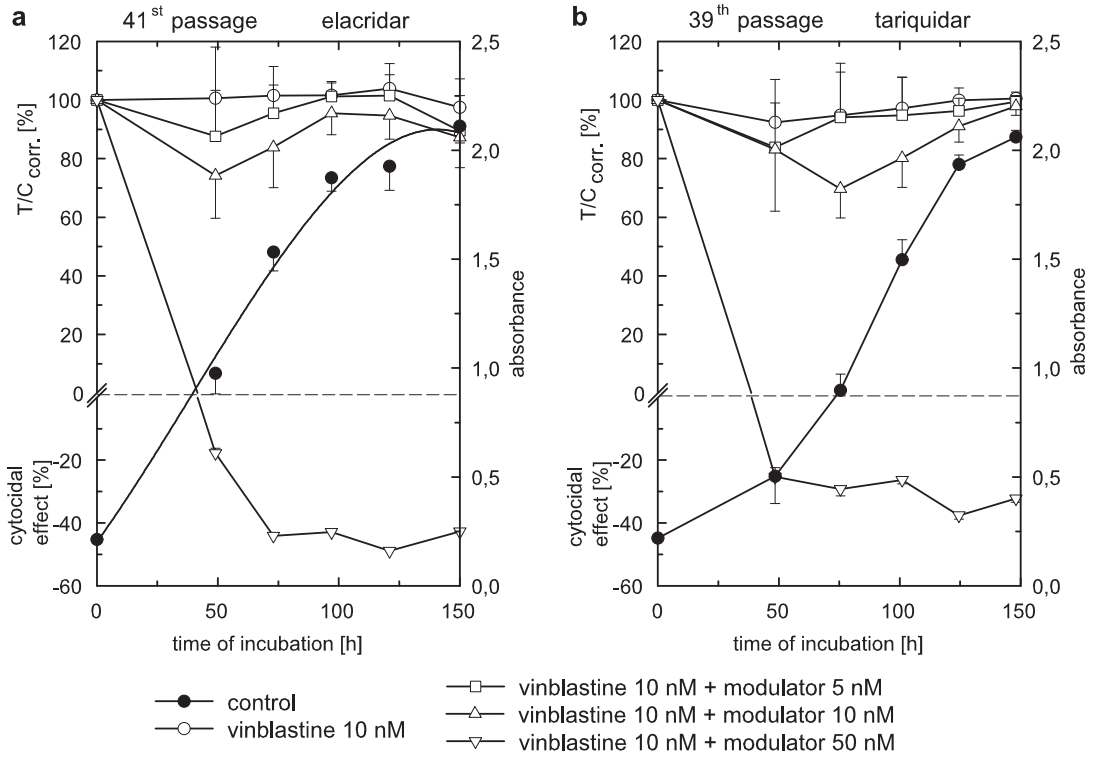

Figure 6.8: Impact of different concentrations of elacridar (a) and tariquidar (b) on the chemosensitivity of Kb-V1/VBL cells against vinblastine (10 nM). The chemoresistance of the cells is completely abrogated after addition of 50 nM of modulator.

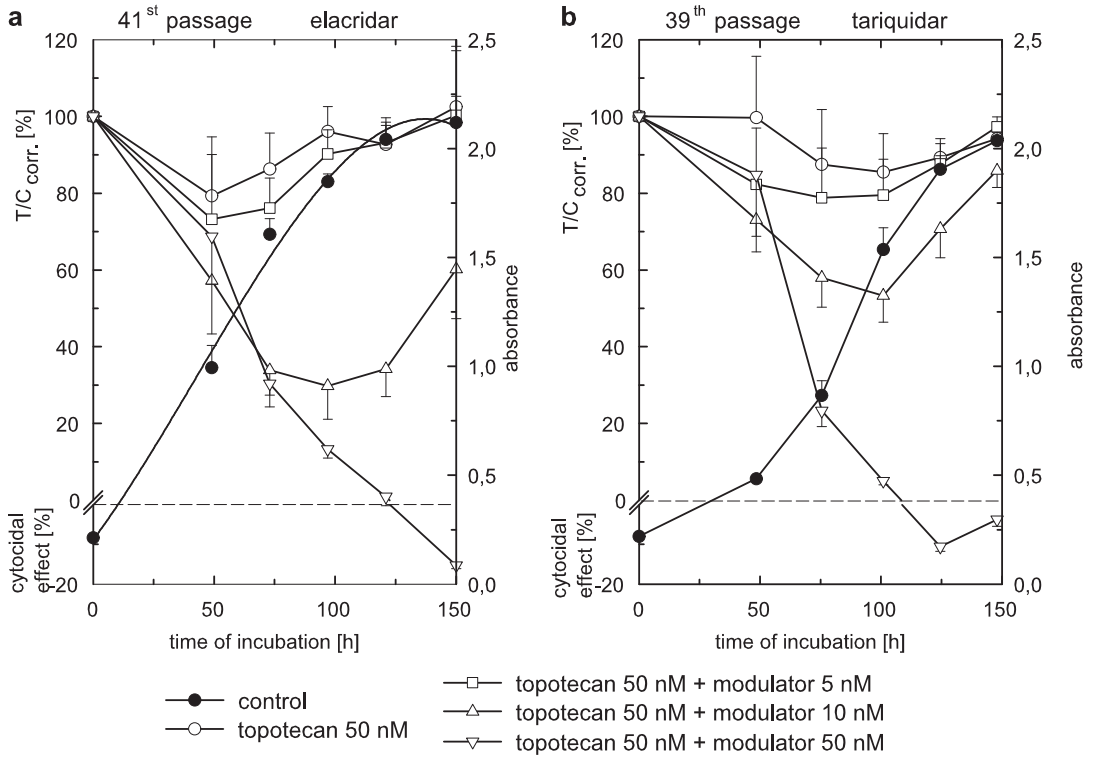

Figure 6.9: Impact of different concentrations of elacridar (a) and tariquidar (b) on the chemosensitivity of Kb-V1/VBL cells against topotecan (50 nM). The chemoresistance of the cells is completely abrogated after addition of 50 nM of modulator.

Fig. 6.10 and Fig. 6.11 compare the effect of paclitaxel on Kb-V1/VBL cells in combination with either the 3^{rd} generation modulators or the 2^{nd} generation modulator valspodar. Almost complete reversal of resistance to paclitaxel was achieved by the addition of 1 μM valspodar. A cytostatic but no cytocidal effect was observed at this valspodar concentration. In contrast, already an addition of 50 nM of elacridar and tariquidar sufficed to restore the paclitaxel resistance completely in case of the new modulators elacridar and tariquidar.

In case of vinblastine (Fig. 6.8) and paclitaxel (Fig. 6.10) it was noticeable that the useful concentration range of the modulators was very narrow. The co-incubation of 10 nM of elacridar or tariquidar with vinblastine had nearly no influence on the growth of Kb-V1/VBL cells, whereas an addition of 50 nM of p-gp inhibitor led already to a clear cytocidal effect of about 40 %.

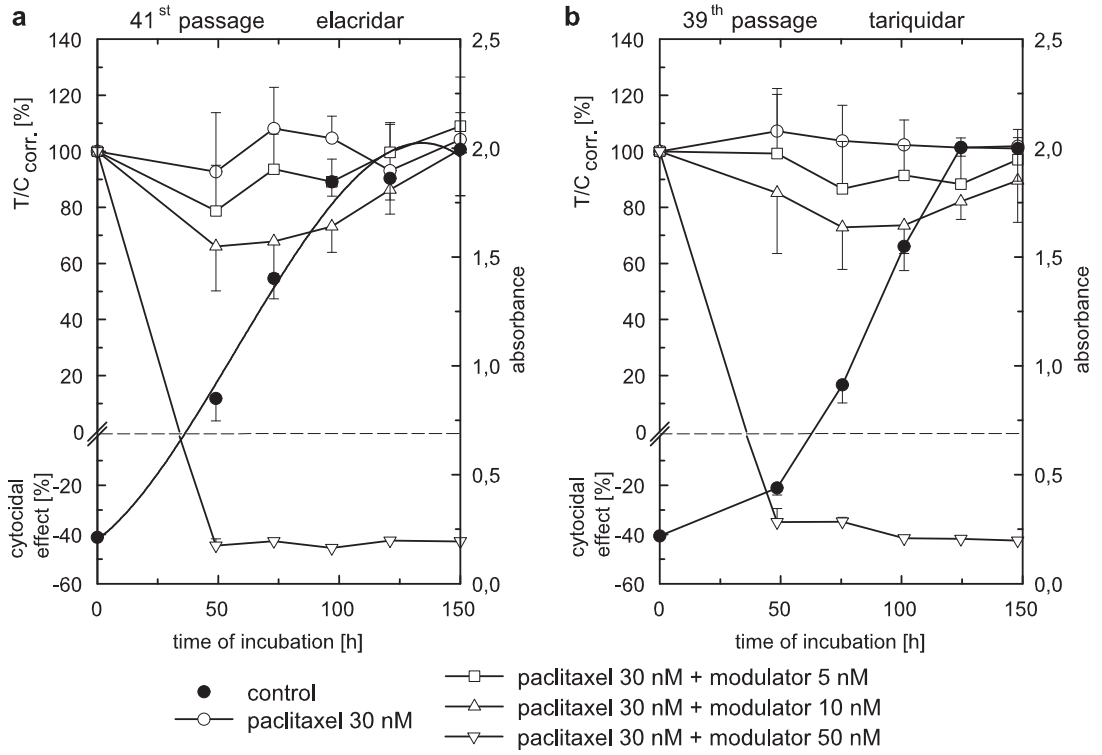

Figure 6.10: Impact of different concentrations of elacridar (a) and tariquidar (b) on the chemosensitivity of Kb-V1/VBL cells against paclitaxel (30 nM). The chemoresistance is fully reversed by the addition of 50 nM of modulators.

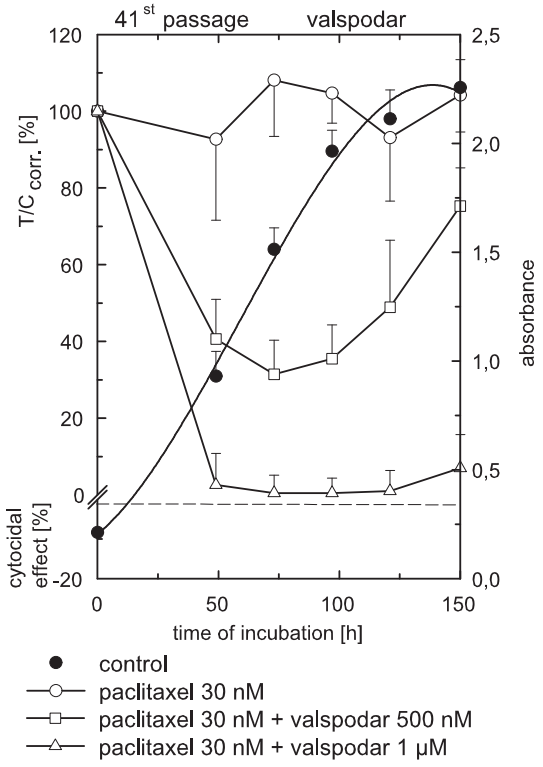

Figure 6.11: Impact of different concentrations of valspodar on the chemosensitivity of Kb-V1/VBL cells against paclitaxel (30 nM). Addition of valspodar (c) leads to a cytostatic inhibition of the Kb-V1/VBL cell proliferation.

The results show that elacridar and tariquidar are highly active p-gp modulators. Both compounds were very potent by fully reversing resistance to various agents associated with the MDR phenotype in the multidrug resistant Kb-V1/VBL cell line. The new modulators were considerably more potent than valspodar. Importantly, they did not affect the activity of cisplatin as presented in Fig. 6.12. This was expected as cisplatin is not a p-gp substrate and hence, the inhibition of the p-gp mediated efflux in the Kb-V1/VBL cells by the new modulators elacridar and tariquidar should not lead to an improvement of the chemosensitivity of the Kb-V1/VBL cells against cisplatin. Moreover, the lack of additive toxicity shown in Fig. 6.12 supports the conclusion that at the used concentrations the modulators do not act as cytotoxic drugs.

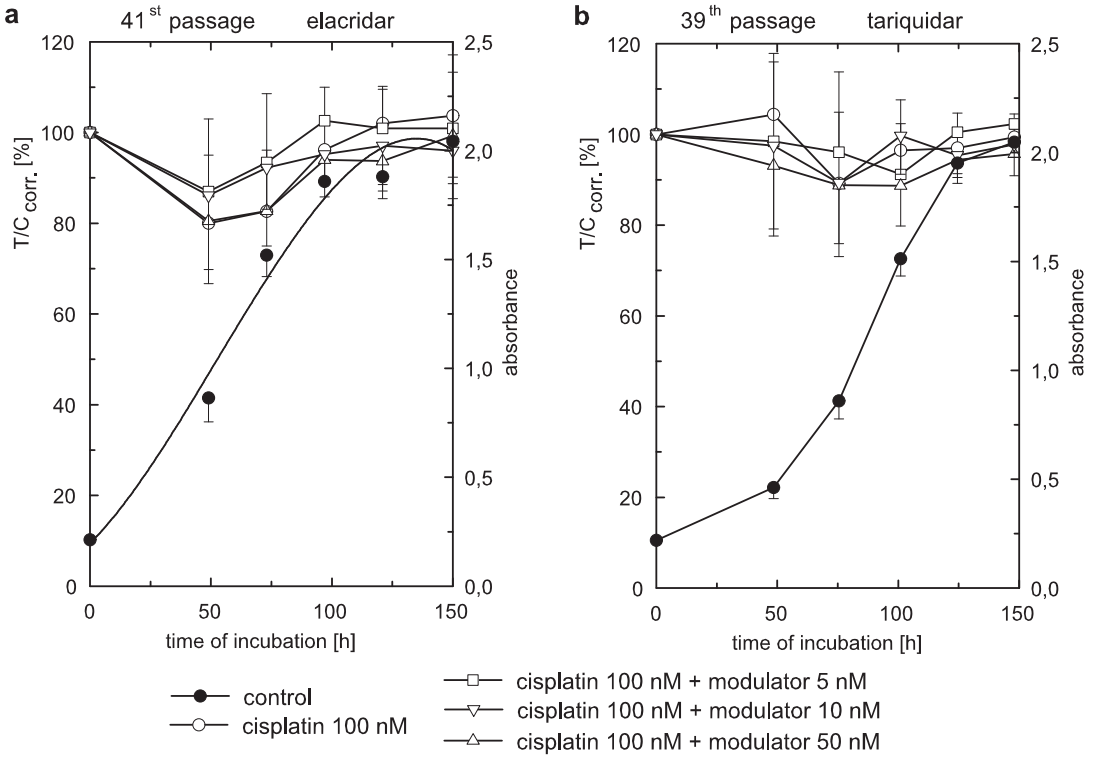

Figure 6.12: Impact of different concentrations of elacridar (a) and tariquidar (b) on the chemosensitivity of Kb-V1/VBL cells against cisplatin (100 nM). Addition of the modulators does not enhance the effect of the non p-gp substrate cisplatin.

6.3.4.2 Determination of the p-gp activity by the calcein-AM efflux assay

The p-gp inhibitory potency (IC_{50} values) of the new modulators was determined in the calcein-AM efflux assay. If p-gp function is blocked by an added test compound, calcein-

AM is hydrolyzed to calcein by esterases after penetration across the cell membrane. Calcein is trapped inside the cells due to its hydrophilicity and its fluorescence is taken as a measure of transport inhibition. The test compounds were used in different concentrations with respect to the construction of concentration response curves. A sample incubated without test compounds served as control and represented 100 % of calcein-AM efflux. The geometric means were calculated from the fluorescence intensity histograms, related to the control and plotted against the test compound concentration. The results of the

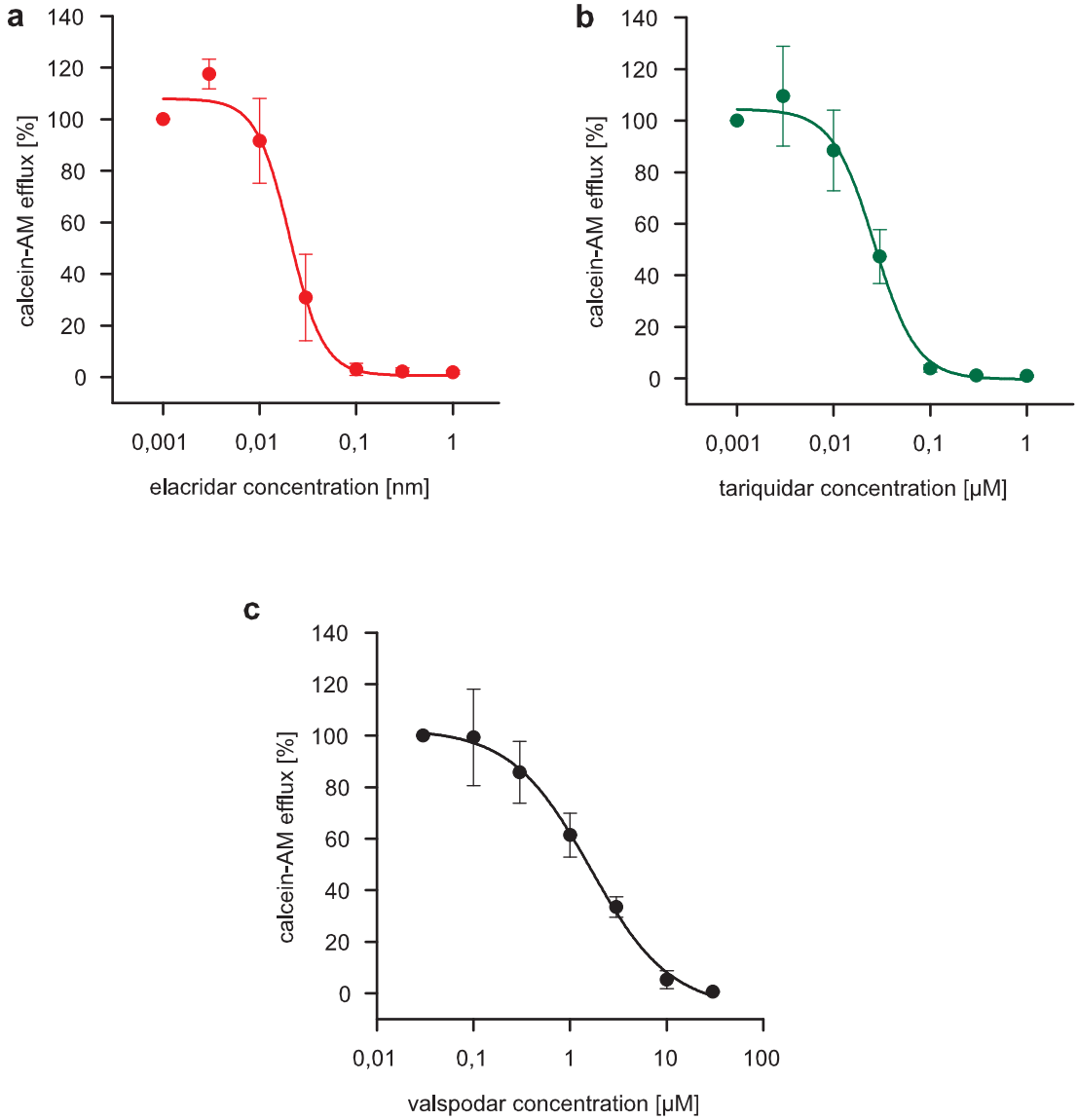

Figure 6.13: P-gp inhibition by the modulators elacridar (a), tariquidar (b) and valspodar (c) in the calcein-AM efflux assay on Kb-V1/VBL cells. Increasing modulator concentrations lead to an enhanced efflux inhibition.

calcein-AM efflux assay for the p-gp modulators elacridar, tariquidar and valspodar are presented in Fig. 6.13.

The addition of increasing concentrations of modulators led to sigmoidal concentration response curves. The IC_{50} values were calculated using the Hill equation (see table 6.4).

Table 6.4: IC_{50} values of the p-gp modulators elacridar, tariquidar and valspodar calculated from the inhibition curves described in Fig. 6.13. The IC_{50} value of valspodar is about 80 times higher than the values of elacridar and tariquidar.

modulator	elacridar	tariquidar	valspodar
IC_{50} value	20.5 ± 1.7 nM	26.5 ± 2.5 nM	1.62 ± 0.3 μM

The shape and the slope of the concentration response curves of elacridar and tariquidar modulation were similar. Moreover, the slopes of the curves were steeper compared to the curve obtained by valspodar modulation. It is obvious that compared to valspodar the 3^{rd} generation p-gp modulators inhibited calcein-AM efflux completely at very low concentrations. According to the IC_{50} values tariquidar and elacridar are 60 and 80 times more potent p-gp inhibitors than valspodar. Therefore, elacridar and tariquidar appeared to be very potent p-gp modulators.

The structures of elacridar and tariquidar are in part identical. The common part, compound **4** (see page 126 and Fig. 6.15), was also tested in the calcein-AM efflux assay to

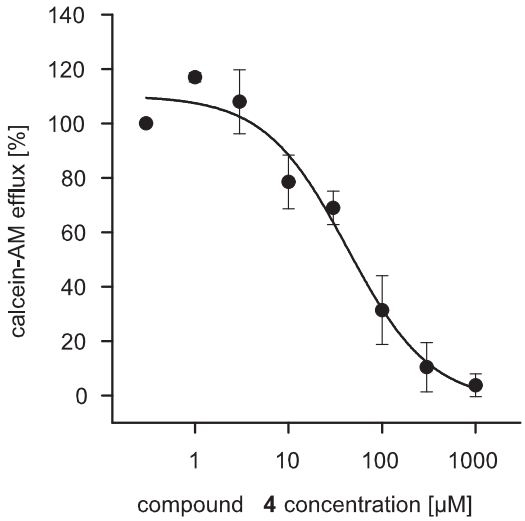

Figure 6.14: Impact of compound **4** on the p-gp mediated calcein-AM efflux. Increasing concentrations lead to enhanced efflux inhibition.

clarify the contribution of this partial structure to the high p-gp inhibitory potency of the modulators. Fig. 6.14 shows the sigmoidal concentration-response curve of compound **4** as an inhibitor of the calcein-AM efflux.

The IC_{50} value of compound **4** (42.7 ± 13.2 μM) was about 5 times lower than the IC_{50} value of the 1^{st} generation modulator verapamil, which was determined to be 248 μM (see chapter 4.5.2). Additionally, in preliminary investigations, both papaverine and compound **2** were tested in the calcein-AM efflux assay. Papaverine was chosen because of its structural similarity to compound **4** (Fig. 6.15). The distance between the ring system and the phenyl ring structure is similar in both compounds as demonstrated by superimposition of the structures in Fig. 6.16.[2] Papaverine produced a 25 % inhibition of the calcein-AM efflux at a concentration of 100 μM. In contrast, compound **2** lacking the phenyl ring did not inhibit the calcein-AM efflux. Thus, both ring systems arranged in a critical distance appear to be crucial for the potent p-gp modulating activity of elacridar and tariquidar.

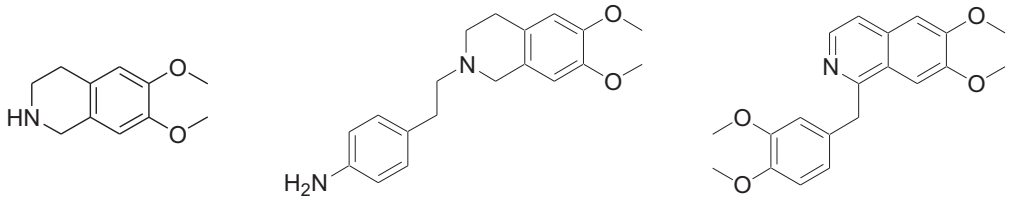

compound **2** compound **4** papaverine

Figure 6.15: Structures of compounds **2** and **4** and papaverine. Compounds **2** and **4** are building blocks for the synthesis of tariquidar.

[2]Both substances were fitted and minimized by means of multifit tool implemented in Sybyl 6.9.2 (Tripos Inc., ST. Louis, Missouri, USA). Gasteiger-Hückel-charges were applied at all atoms. For compound **4** the Tripos Force Field is 15.28 kcal/mol and for papaverine 19.59 kcal/mol, respectively. The analysis was performed by Hendrik Preuß(Institute of Pharmaceutical Chemistry, University of Regensburg, Germany).

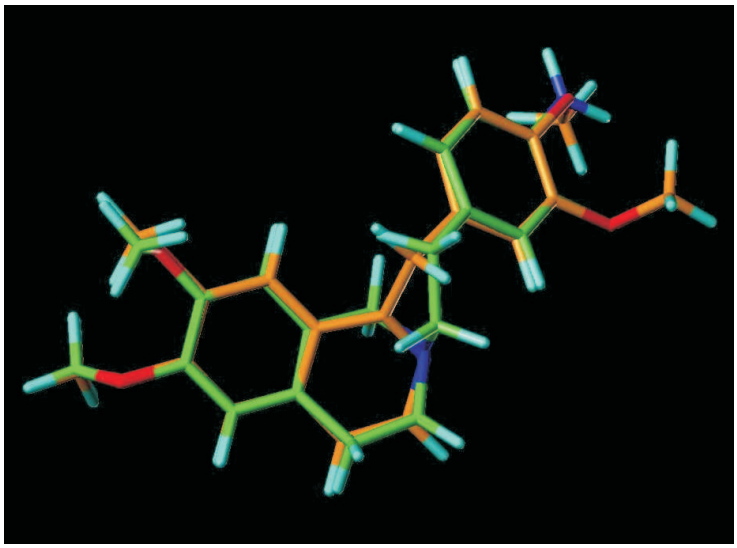

Figure 6.16: Superimposition of compound **4** (green) and papaverine (orange) indicates that both substances are structurally similar.

The results of the chemosensitivity assay were confirmed with the calcein-AM efflux assay. The new substances elacridar and tariquidar are highly potent p-gp modulators, that are able to inhibit the p-gp mediated efflux directly.

6.3.5 Selectivity of the 3^{rd} generation modulators

P-gp is a member of a large superfamily of ABC efflux transporters which contribute to the "impermeability" of the blood-brain barrier (BBB) to numerous drugs. Apart from p-gp the members of the MRP family, MRP1 and MRP2, and the ABCG2 transporter are to be mentioned. To increase the concentration of cytostatic drugs, which are substrates of one or more efflux transporters, inside the human body, multispecific modulators should be administered to block several transporters at the same time. Therefore, the selectivity of the modulators elacridar and tariquidar was investigated. In chapter 6.3.4 the inhibition of the p-gp function by these modulators was described. In another study the ability of elacridar and tariquidar to inhibit the function of the ABCG2 transporter was examined. Again, chemosensitivity assays were used to investigate the potency of the modulators to intensify the effect of cytostatic ABCG2 substrates. The modulation of the ABCG2 function by elacridar and tariquidar was investigated with an optimized flow cytometry assay.

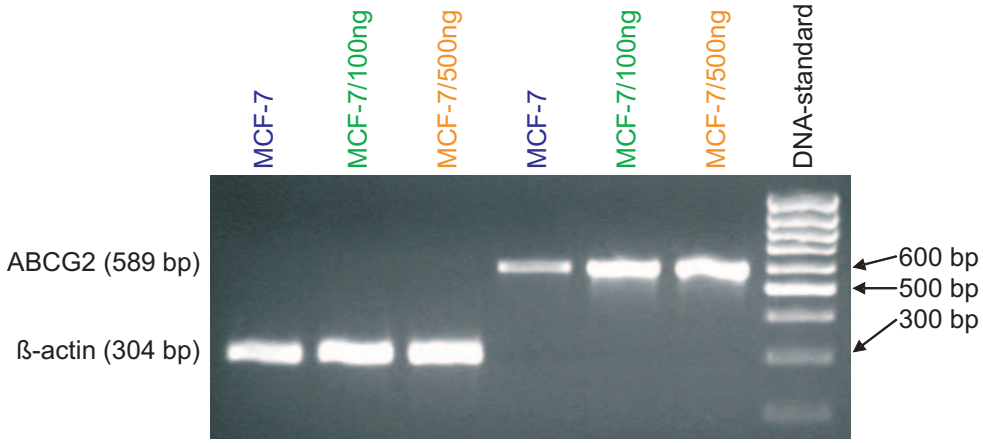

Figure 6.17: Determination of mRNA encoding ABCG2 in wildtype MCF-7 cells and chemoresistant MCF-7/100ng and MCF-7/500ng subclones. The intensity of the ABCG2 bond (589 bp) is higher with increasing topotecan concentrations indicating an intensified ABCG2 expression (ethidiumbromide stained agarose gel after RT-PCR (34 cycles); β-actin served as a control).

In both assays, MCF-7 cells, which possess mRNA encoding ABCG2, were used. These cells expressed functional ABCG2 protein when incubated with increasing concentrations of topotecan up to 500 ng/ml (see Fig. 6.17). The cell line is designated as MCF-7/Topo.

6.3.5.1 Determination of the ABCG2 mediated efflux using the ABCG2 assay

In the literature various test systems are described to determine the functionality of ABCG2 and the potency of different modulating substances. For this purpose, fluorescent dyes such as Lysotracker Green (Litman et al. 2000) and BODIPY-prazosin (Robey et al. 2001a) or the cytostatic drug mitoxantrone (Robey et al. 2001b) were used as fluorescent ABCG2 substrates. In preliminary experiments, mitoxantrone proved to be suitable. The VIS spectrum of mitoxantrone (Fig. 6.18 b) indicated that mitoxantrone is excitable using a red diode laser (λ_{ex} = 635 nm) due to the maxima at wavelengths of 609 and 660 nm. The emitted red fluorescence of mitoxantrone is detectable in channel 4 (FL4-H; λ_{em} = 661 $\pm$ 16 nm) of a flow cytometer.

MCF-7/Topo cells were incubated with mitoxantrone and different concentrations of test substances. After mitoxantrone uptake for 30 minutes, the added substances were removed and the cells were incubated for an additional hour, so that efflux of mitoxantrone

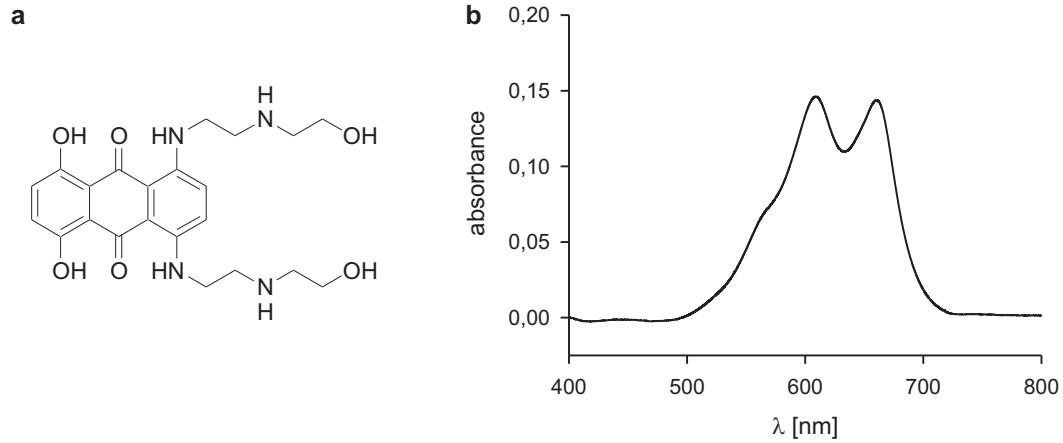

Figure 6.18: Structure of the blue colored chemotherapeutic agent mitoxantrone (a). It is excitable at 635 nm as deduced from the spectrum (b). Mitoxantrone has maxima at 609 and 660 nm.

could take place. The residual mitoxantrone was measured by flow cytometry and the mitoxantrone efflux was calculated from the geometric means of FL4-H histograms. For this purpose, two additional control samples were prepared. One control sample represented

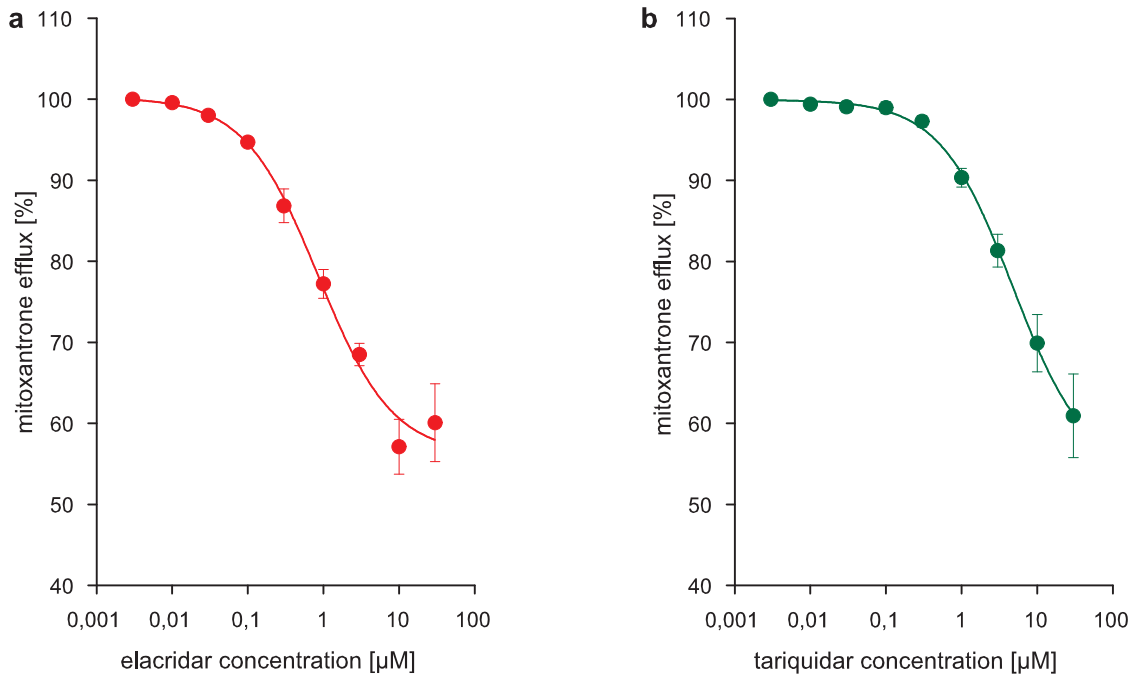

Figure 6.19: Impact of elacridar (a) and tariquidar (b) on the ABCG2 mediated mitoxantrone efflux. Increasing modulator concentrations result in maximum efflux inhibition by about 40 %.

the 100 % mitoxantrone uptake and contained the known ABCG2 inhibitor fumitremorgin C (Rabindran et al. 1998) apart from mitoxantrone. The mitoxantrone fluorescence of this control sample was determined after an incubation for 30 minutes, when mitoxantrone uptake by the cells was finished. The second control sample contained only mitoxantrone and was incubated after the uptake incubation for one further hour in fresh culture medium to allow mitoxantrone efflux. This fluorescence intensity of the residual mitoxantrone in the second control sample is subtracted from the 100 % mitoxantrone uptake value to obtain the 100 % mitoxantrone efflux value. The samples which contain test substances were related to this 100 % efflux value. Fig. 6.19 presents the results of the ABCG2 assay for the 3^{rd} generation modulators elacridar and tariquidar.

Both efflux inhibition curves obtained for the ABCG2 modulation by elacridar and tariquidar showed a sigmoidal and concentration dependent curve. The mitoxantrone efflux was inhibited by about 40 % in both cases. Complete efflux inhibition was not achieved. This can be explained by passive diffusion of mitoxantrone and mitoxantrone efflux that is mediated by transporters other than ABCG2. The following IC_{50} values were calculated from the curves (table 6.5).

Table 6.5: IC_{50} values of elacridar and tariquidar for the modulation of the ABCG2 transporter in MCF-7/Topo cells.

modulator	elacridar	tariquidar
IC_{50} value	0.86 ± 0.23 μM	4.76 ± 2.33 μM

Elacridar as well as tariquidar inhibit the ABCG2 mediated mitoxantrone efflux in MCF-7/Topo cells with IC_{50} values lower than 5 μM. Elacridar was a more potent ABCG2 inhibitor than tariquidar. In both cases, the obtained IC_{50} values were higher than the IC_{50} values in the calcein-AM efflux assay for the p-gp modulation (see page 138). An elacridar concentration 80 times lower than the concentration required for a 50 % inhibition of ABCG2, is sufficient to obtain a half maximum blockade of p-gp function. The IC_{50} value of tariquidar for the ABCG2 transporter modulation is 180 times higher than that for the modulation of the p-gp mediated efflux. Thus, both modulators inhibit predominantly the p-gp mediated efflux. These results are in agreement with the characterization of

elacridar and tariquidar as multispecific modulators in the literature (Han and Zhang 2004, de Bruin et al. 1999, Robey et al. 2004). Because of the great discrepancy between the IC_{50} values for p-gp and ABCG2 modulation in case of tariquidar, it is improbable, that tariquidar concentrations necessary for the inhibition of ABCG2 mediated efflux were achieved in vivo. Therefore, the modulation of the ABCG2 transporter caused by tariquidar seems to be negligible for in vivo pharmacokinetic and treatment studies.

The 2^{nd} generation p-gp modulator valspodar was tested as well. However, no influence on the mitoxantrone efflux was observed (data not shown). Therefore, valspodar is a specific p-gp modulator and inactive on the ABCG2 transporter.

6.3.5.2 Determination of the inhibition of the ABCG2 mediated efflux using the chemosensitivity assay

The results of the ABCG2 assay were reexamined with the chemosensitivity assay. The ability of elacridar and tariquidar to intensify the effect of cytostatic drugs which are ABCG2 substrates on MCF-7/Topo cells was examined within this assay. These cytostatic drugs particularly include camptothecins and anthracyclines. MCF-7/Topo cells were incubated with topotecan and doxorubicin at concentrations that did not affect the cell growth. In addition, various concentrations of elacridar and tariquidar were added, which themselves have no influence on the cell proliferation. Furthermore, paclitaxel, a cytostatic agent that is only transported by p-gp, was included in the study as a negative control. The results of the chemosensitivity tests are summarized in Figs. 6.20 to 6.22.

The effects of both doxorubicin (Fig. 6.20) and topotecan (Fig. 6.21) were enhanced by the co-administration of elacridar and tariquidar. Under the test conditions an inhibition of the cell growth by 80 % was achieved. However, the addition of the modulators did not completely abrogate the drug resistance of MCF-7/Topo cells if administered at a concentration of 1 μM in case of elacridar and 5 μM for tariquidar, respectively.

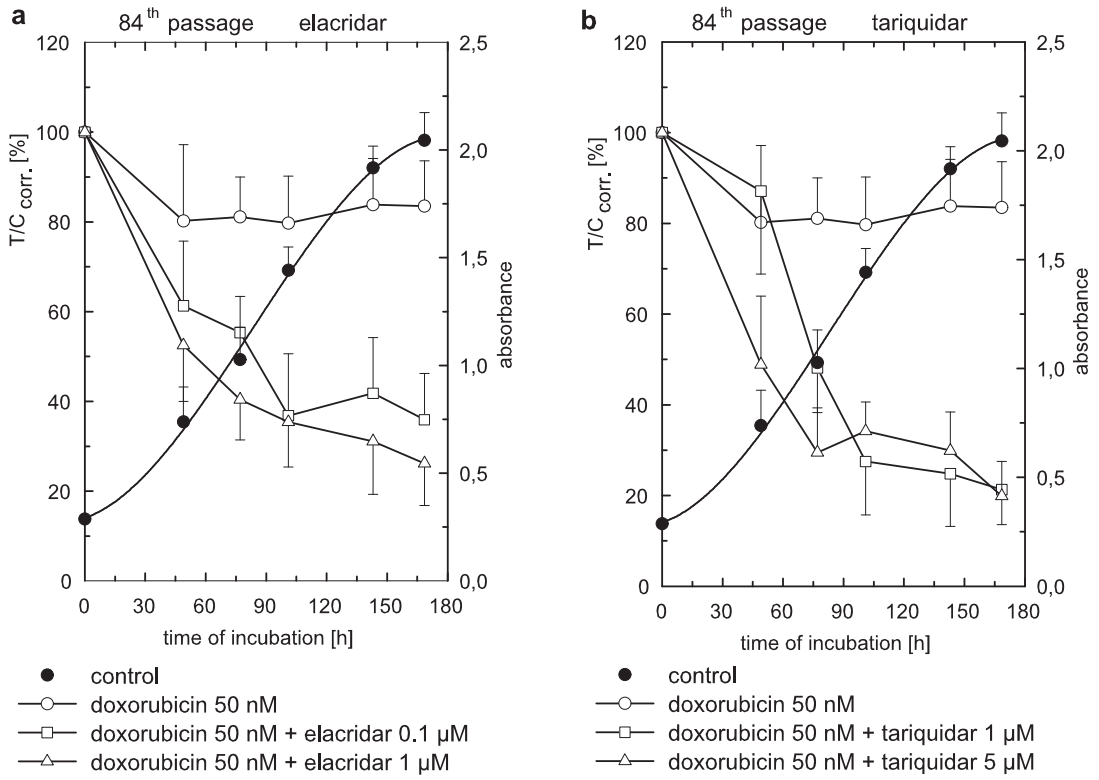

Figure 6.20: Impact of different concentrations of elacridar (a) and tariquidar (b) on the chemosensitivity of MCF-7/Topo cells against doxorubicine (50 nM).

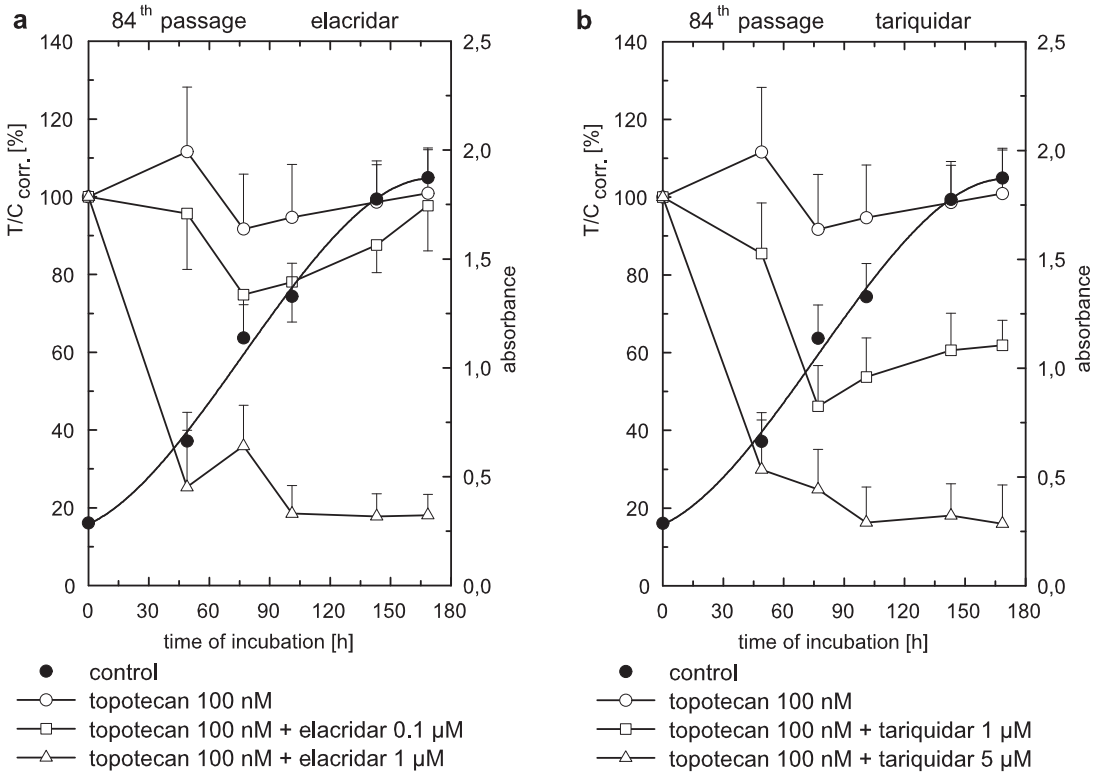

Figure 6.21: Impact of different concentrations of elacridar (a) and tariquidar (b) on the chemosensitivity of MCF-7/Topo cells against topotecan (100 nM).

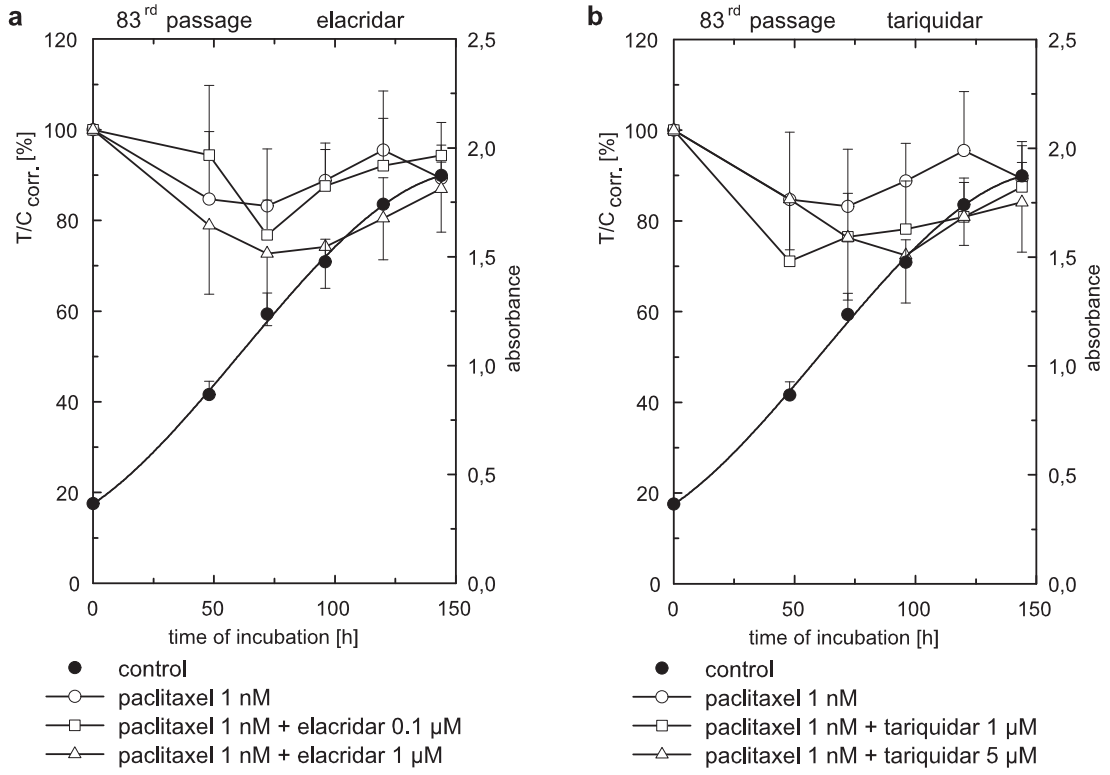

Figure 6.22: Impact of different concentrations of elacridar (a) and tariquidar (b) on the chemosensitivity of MCF-7/Topo cells against paclitaxel (1 nM). Addition of the modulators has no influence on the effect of the non ABCG2 substrate paclitaxel.

As expected, the combination of paclitaxel and the modulators had no effect on the cell growth (Fig. 6.22). MCF-7/Topo cells only expressed the ABCG2 transporter and no p-gp. Because paclitaxel is a selective p-gp substrate, no potentiation of the cytostatic effect of paclitaxel was achieved by combination with elacridar or tariquidar.

It is obvious that higher concentrations were necessary to reverse drug resistance of the MCF-7/Topo cells compared to the experiments with the p-gp expressing Kb-V1/VBL cell line. Hence, the chemosensitivity results confirmed the findings of the ABCG2 assay. In summary, elacridar and tariquidar are modulators of p-gp and ABCG2 mediated drug efflux. Elacridar is more potent on blocking ABCG2 function than tariquidar. In contrast, the potency of the p-gp inhibition is similar for both substances. As the common structural part, 2-[2-[4-aminophenyl)ethyl)-6,7-dimethoxy-1,2,3,4-tetrahydroisoquinoline (compound **4**), seems to be necessary for modulation of p-gp, the residual structural moiety appears to be important for the modulation of the ABCG2 transporter.

6.4 Summary and conclusion

The 3^{rd} generation p-gp modulators elacridar and tariquidar were examined and characterized with regard to their in vitro efficacy and their selectivity to other multidrug transporters. Both substances showed higher p-gp inhibitory potency than any other reported modulator with IC_{50} values of 20.5 nM in case of elacridar and 26.5 nM for tariquidar, respectively. These data are in agreement with the literature. Mistry et al. (2001) observed complete reversal of drug resistance in a multidrug resistant small lung cancer cell line with tariquidar concentrations of 25 to 80 nM. Elacridar in concentrations from 7 to 91 nM was reported to sensitize p-gp expressing human sarcoma cells to various cytostatic drugs (Traunecker et al. 1999). The new modulators were about 80 times more efficient when compared to the 2^{nd} generation p-gp modulator valspodar.

In addition to p-gp modulation, the specificity of elacridar and tariquidar was investigated concerning the ABCG2 transporter. Both modulators proved to be unspecific inhibitors. Elacridar as well as tariquidar inhibited the ABCG2 mediated efflux of several cytotoxic agents such as mitoxantrone or doxorubicin in addition to the aforementioned p-gp activity modulation. However, despite the similar specificity concerning p-gp and ABCG2, the affinity of the two modulators for the ABCG2 efflux pump is different. Whereas the IC_{50} values for inhibition of p-gp are very similar the effect of tariquidar on the ABCG2 transporter was not marked compared to the effect caused by elacridar. There is only little information on the selectivity of the described modulators to MRP, a third relevant ABC transporter responsible for MDR. Some work groups are concerned with this aspect. Germann et al. (1997a), Evers et al. (2000) and Tang et al. (2002) reported that elacridar has no effect on MRP1 as well as on MRP2 function. In case of tariquidar, the affinity to MRP transporters has to be evaluated.

The building block **4** was identified as an important structural part for the high in vitro efficacy of elacridar and tariquidar. Because of the different activity in the ABCG2 assay, the acridine structure of elacridar appears to be necessary for inhibition of ABCG2. Further investigations on the structure activity relationships are required as a basis for the development of another modulator generation. Such studies may contribute to the understanding of the mode of action of ABC transporters and lead to the discovery of

active substances that are not recognized by multidrug transporters.

Elacridar and tariquidar are suited for fluorescence and UV spectroscopic detection. These characteristics are important for in vivo distribution experiments of the two modulators. Ward and Azzarano (2004) demonstrated that elacridar did not inhibit human cytochrome P450 enzymes. This leads to the assumption that elacridar and possibly tariquidar, lack the ability to alter pharmacokinetic parameters of co-administered cytostatic drugs. Thereby, these new modulators will be more suitable for clinical trials in comparison to 2^{nd} generation p-gp modulators (see 6.1). Examinations were carried out by various groups, e.g Bardelmeijer et al. (2000), to investigate the effect of elacridar on the AUC of co-administered cytostatic drugs such as paclitaxel. Bardelmeijer observed that elacridar does not interfere with the elimination of paclitaxel.

In summary, due to the presented results of the in vivo experiments the new p-gp modulators are clearly superior to the 2^{nd} generation modulator valspodar. Therefore, these promising compounds in combination with cytostatics appear to be suitable for the clinical treatment of multidrug resistant tumors and to overcome barriers inside the human body such as the BBB .

Chapter 7

Effect of the p-gp modulators elacridar and tariquidar on the distribution of paclitaxel in nude mice[3]

7.1 Introduction

Paclitaxel (Taxol®, Fig. 7.1) is well established as an anticancer drug in the treatment of various human malignancies (Kroger et al. 1999, Bunn and Kelly 2000, Nathan et al. 2000). It has also been used in the therapy of primary and secondary brain tumors (Glantz et al. 1999). However, the efficacy of paclitaxel in the systemic treatment of these tumors is variable and low. Although paclitaxel is very lipophilic, its access to the brain is limited (Heimans et al. 1994). The brain, often regarded as a "sanctuary site" for cytotoxic drugs, is protected by the blood-brain barrier (BBB), which restricts penetration of drugs into the brain and the brain tumor tissue as well. The BBB consists of endothelial cells of brain capillaries. In the luminal membrane of these endothelial cells the efflux transporter p-glycoprotein 170 (p-gp) is expressed. Experiments with p-gp knockout mice used as a reference model for complete p-gp inhibition have shown that p-gp limits the entry of anticancer drugs such as paclitaxel into the brain (van Asperen et al. 1996). Moreover, several studies done by Tanaka et al. (1994), Sawada et al. (1999) and Gallo et al. (2003)

[3]Parts of this work were presented at the BBB Expertentreffen 2004 in Bad Herrenalb

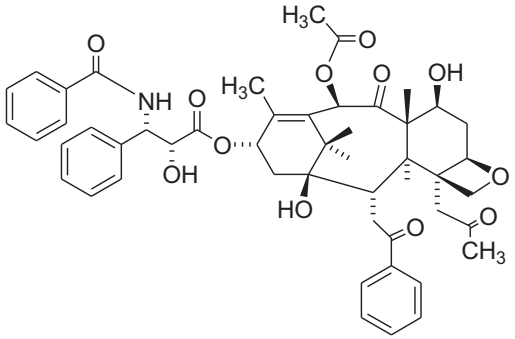

Figure 7.1: Structure of the cytostatic drug paclitaxel

have shown that p-gp is also expressed in the neovasculature of brain tumors, although it is postulated that the BBB is compromised in brain tumor tissue.

However, it is possible to enhance the concentration of p-gp substrates in the brain by blocking the function of the p-gp mediated efflux transport. The p-gp mediated transport is inhibited by certain substances, the so-called p-gp modulators. Experiments with male Wistar rats treated with paclitaxel (8 mg/kg on day 4) demonstrated that addition of the 2^{nd} generation modulator valspodar (100 mg/kg/d over 5 d) led to an 8- to 20-fold increase of paclitaxel in the brain (Donatsch 1996). Fellner et al. (2002) investigated the impact of valspodar co-administration on the paclitaxel distribution in nude mice. They determined a 6-fold increase of the paclitaxel concentration in the brain after pretreatment with valspodar (50 mg/kg, 4 h before 8 mg/kg paclitaxel) compared to the paclitaxel brain levels without valspodar co-application. However, the 2^{nd} generation modulators enhanced not only the concentrations of cytostatic drugs in the brain, but also in liver, kidney and plasma. In addition, they interact with cytochrome P450 enzymes, leading to alterations of pharmacokinetic parameters of cytostatic drug such as delayed elimination (Wandel et al. 1999). Thus, the toxic side effects of chemotherapy increase, and cytostatic drug doses have to be reduced, which in turn results in a lower amount of cytostatic drug in the brain.

To avoid the aforementioned disadvantages new modulators were developed. These were supposed to preferentially modulate p-gp in brain capillaries and lack the interaction with cytochrome P450 enzymes. Two of these 3^{rd} generation modulators, elacridar (GF 120918, Hyafil et al. (1993)) and tariquidar (XR 9576, Mistry et al. (2001)) were

characterized in chapter 6 as highly potent p-gp inhibitors. For elacridar, several studies were carried out that demonstrated the p-gp modulating effect of elacridar at the BBB (Edwards et al. 2002, Huisman et al. 2003). Moreover, combinations of these modulators were well tolerated in phase I studies (Sparreboom et al. 1999, Stewart et al. 2000).

In the present study, the ability of these new p-gp modulators to increase the penetration of paclitaxel into the nude mice brain was examined. The effect of co-administration of elacridar and tariquidar on the distribution of paclitaxel in different nude mice tissues and plasma was investigated as well. For comparison, valspodar (SDZ PSC 833) was included in the study. The impact of valspodar on paclitaxel distribution was already determined by Stephan Fellner (Fellner 2001).

7.2 Material and methods

7.2.1 Drugs and chemicals

Elacridar (GF 120918·HCl) was kindly provided by GSK (Research Triangle Park, North Carolina, United States). Tariquidar (free base) was synthesized at our department as described in chapter 6. Paclitaxel (6 mg/ml) was obtained from the pharmacy of the University Hospital Regensburg as well as Ketamine (Ketanest®, WVD, Garbsen, Germany) and xylazine (Rompun®, Bayer, Leverkusen, Germany). BSA was purchased from Serva (Heidelberg, Germany).

7.2.2 Pharmacokinetic studies in nude mice

The breeding of the NMRI(nu/nu) mice is described in chapter 3.2.7.

Six to 8-week-old NMRI(nu/nu) mice were assigned to groups of three animals per time point. For each experiment only animals of the same sex were used, male mice in case of elacridar experiments and female mice for the tariquidar modulation studies. Elacridar and tariquidar were dissolved in a vehicle that was used in previous studies for valspodar application. This vehicle contained 52.2 g of chremophor RH40 (Caelo, Hilden, Germany), 15 g of absolute ethanol (Merck), 0.1 g of D,L-α-tocopherol (Sigma), 7.5 g of propyl glycol (Merck) and 15 g of Labrafil M2125CS (Gattefosse, Weil am Rhein,

Germany). The solution was treated with ultrasound and heated in a water bath to 37 ℃ to increase the solubility of the compounds. A volume of 0.1 ml was administered by gavage per 10 g of body weight, resulting in a dosage of 5 or 50 mg of modulator per kilogram of body weight. In the same way, the solvent was applied to the control animals.

For intravenous injection paclitaxel (6 mg/ml) was diluted with 0.9 % NaCl solution to a paclitaxcel concentration of 1.6 mg/ml. The drug was injected via the retrobulbar plexus in a volume of 0.1 ml per 20 g of body weight within approximately 10 s. Four hours before the injection of paclitaxel either a dose of 50 mg/kg of modulator (modulator group) or a corresponding volume of the vehicle (control) was orally administered to the mice.

To minimize interferences with the analytical results by drug in the vasculature, ketamine/xylazine-anesthetized mice were killed by cardiac puncture, 1.5, 3, 4.5 and 24 hours after intravenous paclitaxel injection. Heparin-plasma, brain, liver and kidneys were collected. Tissues were homogenized in 4 % BSA solution within 5 minutes and shock-frozen in liquid nitrogen. For homogenization, each organ was cut into small pieces. One milliliter 4 % BSA solution was added per 150 mg tissue. Homogenization was carried out with a Potter-Elvehjem homogenizer by 15 strokes. All samples, except for the brain homogenates, were stored at -78 ℃. The brain homogenates were prepared for paclitaxel analysis immediately after homogenization.

7.2.3 Sample preparation

Tissue extraction was performed by a modification of the method of Sparreboom et al. (1995). Thawed tissue homogenate (1 - 2 ml) was pipetted into a glass centrifugation tube with a ground joint. Samples less than 1 ml were filled up to 1 ml with 4 % BSA solution. Tissue samples underwent diethyl ether extraction (4 ml per sample, 5 min) and were subsequently centrifugated at 1000 rpm for 5 min at 4 ℃. The samples were frozen by a cooling bath and the organic layer was decanted to another centrifugation tube. This extraction procedure was repeated. The combined diethyl ether phases were evaporated under nitrogen at 37 ℃. The residues were resuspended in 250 μl of citrate-phosphate-dextrose (CPD) plasma (BRK, Regensburg, Germany) by ultrasonic treatment for 3 min

and vortexing for 30 s, and were purified by solid-phase-extraction (SPE). Bond Elut CN-E columns (Varian, Darmstadt, Germany) were conditioned with 2 ml of methanol and 2 ml of NH_4OAc buffer (0.01 M, pH 5.0) at 850 to 900 mbar. Samples were mixed with 300 μl of NH_4OAc buffer (0.02, pH 5.0), and the mixtures were loaded on the SPE columns at 700 to 800 mbar. Columns were washed with 2 ml of NH_4OAc buffer (0.01 M, pH 5.0) and 1 ml of 20 % methanol in NH_4OAc buffer (0.01 M, pH 5.0). Samples were eluted with 500 μl of a mixture of acetonitrile and triethylamine (1000:1) into an eppendorf cup (1.5 ml, Eppendorf, Hamburg, Germany). The solvent was evaporated by a SpeedVac Plus 110 A (Thermoquest, Egelsbach, Germany), and the residues were resuspended in 200 μl of mobile phase by vortexing for 30 s. The brain samples were additionally treated with ultrasound for 3 min. All samples were centrifugated at 4000 rpm for 10 min at 4 ℃. The supernatant was either analyzed immediately, as in the case of brain samples, or stored at -78 ℃.

Plasma samples consisted of 250 μl of thawed murine plasma. Samples less than 250 μl were filled up to 250 μl with human CPD plasma. The plasma samples underwent only SPE and were stored at -78 ℃.

7.2.4 Paclitaxel analysis

To each sample 10 μl of a 50 μM docetaxel solution were added as internal standard at the beginning of the sample preparation. For docetaxel stock solutions Taxotere® (80 mg doctaxel per 2 ml of polysorbate 80; Rhone-Poulenc Rorer, Anthony Cedex, France) was diluted with absolute ethanol. HPLC analysis was carried out on a Merck Hitachi liquid chromatograph (Merck, Darmstadt, Germany). A stainless steel (125 x 4 mm) analytical column equipped with a guard column (4 x 4 mm), both packed with 5 μm LiChrospher 100 RP-18 material (Merck), was thermostated to 33 ℃. The mobile phase consisted of acetonitrile, methanol, NH_4OAc buffer (0.2 M, pH 5.0) at the ratio of 35:7.8:57.2 (vol/vol). Ultraviolet detection was performed at 227 nm, and a washing gradient was applied after each run (additional 35 % vol/vol acetonitrile). Injection volumes were either 50 or 100 μl. For calibration, paclitaxel and docetaxel stock solutions in anhydrous ethanol, stored at -20 ℃, were diluted with mobile phase (1:100) on the day of analysis.

The method of analysis was validated for murine plasma, brain, liver, and kidney samples (Fellner 2001). Correlation coefficients for paclitaxel calibration curves in the concentration range 50 - 1000 nM were greater than 0.999. Recovery rates for paclitaxel ranged from 50 to 85 %, depending on the paclitaxel concentration and the type of tissue. The method's accuracy for tissue samples was below 2 % for paclitaxel concentrations between 0.667 and 6.67 nmol/g of tissue and better than 8 % for 0.133 nmol/g. The precision for these determinations was better than 10 %.

7.2.5 Recovery and analysis of elacridar and tariquidar

Stock solutions of the modulators were freshly prepared in mobile phase before sample analysis. For calibration, solutions were diluted with mobile phase (1:100). The modulator and docetaxel (internal standard) solutions used for recovery studies were prepared in absolute ethanol by 1:5 dilution of respective stock solutions.

Homogenized tissues (brain, liver, kidney) and plasma of untreated mice was used for the recovery studies. Prior to diethyl ether extraction 10 μl of a 50 μM solution of the internal standard docetaxel and 10 μl of 3 different concentrations of the modulators (10, 50, 100 μM) were added to blank tissue samples. The analyses of elacridar and tariquidar were performed according to the paclitaxel analysis. The recoveries were determined by comparison of recovery sample peak areas and standard peak areas obtained from directly injected recovery stock solutions after dilution with mobile phase (1:100). For each tissue as well as for murine plasma, 5 samples were analyzed. Additionally, for each recovery concentration one blank tissue and plasma sample was prepared to determine interfering peaks. The peak area of these interfering peaks was subtracted from the corresponding sample areas.

7.3 Results

The paclitaxel concentrations in brain, liver, kidney and plasma of nude mice were determined according to Sparreboom et al. (1995) with slight modifications. The tissue samples were homogenized by a Potter Elvehjem homogenizer and underwent ether extraction and subsequent solid phase extraction. Plasma samples were prepared only by solid phase extraction. Separation was performed on a RP-18 column. Docetaxel was used as internal standard instead of 2'-methyl paclitaxel. The method for examining paclitaxel was established and validated at our department by S. Fellner (Fellner 2001). This method was also used for the determination of elacridar and tariquidar concentrations in these tissues.

7.3.1 Study design

The pharmacokinetic experiments were carried out according to Fig. 7.2. Nude mice received either elacridar or tariquidar at a dosage of 50 mg per kg of body weight. Paclitaxel was administered 4 hours after the p-gp modulators. Brain, liver, kidney and plasma samples were collected after certain periods of time and prepared for HPLC analysis.

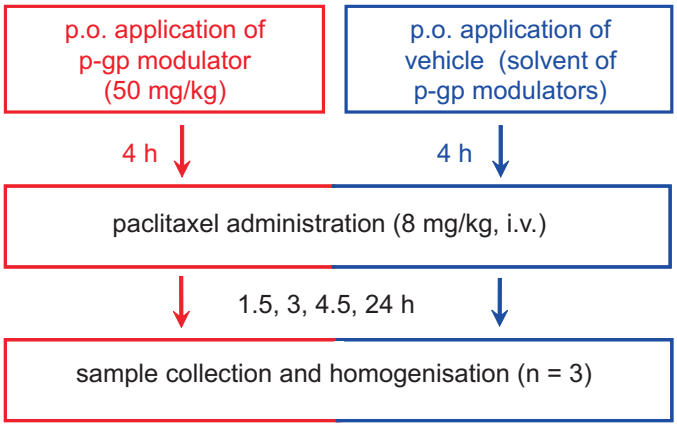

Figure 7.2: Application scheme of the p-gp modulators elacridar and tariquidar, and the cytostatic drug paclitaxel to nude mice. Each group consisted of 3 nude mice per observation time after intravenous injection of paclitaxel.

7.3.2 Determination of elacridar and tariquidar in nude mice tissue

The HPLC chromatograms of mice brain tissues treated with modulator and paclitaxel showed a peak in addition to the paclitaxel and the internal standard peaks. Since this peak only occurred in samples of mice that received either elacridar or tariquidar, the additional peak originated from the modulator. This phenomenon was verified by HPLC analysis of elacridar and tariquidar solutions. Fig. 7.3 shows typical HPLC chromatograms of tissue samples, that consist of either elacridar or tariquidar.

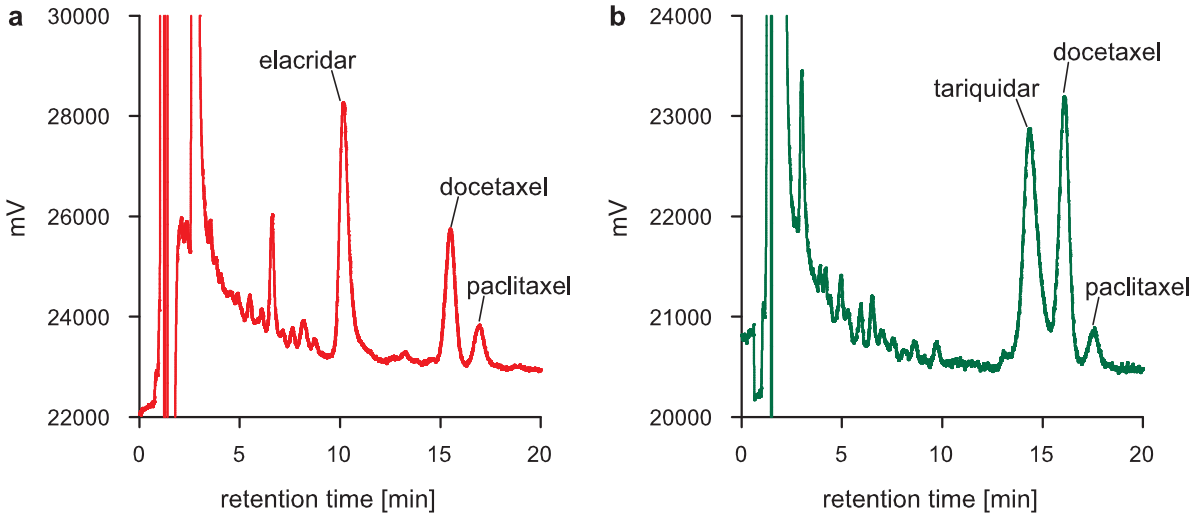

Figure 7.3: HPLC chromatograms of elacridar (a) and tariquidar (b) from mouse brain samples. HPLC conditions: LiChrospher 100 RP-18 (5 μm)(125 mm x 4 mm); acetonitrile/methanol/0.2 M NH_4OAc, pH 5.0, 35:7.8:57.2; flow: 1 ml/min; UV detection at 227 nm; 30 °C.

Elacridar was detected at a retention time of about 10 min. Since the peaks of docetaxel and tariquidar were not well separated, the composition of the mobile phase was changed from that described by Fellner (2001). Thus, tariquidar had a retention time of about 14 min and was distinguishable and separated from the docetaxel signal, which was measured at about 16 min. The separation efficiency was controlled in every analysis due to peak resolution values of just 1.25 for tariquidar and docetaxel peaks. Interfering peaks from tissue and plasma were observed at the same retention times as elacridar and tariquidar. This was especially true for liver and kidney samples. To take these peaks into account,

samples without modulator or blank samples of the different tissues were analyzed. The areas of the interfering peaks at the retention times of the modulators were calculated and subtracted from the determined areas for elacridar and tariquidar.

The recovery of elacridar and tariquidar from mouse brain, liver and kidney tissue homogenates as well as from murine plasma, was determined for 3 different concentrations. Docetaxel was used as internal standard to calculate the modulator content of the different tissues directly from the samples that were prepared for paclitaxel analysis. The same amount of docetaxel was given to all recovery samples (10 μl of 50 μM docetaxel solution in absolute ethanol). The recovery samples were prepared similarly to the procedure for the paclitaxel distribution samples. The recovery of elacridar and tariquidar in the different organs is described in table 7.1 and 7.2.

Table 7.1: Recovery of elacridar and internal standard docetaxel after preparation of brain, liver, kidney and plasma samples (mean values ± SEM). Prior to sample preparation 10 μl of 50 μM of a docetaxel solution were added. For each tissue as well as for murine plasma, 5 samples were analyzed.

tissue	elacridar concentration	elacridar recovery [%]	docetaxel (IS) recovery [%]	recovery ratio elacridar/IS
brain	667 pmol/g	16.47 ± 3.74	58.83 ± 3.88	**0.284 ± 0.085**
	3.33 nmol/g	13.93 ± 3.50	46.08 ± 4.28	**0.299 ± 0.055**
	6.67 nmol/g	21.59 ± 3.56	45.59 ± 4.17	**0.476 ± 0.081**
liver	667 pmol/g	35.44 ± 2.55	62.26 ± 5.22	**0.571 ± 0.047**
	3.33 nmol/g	22.25 ± 3.58	61.69 ± 3.02	**0.358 ± 0.048**
	6.67 nmol/g	23.51 ± 4.95	69.55 ± 4.08	**0.336 ± 0.057**
kidney	667 pmol/g	21.68 ± 5.53	66.32 ± 2.56	**0.329 ± 0.092**
	3.33 nmol/g	18.39 ± 3.18	59.48 ± 2.10	**0.309 ± 0.053**
	6.67 nmol/g	20.75 ± 4.85	62.10 ± 2.21	**0.334 ± 0.078**
plasma	667 pmol/g	10.32 ± 4.40	76.51 ± 3.63	**0.134 ± 0.054**
	3.33 nmol/g	10.36 ± 2.04	80.55 ± 3.05	**0.129 ± 0.025**
	6.67 nmol/g	11.47 ± 5.77	85.24 ± 3.58	**0.134 ± 0.065**

Table 7.2: Recovery of tariquidar and internal standard docetaxel after preparation of brain, liver, kidney and plasma samples (mean values ± SEM). Prior to sample preparation 10 μl of 50 μM of a docetaxel solution were added. For each tissue as well as for murine plasma, 5 samples were analyzed.

tissue	tariquidar concentration	tariquidar recovery [%]	docetaxel (IS) recovery [%]	recovery ratio tariquidar/IS
brain	667 pmol/g	18.09 ± 2.73	58.83 ± 3.88	**0.310 ± 0.062**
	3.33 nmol/g	13.82 ± 3.65	46.08 ± 4.28	**0.299 ± 0.056**
	6.67 nmol/g	18.85 ± 2.94	45.59 ± 4.17	**0.415 ± 0.064**
liver	667 pmol/g	32.39 ± 3.04	62.26 ± 5.22	**0.523 ± 0.061**
	3.33 nmol/g	18.89 ± 2.56	61.69 ± 3.02	**0.304 ± 0.032**
	6.67 nmol/g	17.48 ± 4.11	69.55 ± 4.08	**0.250 ± 0.048**
kidney	667 pmol/g	32.92 ± 6.43	66.32 ± 2.56	**0.438 ± 0.113**
	3.33 nmol/g	17.78 ± 1.57	59.48 ± 2.10	**0.299 ± 0.025**
	6.67 nmol/g	21.86 ± 3.55	62.10 ± 2.21	**0.352 ± 0.056**
plasma	667 pmol/g	9.78 ± 4.86	76.51 ± 3.63	**0.128 ± 0.063**
	3.33 nmol/g	12.17 ± 2.65	80.55 ± 3.05	**0.151 ± 0.032**
	6.67 nmol/g	13.37 ± 5.92	85.24 ± 3.58	**0.156 ± 0.067**

Interestingly, the recovery of the p-gp modulators was much lower compared to the recovery of paclitaxel which had been examined by S. Fellner (Fellner 2001). The elacridar recovery was very low. The values ranged between 10 and 35 % depending on the elacridar concentration and the tissue. The recovery from plasma was the lowest. In brain, liver and kidney a 20 % recovery was determined. The recovery was similar for elacridar and tariquidar. Tariquidar recovery was calculated from 9 to 32 %. In plasma, recovery of tariquidar was lower as well when compared to the other tissues. The average recovery of tariquidar in brain, liver and kidney was 20 %. The recovery of the internal standard docetaxel was about three times greater in brain, liver and kidney compared to the recovery of elacridar and tariquidar in these tissues. In plasma a six times higher recovery was found in case of docetaxel compared to elacridar and tariquidar recovery values, i.e. docetaxel and the two modulators were not extracted to the same extent. For calculation

of the modulator concentrations in the different tissues, the unequal recovery has to be considered.

Correlation coefficients for modulator calibration curves in the concentration range 5 to 5000 nM were higher than 0.99. The method's accuracy was determined for kidney samples (see table 7.3). The accuracy was below 19 % for tariquidar concentrations and 14 % for elacridar concentrations between 0.667 and 6.67 nmol/g of tissue. The precision for these calculations was better than 24 % in case of elacridar and 15 % for tariquidar, respectively.

Table 7.3: Determination of known elacridar and tariquidar concentrations by quanitfication with calibration curves in murine kidney homogenates. Five samples were analyzed per modulator concentration.

modulator concentration [nmol/g]	determined elacridar concentration [nmol/g]	determined tariquidar concentration [nmol/g]
0.667	0.758 ± 0.206	0.791 ± 0.118
3.33	3.60 ± 0.44	3.54 ± 0.25
6.67	6.72 ± 1.62	7.14 ± 1.06

Elacridar and tariquidar levels in different tissues of the nude mice could only be estimated due to the low recovery of the two modulators particularly from murine plasma, and the high variations determined in accuracy and precision calculations.

7.3.3 Distribution of elacridar and tariquidar in nude mice

Based on the recovery data, elacridar and tariquidar concentrations in brain, liver, kidney and plasma were calculated from the HPLC chromatograms of the paclitaxel distribution. Fig. 7.4 and 7.5 presents the modulator levels in the different tissues.

The modulators were detectable in all examined tissues as well as in plasma. Elacridar was quantified in liver and kidney even after 24 hours (Fig. 7.4). The highest elacridar levels were 120 nmol/g after 4.5 hours in liver and kidney. The levels decreased after 4.5 hours to 3.7 nmol/g in liver and 5.5 nmol/g in kidney. After 3 hours approximately 3 times more elacridar was found in brain than in plasma. The maximum concentration

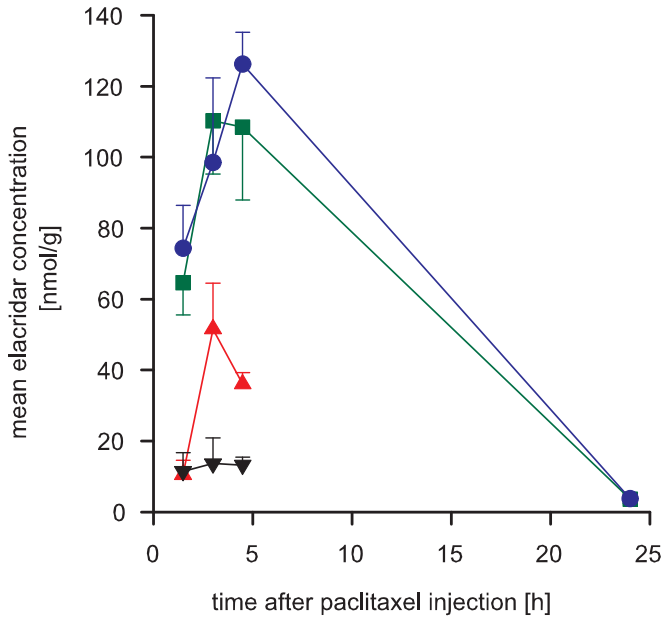

Figure 7.4: Concentrations of p-gp modulator elacridar in brain (▲), liver (●), kidney (■) and plasma (▼) of nude mice (mean values ± SEM).

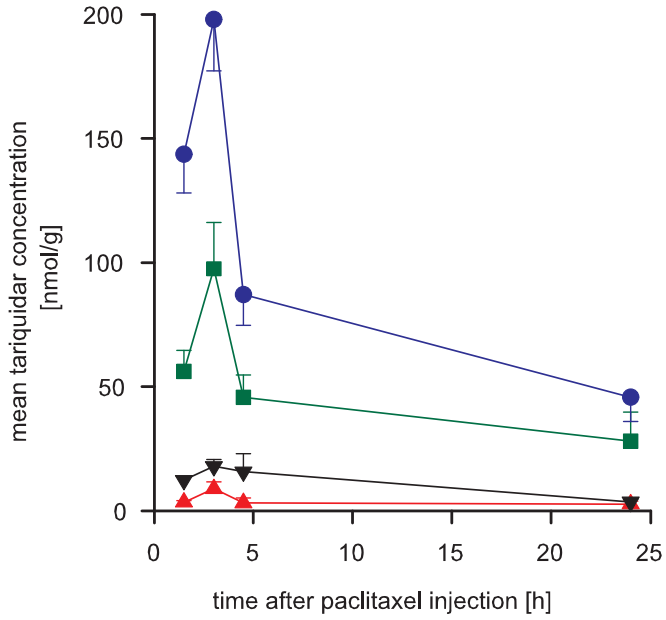

Figure 7.5: Concentrations of p-gp modulator tariquidar in brain (▲), liver (●), kidney (■) and plasma (▼) of nude mice (mean values ± SEM).

in brain was 51.5 nmol elacridar per g tissue. In chapter 6, the IC_{50} value for elacridar was determined to be 20.5 nM. Compared to this value, the elacridar levels in the brain were 500 to 2500 times higher than those required for p-gp inhibition. In case of tariquidar (Fig. 7.5) the modulator was identified in all examined samples during the entire experiment. The highest tariquidar concentrations were measured in liver with a maximum amount of 198 nmol per g of tissue after 3 hours. This is about 40 % higher than the achieved elacridar concentration. Only half of the tariquidar concentration determined in liver was measured in kidney. The tariquidar level in plasma was two-fold higher than in brain. In contrast, the distribution of elacridar was several fold higher in brain tissue compared to plasma. The tariquidar concentrations decreased after 3 hours in all tissues as well as in plasma. The tariquidar brain concentrations were determined to be at least 2.7 nmol/g and at most 8.8 nmol/g. It is important to note that even the lowest tariquidar concentrations measured in these experiments were 100 times higher than those necessary for p-gp modulation (IC_{50} value of 26.5 nM determined in chapter 6). While brain and plasma concentrations of elacridar declined to undetectable levels within 24 hours after paclitaxel administration, the tariquidar levels in plasma and brain remained relatively constant during the 24 hour study period. Obviously, tariquidar has a longer lasting effect than elacridar.

7.3.4 Pharmacokinetic study on the paclitaxel distribution in nude mice

In this study, the influence of the p-gp modulators elacridar and tariquidar on the paclitaxel distribution in brain, liver, kidney and plasma of nude mice was investigated. The analyzed paclitaxel concentrations after elacridar or tariquidar administration were compared to the results obtained in the valspodar study carried out by S. Fellner. The paclitaxel distribution in the different tissues is summarized in Figs. 7.6 to 7.9.

In liver (Fig. 7.6), paclitaxel levels were very high ($>$ 15 nmol/g) after 1.5 hours. The values decreased to similar paclitaxel levels in all four groups. No statistically significant differences were determined between the different p-gp modulator groups and the control group.

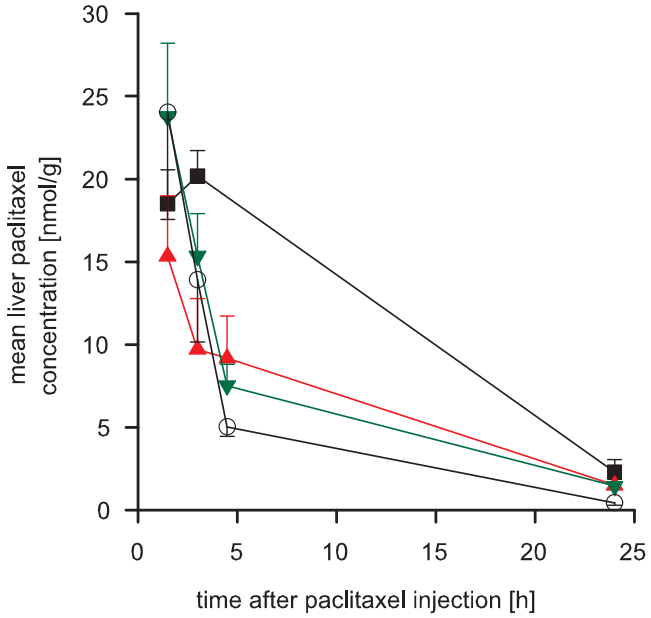

Figure 7.6: Effect of p-gp modulator co-administration (50 mg/kg, p.o.) on paclitaxel levels in liver (mean values ± SEM). Paclitaxel was given intravenously at a dosage of 8 mg/kg. Valspodar (■), elacridar (▲) and tariquidar (▼) were used as p-gp modulators; untreated mice served as a control (○).

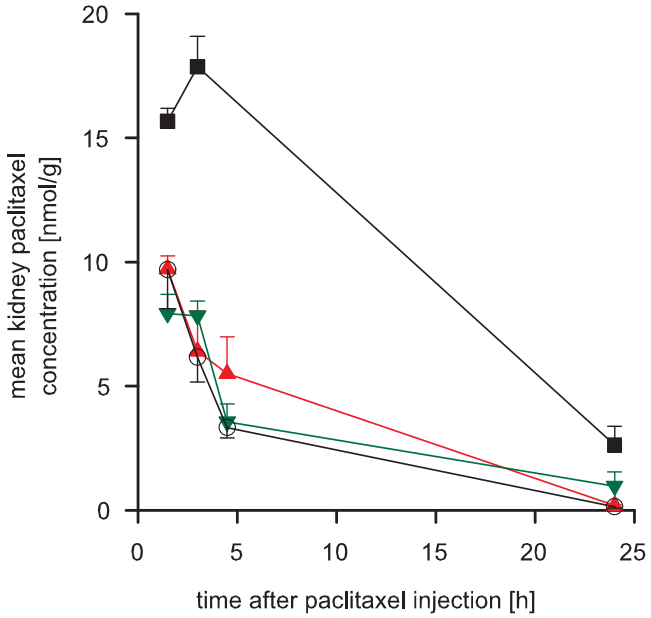

Figure 7.7: Effect of p-gp modulator co-administration (50 mg/kg, p.o.) on paclitaxel levels in kidney (mean values ± SEM). Paclitaxel was given intravenously at a dosage of 8 mg/kg. Valspodar (■), elacridar (▲) and tariquidar (▼) were used as p-gp modulators; untreated mice served as a control (○).

In contrast to the drug levels determined in liver, in the kidney the highest concentration of paclitaxel was found in mice that received valspodar (Fig. 7.7). In fact, 1.5 hours after injection the paclitaxel levels were high in all examined groups with values up to 15.5 nmol paclitaxel per g of tissue. Then in elacridar and tariquidar treated mice, the paclitaxel content in kidney decreased to achieve concentrations similar to those in the untreated control group. In contrast, co-administration of valspodar led to a slight increase in the paclitaxel concentration after 3 hours compared to the values obtained after 1.5 hours. Paclitaxel levels were 7-fold higher after 4.5 hours than after 24 hours. However, this paclitaxel content was still significantly different from the concentrations in the other groups. The paclitaxel concentrations determined in kidney were slightly lower in comparison to the levels measured in liver.

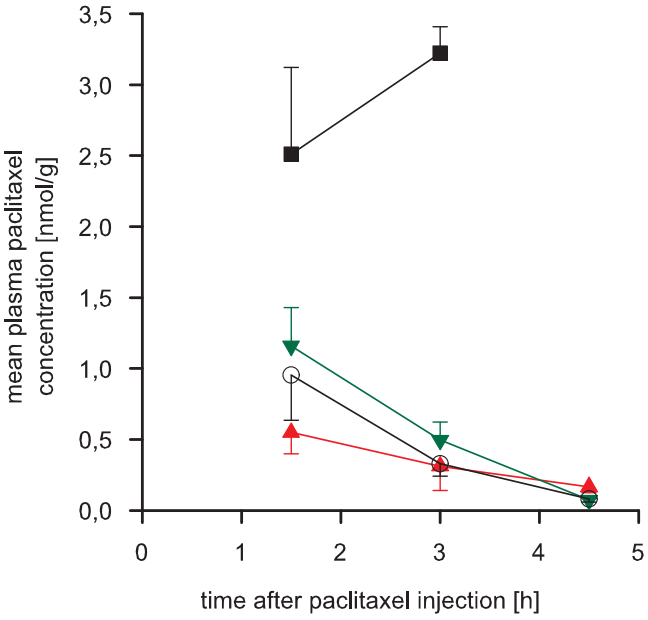

Figure 7.8: Effect of p-gp modulator co-administration (50 mg/kg, p.o.) on paclitaxel levels in plasma (mean values ± SEM). Paclitaxel was given intravenously at a dosage of 8 mg/kg. Valspodar (■), elacridar (▲) and tariquidar (▼) were used as p-gp modulators; untreated mice served as a control (○).

The paclitaxel concentration time profile in plasma (Fig. 7.8) followed a similar pattern as observed in kidney. Relative to the control group the paclitaxel level in plasma of mice that received valspodar increased by 2.5-fold after 1.5 hours and 10-fold after 3 hours. In mice pretreated with elacridar or tariquidar the paclitaxel concentrations were similar to

those in plasma of the control mice and decreased during the experiment to values lower than 0.2 nmol/g after 24 hours. By contrast, in the plasma of valspodar treated mice, no decrease in the paclitaxel concentration was observed.

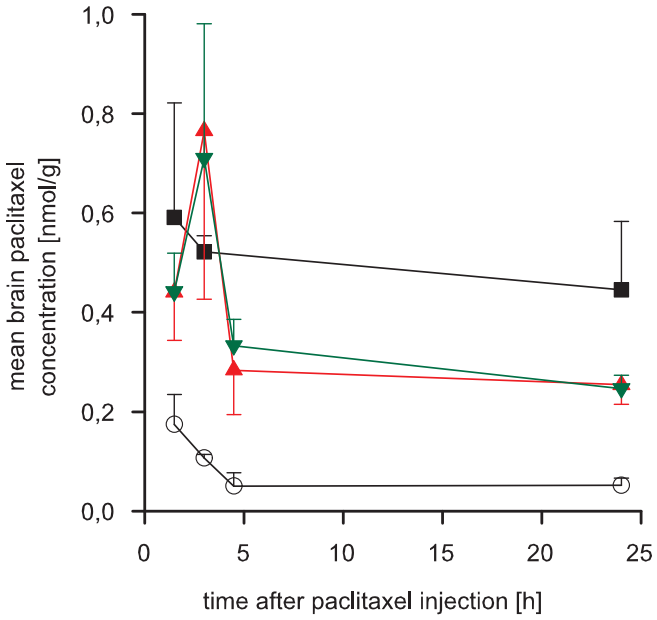

Figure 7.9: Effect of p-gp modulator co-administration (50 mg/kg, p.o.) on paclitaxel levels in brain (mean values ± SEM). Paclitaxel was given intravenously at a dosage of 8 mg/kg. Valspodar (■), elacridar (▲) and tariquidar (▼) were used as p-gp modulators; untreated mice served as a control (○).

The concentration of paclitaxel in the brains of nude mice was also measured (Fig. 7.9). The administration of paclitaxel alone resulted in low levels of the drug in the brain. The concentrations were near the limit of quantitation (0.1 nmol/g). Brain levels were up to 57 times lower (1.5 and 3 hours after injection) compared to those in liver and kidney. Co-administration of valspodar substantially increased the paclitaxel concentration in the brain. Although the levels were 5- to 8.5-fold higher than in the control group the new p-gp modulators elacridar and tariquidar were not able to induce the same increase in the concentration of paclitaxel in the brain as that achieved by valspodar administration. Co-application of elacridar and tariquidar led only to an increase by 4.9 to 7 fold and 4.7 to 6.6 fold, respectively. Despite this slight increase, brain paclitaxel levels observed after pretreatment with elacridar and tariquidar remained significantly different from the control levels. Thus, the brain was the only examined tissue, where administration of

elacridar and tariquidar resulted in different paclitaxel concentrations compared to the control levels. Furthermore, in contrast to liver, kidney and plasma, where paclitaxel concentrations strongly declined after 24 hours, the paclitaxel levels in the brain remained relatively constant within 24 hours.

The different impact of valspodar, elacridar and tariquidar co-administration on the paclitaxel levels in the brain compared to plasma is presented as concentration ratios determined at different points in time in Fig. 7.10. Irrespective of the administered modulator, more paclitaxel was found in plasma than in brain 1.5 hours after paclitaxel injection. However, additional 1.5 hours later, the brain/plasma ratio had changed in case of elacridar or tariquidar co-application: 2.5 and 1.5 times higher paclitaxel levels were detected in brain than in plasma. This effect lasted for 4.5 hours, and was more pronounced with tariquidar (ratio 4.5) than with elacridar (ratio 1.2). The brain/plasma ratios of paclitaxel after valspodar co-administration were 2- to 15-fold lower than in the presence of the new p-gp modulators, indicating that p-gp inhibition by valspodar does

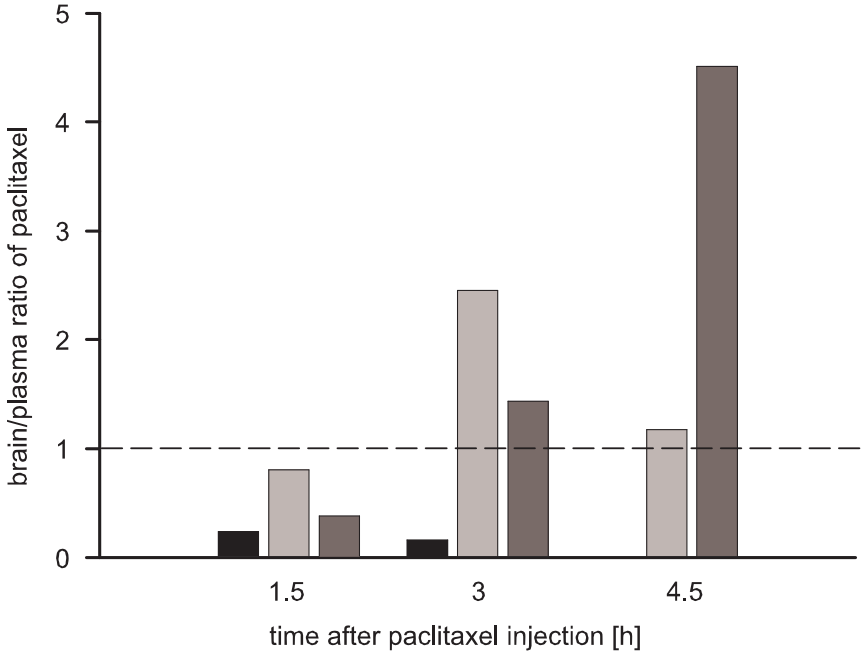

Figure 7.10: Brain-plasma ratio of paclitaxel after co-administration of valspodar (black bar; not determined at 4.5 h), elacridar (light grey bar) and tariquidar (dark grey bar). Three hours after paclitaxel injection more paclitaxel is found in brain than in plasma if elacridar or tariquidar were co-administered.

not lead to a specific accumulation of paclitaxel in the brain of nude mice.

As the measured elacridar concentrations in the brain were at least 50 times higher than the IC_{50} value (ca. 20 nM) determined for p-gp inhibition in vitro, in another experiment the dosage of the modulator was reduced to 5 mg/kg. This dosage should be sufficient by far to achieve the elacridar concentration required for p-gp inhibition. The effect of 5 mg/kg elacridar on the distribution of paclitaxel in different tissues and plasma of nude mice compared to untreated mice is summarized in Fig. 7.11.

In liver, kidney and plasma of mice treated with elacridar at reduced dosage, the paclitaxel concentrations were not significantly different from the control values. As expected, the paclitaxel levels in liver, kidney and plasma obtained after co-administration

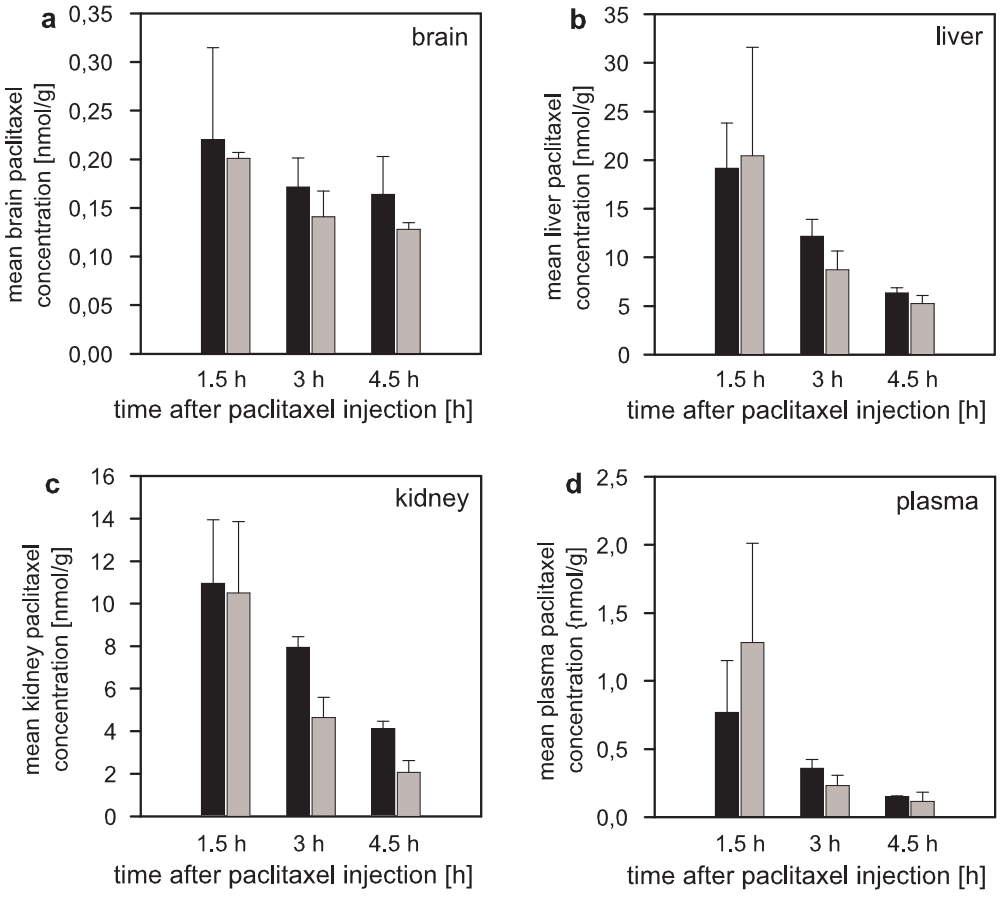

Figure 7.11: Effect of elacridar co-administration (5 mg/kg, p.o.) on paclitaxel levels in brain (a), liver (b), kidney (c) and plasma (d) of nude mice (black bar; mean values ± SEM). Paclitaxel was intravenously given at a dosage of 8 mg/kg. Untreated mice served as a control (light grey bar).

of 5 mg/kg of elacridar were comparable to those after a dosage of 50 mg/kg. However, the reduced dose of elacridar did not result in an increase of the paclitaxel concentration in brain. All measured paclitaxel levels in the brain were near the limit of quantitation. In all tissue and plasma samples a decrease in the paclitaxel concentration was determined during the 4.5 hour study period. Only little information is available on the absorption of the lipophilic elacridar and its distribution into adipose tissue. Due to the lack of increased paclitaxel levels in the brain after p.o. administration of 5 mg/kg elacridar, it may be speculated, that the modulator is only partly absorbed and distributed preferentially to adipose tissue. This would explain why a higher dosage is required to inhibit the p-gp at the BBB.

7.4 Discussion

The 3^{rd} generation p-gp modulators elacridar and tariquidar proved to be highly potent p-gp inhibitors in vitro (see chapter 6). Now, their efficacy was investigated in vivo by quantification of the paclitaxel levels in different tissues of nude mice depending on the co-application of the MDR modulators. Fortunately, the two modulators were detectable in the HPLC chromatograms which were recorded for paclitaxel analysis. The recovery of elacridar and tariquidar was determined afterwards, the calculated modulator distribution in the different tissues could be estimated although sample preparation and HPLC method were developed for the detection and quantification of paclitaxel. The high SEM values in the determination of accuracy and precision were explainable by the following facts. Interfering peaks that were observed particularly in liver and kidney and could only be estimated in control samples might influence the results especially at low modulator concentrations. Since the tariquidar peak was detected close to the peak of the internal standard the separation of both peaks was impaired at higher modulator concentrations. The peak area that is attributed to interfering peaks is negligible at modulator concentrations greater than 2.5 μM. At high elacridar concentrations the pronounced tailing of the peak hampered the exact quantification of elacridar. The asymmetry factor of elacridar peaks at high modulator concentrations was close to the acceptable value of 2.5. Factors higher than 3 result in unprecisely defined peak areas because the point at which the

peak reaches the base line is not well identifiable (Meyer 1992). To determine the concentrations of elacridar and tariquidar correctly, a new method has to be developed. Due to the low recovery, particularly from plasma, the procedure of the sample preparation should be adapted to the modulators. The preparation of modulator samples according to a different method failed due to the small tissue homogenate volume especially in case of brain samples.

Another problem was the poor solubility of elacridar and particularly tariquidar in the vehicle if dosed at 50 mg/kg. Different solvents mentioned in literature such as hydroxypropylmethyl cellulose (HMPC) and tween 80 solutions (Mistry et al. 2001) were tested, but proved to be unsuited, and therefore the modulators were administered in suspension. Thus, the exact dose of soluble modulator that was given to each mouse remained unknown. By improving the solubility of these compounds, the ideal modulator concentration could be determined.

Despite the problems associated with the exact determination of the modulator concentrations, high elacridar and tariquidar levels were analyzed particularly in liver and kidney. Even in the nude mouse brain, the modulator levels were at least 10 to 50 times higher than those required for p-gp inhibition in vitro (see IC_{50} values in the calcein-AM efflux assay). Elacridar and tariquidar were able to significantly increase the paclitaxel concentrations up to 0.3 nmol/g after 24 hours in the brain compared to the control. However, the increase ín brain paclitaxel levels caused by the new modulators was not as high as in case of valspodar administration (about 0.5 nmol/g after 24 hours), indicating an incomplete inhibition of p-gp. This observation should not necessarily lead to the conclusion that elacridar and tariquidar are weaker p-gp modulators in vivo. For the evaluation of the efficacy of a p-gp inhibitor with respect to the increase in brain concentrations of a co-administered drug it is also necessary to take into account the influence of the inhibitor on the drug plasma level. Kemper et al. (2003) examined to what extent increased plasma levels contribute to higher brain levels. They determined the paclitaxel concentrations in the brains of p-gp knockout mice after administration of valspodar. The paclitaxel brain levels were even higher as in untreated knockout mice, suggesting that increased plasma levels due to reduced excretion also account for higher brain levels in wild type mice receiving valspodar. Since the plasma levels of paclitaxel measured by

S. Fellner were markedly increased after valspodar administration compared to the control, the increased levels in the brain might have partly resulted from the high plasma levels in the valspodar group. In case of the new modulators, no marked elevations of the paclitaxel levels in plasma were observed compared to the control. Thus, the elevated paclitaxel concentrations in brain of elacridar and tariquidar treated mice only resulted from the inhibition of p-gp at the BBB. The potency of elacridar found in this study is in line with previous reports on its effects on the brain penetration of docetaxel (Kemper et al. 2004c) and morphine (Letrent et al. 1998).

Another important conclusion can be drawn from the experiment with reduced elacridar dosage. In this case there was no increase in paclitaxel levels at all compared to the control samples. Thus, a relatively high modulator dose is required to show marked elevated paclitaxel levels in the brain. In case of valspodar a further increase in dosage is not reasonable. In experiments done by Kemper et al. (2003) a single dose of 25 mg/kg was found to be sufficient to achieve maximum inhibition of p-gp and other enzymes involved in metabolic elimination of paclitaxel. In addition, higher valspodar doses did not lead to enhanced paclitaxel levels, but could result in toxic side effects if valspodar plasma levels were higher than 3.5 μM. In contrast, elacridar can be administered at high concentrations up to 1 g orally without any toxic side effects to patients (Kruijtzer et al. 2002).

Paclitaxel was specifically accumulated in brain in case of elacridar and tariquidar co-administration. The favorable brain/plasma concentration ratios indicate a preferential modulation of p-gp at the BBB and lower systemic toxicity for the combination of paclitaxel with the new modulators. Several clinical studies in which paclitaxel was combined with a presumed selective and potent p-gp modulator, have shown that dose reductions of the cytostatic were not necessary (Boniface et al. 2002). The fact that no increase in the paclitaxel levels in liver and kidney was measured after co-administration of elacridar and tariquidar, confirmed the suitability of these substances for the combination treatment with cytostatic drugs. By contrast, valspodar caused considerably elevated paclitaxel concentrations in plasma due to substantial reduction of paclitaxel clearance (p-gp inhibition in kidneys). The increased systemic exposure to paclitaxel led to enhanced toxic effects such as bone marrow suppression and neurotoxicity. Hence, it can be concluded that 3^{rd} generation p-gp modulators are not more efficient in inhibiting p-gp in vivo, but

these substances are much more suitable for a well tolerated combination chemotherapy compared to 2^{nd} generation modulators such as valspodar.

7.5 Summary and perspective

The combination of paclitaxel with the newly developed p-gp modulators elacridar or tariquidar led to encouraging results. The compounds were able to increase the brain paclitaxel levels. Thereby, the modulator concentrations in plasma remained lower than 1 nM. These concentrations were well tolerated in patients without any significant side effects (Malingre et al. 2001). Furthermore, elacridar and tariquidar presumably do not enhance the systemic side effects of co-administered cytostatic drugs. Hence, dose reductions of cytostatic drugs are unnecessary and it should be possible to achieve therapeutic benefits in cancer chemotherapy.

The poor solubility of the two examined modulators has to be improved. Moreover, as suggested by the experiments with reduced elacridar dosage the absorption and the distribution into the different compartments has to be optimized. In particular, the modulator accumulation in lipophilic compartments such as adipose tissue should be avoided. Furthermore, it should be investigated whether adjustments of the dosage of the p-gp modulators could help to increase the accumulation and retention of cytostatic drugs in the brain. First experiences concerning this aspect were reported by Kemper et al. (2003). They were able to achieve paclitaxel levels in the brain of wild type mice close to paclitaxel concentrations found in p-gp knockout mice after co-administration of elacridar in two doses of 50 mg/kg at 2 and 8 hours after paclitaxel application. Thus, it is possible to increase cytostatic drugs levels in the brain by repeated dosage of p-gp modulators. Even the order of modulator administration, e.g. before and/or after cytostatic drug application, influences the modulator efficacy. Additional experiments have to be carried out to find the ideal regimen for combination therapies.

Improvements of the aforementioned physicochemical and pharmacokinetic parameters may contribute to the optimization of the treatment of brain tumors with combinations of cytostatics and the new p-gp modulators. In conclusion, cancer chemotherapy in combination with elacridar, tariquidar or other optimized p-gp inhibitors could lead to an

antitumoral efficacy comparable to that described for valspodar by Fellner et al. (2002) on brain tumors, but with less systemic toxicity.

Chapter 8

The transferrin receptor - a possible loophole at the blood-brain barrier

8.1 Introduction

Overcoming the blood-brain barrier (BBB) is a major challenge in the chemotherapy of primary and secondary brain tumors. Research effort is devoted to the inhibition of drug transporters and efflux pumps located at the BBB such as p-glycoprotein 170 or the multidrug resistance related proteins with variable success (Fellner et al. 2002, Kemper et al. 2004b). An alternative approach to selectively increase the brain concentration of cytostatic drugs that normally do not accumulate within the brain, would be to take advantage of a specific transport system present at the BBB. A multiplicity of receptor mediated transport systems responsible for the delivery of peptides and proteins is located at the BBB including receptors for insulin and transferrin (Friden 1993). The transferrin receptor (TfR, CD71) was discovered in 1981 (Trowbridge and Omary 1981). It is expressed in all nucleated cells in the body, but due to the high levels of oxidative metabolism in neuronal cells and the resulting significant requirement of iron the receptor is present in unusually high number on brain capillary endothelial cells (Jefferies et al. 1984). The human TfR is a transmembrane glycoprotein composed of two disulfide-bonded subunits, each of an apparent molecular mass of 95 kDa (Schneider et al. 1982, Trowbridge 1995). TfR mediates the endocytosis of iron into cells with the help of transferrin as iron carrier

(Li and Qian 2002). In addition, transcytosis of iron mediated by the transferrin/TfR system was observed in vitro and in vivo by different work groups. In vitro, Descamps et al. (1996) figured out by pulse-chase and double labelling experiments that in bovine brain capillary endothelial cell cultures the majority of transferrin bound iron was transcytosed to the abluminal side of the cells. Broadwell et al. (1996) and Bickel et al. (1994) used electron microscopic techniques to show that horseradish peroxidase or colloidal gold conjugates of monoclonal antibodies (MAb) targeted to TfR cross the BBB in vivo. Possible transendothelial pathways through the BBB are depicted in Fig. 8.1.

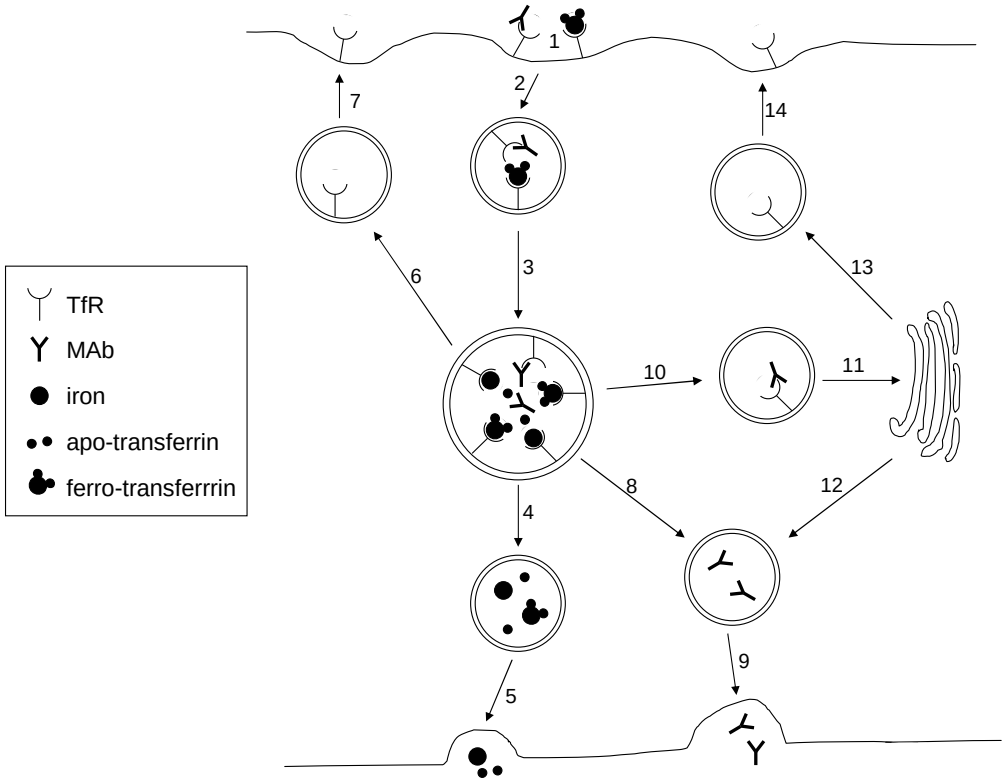

Figure 8.1: Possible transendothelial pathways through the BBB followed by blood-borne transferrin and MAbs directed to the TfR (adapted from Broadwell et al. (1996)). After internalization of the receptor-ligand complex, the formed endocytic vesicle fuses with an endosome, where iron or MAbs dissociate from the receptor. The receptor is recycled to the cell surface. Free iron, apo-transferrin and MAbs are transported to the abluminal membrane for exocytosis. MAbs can also be directed with the receptor to the Golgi complex, where dissociation takes place. The receptor is recycled to the cell surface, whereas MAbs are packaged in a vesicle for migration to the abluminal membrane where they are released by exocytosis.

The first step of TfR-mediated transcytosis of iron across the BBB (Fig. 8.1) is the binding of the transferrin-iron complex (ferro-transferrin) to TfR on the luminal surface of the brain capillary endothelial cells (1). Subsequently, the occupied receptor internalizes into an endocytic vesicle (2), that fuses with an endosome (3). Because of the acid pH inside the endosome the iron dissociates from the transferrin/TfR complex (3). The ferric ions and the iron free apo-transferrin are packaged into export vesicles for migration to the abluminal membrane (4), where exocytosis (5) takes place (Broadwell et al. 1996, Friden 1996). The TfR is recycled to the cell surface (6,7). In non brain tissues the endothelium is sufficiently leaky for passive diffusion of ferro-transferrin. Due to the preferential expression of TfR at the BBB compared to non brain tissues, the TfR mediated transport can be used as a specific drug targeting system across the BBB to increase drug levels in the brain (Friden 1993, Huwyler et al. 1996).

The use of covalently linked compounds to transferrin is limited by the high concentration of transferrin in the blood that leads to competition for binding to the receptor (Friden 1996). Therefore, MAbs directed to the TfR have been introduced into research. Friden et al. (1996) have demonstrated the selective brain distribution of a MAb targeted to the human and monkey TfR after intravenous injection in *Cynomolgus monkeys*. The MAbs were found almost exclusively in brain parenchyma rather than in capillaries, indicating transcytosis of the MAbs across the BBB. A second endothelial pathway for the transcytosis of MAbs directed to TfR is described in literature (Fig. 8.1; Broadwell et al. (1996)). If no dissociation of MAb from TfR takes place in the endosome, the residual MAb/TfR complex is directed within a transfer vesicle (10) to the inner saccule of the Golgi complex (11). The MAb is separated from the TfR by enzymes of the Golgi complex and packaged in transporting vesicles arising from the inner Golgi saccule for exocytosis to the abluminal membrane (9,12), while the free TfR is again inserted into the luminal membrane (13,14). For in vitro and in vivo studies the MAb OX26 (Jefferies et al. 1984) directed to the rat TfR is well established as a drug targeting vector. This antibody has been shown to bind to an extracellular epitope of the receptor, different from the transferrin binding site (Pardridge 1995). However, only 2 or 3 biotinylated drugs can be attached to an OX26 conjugate indicating the low carrying capacity of the OX26 MAb (Huwyler et al. 1996). An answer to this problem is the usage of drug incorporated li-

posomes loaded with MAb (immunoliposomes), where more than 10,000 small molecules may be entrapped in a single 100 nm liposome. The immunoliposomes should be sterically stabilized by insertion of poly(ethylene glycol) (PEG) derivatized lipids within the bilayer of conventional liposomes (Allen 1994). This stabilization leads to a substantial improvement of blood circulation half life (several days in contrast to minutes for conventional liposomes) in humans (Gabizon 2001). Furthermore, the PEG chains enhance the antibody antigen binding as they act as linkers between antibody and liposome, and thus, the antibody is not shielded by the steric barrier of PEG. Schnyder et al. (2004) have investigated a new coupling procedure for the preparation of pegylated immunoliposomes, that is useful for drug targeting to the brain (Fig. 8.2).

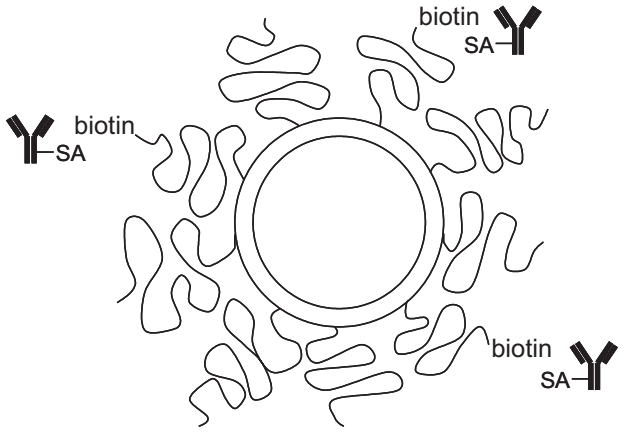

Figure 8.2: Structure of an immunoliposome (adopted from Schnyder et al. (2004)). Streptavidin(SA)-conjugated MAbs are coupled to biotinylated PEG liposomes.

A biotinylated PEG-phospholipid was used for a non-covalent attachment of streptavidin-conjugated OX26 MAb to sterically stabilized liposomes. The prepared immunoliposome has a particle size of 150 nm and contains approximately 5500 strands of 2000 Da PEG and 30 strands of the biotinylated PEG lipid. Biotinylation had no influence on the in vivo pharmacokinetics of the liposomes (Laverman et al. 2000). The use of streptavidin instead of avidin reduced the amount of non-specific binding and thus, the systemic clearance in vivo. The lower isoelectric point of streptavidin (pI 5-6; Kang and Pardridge (1994)) compared to avidin contributes to this effect. As streptavidin can be conjugated to a great variety of MAbs, the presented immunoliposomes represent a delivery system that is easily adapted to special drug targeting problems in vivo.

The well known endocytosis mediated by TfR could be used for the targeting of cytostatic drugs directly to brain tumor cells. Wen et al. (1995) reported that human brain tumors preferentially express TfR rather than normal brain tissue. In treatment studies of human brain tumors implanted in rats a second MAb targeted to the human TfR has to be introduced into the immunoliposome delivery system to transport the incorporated cytostatic drug straight to its target. Further studies demonstrated that therapy with repeated administration of TfR specific MAbs did not result in a down regulation of TfR in tumor cells (Wu and Pardridge 1998).

Therefore, by means of the presented immunoliposome delivery system the concentration of cytostatic drugs could be increased in the brain to sufficient levels for brain tumor therapy. Furthermore, this system can be used to by-pass the efflux pump p-glycoprotein 170 (p- gp) and thus even deliver drugs to the brain, that normally cannot enter the brain due to their high affinity to p-gp (Huwyler et al. 2002). In this chapter the establishment of a tumor model is described that is suitable for the investigation of primary brain tumor therapy with immunoliposome delivery systems that use the TfR mediated transport to overcome the BBB.

8.2 Materials and methods

8.2.1 Cell cultivation

The human glioblastoma cell lines were purchased from the American Type Culture Collection (ATCC, Rockville, MD, USA) and were maintained as "monolayer cultures" in 75 cm^2 flasks (Nunc, Wiesbaden, Germany). The cells were cultured at 37 °C/5 % CO_2 in different culture media. U-87 MG and U-373 MG cells were cultivated in Eagle's minimum essential medium (EMEM, Sigma, München, Germany), supplemented with 110 mg/l sodium pyruvate, 3.7 g/l sodium hydrogen carbonate and 5 % FCS. For U-118 MG cells, Dulbecco's modified eagle medium (DMEM, Sigma) was used, containing 110 mg/l sodium pyruvate, 2.2 g/l sodium hydrogen carbonate and 5 % FCS. All culture media were adjusted to pH 7.4. Subculturing was carried out with 0.2 % trypsin/EDTA (Viralex, Paa Laboratories) in PBS once a week. The human B-cell line RAJI was kindly provided by

the work group of R. Knüchel (Institute of Pathology, University of Regensburg). These cells were maintained as suspension culture in RPMI 1640 culture medium (Sigma) supplemented with 1.5 g/l sodium hydrogen carbonate and 10 % FCS, and subcultured once a week.

8.2.2 Transferrin receptor determination by flow cytometry

The in vitro determination of the transferrin receptor (CD71) was performed according to Krieg et al. (2000) and Brockhoff et al. (1994) with modifications. Cells were harvested and washed with PBS. Subsequently, the cells were adjusted to $1 \cdot 10^6$ cells per 1 ml with PBS, and the samples were centrifugated again at 1100 rpm for 5 min at room temperature. Three different kinds of samples were prepared for the determination of autofluorescence, total staining and unspecific binding of the antibody (negative control). Each sample, except the one for the determination of the autofluorescence, was prepared in triplicate. The cell pellets (autofluorescence and negative control) were resuspended in 50 μl of PBS. The primary mouse anti-human CD71 antibody (M 0734, clone Ber-T9, DAKO, Hamburg, Germany) was used in a dilution of 1:50 (50 μl) to label cell pellets for the total staining. All samples were incubated for 1 h at room temperature. Afterwards, the cells were washed twice with PBS. 50 μl of PBS were given to the autofluorescence sample. All residual cell pellets were resuspended in 50 μl of fluorescein isothiocyanate (FITC)-coupled rabbit anti-mouse antibody (F 0261, DAKO, Hamburg, Germany). The secondary antibody was diluted 1:20 with PBS. After an incubation period of 1 h at room temperature in the dark, the samples were washed once with PBS, resuspended in 250 to 400 μl of PBS and placed on ice in the dark until analysis. The FITC fluorescence was detected after excitation at 488 nm in the FL1-H (530 $\pm$ 30 nm) band pass filter using a FACS Calibur™ (Becton Dickinson, Heidelberg, Germany). The photomultiplier settings were as follows: E-1 for FSC, 200 for SSC and 450 for FL1-H. A threshold of 450 was set up for FL1-H. The samples were gated on forward scatter versus sideward scatter to exclude clumps and debris and a minimum of 10,000 gated events was collected per sample. FL1-H histograms were analyzed by the WinMDI 2.8 software. Mean fluorescence intensity of negative control cells was subtracted from the fluorescence intensities of anti-CD71

labelled cells. Membrane expression of CD71 was quantified in molecules of equivalent soluble fluorescence (MESF) using Quantum™ 26 beads (Bangs Laboratories, Fishers, IN, USA). As FITC fluorescence intensity is strongly dependent on pH values, all samples as well as the microbead populations were prepared in PBS adjusted to pH 7.2. RAJI cells served as a positive control of transferrin receptor expression (Trowbridge 1995).

8.2.3 Immunohistochemistry

Frozen sections were used to detect transferrin receptors in tumor tissue and nude mouse brain. Subcutaneously grown glioblastomas were excised when the tumor growth reached an area of about 150 mm^2 in nude mice (see chapter 3). The tumor tissue was embedded in frozen tissue matrix (Tissue-Tek® O.C.T.™ Compound, Sakura Finetek, Giessen, Germany) to ensure freezing without trapped air and stored in liquid nitrogen. The sections were cut on a freezing microtome (FrigocutE 2800, Reichert-Jung, Nussloch-Heidelberg, Germany) with a thickness of 5 to 8 μm, and two sections each were mounted on Superfrost Plus (Fisher Scientific, Pittsburgh, PA) glass slides. The sections were immersed immediately in acetone for 15 min to fix the sections on the slides. After fixation, the slides were rinsed for 5 min with phosphate-buffered saline (PBS), pH 7.4, and subjected to immunostaining.

Endogenous peroxidase was blocked by incubation in PBS containing 3 % H_2O_2 and 10 % methanol for 30 min, followed by two incubations in PBS with 0.04 % Triton-X-100 (PBST) for 5 min. Nonspecific binding was prevented by incubation for 30 min in 10 % natural donkey serum (NDS, Sigma, München, Germany), 2.5 % skimmed milk powder (Milupa, Friedrichsdorf, Germany), and 0.3 % Triton-X-100 in PBS. Subsequently, cells were washed three times with PBST. Primary mouse anti-human CD71 antibody (M 0734, clone Ber-T9, anti-human CD71, DAKO, Hamburg, Germany) was diluted 1:5 with washing buffer consisting of 10 ml of milk powder solution (2.5 % skimmed milk powder in PBST), 100 μl 1 % NDS, and 0.3 % Triton-X-100. After incubation with the primary antibody for 48 h at 4 ℃, the slides were washed three times with PBST and treated with biotinylated donkey anti-mouse antibody as secondary antibody (1:100, Dianova, Hamburg, Germany) for 2 hours at room temperature. All incubations with antibody

were performed in humid chambers. Afterwards, slides were washed three times in PBST and incubated for 1 hour with horseradish-conjugated avidin-biotin complex (Vectastain Elite Kit ABC, Vectorlabs, Burlingame, United Kingdom) in PBST. Slides were washed for 5 min in PBST before incubation in a diaminobenzidine (DAB) solution for 10 min (0.05 % DAB, 0.02 % ammonium nickel sulfate in PBST). H_2O_2 (10 %) was added to a final concentration of 0.006 %, and slides were incubated for 1.5 min. Afterwards, they were washed three times in PBS and counterstained with Harris' haematoxylin. Then the slides were placed in PBS and demineralized water, processed in an ascending alcohol series and mounted in DePex. All stained sections were evaluated with a BH2 microscope (Olympus, Hamburg, Germany) mounted with a CCD-camera for digital imaging.

8.2.4 Chemosensitivity assay

The chemosensitivity assay was performed according to the procedure described by Bernhardt et al. (1992). Details are given in chapter 3.2.6.

8.2.5 In vivo experiments

Rowett(rnu/rnu) nude rats and NMRI(nu/nu) mice obtained from the nude mice laboratory of the department were used for the in vivo growth studies. The animals were allowed to take water and food, a combined breed and maintenance nutrition (Altromin), ad libitum. The water was supplemented with 1.33 g/l of potassium sorbate, 2 g/l of chloramphenicol and 1 g/l of hydrochloric acid yielding a pH value of 2.5. The animals were housed under specified pathogen free conditions at a 12 h light/dark cycle at a temperature of 25 ℃ and a relative humidity of 70 %. At an age of 6 weeks the rats were used for studies.

The subcutaneous tumor model is discussed in chapter 3.

The intracerebral model has been described by Altenschöpfer (1998). In brief: the parietal bone of anaesthetized nude rats was drilled with a 1-mm-diameter bit 3 mm to the right-hand side of the sagittal line and 3 mm rostral of the coronal line. The rats were anesthesized with sevoflurane (Abbott, Wiesbaden, Germany). Human glioblastoma cells ($3{\cdot}10^5$ cells) suspended in 5 μl of serum-free EMEM were injected 5 mm deep into

the brain tissue, and the wound was closed with a surgical clamp. The body weight was observed to assess the tumor burden and the rats were killed when 20 % weight reduction occurred.

For histological staining of the tumor bearing brains, the nude rat brains were removed and fixed for at least three days in Bouin's solution. The tissues were embedded in paraffin by a standard procedure in a Histokinette (Shandon, Frankfurt/Main, Germany), cut by a Microtome Leitz 1516 (Leitz, Wetzlar, Germany) in sections with a thickness of 6 μm and put on object slides prepared with poly-L-lysin. Prior to each staining procedure, the sections were deparaffinized with xylol and various ethanol solutions with descending concentrations. The sections were stained according to the Masson-Goldner (MG) procedure which is described in detail in chapter 3.2.3. All stained sections were evaluated with a BH2 microscope (Olympus, Hamburg, Germany) mounted with a CCD-camera for digital imaging.

8.3 Results and discussion

The aim of the study was the examination of several human brain tumor cell lines with respect to their suitability for a targeted treatment with an immunoliposome based delivery system. The selected cell lines have to fullfill to the following requirements. The tumor cells should express sufficient quantities of TfR to target the immunoliposomes directly to the tumor cells after they have crossed the BBB. This was investigated in vitro and the TfR expression was confirmed in vivo in tumors growing subcutaneously in nude mice. As a second prerequisite, the cells have to be chemosensitive to low concentrations of the cytostatic drug that is incorporated in the immunoliposome. In addition, the tumor cells have to be tumorigenic in the brains of nude rats. These animals were used for the experiments, because of the possibility to overcome the BBB by means of transcytosis mediated by the OX-26 antibody which is targeted to the rat TfR.

8.3.1 Transferrin receptor content in tumor cells

8.3.1.1 TfR content of various tumor cell lines

The TfR content of several tumor cell lines that include brain and lung cancers was determined in vitro by an indirect immunofluorescence detection procedure at a flow cytometer. The FITC fluorescence intensity was quantified in molecules of equivalent solubility (MESF) by means of four fluorescent standard microbead populations of approximately 7 to 9 μ in diameter. The beads matched both the excitation and emission spectra of FITC labelled antibodies. Each microbead population had a different level of fluorescence intensity that referred to a certain MESF value. This means that microbeads with a MESF value of 10,000 exhibit the same fluorescence intensity as a solution containing 10,000 FITC molecules. A calibration curve was obtained by plotting the fluorescence intensities (relative channel number) of the single bead populations against the corresponding MESF values of the 4 populations. The single bead populations were recorded at the same settings as the analyzed samples (Fig. 8.3). Using this calibration curve, the MESF value of every sample was determined and measurements performed on different days could be compared with each other.

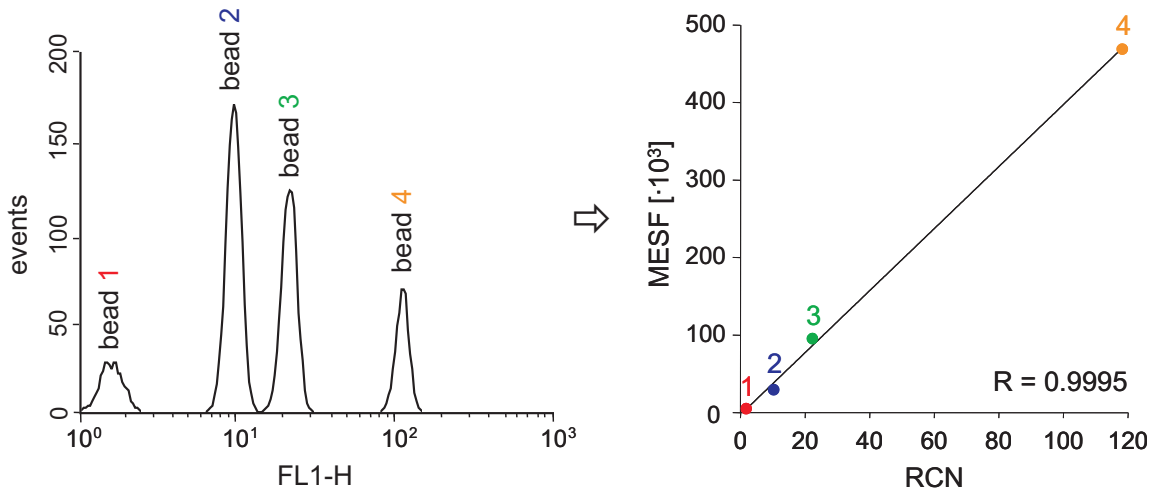

Figure 8.3: (a) fluorescence intensity at FL1-H channel of a mixture consisting of 4 microbead populations. (b) calibration curve of MESF calculated from microbead fluorescence intensities. RCN (relative channel number) is equivalent to FL1-H channel number.

The secondary antibody used for the indirect determination of TfR was labelled with FITC. Since the ratio of fluorescent dye and antibody ranges between 1 and 3, the fluorescence intensity of the different tumor cells can not be transformed directly in antibody binding capacity values or TfR densities. Direct quantification of receptor densities with fluorescent antibodies is only possible at fluorescent dye/antibody ratios of 1 as in case of phycoerythrin (PE) labelling. In consideration of the FITC/antibody ratio only a range for the TfR density of the different cell lines could be estimated. The TfR density ranges of selected glioblastoma and lung cancer cell lines are summarized in table 8.1. The TfR densities of the lung cancer cell lines were determined as these tumor entities metastasize preferentially to the brain. The human B-cell line RAJI served as a positive control for TfR expression.

Table 8.1: MESF values of different cell lines and their corresponding TfR density. Measurements were taken on day 5 after last passage (n= 3-6).

cell line	MESF [$\cdot 10^3$]	transferrin receptor density [$\cdot 10^3$]		
		min.		max.
U-87 MG	347.91 ± 51.96	139	-	348
U-118 MG	714.07 ± 224.46	286	-	714
U-373 MG	**540.36 ± 26.83**	**216**	**-**	**540**
RAJI	158.50 ± 3.37	64	-	159
NCI-H460	266.06 ± 3.05	106	-	266
DMS 53	61.82 ± 1.21	25	-	62
DMS 114	75.86 ± 1.42	30	-	76

The highest TfR densities were detected on U-87 MG, U-118 MG and U-373 MG glioma cells with levels 2 to 4 times higher compared to those of the RAJI control cells. The examined lung cancer cell lines exhibited lower TfR densities than the brain tumor cells, particularly the small cell lung cancer cells DMS 53 and DMS 114. In these cell lines TfR densities under 100,000 were determined. In contrast, in NCI-H460 non-small cell lung cancer cells TfR is expressed at a level similar to that in U-87 MG cells. The TfR

density in the U-118 MG cells was the highest among the analyzed cell lines. However, the expression of TfR seemed to be unequal, since the standard deviation of the calculated MESF value was extremely high. Lower standard deviation combined with high TfR density was found in U-373 MG cells. Therefore, the U-373 MG cell line is the most suitable one among the examined brain tumor cell lines, for a TfR targeted treatment regarding the TfR density in vitro.

8.3.1.2 Growth depended TfR expression

The TfR is essential for cell growth as it mediates the transport of iron into the cell, which is necessary for metabolic processes. Several work groups identified a close relationship between TfR expression and cell proliferation (Trowbridge et al. 1984, Gambari et al. 1986, Chan et al. 1994). Therefore, we investigated the TfR content of various glioblastoma cell lines in different proliferation stages by indirect immunofluorescence detection using FITC labelled antibodies. RAJI cells are described as TfR expressing cells in literature (Laskey et al. 1988) and were used as a positive control. The human glioblastoma cell lines U-87 MG, U-118 MG and U-373 MG were examined 3, 5 and 7 days after passaging to simulate subconfluent and postconfluent growth. The measured fluorescence intensities of the single cell lines plotted against the growth time are depicted in Fig. 8.4.

In all cell lines a FITC fluorescence intensity that correlates with TfR expression was detected at all time points. For the control cell line RAJI (black bars) the highest fluorescence intensities were measured after 3 days. Subsequently, the intensity strongly decreased to values 7 times lower than those measured after 3 days in culture. This indicated that the growth of the RAJI cells is almost complete after 3 days. Thus, there is no need for further TfR expression. In case of the U-87 MG cells (right-hatched bars) the determined fluorescence intensity reached maximum values on day 3 as well. Indeed, the intensities measured on the other two days slowly declined compared to day 3, but the decrease was not as distinct as observed in the RAJI cells. In contrast, the fluorescence intensity of U-118 MG cells (cross-hatched bars) increased up to day 5. After 2 further days of incubation only half of the fluorescence intensity was measured compared to day 5. The fluorescence intensity of U-373 MG cells (left-hatched bars) remained relatively constant over the examination period in consideration of the SEM values. The detected intensity

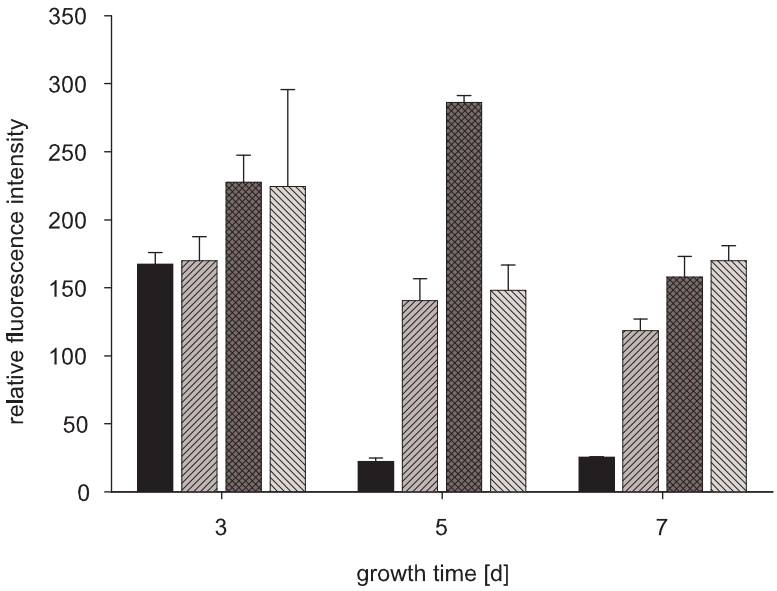

Figure 8.4: Growth dependent TfR expression in different glioblastoma cell lines U-87 MG (right-hatched bars), U-118 MG (cross-hatched bars) and U-373 MG (left-hatched bars). RAJI cell line (black bars) serves as control for measurable TfR expression. (mean values ± SEM)

values were similar to those measured in U-87 MG cells, but U-373 MG cells showed no decrease in fluorescence intensity. This indicated a relatively constant cell growth in vitro. In view of the suitability for the mentioned tumor model, the brain tumor cell line should have a constant TfR expression over a longer period of time. This requirement is best fulfilled by the U-373 MG cells as they showed the most constant TfR expression.

8.3.2 Transferrin receptor expression in tumor tissue

To ensure the relevance of the in vitro data to the in vivo situation, the TfR expression was also analyzed in tumors growing subcutaneously in athymic mice. Immunohistochemical methods were used to detect TfR in solid U-87 MG, U-118 MG and U-373 MG tumors. The sections were counterstained with Harris' haematoxylin to stain nuclei blue for a better contrast to the light brown staining of the TfR. TfR as a transmembrane cell surface receptor is located at the cell membrane. The main part of the receptor is present at the extracellular site and only a small region is found at the cytoplasmic site of the cell

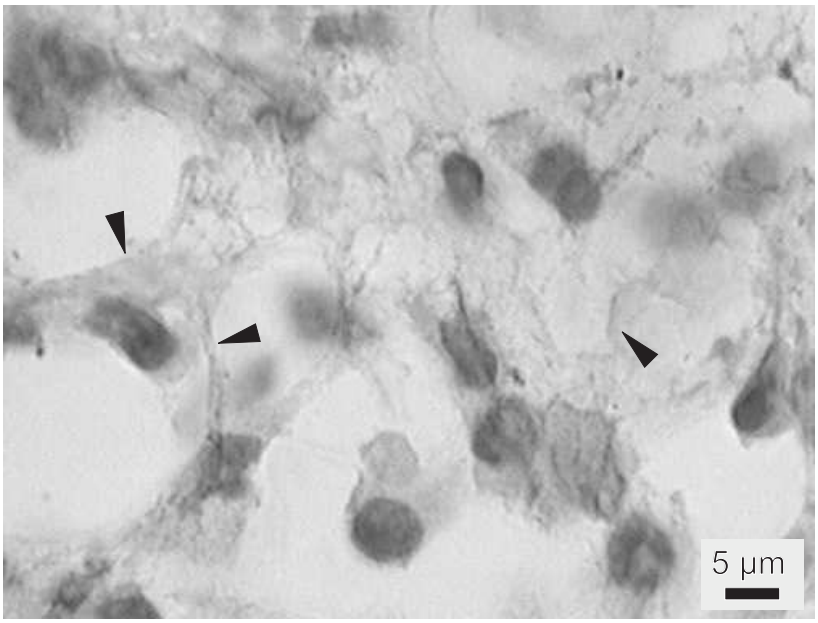

Figure 8.5: Section of subcutaneously grown U-87 MG glioblastoma immunostained with mouse MAb to the human TfR shows positive TfR staining at the cell membrane (clone Ber-T9 (1:5), avidine-biotin-peroxidase staining on frozen sections, hematoxylin counterstaining.)

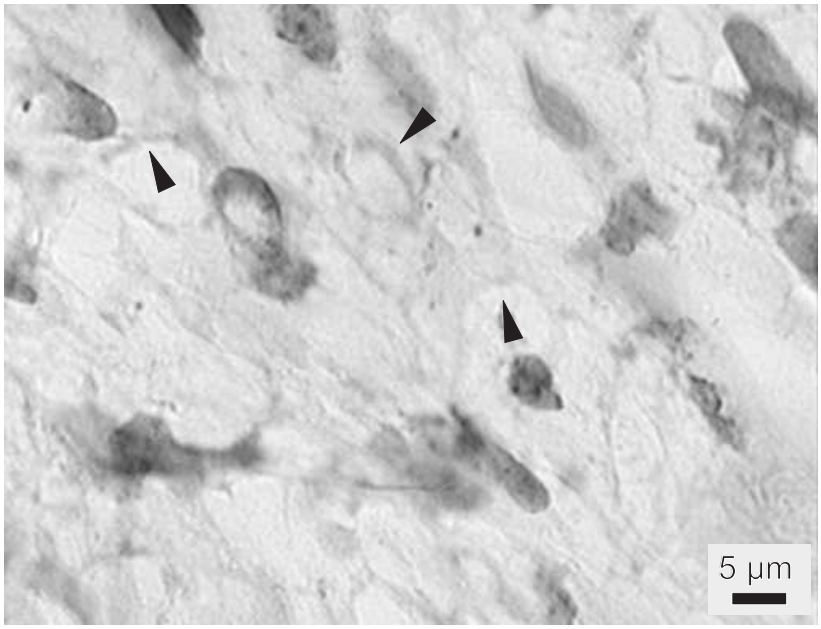

Figure 8.6: Tumor tissue section of subcutaneously grown U-118 MG glioblastoma demonstrates positive TfR staining at the cell membrane with mouse MAb to the human TfR (clone Ber-T9 (1:5), avidine-biotin-peroxidase staining on frozen sections, hematoxylin counterstaining.)

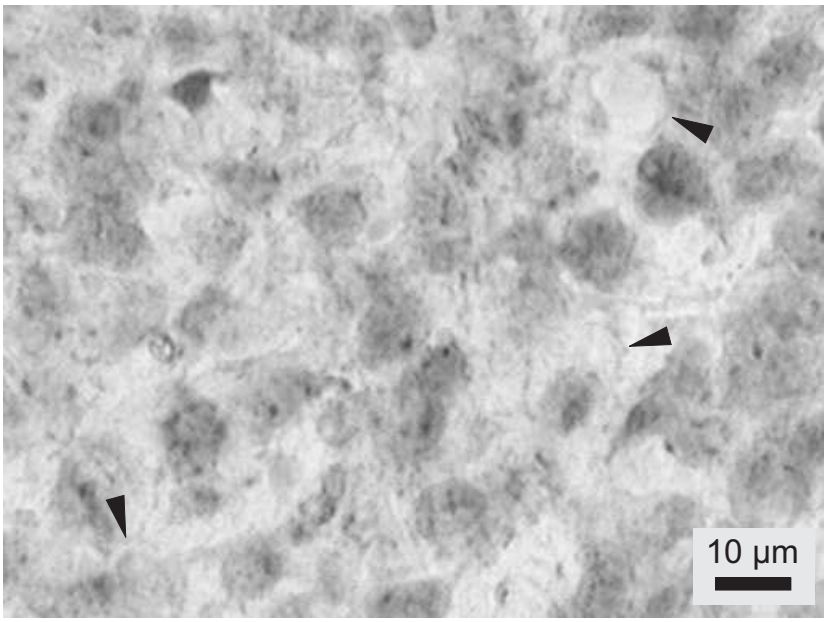

Figure 8.7: Frozen section of subcutaneously grown U-373 MG tumor. Despite the poor quality of the frozen section, positive TfR staining is detectable at the membrane of the tumor cells (clone Ber-T9 (1:5), avidine-biotin-peroxidase staining on frozen sections, hematoxylin counterstaining.)

membrane. The described TfR localization was found in all immunostained sections of the three tumor types (Figs. 8.5 to 8.7). The tumor cells demonstrated a specific positive staining of the cell membrane, but not of the cytoplasm. This is clearly visible in sections of U-87 MG and U-118 MG tumors (Fig. 8.5 and Fig. 8.6). Many blue stained nuclei were visible that were enclosed by the light brown stained cell membrane. Occasionally sections of cells without visible nuclei were observed that were intensely stained at the membrane rather than at the cytoplasm indicating the specific staining of TfR which is a transmembrane protein. In immunostained sections of U-373 MG tumors the TfR staining was difficult to determine because of the poor quality of the frozen tumor sections. However, the tumor section depicted in Fig. 8.7 presents the aforementioned characteristics for a positive TfR staining.

The immunohistochemical staining was very weak and not sensitive enough to stain internalized TfR inside the cells. Furthermore, differences in TfR expression level as determined by flow cytometry were not detected between the single cell lines. Hence, this method could only be used to visualize of TfR expression and not for the quantitative distribution of the receptor.

8.3.3 In vitro chemosensitivity against anthracyclins

Immunoliposomes that are targeted to brain tumors can include a cytostatic drug concentration of 0.2 to 0.5 μM (Huwyler et al. 2002). Hence, for an effective treatment of brain tumors, the cancer cells have to be sensitive to the incorporated cytostatic drug at least at these concentrations. Cytostatic agents like the anthracyclins doxorubicin and daunorubicin (see Fig. 8.8) are well suited for the incorporation into immunoliposomes. However, since both substances are substrates of the p-gp, these compounds cannot reach the brain and consequently, the brain tumors. Masking of such compounds by incorporation in immunoliposomes leads to an enhanced accumulation in the brain, which is a prerequisite for a successful chemotherapy. The three selected glioblastoma cell lines U-87 MG, U-118 MG and U-373 MG were examined with respect to their chemosensitivity against various concentrations of doxorubicin and daunorubicin ranging from 0.1 to 1 μM. For this purpose the tumor cells were exposed to the cytostatic drugs over a period of 150 hours and the cell proliferation was determined. The results shown in Figs. 8.9 to 8.11 demonstrated a marked effect of the selected cytostatic drugs on the cell proliferation of the glioblastoma cells.

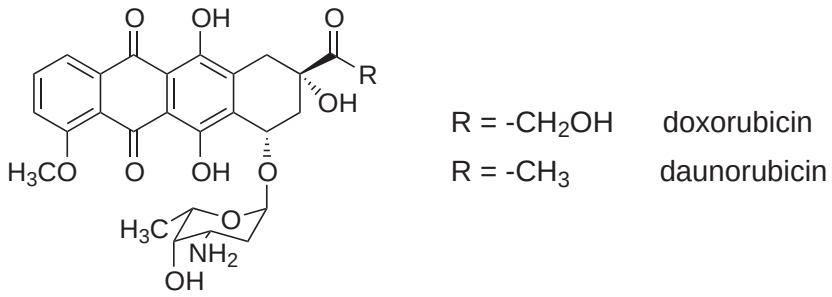

Figure 8.8: Structures of the anthracyclins doxorubicin and daunorubicin. Both chemotherapeutics are easily incorporated in immunoliposomes at concentrations from 0.2 to 0.5 μM.

Long term incubation with doxorubicin and daunorubicin had similar effects on the growth of the three tumor cell lines at all experimental concentrations. Doxorubicin was slightly more potent compared to daunorubicin except for U-118 MG cells. Addition of only 200 nM doxorubicin led to complete decay of U-87 MG cells (Fig. 8.9 a). In case of daunorubicin a concentration of 300 nM was needed to produce the same effect (Fig.

8.9 b). Lower concentrations of both compounds resulted in cell growth inhibition of at least 80 %. To reach complete disintegration of U-118 MG cells, significantly higher concentrations were required (Fig. 8.10). Here, a doxorubicin concentration of 1 μM was necessary for a cytocidal effect (50 % of the cells were killed after 150 hours). Daunorubicin was more effective in inhibiting the proliferation of U-118 MG cells as the addition of 300 nM daunorubicin led to killing of the tumor cell population. If the cytostatic agents were used at lower concentrations, a cytostatic effect on the cell growth was observed. However, doxorubicin added at a concentration of 100 nM inhibited the growth of U-118 MG cells only by 40 %, which was the weakest effect measured in this study. The U-118 MG cell line was the only cell line of the selected ones, where daunorubicin was more active than doxorubicin. The most sensitive glioblastoma cell line was the U-373 MG cell line (Fig. 8.11). Cytocidal effects were observed after incubation with 100 nM doxorubicin and 200 nM daunorubicin. But even 100 nM daunorubicin had a cytostatic effect on the cells and inhibited the cell proliferation by 95 %.

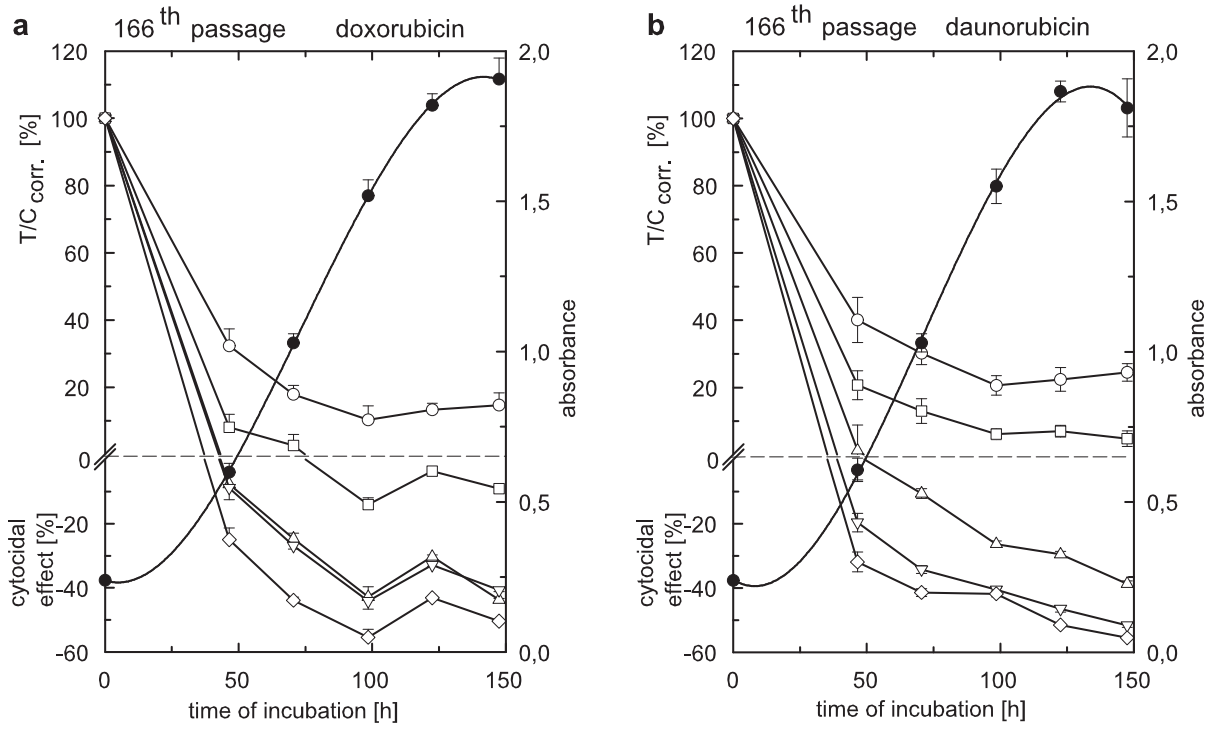

Figure 8.9: Chemosensitivity of U-87 MG cells against the anthracyclins doxorubicin (a) and daunorubicin (b) at concentrations of 100 nM (○), 200 nM (□), 300 nM (△), 500 nM (▽) and 1 μM (◇). Proliferation of untreated cells served as control (●).

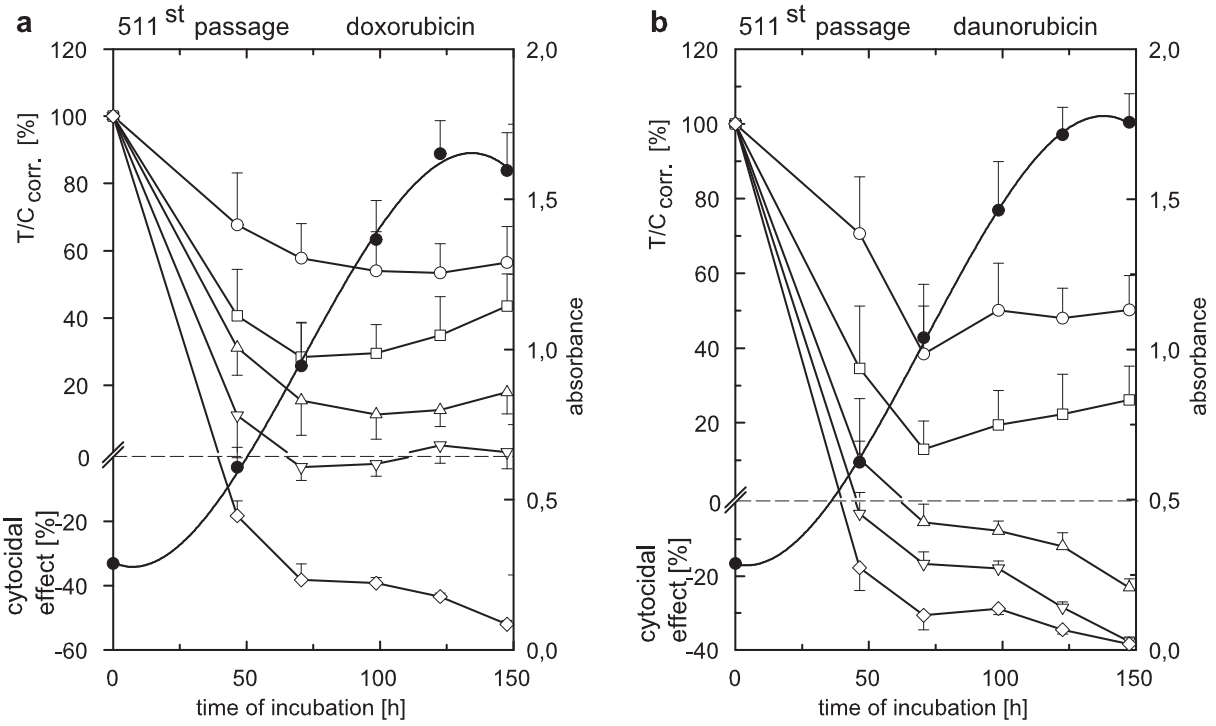

Figure 8.10: Chemosensitivity of U-118 MG cells against the anthracyclins doxorubicin (a) and daunorubicin (b) at concentrations of 100 nM (○), 200 nM (□), 300 nM (△), 500 nM (▽) and 1 μM (◇). Proliferation of untreated cells served as control (●).

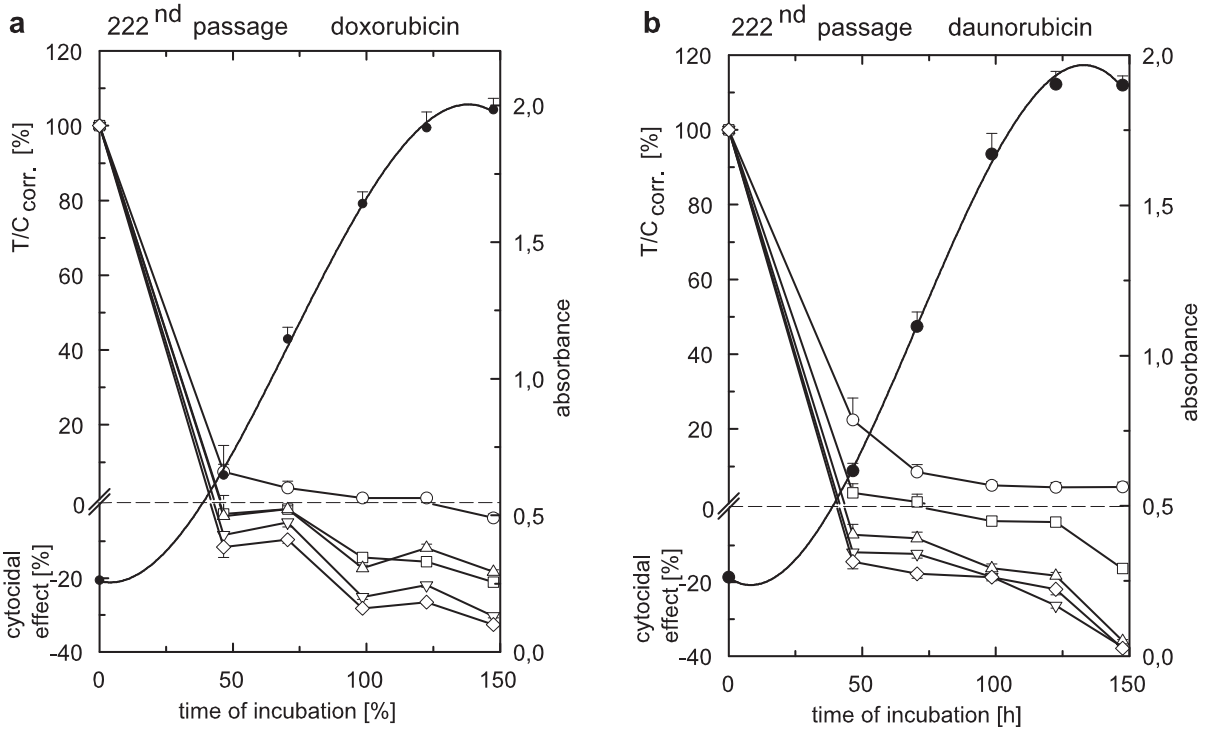

Figure 8.11: Chemosensitivity of U-373 MG cells against the anthracyclins doxorubicin (a) and daunorubicin (b) at concentrations of 100 nM (○), 200 nM (□), 300 nM (△), 500 nM (▽) and 1 μM (◇). Proliferation of untreated cells served as control (●).

When considering the loading capacity of the immunoliposomes, a tumor cell line used for the tumor model has to be chemosensitive to a cytostatic drug concentration of at least 200 nM. U-118 MG cells were indeed chemosensitive against the two chemotherapeutics. However, it is debatable, if the observed growth inhibition of 40 % in case of doxorubicin and 60 % for daunorubicin, is sufficient to provide a therapeutic benefit. U-87 MG cells were more sensitive compared to U-118 MG cells, particularly regarding their chemosensitivity against doxorubicin. Here a cytocidal effect was demonstrated at 200 nM doxorubicin. In contrast, incubation of U-373 MG cells with the same drug concentration led to complete cell disintegration in both cases. Provided that the U-373 MG glioblastoma has the same chemosensitivity in vitro and in vivo, this cell line is preferred for the therapy with anthracyclins loaded immunoliposomes.

8.3.4 Growth of human glioblastomas in the nude rat brain

It is indispensable that brain tumor cell lines are tumorigenic in the laboratory animal in order to study the effect of a brain targeted immunoliposome based chemotherapy in vivo. Another criterion to assess the suitability of a tumor cell line for the use in an animal model is the tumor burden, which results from the intracerebral tumor growth. The OX-26 is a MAb directed to the rat TfR and it was chosen as a vector for targeting immunoliposomes to the brain. Thus, the planned animal tumor model has to be established in nude rats. The three brain tumor cell lines U-87 MG, U-118 MG and U-373 MG were injected into the brains of three nude rats per cell line. The tumor appearance and growth were examined after 4 to 5 weeks by histological staining techniques. Additionally, the body weight of the animals was monitored during the experiment to evaluate the tumor burden.

Fig. 8.12 and Fig. 8.13 illustrate histological sections of an intracerebrally grown U-87 MG tumor. The big, cell-rich tumor is well confined from the normal brain tissue. Many blood vessels, that are not infiltrated by the tumor cells, are observed in the tumor tissue. Besides tumor areas with high content of connective tissue, necrotic areas are also detected within the tumor tissue. The tumor consists of inhomogeneous formed cells with mostly one round to oval nucleus and several pleomorphic nucleoli. Mitotic activity is visible as well.

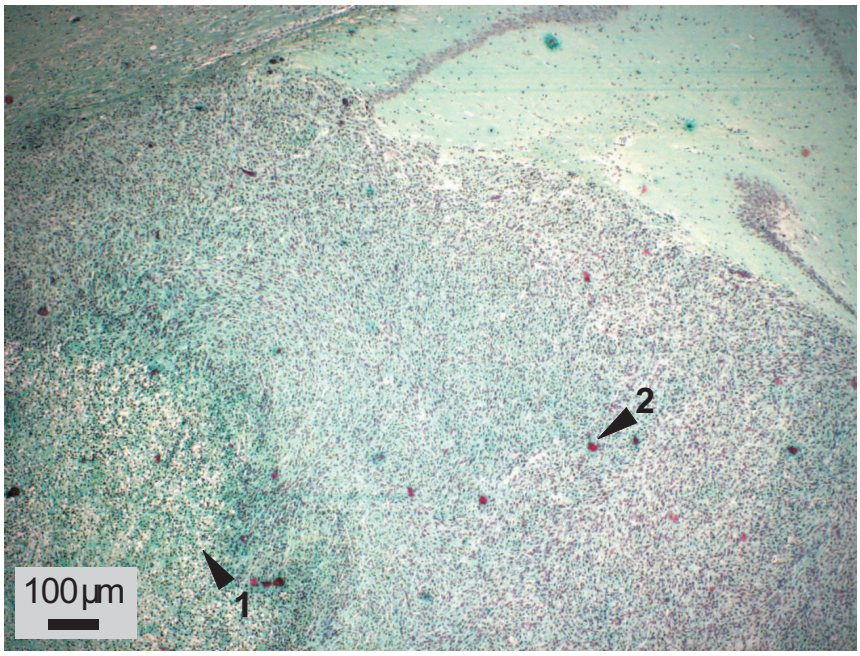

Figure 8.12: MG-stained section of intracerebrally grown U-87 MG glioblastoma in the nude rat. The well-confined tumor is of enormous size and has necrotic areas (indicated by arrow 1). Blood vessels are observed as well (indicated by arrow 2).

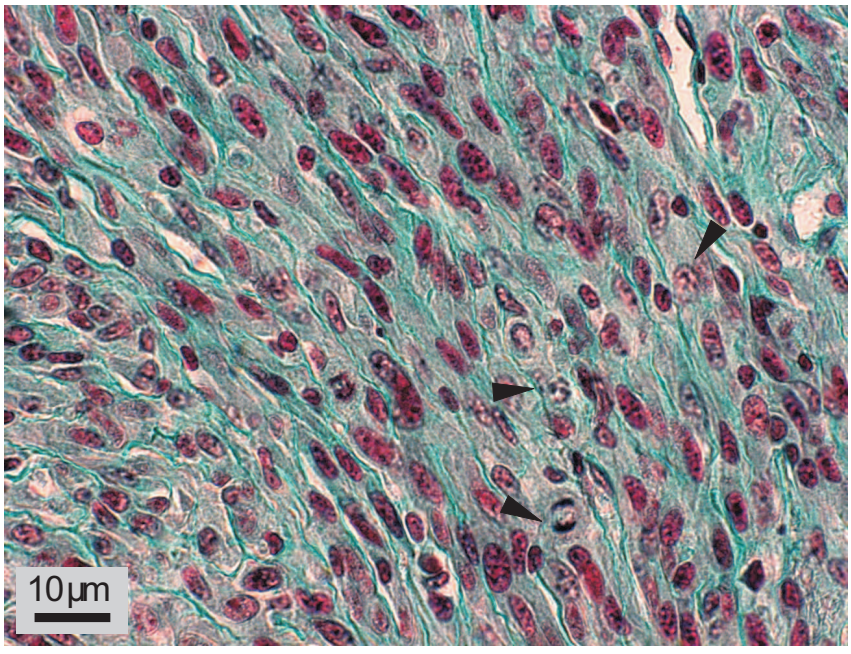

Figure 8.13: MG-stained section of intracerebrally grown U-87 MG glioblastoma in the nude rat. The inhomogeneous formed tumor cells have round to oval nuclei with irregular formed nucleoli. Mitotic activity is observed (indicated by arrows).

The appearance of the intracerebrally grown U-118 MG tumor (Fig. 8.14 and Fig. 8.15) is quite different to that of the U-87 MG tumor. U-118 MG tumors are significantly smaller and the cell density is lower. The high amount of connective tissue indicated by the intensive green color, is an important characteristic of this tumor. The tumor cells with indistinct cytoplasm infiltrate the normal brain tissue. The fusiform cells have readily identifiable oval nuclei with several prominent nucleoli.

In Fig. 8.16 and Fig. 8.17 histological U-373 MG tumor sections of the injection area in the brain are presented. The tumor is spread along the puncture channel, but only slight infiltration of the normal brain tissue is observed. The homogenous tumor consists of fusiform cells with oval nuclei, which are of different size and have mostly one prominent nucleolus. The cell density is comparable to that of the U-87 MG tumor.

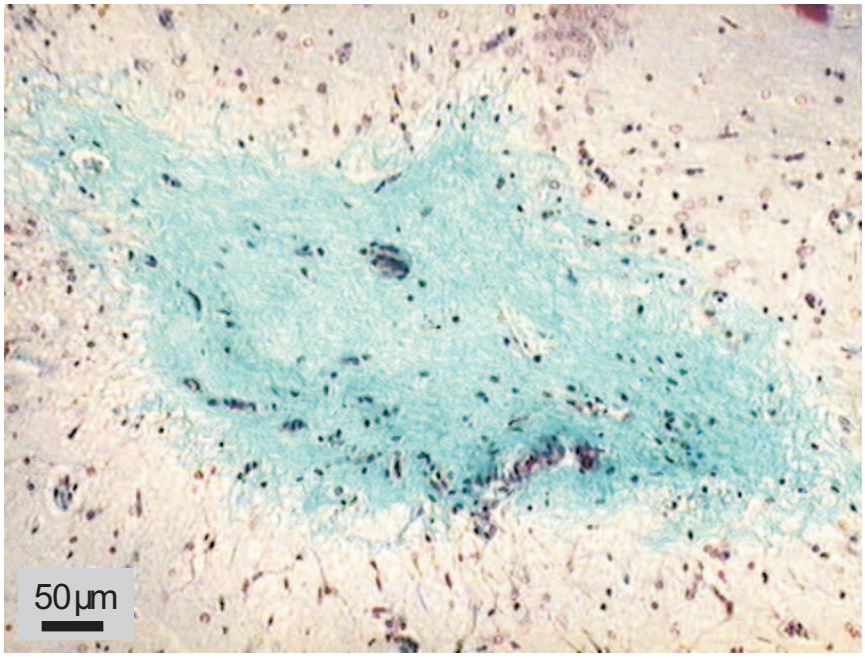

Figure 8.14: MG-stained section of intracerebrally grown U-118 MG glioblastoma in the nude rat. The tumor is characteristically green stained, because of the high content of connective tissue.

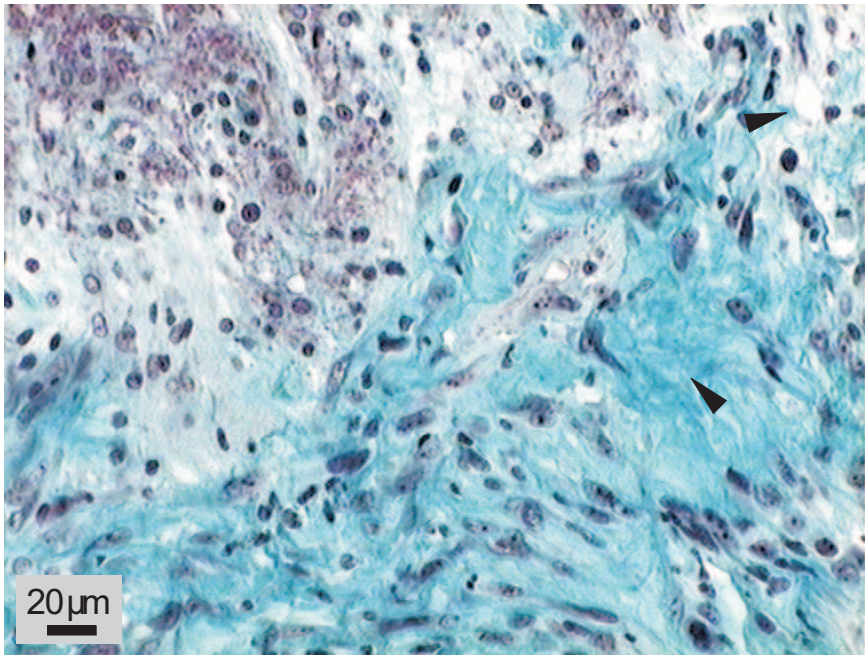

Figure 8.15: MG-stained section of intracerebrally grown U-118 MG glioblastoma in the nude rat. The fusiform cells with indistinct cytoplasm have readily identifiable oval nuclei with several prominent nucleoli. The high content of connective tissue and necrotic areas are marked by arrows.

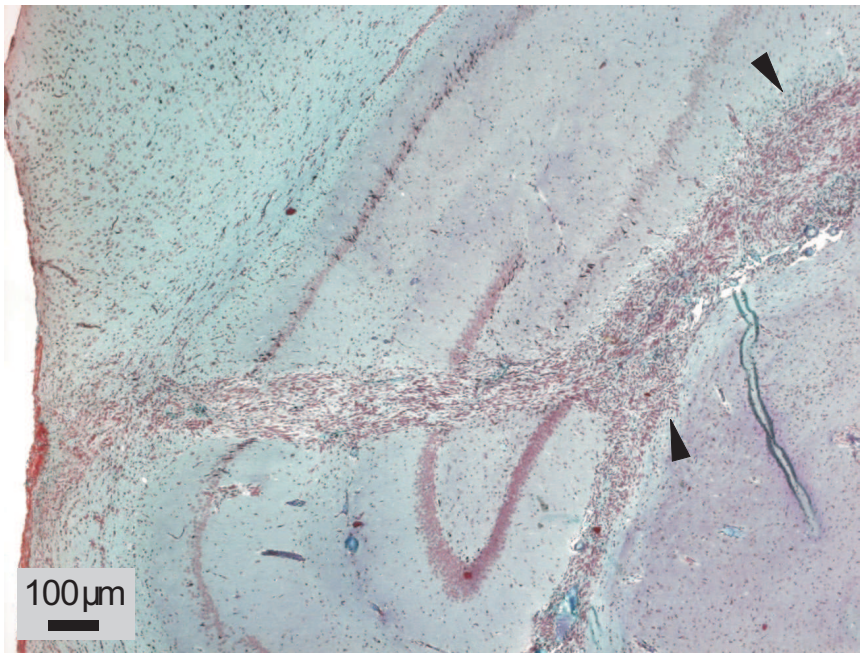

Figure 8.16: MG-stained section of intracerebrally grown U-373 MG glioblastoma in the nude rat. The cell rich tumor slightly infiltrates normal brain tissue (indicated by arrows).

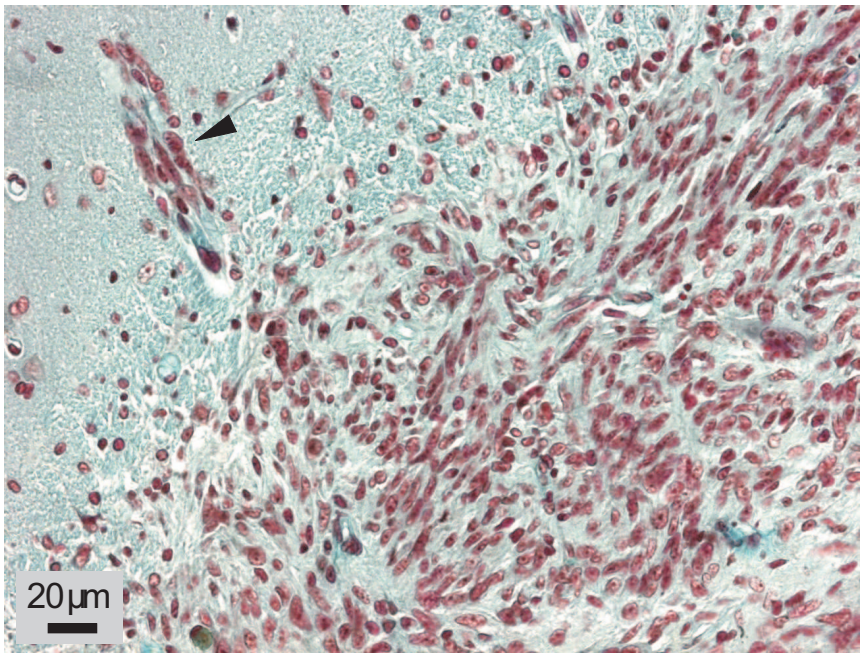

Figure 8.17: MG-stained section of intracerebrally grown U-87 MG glioblastoma in the nude rat. The tumor cells appear homogenous and fusiform with different sized nuclei. Infiltration of normal brain tissue is indicated by arrow.

All controlled rats developed brain tumors, which led to a loss of body weight of up to 20 % within 3 to 4 weeks after tumor cell injection. The changes of body weight depicted in Fig. 8.18, indicate that the developed tumors are tolerated by the rats. Negative values reflect an increasing tumor burden in the rat brain.

Rats bearing U-373 MG tumors were the only ones that put on weight during the first 3 weeks. However, a clear decrease in body weight was observed 4 weeks after the injection of U-373 MG cell into the brain. At this time rats bearing U-87 MG or U-118 MG tumors appeared lethargic and lost so much strength, that the experiment had to be stopped.

The intracerebrally growing tumors should enfeeble the experimental animals only to such an extent that they can withstand subsequent chemotherapy. Therefore, no detraction of the animals should be observable over a longer period. This is true in case of U-373 MG glioblastoma, as the development of the brain tumor had no influence on growth, behavior and general condition of the rats in the first 3 to 4 weeks of the experiment.

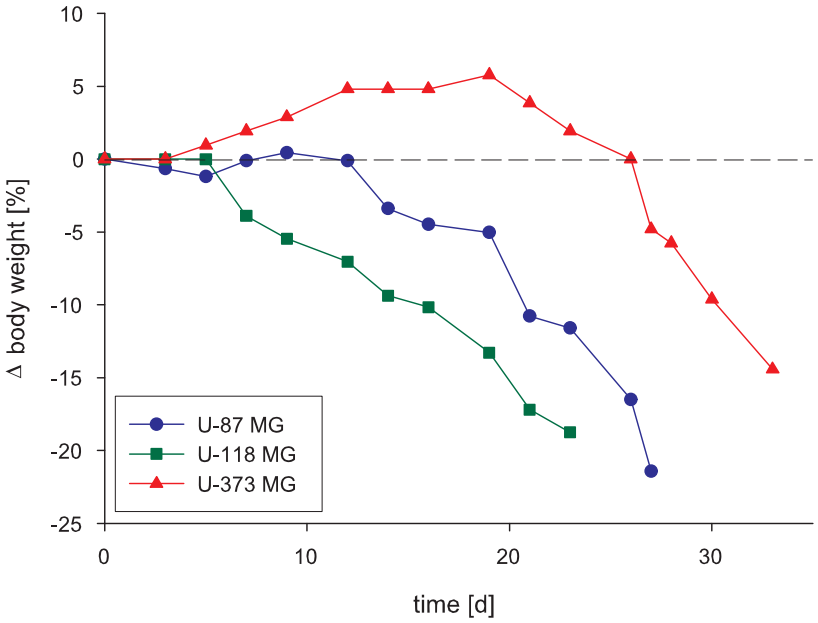

Figure 8.18: Change of mean body weight as an indicator for tumor aggressiveness. Negative values reflect an increasing tumor burden in the rat brain.

8.3.5 Discussion

The three human glioblastoma cell lines U-87 MG, U-118 MG and U-373 MG were examined with respect to the following characteristics. The TfR density and the TfR expression in various stages of growth were determined in vitro as well as the TfR expression in subcutaneously grown tumors. Furthermore, the chemosensitivity of the cell lines against the anthracyclins doxorubicin and daunorubicin was investigated. In addition, the tumorigenicity of the human brain tumors in the nude rat brain was studied. These examinations indicate, which of the tested cell lines is most suitable for a brain tumor model in nude rats. By means of that model, treatment experiments with brain targeted immunoliposomes should be carried out.

The TfR density of the U-118 MG cells was very high, and TfR was detected in subcutaneously grown tumor tissue as well. However, the TfR expression in this cell line did not remain constant during cultivation. Furthermore, the anthracyclins doxorubicin and daunorubicin used at a concentration of 200 nM, led to an inhibition of the proli-

feration by only 60 and 80 %, respectively. However, this anticancer drug concentration is required as immunoliposomes can be loaded with a cytostatic drug concentration from 200 to 500 nM. U-118 MG cells were tumorigenic in the brain of nude rats, but the resulting tumor enfeebled the rats. It is debatable, if rats bearing U-118 MG tumors will sustain the additional burden of chemotherapy. As the body weight of tumor bearing rats significantly decreased, the distinction between weight reduction as a result of tumor aggressiveness or because of the toxicity of administered cytostatic drugs will be impossible. Thus, the U-118 MG cells are unsuited as a brain tumor model.

The U-87 MG cell line was used in former studies to demonstrate imaging of intracerebrally grown U-87 MG tumors in rat brains with a conjugate of peptide radiopharmaceuticals and the OX-26 MAb targeted to the TfR (Kurihara and Pardridge 1999). In the present study the suitability of this tumor for treatment experiments in rats was studied. The determined TfR density was half that of U-118 MG cells. In contrast, the TfR expression did not change significantly during cultivation. U-87 MG cells have a TfR density twice as high compared to RAJI cells, which served as a positive control for TfR expression. Hence, the lower TfR expression of U-87 MG cells compared to U-118 MG cells should be sufficient for the targeted therapy. In addition, TfR was discovered in subcutaneously grown tumor tissue. Moreover, the U-87 MG cell line was sufficiently sensitive against the selected cytostatic drugs. Doxorubicin is preferred over daunorubicin because of the complete disintegration of the cells by incubation with 200 nM doxorubicin. Assuming that chemosensitivity of the cells is similar in vitro and in vivo, U-87 MG tumors might be successfully treated with doxorubicin loaded immunoliposomes. Unfortunately, U-87 MG cells injected into nude rat brain developed very large tumors of about half the size of the rat's brain. Tumors of this size are not treatable any more. The enormous extensions of these tumors led to a marked reduction of body weight of U-87 MG tumor bearing rats by 20 %. It becomes obvious from these results, that the U-87 MG glioblastoma is unsuited for the establishment of a brain tumor model.

The last examined human brain cancer cell line was the U-373 MG cell line. The determined TfR density was similar to that in U-118 MG cells, but changes in TfR expression in U-373 MG cells during cultivation were not as distinct as in U-118 MG cells. The evidence of TfR in vivo was hampered by the poor quality of the tumor

tissue section. However, slight positive staining of TfR was detected. The U-373 MG cell line was most sensitive against doxorubicin and daunorubicin. The incubation of U-373 MG cells with cytostatic drugs at a concentration of 200 nM led to a complete disintegration of the cell culture in both cases. Cell death of the whole population is desired in in vivo therapy experiments. Furthermore, the U-373 cells are tumorigenic in the nude rat brain and developed solid tumors of a tolerable size. Up to 3 weeks after the tumor cell injection the body weight was not affected. These results demonstrate, that a nude rat brain tumor model could be established using the U-373 MG cells to study the effect of an immunoliposome based, brain targeted chemotherapy on brain tumors. The suitability of the U-373 MG cell line was proven by the work group of Martell et al. (1993). Martell et al. demonstrated, that U-373 MG cells were extremely sensitive to TfR targeted immunotoxins, indicating an successful drug targeting to these tumor cells by using TfR as a vector. Therefore, U-373 MG has most promising prerequisites for a successful therapy with the TfR targeted immunoliposomes.

8.4 Perspectives

As described in this chapter the human brain tumor cell line U-373 MG proved to be suitable for the establishment of a tumor model in the nude rat brain. The therapeutic effects of a brain targeted immunoliposome based drug delivery system can be evaluated by using this model. Further investigations have to focus on the toxicity of unloaded immunoliposomes at the U-373 MG cell line as well as on the chemosensitivity of U-373 MG cells against incorporated anthracyclins. Afterwards, in vivo experiments in nude rats must show, if drug delivery systems targeted to the TfR at both the BBB and the brain tumor, can improve the treatment of brain tumors and lower the negative side effects of chemotherapy.

Because of the possibility to easily exchange the coupled MAb of the immunoliposomes the presented drug delivery system can be targeted to other specific transport systems that are located in certain organs or are highly expressed in tumor cells like insulin or EGFP receptors (Friden 1996, Zhang et al. 2004).

The principle of the TfR mediated transcytosis which is the basis of the introduced drug

delivery system is used by other work groups to increase the concentration of different compounds in tumor cells or in the brain. In vitro studies were carried out to improve the cellular delivery of antisense oligonucleotides to U-87 MG cells (Walker et al. 1995). Zhu et al. (2004) demonstrated the TfR mediated transcytosis of adenoviral vectors in Caco-2 cells. Such vectors could be used in lung, urogenital and brain disorders. In vivo studies of noninvasive gene targeting to the brain mediated by TfR at the BBB in rodents were also reported (Shi and Pardridge 2000). Bickel et al. (2001) reviewed the possibility of delivery of neuropeptides and proteins to the brain with the use of a chimeric peptide strategy. Pharmacological effects were observed in the brain after the systemic administration of relatively low doses of chimeric neuropeptide.

Therefore, the TfR as a drug delivery vehicle using the naturally occurring TfR mediated transcytosis pathway is a promising model for the targeted delivery to so-called "sanctuary sites" in the human body such as the brain. Furthermore, the use of TfR targeted compounds or immunoliposomes may lead to a better tolerated cancer therapy with less negative side effects.

Chapter 9

Summary

The treatment of malignant brain tumors is a major challenge for modern oncology. Only minor success has been achieved by the application of current treatments including surgery and radiotherapy. By means of chemotherapy, in contrast to surgery, the whole brain is treated theoretically, but the brain concentrations of chemotherapeutic agents are usually very low due to the existence of the blood-brain barrier (BBB). At the BBB special efflux transport proteins, members of the ABC family, are present, which are transporting a broad variety of compounds including most of the lipophilic cytostatic drugs such as paclitaxel. The most common ABC transporter at the BBB is the p-glycoprotein 170 (p-gp, MDR1). Inhibitors, which block the ABC transporter mediated efflux, should increase the concentrations of chemotherapeutic agents in the brain.

This work is based on the results of previous studies done by P. Altenschöpfer and S. Fellner, who established a nude mouse model to study the treatment of human primary brain tumors (Altenschöpfer 1998) and demonstrated a therapeutic benefit by combining the cytostatic agent paclitaxel with the p-gp inhibitor valspodar against U-118 MG glioblastoma (Fellner 2001). The main goal of this thesis was the adaptation of the combination strategy to the therapy of brain metastases of lung cancer, occurring at a much higher incidence than malignant primary brain tumors. To refine the combinatorial approach, the new p-gp modulators elacridar and tariquidar were included in the studies.

First, three human lung cancer cell lines were characterized with respect to in vitro growth, chromosome distribution, chemosensitivity against clinically established cytostatic drugs, being p-gp substrates. Then, tumorigenicity was determined after subcuta-

neous injection of the human lung cancer cells into nude mice. The NCI-H460 non-small cell lung cancer cells and the DMS 114 small cell lung cancer cells proved to be particularly suited for the establishment of a subcutaneous tumor model. NCI-H460 cells are very aggressive becoming obvious by the abundant abnormal mitotic figures. These cells grow very rapidly (minimal doubling time: 9 hours) in vitro. In contrast, DMS 114 cells grew markedly slower (minimal doubling time: 28 hours), but were more sensitive to chemotherapeutic agents compared to the NCI-H460 cells.

Additionally, a flow cytometric assay for the assessment of p-gp activity in living cells and for the determination of the inhibitory activity of p-gp modulators was established, using the p-gp substrate calcein-AM.

Subsequently, the selected human lung cancer cells (NCI-H460 and DMS 114) were examined with regard to the establishment of an intracerebral tumor model in nude mice to simulate brain metastases. The presence of a MDR1 phenotype was also investigated. Both, the NCI-H460 and the DMS 114 cells, were tumorigenic in the brains of nude mice. Tumorigenicity of the DMS 114 cells strongly depended on the number of injected cells. Moreover, no functional MDR1 protein was detected, despite the identification of mRNA, encoding for p-gp in NCI-H460 cells. Hence, in case of a therapeutical benefit due to a co-administration of a p-gp inhibitor with an antitumor agent in vivo, the effect is attributable to the modulation of the p-gp mediated efflux of the chemotherapeutic at the BBB. Two different therapeutic experiments were performed. As a model of non-small cell lung cancer metastases, intacerebrally implanted human NCI-H460 cells were treated with a combination of valspodar and vinblastine (50 mg/kg of valspodar p.o.; 0.8 mg/kg of vinblastine i.p., every 5 day). Brain metastases of small cell lung cancer were simulated by the intracerebral injection of DMS 114 cells. These tumors were treated with a combination of valspodar and paclitaxel (50 mg/kg of valspodar p.o.; 3 mg/kg of paclitaxel i.v. on day 8, and 2 mg/kg on day 15). Although the combination of the p-gp modulator with the aforementioned chemotherapeutic agents resulted in a recovery of the chemosensitivity of p-gp overexpressing Kb-V1/VBL cells in vitro, no therapeutic benefit was observed in the intracerebral tumor models. The high aggressiveness of NCI-H460 cells together with the rapid cell proliferation may be the reason for the negative in vivo result. Furthermore, the increase in the vinblastine concentration in the brain, resulting

from the p-gp inhibition by valspodar seemed to be extremely low. In case of intracranial DMS 114 tumors chemosensitivity of DMS 114 cells against paclitaxel seemed to be lower compared to the in vitro sensitivity, because, despite of paclitaxel concentrations sufficient for a cytocidal effect in vitro, tumor growth was not affected in vivo.

Recently, new p-gp modulators had been developed, which were reported to be more potent compared to valspodar and could therefore be superior to valspodar in a combination therapy approach to the treatment of secondary brain tumors. These new modulators include the compounds elacridar and tariquidar. Both modulators were characterized with respect to their activity to inhibit p-gp mediated efflux and their specificity against other ABC proteins present at the BBB, particularly the ABCG2 transporter. Both compounds showed an up to 80 times higher inhibitory activity against p-gp than valspodar with IC_{50} values of 20.5 nM for elacridar and 26.5 nM in case of tariquidar. Since elacridar and tariquidar are structurally related, the common moiety 4-[2-(6,7-dimethoxy-3,4-dihydro-1*H*-isoquinolin-2-yl)ethyl]phenylamine, designated as compound **4**, was examined with regard to its inhibitory activity, too. Compound **4** has an IC_{50} value of 42.7 μM, which is 6 times lower compared to the IC_{50} value of the 1^{st} generation p-gp modulator *(R)*-verapamil (248 μM). Hence, it was assumed that this structural element is important for the inhibition of p-gp mediated drug efflux. Elacridar and tariquidar are non-specific modulators as both compounds were able to inhibit not only the p-gp mediated efflux but also ABCG2 transport. However, they differed concerning the selectivity for the two ABC transport proteins. The IC_{50} values of elacridar and tariquidar were similar in case of p-gp inhibition. However, the IC_{50} value of elacridar concerning ABCG2 transport inhibition (0.86 μM) was 5.5 times lower compared to the corresponding IC_{50} value of tariquidar (4.76 μM).

After the in vitro characterization of the new modulators elacridar and tariquidar, the two compounds were examined with respect to their effect on the paclitaxel distribution in nude mice, particularly on the brain penetration of paclitaxel. The paclitaxel levels were detected in liver, kidney, plasma and brain of nude mice 1.5, 3, 4.5 and 24 hours after the intravenous injection of paclitaxel by HPLC. One group of the animals received either elacridar or tariquidar 4 hours before the paclitaxel administration. Animals, which served as control, received the vehicle of the modulator. The results were

compared to the paclitaxel distribution determined by Fellner (2001) after valspodar co-administration. In contrast to valspodar, elacridar and tariquidar were detectable in the HPLC chromatograms. Therefore, the distribution of the two modulators was determined as well. Due to the high SEM values in the determination of accuracy and precision of the modulator recovery, the modulator distribution was only estimated. Compared to the IC_{50} values for p-gp inhibition determined in vitro, 500 to 2500 times higher elacridar concentrations were detected in the brain samples. In case of tariquidar at least 100 times higher concentrations were determined in the brains of nude mice. Therefore, elacridar and tariquidar reached tissue levels sufficient for p-gp modulation. In liver and kidney the paclitaxel concentrations were similar in the control, the elacridar and the tariquidar group, whereas in the valspodar group the paclitaxel concentrations were significantly higher. In the plasma of valspodar treated mice the paclitaxel levels were about 10 times higher than in the plasma of mice treated with tariquidar, elacridar or vehicle. Without modulator the paclitaxel levels in the brain were close to the limit of quantification. The paclitaxel concentrations in the brains of the valspodar group were 5 to 8.5 times higher than in the control group, whereas in the elacridar and tariquidar groups an only 4-fold increase compared to the control group was measured. Compared with valspodar, the brain/plasma ratio of paclitaxel in mice treated with elacridar or tariquidar indicates a more specific accumulation of paclitaxel in the brain. Although the increase in paclitaxel brain concentration in case of elacridar and tariquidar co-administration was not as pronounced as in case of valspodar, a dose reduction of anticancer drugs, as in case of valspodar paclitaxel co-administration, seems unnecessary with the new modulators, due to the lack of p-gp modulation in liver and kidney, and the low cytostatic drugs concentrations in plasma.

Another method to increase intracerebral drug concentrations is the utilization of the transferrin receptor (TfR) mediated transcytosis at the BBB for drug delivery to the brain. To be able to perform treatment studies with cytostatic drug loaded immunoliposomes targeted to the transferrin receptor both at the BBB and in tumor cells, a tumor model of primary brain tumors in the brain of nude rats was established. For this purpose, three human glioblastoma cell lines were examined, but only the U-373 MG cells turned out to be suited as an orthotopic tumor model. U-373 MG cells express a sufficient amount

of TfR and were most sensitive to the cytostatic drugs doxorubicin and daunorubicin, which are planned to be used in in vivo experiments. The developed U-373 MG tumors in brains of nude rats three weeks after cell implantation were of sufficient size and were well tolerated by the animals.

In summary, the administration of p-gp modulators of the 3^{rd} generation in combination with anticancer drugs is a promising strategy for the treatment of primary and secondary brain tumors. Approaches exploiting specific transcytotic pathways at the BBB might also enhance the concentrations of cytostatic drugs in the brain, a prerequisite for a successful therapy of malignant brain tumors.

List of abbreviations

ABC	ATP-binding cassette
ABCP	ABC transporter highly expressed in placenta
ADP	adenosine-5'diphosphate
AM	acetoxymethyl ester
AMT	absorption mediated transcytosis
ATCC	American Type Culture Collection
ATP	adenosine-5' triphosphate
AUC	area under the concentration/time curve
BBB	blood-brain barrier
BCB	blood-cerebrospinal fluid barrier
BCEC	brain capillary endothelial cells
BCRP	breast cancer resistant protein
bp	base pairs
BSA	bovine serum albumin
cDNA	copy DNA
CNS	central nervous system
CPD	citrate-phosphate-dextrose
CSF	cerebrospinal fluid
CVO	circumventricular organs
Da	dalton
DCC	1,3-dicyclohexylcarbodiimide
DEPC	diethyl pyrocarbonate
DMF	N,N-dimethylformamide
DMEM	Dulbecco's Modified Eagle Medium
DMS	Dartmouth Medical School
DMSO	dimethyl sulfoxide
DNA	desoxyribonucleic acid
DTT	dithiothreitol
EDTA	ethylenediaminetetraacetic acid
EGFP	enhanced green fluorescent protein
EMEM	Eagles Minimum Essential Medium
FCS	fetal calf serum
FITC	fluorescein-5-isothiocyanate
GFAP	glial fibrillary acidic protein
GFP	green fluorescent protein
GLUT	glucose transporter
h	hour
HE	haematoxyline-eosin
HOBt	1-hydroxybenzotriazole
HPLC	high performance liquid chromatography

HUGO	Human Genome Organisation
IC_{50}	concentration of inhibitor required to give a 50 % inhibition of activity
i.p.	intraperitoneal
i.v.	intravenous
λ	wave length
LAT	large neutral amino acid transporter
LDL	low density lipoprotein
log $P_{o/w}$	logarithm of the partition coefficient octanol/water
MAb	monoclonal antibody
MDR	multidrug resistance
MESF	molecules of equivalent soluble fluorescence
MG	Masson-Goldner
min	minute
Mp	melting point
mRNA	messenger RNA
MRP	multidrug resistance-associated protein
MS	mass spectrometry
MSD	membrane spanning domains
MW	molecular weight
MXR	mitoxantrone resistance
NAD	nicotinamide adenine dinucleotide
NADH	1,4-dihydronicotinamide adenine dinucleotide
NBD	nucleotide binding domain
NCI	National Cancer Institute
N-SCLC	non small cell lung cancer
PBS	phosphate buffered saline
PCR	polymerase chain reaction
PE	phycoerythrin
PEG	polyethylene glycol
p-gp	p-glycoprotein 170
pH	negative logarithm of the hydrogen ion concentration
p.o.	per os
RMT	receptor mediated transcytosis
RNA	ribonucleic acid
RP	reversed phase
RPMI	Roswell Park Memorial Institute
RT-PCR	reverse transcription-polymerase chain reaction
s	second
SCLC	small cell lung cancer
SEM	standard error of the mean
SPE	solid phase extraction
TfR	transferrin receptor
TMD	transmembrane domain
Topo	topotecan
UV	ultra violet
VBL	vinblastine
VP	verapamil
WHO	World health organization

List of Figures

Bibliography

Abbott, N. J. (2002). Astrocyte-endothelial interactions and blood-brain barrier permeability. *J Anat*, 200(6):629–38.

Advani, R., Fisher, G. A., Lum, B. L., Hausdorff, J., Halsey, J., Litchman, M., and Sikic, B. I. (2001). A phase I trial of doxorubicin, paclitaxel, and valspodar (PSC 833), a modulator of multidrug resistance. *Clin Cancer Res*, 7(5):1221–9.

Allen, T. M. (1994). Long-circulating (sterically stabilized) liposomes for targeted drug delivery. *Trends Pharmacol Sci*, 15(7):215–20.

Allikmets, R., Schriml, L. M., Hutchinson, A., Romano-Spica, V., and Dean, M. (1998). A human placenta-specific ATP-binding cassette gene (abcp) on chromosome 4q22 that is involved in multidrug resistance. *Cancer Res*, 58(23):5337–9.

Altenschöpfer, P. (1998). *Tumorpharmakologische und analytische Untersuchungen zur Optimierung neuer Zytostatika-beladener bioabbaubarer Implantate für die interstitielle Chemotherapie maligner Hirntumore*. PhD thesis, University of Regensburg.

Alyautdin, R., Gothier, D., Petrov, V., Kharkevich, D., and Kreuter, J. (1995). Analgesic activity of the hexapeptide dalargin adsorbed on the surface of polysorbate 80-coated poly(butyl cyanoacrylate) nanoparticles. *European Journal of Pharmaceutics and Biopharmaceutics*, 41(1):44–8.

Ambudkar, S. V., Kimchi-Sarfaty, C., Sauna, Z. E., and Gottesman, M. M. (2003). P-glycoprotein: from genomics to mechanism. *Oncogene*, 22(47):7468–85.

Bakos, E., Evers, R., Szakacs, G., Tusnady, G. E., Welker, E., Szabo, K., de Haas, M., van Deemter, L., Borst, P., Varadi, A., and Sarkadi, B. (1998). Functional multidrug resistance protein (MRP1) lacking the N-terminal transmembrane domain. *J Biol Chem*, 273(48):32167–75.

Bardelmeijer, H. A., Beijnen, J. H., Brouwer, K. R., Rosing, H., Nooijen, W. J., Schellens, J. H., and van Tellingen, O. (2000). Increased oral bioavailability of paclitaxel by GF 120918 in mice through selective modulation of p-glycoprotein. *Clin Cancer Res*, 6(11):4416–21.

Bardelmeijer, H. A., Ouwehand, M., Beijnen, J. H., Schellens, J. H., and van Tellingen, O. (2004). Efficacy of novel p-glycoprotein inhibitors to increase the oral uptake of paclitaxel in mice. *Invest New Drugs*, 22(3):219–29.

Bart, J., Groen, H. J., Hendrikse, N. H., van der Graaf, W. T., Vaalburg, W., and de Vries, E. G. (2000). The blood-brain barrier and oncology: new insights into function and modulation. *Cancer Treat Rev*, 26(6):449–62.

Bates, S., Kang, M., Meadows, B., Bakke, S., Choyke, P., Merino, M., Goldspiel, B., Chico, I., Smith, T., Chen, C., Robey, R., Bergan, R., Figg, W. D., and Fojo, T. (2001). A phase I study of infusional vinblastine in combination with the p-glycoprotein antagonist PSC 833 (valspodar). *Cancer*, 92(6):1577–90.

Bates, S. E., Bakke, S., Kang, M., Robey, R. W., Zhai, S., Thambi, P., Chen, C. C., Patil, S., Smith, T., Steinberg, S. M., Merino, M., Goldspiel, B., Meadows, B., Stein, W. D., Choyke, P., Balis, F., Figg, W. D., and Fojo, T. (2004). A phase I/II study of infusional vinblastine with the p-glycoprotein antagonist valspodar (PSC 833) in renal cell carcinoma. *Clin Cancer Res*, 10(14):4724–33.

Bates, S. E., Robey, R., Knutsen, T., Honjo, Y., Litman, T., and Dean, M. (2000). New ABC transporters in multi-drug resistance. *Emerging Therapeutic Targets*, 4(5):561–580.

Bauer, B., Miller, D. S., and Fricker, G. (2003). Compound profiling for p-glycoprotein at the blood-brain barrier using a microplate screening system. *Pharm Res*, 20(8):1170–6.

Beaulieu, E., Demeule, M., Ghitescu, L., and Beliveau, R. (1997). P-glycoprotein is strongly expressed in the luminal membranes of the endothelium of blood vessels in the brain. *Biochem J*, 326 (Pt 2):539–44.

Begley, D. J. (1996). The blood-brain barrier: principles for targeting peptides and drugs to the central nervous system. *J Pharm Pharmacol*, 48(2):136–46.

Begley, D. J. (2003). Understanding and circumventing the blood-brain barrier. *Acta Paediatr Suppl*, 92(443):83–91.

Begley, D. J. (2004). Delivery of therapeutic agents to the central nervous system: the problems and the possibilities. *Pharmacol Ther*, 104(1):29–45.

Begley, D. J. and Brightman, M. W. (2003). Structural and functional aspects of the blood-brain barrier. In Prokai, L. and Prokai-Tatrai, K., editors, *Peptide Transport and Delivery into the Central Nervous System. Progress in Drug Research*, 39–78. Birkhauser Verlag, Basel, Switzeerland.

Begley, D. J., Khan, E. U., Rollinson, C., and Abbott, N. J. (2000). The role of brain extracellular fluid production and efflux mechanisms in drug transport to the brain. In Begley, D. J., Bradbury, M., and Kreuter, J., editors, *The Blood-brain Barrier and Drug Delivery to the CNS*, 93–108. Dekker, New York.

Begley, D. J., Lechardeur, D., Chen, Z. D., Rollinson, C., Bardoul, M., Roux, F., Scherman, D., and Abbott, N. J. (1996). Functional expression of p-glycoprotein in an immortalised cell line of rat brain endothelial cells, RBE4. *J Neurochem*, 67(3):988–95.

Bendayan, R., Lee, G., and Bendayan, M. (2002). Functional expression and localization of p-glycoprotein at the blood brain barrier. *Microsc Res Tech*, 57(5):365–80.

Benoit, J. P., Faisant, N., Venier-Julienne, M. C., and Menei, P. (2000). Development of microspheres for neurological disorders: from basics to clinical applications. *J Control Release*, 65(1-2):285–96.

Bernhardt, G., Reile, H., Birnbock, H., Spruss, T., and Schonenberger, H. (1992). Standardized kinetic microassay to quantify differential chemosensitivity on the basis of proliferative activity. *J Cancer Res Clin Oncol*, 118(1):35–43.

Bickel, U., Kang, Y. S., Yoshikawa, T., and Pardridge, W. M. (1994). In vivo demonstration of subcellular localization of anti-transferrin receptor monoclonal antibody-colloidal gold conjugate in brain capillary endothelium. *J Histochem Cytochem*, 42(11):1493–7.

Bickel, U., Yoshikawa, T., Landaw, E. M., Faull, K. F., and Pardridge, W. M. (1993). Pharmacologic effects in vivo in brain by vector-mediated peptide drug delivery. *Proc Natl Acad Sci U S A*, 90(7):2618–22.

Bickel, U., Yoshikawa, T., and Pardridge, W. M. (2001). Delivery of peptides and proteins through the blood-brain barrier. *Adv Drug Deliv Rev*, 46(1-3):247–79.

Black, K. L., Baba, T., and Pardridge, W. M. (1994). Enzymatic barrier protects brain capillaries from leukotriene C4. *J Neurosurg*, 81(5):745–51.

Boado, R. J., Li, J. Y., Nagaya, M., Zhang, C., and Pardridge, W. M. (1999). Selective expression of the large neutral amino acid transporter at the blood-brain barrier. *Proc Natl Acad Sci U S A*, 96(21):12079–84.

Bodor, N. and Brewster, M. (1991). Chemical deivery systems. In Juliano, R., editor, *Targeted Drug Delivery*, 231–284. Springer-Verlag, Berlin.

Bodor, N. and Buchwald, P. (1999). Recent advances in the brain targeting of neuropharmaceuticals by chemical delivery systems. *Adv Drug Deliv Rev*, 36(2-3):229–254.

Bodor, N. and Buchwald, P. (2002). Barriers to remember: brain-targeting chemical delivery systems and alzheimer's disease. *Drug Discov Today*, 7(14):766–74.

Boesch, D., Gaveriaux, C., Jachez, B., Pourtier-Manzanedo, A., Bollinger, P., and Loor, F. (1991). In vivo circumvention of p-glycoprotein-mediated multidrug resistance of tumor cells with SDZ PSC 833. *Cancer Res*, 51(16):4226–33.

Boniface, G. R., Ferry, D. R., Atsmon, J., Inbar, M., van Tellingen, O., Abraham, J., Bates, S. E., Fojo, A. T., Thomas, H., Mould, G., Steiner, J., and Mellows, G. (2002). XR 9576 (tariquidar), a potent and specific p-glycoprotein inhibitor, has minimal effects on the pharmacokinetics of paclitaxel, doxorubicin, and vinorelbine and can be administered with full-dose chemotherapy in patients with cancer. *Proc. Am. Soc. Clin. Oncol.*, 39:2173.

Brem, H. and Gabikian, P. (2001). Biodegradable polymer implants to treat brain tumors. *J Control Release*, 74(1-3):63–7.

Brightman, M. (1992). Ultrastructure of brain endothelium. In Bradbury, M., editor, *Physiology and pharmacology of the blood brain barrier. Handbook of experimental pharmacology 103*, 1–22. Springer Verlag, Berlin.

Brightman, M. W. and Reese, T. S. (1969). Junctions between intimately apposed cell membranes in the vertebrate brain. *J Cell Biol*, 40(3):648–77.

Broadwell, R. D., Baker-Cairns, B. J., Friden, P. M., Oliver, C., and Villegas, J. C. (1996). Transcytosis of protein through the mammalian cerebral epithelium and endothelium. III. receptor-mediated transcytosis through the blood-brain barrier of blood-borne transferrin and antibody against the transferrin receptor. *Exp Neurol*, 142(1):47–65.

Brockhoff, G., Hofstaedter, F., and Knuechel, R. (1994). Flow cytometric detection and quantitation of the epidermal growth factor receptor in comparison to scatchard analysis in human bladder carcinoma cell lines. *Cytometry*, 17(1):75–83.

Brownlees, J. and Williams, C. H. (1993). Peptidases, peptides, and the mammalian blood-brain barrier. *J Neurochem*, 60(3):793–803.

Bruggemann, E. P., Currier, S. J., Gottesman, M. M., and Pastan, I. (1992). Characterization of the azidopine and vinblastine binding site of p-glycoprotein. *J Biol Chem*, 267(29):21020–6.

Bunn, P. A., J. and Kelly, K. (2000). New combinations in the treatment of lung cancer: a time for optimism. *Chest*, 117(4 Suppl 1):138S–143S.

Butt, A. M., Jones, H. C., and Abbott, N. J. (1990). Electrical resistance across the blood-brain barrier in anaesthetized rats: a developmental study. *J Physiol*, 429:47–62.

Carney, D. N., Gazdar, A. F., Bepler, G., Guccion, J. G., Marangos, P. J., Moody, T. W., Zweig, M. H., and Minna, J. D. (1985). Establishment and identification of small cell lung cancer cell lines having classic and variant features. *Cancer Res*, 45(6):2913–23.

Chan, R. Y., Seiser, C., Schulman, H. M., Kuhn, L. C., and Ponka, P. (1994). Regulation of transferrin receptor mRNA expression. Distinct regulatory features in erythroid cells. *Eur J Biochem*, 220(3):683–92.

Chandler, W. F., Greenberg, H. S., Ensminger, W. D., Diaz, R. F., Junck, L. R., Hood, T. W., Gebarski, S. S., and Page, M. A. (1988). Use of implantable pump systems for intraarterial, intraventricular and intratumoral treatment of malignant brain tumors. *Ann N Y Acad Sci*, 531:206–12.

Chang, G. (2003). Structure of MsbA from vibrio cholera: a multidrug resistance ABC transporter homolog in a closed conformation. *J Mol Biol*, 330(2):419–30.

Chang, G. and Roth, C. B. (2001). Structure of MsbA from E. coli: a homolog of the multidrug resistance ATP binding cassette (ABC) transporters. *Science*, 293(5536):1793–800.

Chervinsky, D. S., Brecher, M. L., and Hoelcle, M. J. (1993). Cremophor-el enhances taxol efficacy in a multi-drug resistant C1300 neuroblastoma cell line. *Anticancer Res*, 13(1):93–6.

Chio, C. C., Baba, T., and Black, K. L. (1992). Selective blood-tumor barrier disruption by leukotrienes. *J Neurosurg*, 77(3):407–10.

Chomczynski, P. and Sacchi, N. (1987). Single-step method of RNA isolation by acid guanidinium thiocyanate-phenol-chloroform extraction. *Anal Biochem*, 162(1):156–9.

Cloughesy, T. F. and Black, K. L. (1995). Pharmacological blood-brain barrier modification for selective drug delivery. *J Neurooncol*, 26(2):125–32.

Cole, S. P., Bhardwaj, G., Gerlach, J. H., Mackie, J. E., Grant, C. E., Almquist, K. C., Stewart, A. J., Kurz, E. U., Duncan, A. M., and Deeley, R. G. (1992). Overexpression of a transporter gene in a multidrug-resistant human lung cancer cell line. *Science*, 258(5088):1650–4.

Cooray, H. C., Blackmore, C. G., Maskell, L., and Barrand, M. A. (2002). Localisation of breast cancer resistance protein in microvessel endothelium of human brain. *Neuroreport*, 13(16):2059–63.

Cornford, E. M., Braun, L. D., Oldendorf, W. H., and Hill, M. A. (1982). Comparison of lipid-mediated blood-brain-barrier penetrability in neonates and adults. *Am J Physiol*, 243(3):C161–8.

Covelli, A. (1998). Clinical research: SDZ PSC 833. *Investigators' Brochure*, (40).

Cserr, H. and Patlak, C. (1992). Secretion and bulk flow of intestinal fluid. In Bradbury, M., editor, *Physiology and Pharmacology of the Blood-Brain Barrier. Handbook of Experimental Pharmacology*, 245–261. Springer-Verlag, Berlin.

Dalton, W. S., Grogan, T. M., Meltzer, P. S., Scheper, R. J., Durie, B. G., Taylor, C. W., Miller, T. P., and Salmon, S. E. (1989). Drug-resistance in multiple myeloma and non-hodgkin's lymphoma: detection of p-glycoprotein and potential circumvention by addition of verapamil to chemotherapy. *J Clin Oncol*, 7(4):415–24.

Dano, K. (1973). Active outward transport of daunomycin in resistant ehrlich ascites tumor cells. *Biochim Biophys Acta*, 323(3):466–83.

Dantzig, A. H., Shepard, R. L., Cao, J., Law, K. L., Ehlhardt, W. J., Baughman, T. M., Bumol, T. F., and Starling, J. J. (1996). Reversal of p-glycoprotein-mediated multidrug resistance by a potent cyclopropyldibenzosuberane modulator, LY 335979. *Cancer Res*, 56(18):4171–9.

de Bruin, M., Miyake, K., Litman, T., Robey, R., and Bates, S. E. (1999). Reversal of resistance by GF 120918 in cell lines expressing the ABC half-transporter, MXR. *Cancer Lett*, 146(2):117–26.

Decleves, X., Regina, A., Laplanche, J. L., Roux, F., Boval, B., Launay, J. M., and Scherrmann, J. M. (2000). Functional expression of p-glycoprotein and multidrug resistance-associated protein (MRP1) in primary cultures of rat astrocytes. *J Neurosci Res*, 60(5):594–601.

Demmer, A., Thole, H., Kubesch, P., Brandt, T., Raida, M., Fislage, R., and Tummler, B. (1997). Localization of the iodomycin binding site in hamster p-glycoprotein. *J Biol Chem*, 272(33):20913–9.

Descamps, L., Dehouck, M. P., Torpier, G., and Cecchelli, R. (1996). Receptor-mediated transcytosis of transferrin through blood-brain barrier endothelial cells. *Am J Physiol*, 270(4 Pt 2):H1149–58.

Dey, S., Ramachandra, M., Pastan, I., Gottesman, M. M., and Ambudkar, S. V. (1997). Evidence for two nonidentical drug-interaction sites in the human p-glycoprotein. *Proc Natl Acad Sci U S A*, 94(20):10594–9.

Dhainaut, A., Regnier, G., Atassi, G., Pierre, A., Leonce, S., Kraus-Berthier, L., and Prost, J. F. (1992). New triazine derivatives as potent modulators of multidrug resistance. *J Med Chem*, 35(13):2481–96.

Dodic, N., Dumaitre, B., Daugan, A., and Pianetti, P. (1995). Synthesis and activity against multidrug resistance in chinese hamster ovary cells of new acridone-4-carboxamides. *J Med Chem*, 38(13):2418–26.

Donatsch, P. (1996). Summary of toxicity data (update). In *Document*, 203–324. Sandoz Pharma LTD, Basel Switzerland.

Dougherty, D. (1996). Cation-p interactions in chemistry and biology: a new view of benzene, phe, tyr, and trp. *Science (Washington, D. C.)*, 271(5246):163–8.

Doyle, L. A., Yang, W., Abruzzo, L. V., Krogmann, T., Gao, Y., Rishi, A. K., and Ross, D. D. (1998). A multidrug resistance transporter from human MCF-7 breast cancer cells. *Proc Natl Acad Sci U S A*, 95(26):15665–70.

Drion, N., Lemaire, M., Lefauconnier, J. M., and Scherrmann, J. M. (1996). Role of p-glycoprotein in the blood-brain transport of colchicine and vinblastine. *J Neurochem*, 67(4):1688–93.

Druley, T. E., Stein, W. D., and Roninson, I. B. (2001). Analysis of MDR1 p-glycoprotein conformational changes in permeabilized cells using differential immunoreactivity. *Biochemistry*, 40(14):4312–22.

Eberhardt, W., Wilke, H., Stamatis, G., Stuschke, M., Harstrick, A., Menker, H., Krause, B., Mueller, M. R., Stahl, M., Flasshove, M., Budach, V., Greschuchna, D., Konietzko, N., Sack, H., and Seeber, S. (1998). Preoperative chemotherapy followed by concurrent chemoradiation therapy based on hyperfractionated accelerated radiotherapy and definitive surgery in locally advanced non-small-cell lung cancer: mature results of a phase II trial. *J Clin Oncol*, 16(2):622–34.

Edwards, J. E., Brouwer, K. R., and McNamara, P. J. (2002). GF 120918, a p-glycoprotein modulator, increases the concentration of unbound amprenavir in the central nervous system in rats. *Antimicrob Agents Chemother*, 46(7):2284–6.

Ehrlich, P. (1902). Über die Beziehungen von chemischer Constitution, Verteilung und pharmakologischer Wirkung. In *Collected Studies in Immunity (1906)*. John Wiley, New York.

Ekins, S., Kim, R. B., Leake, B. F., Dantzig, A. H., Schuetz, E. G., Lan, L. B., Yasuda, K., Shepard, R. L., Winter, M. A., Schuetz, J. D., Wikel, J. H., and Wrighton, S. A. (2002). Three-dimensional quantitative structure-activity relationships of inhibitors of p-glycoprotein. *Mol Pharmacol*, 61(5):964–73.

Emerich, D. F., Dean, R. L., Osborn, C., and Bartus, R. T. (2001). The development of the bradykinin agonist labradimil as a means to increase the permeability of the blood-brain barrier: from concept to clinical evaluation. *Clin Pharmacokinet*, 40(2):105–23.

Erdlenbruch, B., Alipour, M., Fricker, G., Miller, D. S., Kugler, W., Eibl, H., and Lakomek, M. (2003a). Alkylglycerol opening of the blood-brain barrier to small and large fluorescence markers in normal and c6 glioma-bearing rats and isolated rat brain capillaries. *Br J Pharmacol*, 140(7):1201–10.

Erdlenbruch, B., Schinkhof, C., Kugler, W., Heinemann, D. E., Herms, J., Eibl, H., and Lakomek, M. (2003b). Intracarotid administration of short-chain alkylglycerols for increased delivery of methotrexate to the rat brain. *Br J Pharmacol*, 139(4):685–94.

Evers, R., Kool, M., Smith, A. J., van Deemter, L., de Haas, M., and Borst, P. (2000). Inhibitory effect of the reversal agents V-104, GF 120918 and pluronic l61 on MDR1 pgp-, MRP1- and MRP2-mediated transport. *Br J Cancer*, 83(3):366–74.

Fardel, O., Lecureur, V., and Guillouzo, A. (1996). The p-glycoprotein multidrug transporter. *Gen Pharmacol*, 27(8):1283–91.

Fehm, H. L., Perras, B., Smolnik, R., Kern, W., and Born, J. (2000). Manipulating neuropeptidergic pathways in humans: a novel approach to neuropharmacology? *Eur J Pharmacol*, 405(1-3):43–54.

Feller, N., Kuiper, C. M., Lankelma, J., Ruhdal, J. K., Scheper, R. J., Pinedo, H. M., and Broxterman, H. J. (1995). Functional detection of MDR1/P170 and MRP/p190-mediated multidrug resistance in tumour cells by flow cytometry. *Br J Cancer*, 72(3):543–9.

Fellner, S. (2001). *Pharmakokinetische und pharmakodynamische Untersuchungen zur Koapplikation von MDR-Modulatoren (SDZ PSC 833) und Hyaluronidase bei der Chemotherapie maligner Gliome*. PhD thesis, Univeristy of Regensburg.

Fellner, S., Bauer, B., Miller, D. S., Schaffrik, M., Fankhanel, M., Spruss, T., Bernhardt, G., Graeff, C., Farber, L., Gschaidmeier, H., Buschauer, A., and Fricker, G. (2002). Transport of paclitaxel (taxol) across the blood-brain barrier in vitro and in vivo. *J Clin Invest*, 110(9):1309–18.

Fenstermacher, J. (2001). Overview of the structure and function of the blood-brain-barrier in vivo. In Kobiler, D., Lustig, S., and Shapira, S., editors, *Blood-Brain-Barrier: Drug Delivery and brain pathology*, 1–8. Kluwer Academic/Plenum Publisher, New York.

Ferry, D. R., Traunecker, H., and Kerr, D. J. (1996). Clinical trials of p-glycoprotein reversal in solid tumours. *Eur J Cancer*, 32A(6):1070–81.

Fischer, V., Rodriguez-Gascon, A., Heitz, F., Tynes, R., Hauck, C., Cohen, D., and Vickers, A. E. (1998). The multidrug resistance modulator valspodar (PSC 833) is metabolized by human cytochrome P450 3A. Implications for drug-drug interactions and pharmacological activity of the main metabolite. *Drug Metab Dispos*, 26(8):802–11.

Fisher, G. A., Lum, B. L., Hausdorff, J., and Sikic, B. I. (1996). Pharmacological considerations in the modulation of multidrug resistance. *Eur J Cancer*, 32A(6):1082–8.

Ford, J. M. (1996). Experimental reversal of p-glycoprotein-mediated multidrug resistance by pharmacological chemosensitisers. *Eur J Cancer*, 32A(6):991–1001.

Fracasso, P. M., Westervelt, P., Fears, C. L., Rosen, D. M., Zuhowski, E. G., Cazenave, L. A., Litchman, M., Egorin, M. J., Westerveldt, P., and Fears, C. A. (2000). Phase I study of paclitaxel in combination with a multidrug resistance modulator, PSC 833 (valspodar), in refractory malignancies. *J Clin Oncol*, 18(5):1124–34.

Fricker, G. and Miller, D. S. (2004). Modulation of drug transporters at the blood-brain barrier. *Pharmacology*, 70(4):169–76.

Friden, P. (1993). Receptor-mediated transport of peptides and proteins across the blood-brain barrier. In Pardridge, W. M., editor, *The Blood-Brain Barrier: Cellular and Molecular Biology*, 229–248. Raven Press, New York.

Friden, P. M. (1996). Utilization of an endogenous cellular transport system for the delivery of theraeputics across the blood-brain barrier. *Journal of Controlled Release*, 46(1-2):117–128.

Friden, P. M., Olson, T. S., Obar, R., Walus, L. R., and Putney, S. D. (1996). Characterization, receptor mapping and blood-brain barrier transcytosis of antibodies to the human transferrin receptor. *J Pharmacol Exp Ther*, 278(3):1491–8.

Gabizon, A. A. (2001). Pegylated liposomal doxorubicin: metamorphosis of an old drug into a new form of chemotherapy. *Cancer Invest*, 19(4):424–36.

Gaillard, P. J., van der Sandt, I. C., Voorwinden, L. H., Vu, D., Nielsen, J. L., de Boer, A. G., and Breimer, D. D. (2000). Astrocytes increase the functional expression of p-glycoprotein in an in vitro model of the blood-brain barrier. *Pharm Res*, 17(10):1198–205.

Gallo, J. M., Li, S., Guo, P., Reed, K., and Ma, J. (2003). The effect of p-glycoprotein on paclitaxel brain and brain tumor distribution in mice. *Cancer Res*, 63(16):5114–7.

Gambari, R., Barbieri, R., Buzzoni, D., Bernardi, F., Marchetti, G., Amelotti, F., Piva, R., Viola, L., and del Senno, L. (1986). Human leukemic K562 cells: suppression of hemoglobin accumulation by a monoclonal antibody to human transferrin receptor. *Biochim Biophys Acta*, 886(2):203–13.

Gekeler, V., Ise, W., Sanders, K. H., Ulrich, W. R., and Beck, J. (1995). The leukotriene LTD4 receptor antagonist MK571 specifically modulates MRP associated multidrug resistance. *Biochem Biophys Res Commun*, 208(1):345–52.

Germann, U. A., Ford, P. J., Shlyakhter, D., Mason, V. S., and Harding, M. W. (1997a). Chemosensitization and drug accumulation effects of vx-710, verapamil, cyclosporin A, MS-209 and GF 120918 in multidrug resistant HL60/ADR cells expressing the multidrug resistance-associated protein MRP. *Anticancer Drugs*, 8(2):141–55.

Germann, U. A., Shlyakhter, D., Mason, V. S., Zelle, R. E., Duffy, J. P., Galullo, V., Armistead, D. M., Saunders, J. O., Boger, J., and Harding, M. W. (1997b). Cellular and biochemical characterization of VX-710 as a chemosensitizer: reversal of p-glycoprotein-mediated multidrug resistance in vitro. *Anticancer Drugs*, 8(2):125–40.

Glantz, M. J., Chamberlain, M. C., Chang, S. M., Prados, M. D., and Cole, B. F. (1999). The role of paclitaxel in the treatment of primary and metastatic brain tumors. *Semin Radiat Oncol*, 9(2 Suppl 1):27–33.

Globocan (2000). Cancer incidence, mortality and prevalence worldwide, version 1.0. http://www.who.int/cancer/resources/incidences/en/.

Goldmann, E. (1909). Die äußere u. innere Sekretion des gesunden und kranken Organismus im Lichte der vitalen Färbung. *Beit. Klin. Chirug.*, 64:192–265.

Gottesman, M. M. and Pastan, I. (1993). Biochemistry of multidrug resistance mediated by the multidrug transporter. *Annu Rev Biochem*, 62:385–427.

Granados, M. E., Soriano, E., and Saavedra-Molina, A. (1997). Use of pluronic acid F-127 with fluo-3/AM probe to determine intracellular calcium changes elicited in bean protoplasts. *Phytochemical Analysis*, 8(4):204–208.

Gulyaev, A. E., Gelperina, S. E., Skidan, I. N., Antropov, A. S., Kivman, G. Y., and Kreuter, J. (1999). Significant transport of doxorubicin into the brain with polysorbate 80-coated nanoparticles. *Pharm Res*, 16(10):1564–9.

Han, B. and Zhang, J. T. (2004). Multidrug resistance in cancer chemotherapy and xenobiotic protection mediated by the half ATP-binding cassette transporter ABCG2. *Curr Med Chem Anti-Canc Agents*, 4(1):31–42.

Hay, R. J. (1988). The seed stock concept and quality control for cell lines. *Anal Biochem*, 171(2):225–37.

Hay, R. J., Pak, J., and Gazdar, A. F. (1994). *Atlas of human tumor cell lines*. Academic Press, London.

Heimans, J. J., Vermorken, J. B., Wolbers, J. G., Eeltink, C. M., Meijer, O. W., Taphoorn, M. J., and Beijnen, J. H. (1994). Paclitaxel (taxol) concentrations in brain tumor tissue. *Ann Oncol*, 5(10):951–3.

Heruth, K. T. (1988). Medtronic synchromed drug administration system. *Ann N Y Acad Sci*, 531:72–5.

Higgins, C. F. (1995). The ABC of channel regulation. *Cell*, 82(5):693–6.

Higgins, C. F. and Gottesman, M. M. (1992). Is the multidrug transporter a flippase? *Trends Biochem Sci*, 17(1):18–21.

Hoffman, R. M. (2002). Green fluorescent protein imaging of tumour growth, metastasis, and angiogenesis in mouse models. *Lancet Oncology*, 3(9):546–556.

Holland, B., Cole, S., Kuchler, K., and Higgins, C. (2003). *ABC Proteins: From Bacteria to Man*. Academic Press, London.

Hollo, Z., Homolya, L., Davis, C. W., and Sarkadi, B. (1994). Calcein accumulation as a fluorometric functional assay of the multidrug transporter. *Biochim Biophys Acta*, 1191(2):384–8.

Homolya, L., Hollo, M., Muller, M., Mechetner, E. B., and Sarkadi, B. (1996). A new method for a quantitative assessment of p-glycoprotein-related multidrug resistance in tumour cells. *Br J Cancer*, 73(7):849–55.

Homolya, L., Hollo, Z., Germann, U. A., Pastan, I., Gottesman, M. M., and Sarkadi, B. (1993). Fluorescent cellular indicators are extruded by the multidrug resistance protein. *J Biol Chem*, 268(29):21493–6.

Honjo, Y., Hrycyna, C. A., Yan, Q. W., Medina-Perez, W. Y., Robey, R. W., van de Laar, A., Litman, T., Dean, M., and Bates, S. E. (2001). Acquired mutations in the mxr/bcrp/abcp gene alter substrate specificity in MXR/BCRP/ABCP-overexpressing cells. *Cancer Res*, 61(18):6635–9.

Horio, M., Chin, K. V., Currier, S. J., Goldenberg, S., Williams, C., Pastan, I., Gottesman, M. M., and Handler, J. (1989). Transepithelial transport of drugs by the multidrug transporter in cultured madin-darby canine kidney cell epithelia. *J Biol Chem*, 264(25):14880–4.

Huisman, M. T., Smit, J. W., Wiltshire, H. R., Beijnen, J. H., and Schinkel, A. H. (2003). Assessing safety and efficacy of directed p-glycoprotein inhibition to improve the pharmacokinetic properties of saquinavir coadministered with ritonavir. *J Pharmacol Exp Ther*, 304(2):596–602.

Huwyler, J., Cerletti, A., Fricker, G., Eberle, A. N., and Drewe, J. (2002). By-passing of p-glycoprotein using immunoliposomes. *J Drug Target*, 10(1):73–9.

Huwyler, J., Wu, D., and Pardridge, W. M. (1996). Brain drug delivery of small molecules using immunoliposomes. *Proc Natl Acad Sci U S A*, 93(24):14164–9.

Hyafil, F., Vergely, C., Du Vignaud, P., and Grand-Perret, T. (1993). In vitro and in vivo reversal of multidrug resistance by GF 120918, an acridonecarboxamide derivative. *Cancer Res*, 53(19):4595–602.

Illum, L. (2002). Nasal drug delivery: new developments and strategies. *Drug Discov Today*, 7(23):1184–9.

Illum, L. (2003). Nasal drug delivery–possibilities, problems and solutions. *J Control Release*, 87(1-3):187–98.

Jain, R. K. (1994). Barriers to drug delivery in solid tumors. *Sci Am*, 271(1):58–65.

Janvilisri, T., Venter, H., Shahi, S., Reuter, G., Balakrishnan, L., and van Veen, H. W. (2003). Sterol transport by the human breast cancer resistance protein (ABCG2) expressed in lactococcus lactis. *J Biol Chem*, 278(23):20645–51.

Janzer, R. C. and Raff, M. C. (1987). Astrocytes induce blood-brain barrier properties in endothelial cells. *Nature*, 325(6101):253–7.

Jefferies, W. A., Brandon, M. R., Hunt, S. V., Williams, A. F., Gatter, K. C., and Mason, D. Y. (1984). Transferrin receptor on endothelium of brain capillaries. *Nature*, 312(5990):162–3.

Juliano, R. L. and Ling, V. (1976). A surface glycoprotein modulating drug permeability in chinese hamster ovary cell mutants. *Biochim Biophys Acta*, 455(1):152–62.

Kabanov, A. V., Batrakova, E. V., and Miller, D. W. (2003). Pluronic block copolymers as modulators of drug efflux transporter activity in the blood-brain barrier. *Adv Drug Deliv Rev*, 55(1):151–64.

Kage, K., Tsukahara, S., Sugiyama, T., Asada, S., Ishikawa, E., Tsuruo, T., and Sugimoto, Y. (2002). Dominant-negative inhibition of breast cancer resistance protein as drug efflux pump through the inhibition of s-s dependent homodimerization. *Int J Cancer*, 97(5):626–30.

Kajiji, S., Dreslin, J. A., Grizzuti, K., and Gros, P. (1994). Structurally distinct MDR modulators show specific patterns of reversal against p-glycoproteins bearing unique mutations at serine 939/941. *Biochemistry*, 33(17):5041–8.

Kang, Y. S. and Pardridge, W. M. (1994). Use of neutral avidin improves pharmacokinetics and brain delivery of biotin bound to an avidin-monoclonal antibody conjugate. *J Pharmacol Exp Ther*, 269(1):344–50.

Kaye, A. and Laws, R. (1995). *Brain Tumors, an Encyclopedic Approach*. Churchill Livingstone, Edinburgh.

Kaye, F. J. (2001). Molecular biology of lung cancer. *Lung Cancer*, 34 Suppl 2:S35–41.

Kemper, E. M., Boogerd, W., Thuis, I., Beijnen, J. H., and van Tellingen, O. (2004a). Modulation of the blood-brain barrier in oncology: therapeutic opportunities for the treatment of brain tumours? *Cancer Treat Rev*, 30(5):415–23.

Kemper, E. M., Cleypool, C., Boogerd, W., Beijnen, J. H., and van Tellingen, O. (2004b). The influence of the p-glycoprotein inhibitor zosuquidar trihydrochloride (LY 335979) on the brain penetration of paclitaxel in mice. *Cancer Chemother Pharmacol*, 53(2):173–8.

Kemper, E. M., van Zandbergen, A. E., Cleypool, C., Mos, H. A., Boogerd, W., Beijnen, J. H., and van Tellingen, O. (2003). Increased penetration of paclitaxel into the brain by inhibition of p-glycoprotein. *Clin Cancer Res*, 9(7):2849–55.

Kemper, E. M., Verheij, M., Boogerd, W., Beijnen, J. H., and van Tellingen, O. (2004c). Improved penetration of docetaxel into the brain by co-administration of inhibitors of p-glycoprotein. *Eur J Cancer*, 40(8):1269–74.

Khosla, A. (2004). Brain, metastases. http://www. emedicine.com/radio/topic101.htm.

Kim, R. B., Fromm, M. F., Wandel, C., Leake, B., Wood, A. J., Roden, D. M., and Wilkinson, G. R. (1998). The drug transporter p-glycoprotein limits oral absorption and brain entry of HIV-1 protease inhibitors. *J Clin Invest*, 101(2):289–94.

Klein, I., Sarkadi, B., and Varadi, A. (1999). An inventory of the human ABC proteins. *Biochim Biophys Acta*, 1461(2):237–62.

Kniesel, U. and Wolburg, H. (2000). Tight junctions of the blood-brain barrier. *Cell Mol Neurobiol*, 20(1):57–76.

Kreis, W., Budman, D. R., and Calabro, A. (2001). A reexamination of PSC 833 (valspodar) as a cytotoxic agent and in combination with anticancer agents. *Cancer Chemother Pharmacol*, 47(1):78–82.

Kreuter, J., Ramge, P., Petrov, V., Hamm, S., Gelperina, S. E., Engelhardt, B., Alyautdin, R., von Briesen, H., and Begley, D. J. (2003). Direct evidence that polysorbate-80-coated poly(butylcyanoacrylate) nanoparticles deliver drugs to the CNS via specific mechanisms requiring prior binding of drug to the nanoparticles. *Pharm Res*, 20(3):409–16.

Kreuter, J., Shamenkov, D., Petrov, V., Ramge, P., Cychutek, K., Koch-Brandt, C., and Alyautdin, R. (2002). Apolipoprotein-mediated transport of nanoparticle-bound drugs across the blood-brain barrier. *J Drug Target*, 10(4):317–25.

Krewson, C. E., Klarman, M. L., and Saltzman, W. M. (1995). Distribution of nerve growth factor following direct delivery to brain interstitium. *Brain Res*, 680(1-2):196–206.

Krieg, R. C., Fickweiler, S., Wolfbeis, O. S., and Knuechel, R. (2000). Cell-type specific protoporphyrin ix metabolism in human bladder cancer in vitro. *Photochem Photobiol*, 72(2):226–33.

Krishan, A., Fitz, C. M., and Andritsch, I. (1997). Drug retention, efflux, and resistance in tumor cells. *Cytometry*, 29(4):279–85.

Krishna, R. and Mayer, L. D. (2000). Multidrug resistance (MDR) in cancer. Mechanisms, reversal using modulators of MDR and the role of MDR modulators in influencing the pharmacokinetics of anticancer drugs. *Eur J Pharm Sci*, 11(4):265–83.

Kroger, N., Achterrath, W., Hegewisch-Becker, S., Mross, K., and Zander, A. R. (1999). Current options in treatment of anthracycline-resistant breast cancer. *Cancer Treat Rev*, 25(5):279–91.

Kruh, G. D. and Belinsky, M. G. (2003). The MRP family of drug efflux pumps. *Oncogene*, 22(47):7537–52.

Kruijtzer, C. M., Beijnen, J. H., Rosing, H., ten Bokkel Huinink, W. W., Schot, M., Jewell, R. C., Paul, E. M., and Schellens, J. H. (2002). Increased oral bioavailability of topotecan in combination with the breast cancer resistance protein and p-glycoprotein inhibitor GF 120918. *J Clin Oncol*, 20(13):2943–50.

Kurihara, A. and Pardridge, W. M. (1999). Imaging brain tumors by targeting peptide radiopharmaceuticals through the blood-brain barrier. *Cancer Res*, 59(24):6159–63.

Kwan, T., Loughrey, H., Brault, M., Gruenheid, S., Urbatsch, I. L., Senior, A. E., and Gros, P. (2000). Functional analysis of a tryptophan-less p-glycoprotein: a tool for tryptophan insertion and fluorescence spectroscopy. *Mol Pharmacol*, 58(1):37–47.

Lal, B., Indurti, R. R., Couraud, P. O., Goldstein, G. W., and Laterra, J. (1994). Endothelial cell implantation and survival within experimental gliomas. *Proc Natl Acad Sci U S A*, 91(21):9695–9.

Landwojtowicz, E., Nervi, P., and Seelig, A. (2002). Real-time monitoring of p-glycoprotein activation in living cells. *Biochemistry*, 41(25):8050–7.

Laskey, J., Webb, I., Schulman, H. M., and Ponka, P. (1988). Evidence that transferrin supports cell proliferation by supplying iron for DNA synthesis. *Exp Cell Res*, 176(1):87–95.

Laverman, P., Zalipsky, S., Oyen, W. J., Dams, E. T., Storm, G., Mullah, N., Corstens, F. H., and Boerman, O. C. (2000). Improved imaging of infections by avidin-induced clearance of 99mTc-biotin-peg liposomes. *J Nucl Med*, 41(5):912–8.

Lee, H. J., Zhang, Y., and Pardridge, W. M. (2002). Blood-brain barrier disruption following the internal carotid arterial perfusion of alkyl glycerols. *J Drug Target*, 10(6):463–7.

Lee, J. S., Paull, K., Alvarez, M., Hose, C., Monks, A., Grever, M., Fojo, A. T., and Bates, S. E. (1994). Rhodamine efflux patterns predict p-glycoprotein substrates in the national cancer institute drug screen. *Mol Pharmacol*, 46(4):627–38.

Legrand, O., Simonin, G., Perrot, J. Y., Zittoun, R., and Marie, J. P. (1998). Pgp and MRP activities using calcein-am are prognostic factors in adult acute myeloid leukemia patients. *Blood*, 91(12):4480–8.

Lemaire, M., Bruelisauer, A., Guntz, P., and Sato, H. (1996). Dose-dependent brain penetration of SDZ PSC 833, a novel multidrug resistance-reversing cyclosporin, in rats. *Cancer Chemother Pharmacol*, 38(5):481–6.

Lentz, K. A., Polli, J. W., Wring, S. A., Humphreys, J. E., and Polli, J. E. (2000). Influence of passive permeability on apparent p-glycoprotein kinetics. *Pharm Res*, 17(12):1456–60.

Letrent, S. P., Pollack, G. M., Brouwer, K. R., and Brouwer, K. L. (1998). Effect of GF 120918, a potent p-glycoprotein inhibitor, on morphine pharmacokinetics and pharmacodynamics in the rat. *Pharm Res*, 15(4):599–605.

Levin, V. A. (1980). Relationship of octanol/water partition coefficient and molecular weight to rat brain capillary permeability. *J Med Chem*, 23(6):682–4.

Li, H. and Qian, Z. M. (2002). Transferrin/transferrin receptor-mediated drug delivery. *Med Res Rev*, 22(3):225–50.

Liminga, G., Nygren, P., and Larsson, R. (1994). Microfluorometric evaluation of calcein acetoxymethyl ester as a probe for p-glycoprotein-mediated resistance: effects of cyclosporin A and its nonimmunosuppressive analogue SDZ PSC 833. *Exp Cell Res*, 212(2):291–6.

Linton, K., Rosenberg, M., Kerr, I., and Higgins, C. F. (2003). Structure of ABC transporters. In Holland, B., Cole, S., Kuchler, K., and Higgins, C. F., editors, *ABC Proteins: From Bacteria to Man*, 65–80. Academic Press, London.

Litman, T., Brangi, M., Hudson, E., Fetsch, P., Abati, A., Ross, D. D., Miyake, K., Resau, J. H., and Bates, S. E. (2000). The multidrug-resistant phenotype associated with overexpression of the new ABC half-transporter, MXR (ABCG2). *J Cell Sci*, 113 (Pt 11):2011–21.

Litman, T., Druley, T. E., Stein, W. D., and Bates, S. E. (2001). From MDR to MXR: new understanding of multidrug resistance systems, their properties and clinical significance. *Cell Mol Life Sci*, 58(7):931–59.

Litman, T., Jensen, U., Hansen, A., Covitz, K. M., Zhan, Z., Fetsch, P., Abati, A., Hansen, P. R., Horn, T., Skovsgaard, T., and Bates, S. E. (2002). Use of peptide antibodies to probe for the mitoxantrone resistance-associated protein MXR/BCRP/ABCP/ACBG2. *Biochim Biophys Acta*, 1565(1):6–16.

Liu, R. and Sharom, F. J. (1996). Site-directed fluorescence labeling of p-glycoprotein on cysteine residues in the nucleotide binding domains. *Biochemistry*, 35(36):11865–73.

Lo, E. H., Singhal, A. B., Torchilin, V. P., and Abbott, N. J. (2001). Drug delivery to damaged brain. *Brain Res Brain Res Rev*, 38(1-2):140–8.

Locher, K. P., Lee, A. T., and Rees, D. C. (2002). The E. coli BtuCD structure: a framework for ABC transporter architecture and mechanism. *Science*, 296(5570):1091–8.

Loo, T. W. and Clarke, D. M. (2000). Identification of residues within the drug-binding domain of the human multidrug resistance p-glycoprotein by cysteine-scanning mutagenesis and reaction with dibromobimane. *J Biol Chem*, 275(50):39272–8.

Loo, T. W. and Clarke, D. M. (2001). Defining the drug-binding site in the human multidrug resistance p-glycoprotein using a methanethiosulfonate analog of verapamil, MTS-verapamil. *J Biol Chem*, 276(18):14972–9.

Lord, P., Allami, H., Davis, M., Diaz, R., Heck, P., and Fischell, R. (1988). Minimed technologies programmable implantable infusion system. *Ann N Y Acad Sci*, 531:66–71.

Lyubimov, E., Lan, L. B., Pashinsky, I., and Stein, W. D. (1996). Effect of modulators of the multidrug resistance pump on the distribution of vinblastine in tissues of the mouse. *Anticancer Drugs*, 7(1):60–9.

Mabry, M., Nakagawa, T., Baylin, S., Pettengill, O., Sorenson, G., and Nelkin, B. (1989). Insertion of the v-ha-ras oncogene induces differentiation of calcitonin-producing human small cell lung cancer. *J Clin Invest*, 84(1):194–9.

Madrid, Y., Langer, L. F., Brem, H., and Langer, R. (1991). New directions in the delivery of drugs and other substances to the central nervous system. *Adv Pharmacol*, 22:299–324.

Maliepaard, M., van Gastelen, M. A., de Jong, L. A., Pluim, D., van Waardenburg, R. C., Ruevekamp-Helmers, M. C., Floot, B. G., and Schellens, J. H. (1999). Overexpression of the BCRP/MXR/ABCP gene in a topotecan-selected ovarian tumor cell line. *Cancer Res*, 59(18):4559–63.

Malingre, M. M., Beijnen, J. H., Rosing, H., Koopman, F. J., Jewell, R. C., Paul, E. M., Ten Bokkel Huinink, W. W., and Schellens, J. H. (2001). Co-administration of GF 120918 significantly increases the systemic exposure to oral paclitaxel in cancer patients. *Br J Cancer*, 84(1):42–7.

Marquardt, D., McCrone, S., and Center, M. S. (1990). Mechanisms of multidrug resistance in HL60 cells: detection of resistance-associated proteins with antibodies against synthetic peptides that correspond to the deduced sequence of p-glycoprotein. *Cancer Res*, 50(5):1426–30.

Martell, L. A., Agrawal, A., Ross, D. A., and Muraszko, K. M. (1993). Efficacy of transferrin receptor-targeted immunotoxins in brain tumor cell lines and pediatric brain tumors. *Cancer Res*, 53(6):1348–53.

Martin, C., Berridge, G., Higgins, C. F., Mistry, P., Charlton, P., and Callaghan, R. (2000). Communication between multiple drug binding sites on p-glycoprotein. *Mol Pharmacol*, 58(3):624–32.

Martin, C., Berridge, G., Mistry, P., Higgins, C., Charlton, P., and Callaghan, R. (1999). The molecular interaction of the high affinity reversal agent XR 9576 with p-glycoprotein. *Br J Pharmacol*, 128(2):403–11.

Matsukado, K., Inamura, T., Nakano, S., Fukui, M., Bartus, R. T., and Black, K. L. (1996). Enhanced tumor uptake of carboplatin and survival in glioma-bearing rats by intracarotid infusion of bradykinin analog, RMP-7. *Neurosurgery*, 39(1):125–33; discussion 133–4.

Matsumoto, T., Tani, E., Kaba, K., Shindo, H., and Miyaji, K. (1991). Expression of p-glycoprotein in human glioma cell lines and surgical glioma specimens. *J Neurosurg*, 74(3):460–6.

McConnell, H. M., Owicki, J. C., Parce, J. W., Miller, D. L., Baxter, G. T., Wada, H. G., and Pitchford, S. (1992). The cytosensor microphysiometer: biological applications of silicon technology. *Science*, 257(5078):1906–12.

McGrath, T. and Center, M. S. (1987). Adriamycin resistance in HL60 cells in the absence of detectable p-glycoprotein. *Biochem Biophys Res Commun*, 145(3):1171–6.

Meyer, V. R. (1992). *Praxis der Hochleistungs-Flüssigchromatographie*. Otto Salle, Frankfurt, 7 edition.

Miller, G. (2002). Drug targeting. breaking down barriers. *Science*, 297(5584):1116–8.

Miller, T. P., Grogan, T. M., Dalton, W. S., Spier, C. M., Scheper, R. J., and Salmon, S. E. (1991). P-glycoprotein expression in malignant lymphoma and reversal of clinical drug resistance with chemotherapy plus high-dose verapamil. *J Clin Oncol*, 9(1):17–24.

Misra, A., Ganesh, S., Shahiwala, A., and Shah, S. P. (2003). Drug delivery to the central nervous system: a review. *J Pharm Pharm Sci*, 6(2):252–73.

Mistry, P., Stewart, A. J., Dangerfield, W., Okiji, S., Liddle, C., Bootle, D., Plumb, J. A., Templeton, D., and Charlton, P. (2001). In vitro and in vivo reversal of p-glycoprotein-mediated multidrug resistance by a novel potent modulator, XR 9576. *Cancer Res*, 61(2):749–58.

Mitsuuchi, Y. and Testa, J. R. (2002). Cytogenetics and molecular genetics of lung cancer. *Am J Med Genet*, 115(3):183–8.

Miyake, K., Mickley, L., Litman, T., Zhan, Z., Robey, R., Cristensen, B., Brangi, M., Greenberger, L., Dean, M., Fojo, T., and Bates, S. E. (1999). Molecular cloning of cDNAs which are highly overexpressed in mitoxantrone-resistant cells: demonstration of homology to ABC transport genes. *Cancer Res*, 59(1):8–13.

Myer, M. S., Joone, G., Chasen, M. R., and van Rensburg, C. E. (1999). The chemosensitizing potential of GF 120918 is independent of the magnitude of p-glycoprotein-mediated resistance to conventional chemotherapeutic agents in a small cell lung cancer line. *Oncol Rep*, 6(1):217–8.

Nathan, F. E., Berd, D., Sato, T., and Mastrangelo, M. J. (2000). Paclitaxel and tamoxifen: An active regimen for patients with metastatic melanoma. *Cancer*, 88(1):79–87.

Neuwelt, E. A., Wiliams, P. C., Mickey, B. E., Frenkel, E. P., and Henner, W. D. (1994). Therapeutic dilemma of disseminated CNS germinoma and the potential of increased platinum-based chemotherapy delivery with osmotic blood-brain barrier disruption. *Pediatr Neurosurg*, 21(1):16–22.

Newman, M. J., Rodarte, J. C., Benbatoul, K. D., Romano, S. J., Zhang, C., Krane, S., Moran, E. J., Uyeda, R. T., Dixon, R., Guns, E. S., and Mayer, L. D. (2000). Discovery and characterization of OC 144-093, a novel inhibitor of p-glycoprotein-mediated multidrug resistance. *Cancer Res*, 60(11):2964–72.

Pardridge, W. M. (1988). Recent advances in blood-brain barrier transport. *Annu Rev Pharmacol Toxicol*, 28:25–39.

Pardridge, W. M. (1995). Vector-mediated peptide drug delivery to the brain. *Advanced Drug Delivery Reviews*, 15(1-3):109–46.

Pardridge, W. M. (1997). Drug delivery to the brain. *J Cereb Blood Flow Metab*, 17(7):713–31.

Pardridge, W. M. (1999). Vector-mediated drug delivery to the brain. *Adv Drug Deliv Rev*, 36(2-3):299–321.

Pardridge, W. M., Boado, R. J., and Farrell, C. R. (1990a). Brain-type glucose transporter (GLUT-1) is selectively localized to the blood-brain barrier. Studies with quantitative western blotting and in situ hybridization. *J Biol Chem*, 265(29):18035–40.

Pardridge, W. M., Golden, P. L., Kang, Y. S., and Bickel, U. (1997). Brain microvascular and astrocyte localization of p-glycoprotein. *J Neurochem*, 68(3):1278–85.

Pardridge, W. M., Triguero, D., Buciak, J., and Yang, J. (1990b). Evaluation of cationized rat albumin as a potential blood-brain barrier drug transport vector. *J Pharmacol Exp Ther*, 255(2):893–9.

Penzotti, J. E., Lamb, M. L., Evensen, E., and Grootenhuis, P. D. (2002). A computational ensemble pharmacophore model for identifying substrates of p-glycoprotein. *J Med Chem*, 45(9):1737–40.

Pettengill, O. S., Curphey, T. J., Cate, C. C., Flint, C. F., Maurer, L. H., and Sorenson, G. D. (1980a). Animal model for small cell carcinoma of the lung. Effect of immunosuppression and sex of mouse on tumor growth in nude athymic mice. *Exp Cell Biol*, 48(4):279–97.

Pettengill, O. S., Sorenson, G. D., Wurster-Hill, D. H., Curphey, T. J., Noll, W. W., Cate, C. C., and Maurer, L. H. (1980b). Isolation and growth characteristics of continuous cell lines from small-cell carcinoma of the lung. *Cancer*, 45(5):906–18.

Polli, J. W., Wring, S. A., Humphreys, J. E., Huang, L., Morgan, J. B., Webster, L. O., and Serabjit-Singh, C. S. (2001). Rational use of in vitro p-glycoprotein assays in drug discovery. *J Pharmacol Exp Ther*, 299(2):620–8.

Prados, M. D., Schold, S. J. S., Fine, H. A., Jaeckle, K., Hochberg, F., Mechtler, L., Fetell, M. R., Phuphanich, S., Feun, L., Janus, T. J., Ford, K., and Graney, W. (2003). A randomized, double-blind, placebo-controlled, phase 2 study of RMP-7 in combination with carboplatin administered intravenously for the treatment of recurrent malignant glioma. *Neuro-oncol*, 5(2):96–103.

Rabindran, S. K., He, H., Singh, M., Brown, E., Collins, K. I., Annable, T., and Greenberger, L. M. (1998). Reversal of a novel multidrug resistance mechanism in human colon carcinoma cells by fumitremorgin C. *Cancer Res*, 58(24):5850–8.

Rabindran, S. K., Ross, D. D., Doyle, L. A., Yang, W., and Greenberger, L. M. (2000). Fumitremorgin C reverses multidrug resistance in cells transfected with the breast cancer resistance protein. *Cancer Res*, 60(1):47–50.

Ramakrishnan, P. (2003). The role of p-glycoprotein in the blood-brain barrier. *Einstein Quarterly Journal of Biology and Medicine*, 19(4):160–165.

Ramge, P., Unger, R. E., Oltrogge, J. B., Zenker, D., Begley, D., Kreuter, J., and Von Briesen, H. (2000). Polysorbate-80 coating enhances uptake of polybutylcyanoacrylate (PBCA)-nanoparticles by human and bovine primary brain capillary endothelial cells. *Eur J Neurosci*, 12(6):1931–40.

Rao, V. V., Dahlheimer, J. L., Bardgett, M. E., Snyder, A. Z., Finch, R. A., Sartorelli, A. C., and Piwnica-Worms, D. (1999). Choroid plexus epithelial expression of MDR1 p-glycoprotein and multidrug resistance-associated protein contribute to the blood-cerebrospinal-fluid drug-permeability barrier. *Proc Natl Acad Sci U S A*, 96(7):3900–5.

Rapoport, S. I. (2000). Osmotic opening of the blood-brain barrier: principles, mechanism, and therapeutic applications. *Cell Mol Neurobiol*, 20(2):217–30.

Rapoport, S. I., Hori, M., and Klatzo, I. (1972). Testing of a hypothesis for osmotic opening of the blood-brain barrier. *Am J Physiol*, 223(2):323–31.

Ratcheson, R. A. and Ommaya, A. K. (1968). Experience with the subcutaneous cerebrospinal-fluid reservoir. preliminary report of 60 cases. *N Engl J Med*, 279(19):1025–31.

Rautio, J. and Chikhale, P. J. (2004). Drug delivery systems for brain tumor therapy. *Current Pharmaceutical Design*, 10(12):1341–1353.

Reile, H., Birnbock, H., Bernhardt, G., Spruss, T., and Schonenberger, H. (1990). Computerized determination of growth kinetic curves and doubling times from cells in microculture. *Anal Biochem*, 187(2):262–7.

Rennels, M. L., Gregory, T. F., and Fujimoto, K. (1983). Innervation of capillaries by local neurons in the cat hypothalamus: a light microscopic study with horseradish peroxidase. *J Cereb Blood Flow Metab*, 3(4):535–42.

Richard, J. P., Melikov, K., Vives, E., Ramos, C., Verbeure, B., Gait, M. J., Chernomordik, L. V., and Lebleu, B. (2003). Cell-penetrating peptides. A reevaluation of the mechanism of cellular uptake. *J Biol Chem*, 278(1):585–90.

Robert, J. and Jarry, C. (2003). Multidrug resistance reversal agents. *J Med Chem*, 46(23):4805–17.

Robey, R. W., Honjo, Y., van de Laar, A., Miyake, K., Regis, J. T., Litman, T., and Bates, S. E. (2001a). A functional assay for detection of the mitoxantrone resistance protein, MXR (ABCG2). *Biochim Biophys Acta*, 1512(2):171–82.

Robey, R. W., Medina-Perez, W. Y., Nishiyama, K., Lahusen, T., Miyake, K., Litman, T., Senderowicz, A. M., Ross, D. D., and Bates, S. E. (2001b). Overexpression of the ATP-binding cassette half-transporter, ABCG2 (MXR/BCRP/ABCP1), in flavopiridol-resistant human breast cancer cells. *Clin Cancer Res*, 7(1):145–52.

Robey, R. W., Steadman, K., Polgar, O., Morisaki, K., Blayney, M., Mistry, P., and Bates, S. E. (2004). Pheophorbide A is a specific probe for ABCG2 function and inhibition. *Cancer Res*, 64(4):1242–6.

Roe, M., Folkes, A., Ashworth, P., Brumwell, J., Chima, L., Hunjan, S., Pretswell, I., Dangerfield, W., Ryder, H., and Charlton, P. (1999). Reversal of p-glycoprotein mediated multidrug resistance by novel anthranilamide derivatives. *Bioorg Med Chem Lett*, 9(4):595–600.

Roepe, P. D., Wei, L. Y., Cruz, J., and Carlson, D. (1993). Lower electrical membrane potential and altered phi homeostasis in multidrug-resistant (MDR) cells: further characterization of a series of MDR cell lines expressing different levels of p-glycoprotein. *Biochemistry*, 32(41):11042–56.

Romeis, B. (1989). *Mikroskopische Technik*. Urban & Schwarzenberg Verlag, München, 17. edition.

Rooney, D. and Czepulkowski, B. (1986). *Human cytogenesis: a practical approach*. IRL Press ltd, OIxford, Great Britain.

Rosenberg, M. F., Callaghan, R., Ford, R. C., and Higgins, C. F. (1997). Structure of the multidrug resistance p-glycoprotein to 2.5 nm resolution determined by electron microscopy and image analysis. *J Biol Chem*, 272(16):10685–94.

Rosenberg, M. F., Mao, Q., Holzenburg, A., Ford, R. C., Deeley, R. G., and Cole, S. P. (2001a). The structure of the multidrug resistance protein 1 (MRP1/ABCC1). crystallization and single-particle analysis. *J Biol Chem*, 276(19):16076–82.

Rosenberg, M. F., Velarde, G., Ford, R. C., Martin, C., Berridge, G., Kerr, I. D., Callaghan, R., Schmidlin, A., Wooding, C., Linton, K. J., and Higgins, C. F. (2001b). Repacking of the transmembrane domains of p-glycoprotein during the transport ATPase cycle. *Embo J*, 20(20):5615–25.

Ross, D. D., Yang, W., Abruzzo, L. V., Dalton, W. S., Schneider, E., Lage, H., Dietel, M., Greenberger, L., Cole, S. P., and Doyle, L. A. (1999). Atypical multidrug resistance: breast cancer resistance protein messenger RNA expression in mitoxantrone-selected cell lines. *J Natl Cancer Inst*, 91(5):429–33.

Rousselle, C., Clair, P., Lefauconnier, J. M., Kaczorek, M., Scherrmann, J. M., and Temsamani, J. (2000). New advances in the transport of doxorubicin through the blood-brain barrier by a peptide vector-mediated strategy. *Mol Pharmacol*, 57(4):679–86.

Rowinsky, E. K., Smith, L., Wang, Y. M., Chaturvedi, P., Villalona, M., Campbell, E., Aylesworth, C., Eckhardt, S. G., Hammond, L., Kraynak, M., Drengler, R., Stephenson, J., J., Harding, M. W., and Von Hoff, D. D. (1998). Phase I and pharmacokinetic study of paclitaxel in combination with biricodar, a novel agent that reverses multidrug resistance conferred by overexpression of both MDR1 and MRP. *J Clin Oncol*, 16(9):2964–76.

Rubin, L. L. and Staddon, J. M. (1999). The cell biology of the blood-brain barrier. *Annu Rev Neurosci*, 22:11–28.

Sakane, T., Akizuki, M., Yamashita, S., Nadai, T., Hashida, M., and Sezaki, H. (1991). The transport of a drug to the cerebrospinal fluid directly from the nasal cavity: the relation to the lipophilicity of the drug. *Chem Pharm Bull (Tokyo)*, 39(9):2456–8.

Sauna, Z. E. and Ambudkar, S. V. (2000). Evidence for a requirement for ATP hydrolysis at two distinct steps during a single turnover of the catalytic cycle of human p-glycoprotein. *Proc Natl Acad Sci U S A*, 97(6):2515–20.

Sauna, Z. E. and Ambudkar, S. V. (2001). Characterization of the catalytic cycle of ATP hydrolysis by human p-glycoprotein. The two ATP hydrolysis events in a single catalytic cycle are kinetically similar but affect different functional outcomes. *J Biol Chem*, 276(15):11653–61.

Saunders, N. R., Habgood, M. D., and Dziegielewska, K. M. (1999). Barrier mechanisms in the brain, I. adult brain. *Clin Exp Pharmacol Physiol*, 26(1):11–9.

Sawada, T., Kato, Y., Sakayori, N., Takekawa, Y., and Kobayashi, M. (1999). Expression of the multidrug-resistance p-glycoprotein (pgp, MDR-1) by endothelial cells of the neovasculature in central nervous system tumors. *Brain Tumor Pathol*, 16(1):23–7.

Sawaya, R. and Bindal, R. (1995). Metstatic brain tumors. In Kaye, A. and Laws, R., editors, *Brain Tumors, an Encyclopedic approach*. Chruchill Livingstone, Edinburgh.

Scaduto, R. C., J. and Grotyohann, L. W. (1999). Measurement of mitochondrial membrane potential using fluorescent rhodamine derivatives. *Biophys J*, 76(1 Pt 1):469–77.

Scarborough, G. A. (1995). Drug-stimulated ATPase activity of the human p-glycoprotein. *J Bioenerg Biomembr*, 27(1):37–41.

Schaddelee, M. P., Voorwinden, H. L., Groenendaal, D., Hersey, A., Ijzerman, A. P., Danhof, M., and De Boer, A. G. (2003). Blood-brain barrier transport of synthetic adenosine A1 receptor agonists in vitro: structure transport relationships. *Eur J Pharm Sci*, 20(3):347–56.

Schinkel, A. H., Wagenaar, E., van Deemter, L., Mol, C. A., and Borst, P. (1995). Absence of the MDR1a p-glycoprotein in mice affects tissue distribution and pharmacokinetics of dexamethasone, digoxin, and cyclosporin A. *J Clin Invest*, 96(4):1698–705.

Schlageter, K. E., Molnar, P., Lapin, G. D., and Groothuis, D. R. (1999). Microvessel organization and structure in experimental brain tumors: microvessel populations with distinctive structural and functional properties. *Microvasc Res*, 58(3):312–28.

Schneider, C., Sutherland, R., Newman, R., and Greaves, M. (1982). Structural features of the cell surface receptor for transferrin that is recognized by the monoclonal antibody OKT9. *J Biol Chem*, 257(14):8516–22.

Schneider, E., Mayer, M., Bernhardt, G., and Buschauer, A. (2002). Simultaneous determination of ligand binding and cellular response by flow cytometry. In *Jahrestagung der DPhG*, volume 335, Suppl.1, Berlin, Germany. Arch. Pharm. Pharm. Med. Chem.

Schnyder, A., Krahenbuhl, S., Torok, M., Drewe, J., and Huwyler, J. (2004). Targeting of skeletal muscle in vitro using biotinylated immunoliposomes. *Biochem J*, 377(Pt 1):61–7.

Schwab, D., Fischer, H., Tabatabaei, A., Poli, S., and Huwyler, J. (2003). Comparison of in vitro p-glycoprotein screening assays: recommendations for their use in drug discovery. *J Med Chem*, 46(9):1716–25.

Schwarze, S. R., Ho, A., Vocero-Akbani, A., and Dowdy, S. F. (1999). In vivo protein transduction: delivery of a biologically active protein into the mouse. *Science*, 285(5433):1569–72.

Seelig, A. (1998). A general pattern for substrate recognition by p-glycoprotein. *Eur J Biochem*, 251(1-2):252–61.

Sekido, Y., Fong, K., and Minna, J. D. (2001). Molecular biology of lung cancer. In De Vita, V., Hellman, S., and Rosenberg, S., editors, *Cancer: principles and practice of oncology*, 917–925. Lippincott Williams & Wilkins, Philadelphia.

Sharom, F. J. (2003). Probing of conformational changes, catalytic cycle and ABC transporter function. In Holland, B., Cole, S. P. C., Kuchler, K., and Higgins, C., editors, *ABC Proteins: From Bacteria to Man*, 107–133. Academic Press, London.

Sharp, M. J., Mader, C. J., and Strachan, C. (1998). Synthesis of acridine derivative as multidrug-resistant inhibitor.

Shepard, R. L., Cao, J., Starling, J. J., and Dantzig, A. H. (2003). Modulation of p-glycoprotein but not MRP1- or BCRP-mediated drug resistance by LY 335979. *Int J Cancer*, 103(1):121–5.

Shi, N. and Pardridge, W. M. (2000). Noninvasive gene targeting to the brain. *Proc Natl Acad Sci U S A*, 97(13):7567–72.

Siegal, T. (2001). Strategies for increasing drug delivery to the brain (lessons derived from the treament of brain tumors). In Kobiler, D., Lustig, S., and Shapira, S., editors, *Blood-Brain-Barrier: Drug Delivery and brain pathology*, 251–272. Kluwer Academic/Plenum Publisher, New York.

Smith, Q. R. (2000). Transport of glutamate and other amino acids at the blood-brain barrier. *J Nutr*, 130(4S Suppl):1016S–22S.

Smith, Q. R. and Stoll, J. (1999). Molecular characterization of amino acid transporters at the blood-brain barrier. In Paulson, O., Moos Knudsen, G., and Moos, T., editors, *Brain Barrier Systems. Alfred Benzon Symposium*, 303–320. Munksgaard, Copenhagen.

Sparreboom, A., Planting, A. S., Jewell, R. C., van der Burg, M. E., van der Gaast, A., de Bruijn, P., Loos, W. J., Nooter, K., Chandler, L. H., Paul, E. M., Wissel, P. S., and Verweij, J. (1999). Clinical pharmacokinetics of doxorubicin in combination with GF 120918, a potent inhibitor of MDR1 p-glycoprotein. *Anticancer Drugs*, 10(8):719–28.

Sparreboom, A., van Tellingen, O., Nooijen, W. J., and Beijnen, J. H. (1995). Determination of paclitaxel and metabolites in mouse plasma, tissues, urine and faeces by semi-automated reversed-phase high-performance liquid chromatography. *J Chromatogr B Biomed Appl*, 664(2):383–91.

Spruss, T., Bernhardt, G., Schonenberger, H., and Schiess, W. (1995). Hyaluronidase significantly enhances the efficacy of regional vinblastine chemotherapy of malignant melanoma. *J Cancer Res Clin Oncol*, 121(4):193–202.

Staab, H. and Drlicek, M. (1988). *Hirnmetastasen - eine interdisziplinäre Herausforderung.* Thieme Verlag, Stuttgart, New York.

Steiniger, S. C., Kreuter, J., Khalansky, A. S., Skidan, I. N., Bobruskin, A. I., Smirnova, Z. S., Severin, S. E., Uhl, R., Kock, M., Geiger, K. D., and Gelperina, S. E. (2004). Chemotherapy of glioblastoma in rats using doxorubicin-loaded nanoparticles. *Int J Cancer*, 109(5):759–67.

Stella, V. J., Charman, W. N., and Naringrekar, V. H. (1985). Prodrugs. Do they have advantages in clinical practice? *Drugs*, 29(5):455–73.

Stewart, A., Steiner, J., Mellows, G., Laguda, B., Norris, D., and Bevan, P. (2000). Phase I trial of XR 9576 in healthy volunteers demonstrates modulation of p-glycoprotein in CD56+ lymphocytes after oral and intravenous administration. *Clin Cancer Res*, 6(11):4186–91.

Takada, Y., Vistica, D. T., Greig, N. H., Purdon, D., Rapoport, S. I., and Smith, Q. R. (1992). Rapid high-affinity transport of a chemotherapeutic amino acid across the blood-brain barrier. *Cancer Res*, 52(8):2191–6.

Takahashi, M. (1987). *Farbatlas der onkologischen Zytologie.* Perimed Fachbuch-Verlagsgesellschaft mbH, Erlangen, Deutschland.

Tamai, I., Sai, Y., Kobayashi, H., Kamata, M., Wakamiya, T., and Tsuji, A. (1997). Structure-internalization relationship for adsorptive-mediated endocytosis of basic peptides at the blood-brain barrier. *J Pharmacol Exp Ther*, 280(1):410–5.

Tamai, I. and Tsuji, A. (2000). Transporter-mediated permeation of drugs across the blood-brain barrier. *J Pharm Sci*, 89(11):1371–88.

Tan, B., Piwnica-Worms, D., and Ratner, L. (2000). Multidrug resistance transporters and modulation. *Curr Opin Oncol*, 12(5):450–8.

Tanaka, Y., Abe, Y., Tsugu, A., Takamiya, Y., Akatsuka, A., Tsuruo, T., Yamazaki, H., Ueyama, Y., Sato, O., Tamaoki, N., and et al. (1994). Ultrastructural localization of p-glycoprotein on capillary endothelial cells in human gliomas. *Virchows Arch*, 425(2):133–8.

Tang, F., Horie, K., and Borchardt, R. T. (2002). Are MDCK cells transfected with the human MRP2 gene a good model of the human intestinal mucosa? *Pharm Res*, 19(6):773–9.

Thiebaut, F., Tsuruo, T., Hamada, H., Gottesman, M. M., Pastan, I., and Willingham, M. C. (1987). Cellular localization of the multidrug-resistance gene product p-glycoprotein in normal human tissues. *Proc Natl Acad Sci U S A*, 84(21):7735–8.

Thiebaut, F., Tsuruo, T., Hamada, H., Gottesman, M. M., Pastan, I., and Willingham, M. C. (1989). Immunohistochemical localization in normal tissues of different epitopes in the multidrug transport protein p170: evidence for localization in brain capillaries and crossreactivity of one antibody with a muscle protein. *J Histochem Cytochem*, 37(2):159–64.

Thomas, H. and Coley, H. M. (2003). Overcoming multidrug resistance in cancer: an update on the clinical strategy of inhibiting p-glycoprotein. *Cancer Control*, 10(2):159–65.

Thomas, M., Baumann, M., Deppermann, M., Freitag, L., Gatzemeier, U., Huber, R., Passlick, B., Serke, M., and Ukena, D. (2002). Recommendations on the therapy of bronchial carcinoma. *Pneumologie*, 56(2):113–31.

Torchilin, V. P., Rammohan, R., Weissig, V., and Levchenko, T. S. (2001). TAT peptide on the surface of liposomes affords their efficient intracellular delivery even at low temperature and in the presence of metabolic inhibitors. *Proc Natl Acad Sci U S A*, 98(15):8786–91.

Toth, K., Vaughan, M. M., Peress, N. S., Slocum, H. K., and Rustum, Y. M. (1996). MDR1 p-glycoprotein is expressed by endothelial cells of newly formed capillaries in human gliomas but is not expressed in the neovasculature of other primary tumors. *Am J Pathol*, 149(3):853–8.

Traunecker, H. C., Stevens, M. C., Kerr, D. J., and Ferry, D. R. (1999). The acridonecarboxamide GF 120918 potently reverses p-glycoprotein-mediated resistance in human sarcoma MES-DX5 cells. *Br J Cancer*, 81(6):942–51.

Travis, W., Colby, T., and Corrin, B. (1999). *Histological typing of lung and pleural tumors. WHO international histological classification of tumors*, volume 29. Springer Verlag, Berlin, 3 edition.

Trowbridge, I. (1995). Overview of CD71. In *Leucocyte Typing*, 1139–1142. Oxford Univ. Press, Oxford.

Trowbridge, I. S., Newman, R. A., Domingo, D. L., and Sauvage, C. (1984). Transferrin receptors: structure and function. *Biochem Pharmacol*, 33(6):925–32.

Trowbridge, I. S. and Omary, M. B. (1981). Human cell surface glycoprotein related to cell proliferation is the receptor for transferrin. *Proc Natl Acad Sci U S A*, 78(5):3039–43.

Tsuji, A. (2000). Specific mechanisms for transporting drugs into brain. *Blood-Brain Barrier and Drug Delivery to the CNS*, 121–144.

Tuveson, D. A. and Jacks, T. (1999). Modeling human lung cancer in mice: similarities and shortcomings. *Oncogene*, 18(38):5318–24.

Urbatsch, I. L., al Shawi, M. K., and Senior, A. E. (1994). Characterization of the ATPase activity of purified chinese hamster p-glycoprotein. *Biochemistry*, 33(23):7069–76.

van Asperen, J., Mayer, U., van Tellingen, O., and Beijnen, J. H. (1997). The functional role of p-glycoprotein in the blood-brain barrier. *J Pharm Sci*, 86(8):881–4.

van Asperen, J., Schinkel, A. H., Beijnen, J. H., Nooijen, W. J., Borst, P., and van Tellingen, O. (1996). Altered pharmacokinetics of vinblastine in MDR1a p-glycoprotein-deficient mice. *J Natl Cancer Inst*, 88(14):994–9.

Van Houtte, P. and Albain, K. S. (1999). *Progress and perspective in the treatment of lung cancer*. Springer Verlag, Berlin.

Van Veem, H. and Callaghan, R. (2003). Substrate-binding sites in ABC transportes. In Holland, B., Cole, S. P. C., Kuchler, K., and Higgins, C., editors, *ABC Proteins: From Bacteria to Man*, 81–105. Academic Press, London.

van Veen, H. W., Margolles, A., Muller, M., Higgins, C. F., and Konings, W. N. (2000). The homodimeric ATP-binding cassette transporter Lmra mediates multidrug transport by an alternating two-site (two-cylinder engine) mechanism. *Embo J*, 19(11):2503–14.

van Zuylen, L., Sparreboom, A., van der Gaast, A., van der Burg, M. E., van Beurden, V., Bol, C. J., Woestenborghs, R., Palmer, P. A., and Verweij, J. (2000). The orally administered p-glycoprotein inhibitor R 101933 does not alter the plasma pharmacokinetics of docetaxel. *Clin Cancer Res*, 6(4):1365–71.

Walker, I., Irwin, W. J., and Akhtar, S. (1995). Improved cellular delivery of antisense oligonucleotides using transferrin receptor antibody-oligonucleotide conjugates. *Pharm Res*, 12(10):1548–53.

Walker, I., Nicholls, D., Irwin, W. J., and Freeman, S. (1994). Drug delivery via active transport at the blood-brain barrier: II. Investigation of monocarboxylic acid transport in vitro. *International Journal of Pharmaceutics*, 108(3):225–32.

Wall, D. M., Sparrow, R., Hu, X. F., Nadalin, G., Zalcberg, J. R., Marschner, I. C., Van der Weyden, M., and Parkin, J. D. (1993). Clinical application of a rapid, functional assay for multidrug resistance based on accumulation of the fluorescent dye, fluo-3. *Eur J Cancer*, 29A(7):1024–7.

Walter, K. A., Tamargo, R. J., Olivi, A., Burger, P. C., and Brem, H. (1995). Intratumoral chemotherapy. *Neurosurgery*, 37(6):1128–45.

Wandel, C., Kim, R. B., Kajiji, S., Guengerich, P., Wilkinson, G. R., and Wood, A. J. (1999). P-glycoprotein and cytochrome P-450 3A inhibition: dissociation of inhibitory potencies. *Cancer Res*, 59(16):3944–8.

Wang, R. B., Kuo, C. L., Lien, L. L., and Lien, E. J. (2003). Structure-activity relationship: analyses of p-glycoprotein substrates and inhibitors. *J Clin Pharm Ther*, 28(3):203–28.

Ward, K. W. and Azzarano, L. M. (2004). Preclinical pharmacokinetic properties of the p-glycoprotein inhibitor GF 120918a (HCl salt of GF 120918, 9,10-dihydro-5-methoxy-9-oxo-n-[4-[2-(1,2,3,4-tetrahydro-6,7-dimethoxy-2-i soquinolinyl)ethyl]phenyl]-4-acridine-carboxamide) in the mouse, rat, dog, and monkey. *J Pharmacol Exp Ther*, 310(2):703–9.

Wen, D. Y., Hall, W. A., Conrad, J., Godal, A., Florenes, V. A., and Fodstad, O. (1995). In vitro and in vivo variation in transferrin receptor expression on a human medulloblastoma cell line. *Neurosurgery*, 36(6):1158–63; discussion 1163–4.

Wen, P. Y. and Loeffler, J. S. (1999). Management of brain metastases. *Oncology (Huntingt)*, 13(7):941–54, 957–61; discussion 961–2, 9.

Whang-Peng, J., Kao-Shan, C. S., Lee, E. C., Bunn, P. A., Carney, D. N., Gazdar, A. F., and Minna, J. D. (1982). Specific chromosome defect associated with human small-cell lung cancer; deletion 3p(14-23). *Science*, 215(4529):181–2.

Wijnholds, J., Evers, R., van Leusden, M. R., Mol, C. A., Zaman, G. J., Mayer, U., Beijnen, J. H., van der Valk, M., Krimpenfort, P., and Borst, P. (1997). Increased sensitivity to anticancer drugs and decreased inflammatory response in mice lacking the multidrug resistance-associated protein. *Nat Med*, 3(11):1275–9.

Witt, K. A., Huber, J. D., Egleton, R. D., and Davis, T. P. (2002). Pluronic p85 block copolymer enhances opioid peptide analgesia. *J Pharmacol Exp Ther*, 303(2):760–7.

Wolburg, H., Wolburg-Buchholz, K., Liebner, S., and Engelhardt, B. (2001). Claudin-1, claudin-2 and claudin-11 are present in tight junctions of choroid plexus epithelium of the mouse. *Neurosci Lett*, 307(2):77–80.

Woodcock, D. M., Jefferson, S., Linsenmeyer, M. E., Crowther, P. J., Chojnowski, G. M., Williams, B., and Bertoncello, I. (1990). Reversal of the multidrug resistance phenotype with cremophor EL, a common vehicle for water-insoluble vitamins and drugs. *Cancer Res*, 50(14):4199–203.

Wozniak, A. J., Crowley, J. J., Balcerzak, S. P., Weiss, G. R., Spiridonidis, C. H., Baker, L. H., Albain, K. S., Kelly, K., Taylor, S. A., Gandara, D. R., and Livingston, R. B. (1998). Randomized trial comparing cisplatin with cisplatin plus vinorelbine in the treatment of advanced non-small-cell lung cancer: a southwest oncology group study. *J Clin Oncol*, 16(7):2459–65.

Wu, D. and Pardridge, W. M. (1998). Pharmacokinetics and blood-brain barrier transport of an anti-transferrin receptor monoclonal antibody (OX26) in rats after chronic treatment with the antibody. *Drug Metab Dispos*, 26(9):937–9.

Yang, M., Baranov, E., Jiang, P., Sun, F. X., Li, X. M., Li, L., Hasegawa, S., Bouvet, M., Al-Tuwaijri, M., Chishima, T., Shimada, H., Moossa, A. R., Penman, S., and Hoffman, R. M. (2000). Whole-body optical imaging of green fluorescent protein-expressing tumors and metastases. *Proc Natl Acad Sci U S A*, 97(3):1206–11.

Zenker, D., Begley, D., Bratzke, H., Rubsamen-Waigmann, H., and von Briesen, H. (2003). Human blood-derived macrophages enhance barrier function of cultured primary bovine and human brain capillary endothelial cells. *J Physiol*, 551(Pt 3):1023–32.

Zhang, Y., Zhang, Y. F., Bryant, J., Charles, A., Boado, R. J., and Pardridge, W. M. (2004). Intravenous RNA interference gene therapy targeting the human epidermal growth factor receptor prolongs survival in intracranial brain cancer. *Clin Cancer Res*, 10(11):3667–77.

Zhou, S., Morris, J. J., Barnes, Y., Lan, L., Schuetz, J. D., and Sorrentino, B. P. (2002). Bcrp1 gene expression is required for normal numbers of side population stem cells in mice, and confers relative protection to mitoxantrone in hematopoietic cells in vivo. *Proc Natl Acad Sci U S A*, 99(19):12339–44.

Zhu, Z. B., Makhija, S. K., Lu, B., Wang, M., Rivera, A. A., Preuss, M., Zhou, F., Siegal, G. P., Alvarez, R. D., and Curiel, D. T. (2004). Transport across a polarized monolayer of caco-2 cells by transferrin receptor-mediated adenovirus transcytosis. *Virology*, 325(1):116–28.